M 2014

U.PORTO
FEUP FACULDADE DE ENGENHARIA
UNIVERSIDADE DO PORTO

NUMERICAL ANALYSIS OF THE EXCAVATION OF A SHAFT IN LONDON CLAY

JOSÉ ALEXANDRE C. GUEDES B. ADRÊGO

DISSERTAÇÃO DE MESTRADO APRESENTADA
À FACULDADE DE ENGENHARIA DA UNIVERSIDADE DO PORTO EM
MESTRADO INTEGRADO EM ENGENHARIA CIVIL

U.PORTO

FEUP FACULDADE DE ENGENHARIA
UNIVERSIDADE DO PORTO

NUMERICAL ANALYSIS OF THE EXCAVATION OF A SHAFT IN LONDON CLAY

JOSÉ ALEXANDRE C. GUEDES B. ADRÊGO

Dissertação submetida para satisfação parcial dos requisitos do grau de

MESTRE EM ENGENHARIA CIVIL — ESPECIALIZAÇÃO EM GEOTECNIA

Orientador: Professor Doutor António Topa Gomes

Coorientador: Professor Doutor António Viana da Fonseca

Coorientador: Professor Doutor Pedro Ferreira (University College London)

JULHO DE 2014

MESTRADO INTEGRADO EM ENGENHARIA CIVIL 2013/2014

DEPARTAMENTO DE ENGENHARIA CIVIL

Tel. +351-22-508 1901

Fax +351-22-508 1446

✉ miec@fe.up.pt

Editado por

FACULDADE DE ENGENHARIA DA UNIVERSIDADE DO PORTO

Rua Dr. Roberto Frias

4200-465 PORTO

Portugal

Tel. +351-22-508 1400

Fax +351-22-508 1440

✉ feup@fe.up.pt

🌍 http://www.fe.up.pt

To Dulce and Alexandre,

"(..)Some things in life are bad
They can really make you mad
Other things just make you swear and curse.
When you're chewing on life's gristle
Don't grumble, give a whistle
And this'll help things turn out for the best... And...Always look on the bright side of life...."
Monty Python, in Life of Brian

AKNOWLEDGMENTS

First, I would like to thank to my parents, who have always been my number one supporters throughout my academic career. Without their attention, effort, constant guidance and all the love a son could wish for, I would certainly not be in the position of writing a dissertation for Master's Degree.

To my supervisor at FEUP, Professor Dr. António Topa Gomes, for all the attention, availability, friendship and some patience, at times, for all my "last questions" by the end of our meetings. It was a real honour being your student I learned so much from you as a student and as person.

To my co-supervisor at FEUP, Professor Dr. António Viana da Fonseca, who showed such a great availability for helping me to develop this work at University College London (UCL), which was a big dream of mine.

To Professor Dr. Pedro Ferreira, my co-supervisor at UCL and friend who welcomed me and provided me all the means necessary to produce a good work. It was a real pleasure having worked and learned from him.

Also, to Professor Dr. Anthony Swain from UCL, for showing an instant interest towards my work and for his advice regarding numerical analysis using the Finite Element Method.

To Professor Dr. Manuel Matos Fernandes whose teaching skills developed my interest in Geotechnics.

To Sérgio Bernardes, who turned out to be the first teacher who opened me the doors of Geotechnical Engineering. A big thanks for all the advice and help throughout my academic life.

To Rica, who was willing to help promptly when I most needed.

To all my colleagues and friends at FEUP, whose support and friendship made my time as an engineering student unforgettable.

A big thanks to my friends Pedro João and Pedro Reis for their friendship, companionship and help on these stressful last days of work.

A very special thanks to Patrícia for being there, literally, from the very first day at FEUP until the very last one. Thank you so much for being so kind, so patient and so supportive throughout our time as colleagues and friends. Staying up late working at FEUP would be dreadful without your company.

A special thanks to Rita and Manolo for being so supportive and kind to me during my time in London.

At last, to all my "London's Friends", "NP" and my two Greek UCL colleagues for being the best people someone could have ever wished to meet while so far away from home for the very first time.

RESUMO

Esta dissertação foi desenvolvida no âmbito do Mestrado Integrado em Engenharia Civil na Faculdade de Engenharia da Universidade do Porto.

O trabalho desenvolvido consiste na análise numérica de um poço circular construído que atravessa quase na totalidade uma camada de Argila de Londres. A análise numérica foi feita com recurso ao software MIDAS GTS NX. Apesar de, até metade da sua altura a estrutura em análise ter sido construída por elementos anelares pré-fabricados de betão, previamente inseridos no solo antes da escavação do solo, a análise numérica e o desenvolvimento desta tese irá incidir um pouco mais na segunda fase de construção, executada em escavação sequencial com aplicação de betão projetado.

Portanto, este trabalho inicia-se com uma descrição das principais características geológicas e geotécnicas da Argila de Londres e em seguida apresenta e discute o comportamento típico de poços circulares de grande diâmetro durante a construção, assim como algumas noções sobre o dimensionamento e processo de endurecimento do betão projetado.

Relativamente ao caso de estudo, primeiramente são descritas as suas características geométricas, construtivas e geológicas e de seguida é feito um tratamento dos dados obtidos a partir do plano de monitorização.

Por fim, procedeu-se à análise numérica do problema, começando por estudar o comportamento do poço para um cálculo base, recorrendo a um modelo de rotura de Mohr-Coloumb e depois realizou-se um estudo paramétrico, já fazendo variar as características do suporte em função do tempo, aplicando o modelo "Cam-Clay" modificado e incluindo o efeito do rebaixamento do nível freático.

PALAVRAS-CHAVE: Poços Circulares, Argila de Londres, Betão Projetado, MIDAS GTS NX, Análise Numérica

ABSTRACT

This dissertation was developed in the context of the Integrated Master Degree in Civil Engineering in the Faculty of Engineering of University of Porto.

This work consists in a numerical analysis of a circular shaft fully excavated within a soil layer of London Clay, performed with MIDAS GTS NX software. Although only half depth of the studied shaft was constructed using a wet-caisson sinking technique, the analysis of this work will focus on the second phase of construction, done by a sequential excavation process where shotcrete was applied as a support.

Therefore, this work begins with a description of the main geological and geotechnical characteristics of London Clay and then, presents and discusses the typical behavior of shafts during construction and also a few notions regarding design and shotcrete hardening.

Regarding the study case, primarily, its geometrical, constructive and geological characteristics are described and then, the data obtained from the monitoring plan is processed.

In the end, the numerical analysis was performed, firstly by studying the shaft behaviour for a baseline situation using Mohr-Coloumb as a failure criteria and then, a parametric study was done, now applying the Modified Cam-Clay model, considering the hardening process of shotcrete throughout time and including the effect of the water level lowering.

KEYWORDS: Circular Shafts, London Clay, Shotcrete, MIDAS GTS NX, Numerical Analysis

GENERAL INDEX

FIGURES INDEX

1. INTRODUCTION

2. London Clay

3. Construction, Phenomenology and Design of Shafts

4. Shaft Excavation at MILE END

5. Numerical Analysis

TABLES INDEX

2. London Clay

3. Construction, Phenomenology and Design of Shafts

4. Shaft Excavation at Mile END

5. Numerical Analysis

NOTATIONS AND ABBREVIATIONS

Latin alphabet:

c' – Effective cohesion of soil

CPT – Cone Penetration Test

D – Diameter

E – Young's Modulus

E_{cm} – Average Young's Modulus for the concrete at the age of 28 days

E_u – Undrained Young's Modulus

f_{cm} – Concrete's mean compressive strength at 28 days

FEM – Finite Element Method

G – Shear Modulus

JLE – Waterloo Jubilee Line Extension

k – Slope of over consolidated line

K_0 – Coefficient of Earth Pressure at Rest

K_{NC} – Coefficient of Earth Pressure for the Normally Consolidated State

K_{OC} - Coefficient of Earth Pressure for the Over Consolidated State

LC – London Clay

M – Bending moment

M – Slope of critical state line

N – Axial (Hoop) force

N_{60} – SPT blow count, where 60 is the percentage of the theoretical free-fall hammer energy

NATM – New Austrian Tunnelling Method

NC – Normally Consolidated state

OC – Over Consolidated State

OCR – Over Consolidation Ratio

p' – Mean effective stress

PC – Precast Concrete

PD – Project Datum

PI – Plasticity Index

R – Radius

SC – Shotcrete

SCL – Shotcrete Lining

SEM – Sequential Excavation Method

SPT – Standard Penetration Test

S_u – Undrained Shear Strength

S-XX – Midas GTS NX notation for stresses on the X axis

S-YY – Midas GTS NX notation for stresses on the Y axis

T – Shear force

T5 – Heathrow's airport, Terminal 5

TBM – Tunnelling Boring Machine

Tx – Midas GTS NX notation for translation on the X axis

Ty – Midas GTS NX notation for translation on the Y axis

u_a – pore air pressure of soil

u_w – pore water pressure of soil

WIT – Waterloo International Terminal

z – Depth

Greek alphabet:

ψ - Dilation angle

ν - Poisson's ratio

τ - Shear stress

γ - Unit weight

ω - Water content of soil

ω_L - Liquid limit

σ'_{h0} – Effective horizontal stress at rest

σ'_{v0} – Effective vertical stress at rest

Φ' – Effective friction angle

Φ^b – Friction angle due to suction

1
Introduction

1.1. Motivation and Goals

Shafts are vertical structures, usually with circular section, constructed downwards from ground level and designed to retain the surrounding soil. These structures have a key role in most of underground constructions (mainly tunnelling), since they are used as a passageway from the surface to the underground works.

In recent years, their use has been increasing in tunnelling works in urban areas, with greater depths and larger sections and so, it is essential to fully understand how these structures behave during construction, so that the surrounding constructions at the ground surface are not affected. In fact, large diameter shafts constructed employing a sequential excavation method (based on the New Austrian Tunnelling Method – NATM – or "conventional tunnelling method"), have been used in some major engineering projects. A relatively recent example is the construction of the Metropolitan in Porto – see Fig. 1.1 – where large diameter shafts were constructed instead of other "traditional" solutions, using anchored or strutted pile walls, for instance. Choosing this solution can be economically advantageous, since, due to its circular section (or close to circular) the structure is mainly subjected to compression stresses, to which concrete on its own presents a good resistance.

Fig. 1.1 – Photo from a large diameter shaft in Marquês for the construction of Porto's Metropolitan (Topa Gomes, 2008)

Currently in London (United Kingdom), a major tunnelling project is still in the construction phase and a few shafts with large diameters are being constructed. These circumstances gave the author a good opportunity to study the behaviour of one of those structures, located at Mile End Park, London – see Fig. 1.2. This shaft is around 30 m deep, has a diameter of 11.5 m and intercepts 22 m of London Clay. The structure was constructed in two phases and, in each one, a different construction method was employed, one of them being the Sequential Excavation Method. From the site, the author was provided with several reports, from the companies in charge of the works. Those reports describe the construction conditions, geotechnical background, and the structure geometry and provide data from the monitoring plan of the construction.

The study developed in this work, will be based on a numerical analysis of the mentioned shaft, performed with a software that uses the finite element method – Midas GTS NX. The results from this analysis will be further compared to the data obtained from the monitoring plan at the site.

Fig. 1.2 - Location of the case study

1.2. THESIS ORGANIZATION

This dissertation is divided in two main groups. Chapter 2 and 3 can be considered as part of the state of art, while all the others concern the case study. The subjects developed in this dissertation are organized as follows.

Chapter 2 – The shaft analysed in this work intercepts a thick layer of London Clay that represents more than 2/3 of its depth, which reflects the relevant influence this soil mass has on the structure's behaviour. London Clay is a natural material thoroughly studied and referenced in academic studies, mostly in the UK. However, being the author a Portuguese student developing the present work in London and with a limited knowledge of this soil, it was felt relevant to present a chapter providing a brief geological and geotechnical background regarding that material. In addition, the author presents and discusses the geotechnical soil parameters conventionally used in engineering practice, which will be employed in the numerical analysis in Chapter 5.

Chapter 3 – This chapter starts by describing in a general perspective the two construction methods employed in the case study. Then, follows a sub-chapter discussing the behaviour of a circular shaft when built with the conventional tunnelling method based on numerical analysis performed by Topa Gomes (2008). Finally, a parametric study is also presented focusing on the impact the various parameters have in the support internal forces and soil horizontal displacements. The final sub-chapter refers what design approaches there are nowadays for shafts and what considerations should one have concerning the support (shotcrete). The main goal of this chapter is to provide a base for a good understanding of points discussed in chapters 4 and 5.

Chapter 4 – The case study of this dissertation starts to be discussed in this chapter. Primarily, a description of the project framework is presented. Then, based on documents provided to the author by the companies that took charge of shaft construction, there is a description of the main features regarding construction methods employed, shaft's geometry and geological conditions. Then, the data from the monitoring plan reports is presented and discussed, which includes lining convergence, ground settlements, soil's horizontal displacements and shotcrete hardening.

Chapter 5 – As mentioned above, this chapter will focus on the numerical analysis of the case study based on the finite element method (FEM). First, a validation of the software used in this analysis (MIDAS GTS NX) is done by comparing the results to the ones presented in Chapter 3. The numerical analysis of the case study is split into two major parts:

- In the first one, a "baseline" analysis is performed using the Mohr-Coloumb failure criterion and not considering the effect of water table dropdown before excavation. Here, the general behaviour of the structure is presented and discussed by analysing displacements, stress variations, ground settlements and internal forces.
- The second part presents a parametric study of the case, which not only discusses the impact of the variation of some parameters, but also includes the effect of the water level lowering (suction) and the shotcrete hardening. In the end, the modified Cam Clay model is used and the results compared with Mohr-Coloumb.

Chapter 6 – This last chapter summarizes the final notes and main conclusions presented throughout the previous chapters and suggests further studies within the topic of this thesis.

2
London Clay

2.1. Geological Background, Stratigraphy And Properties

2.1.1. Depositional Environment

London Clay is a stiff, overconsolidated marine clay, deposited across the London and Hampshire Basins of southeast England in a shallow sea environment in the early Eocene age (Pantelidou, Simpson, 2007) – see Fig. 2.1. Its deposition occurred after a transgressional series of sands, silts and clays, which together constitute the Lambeth Group. Between this layer and the London Clay (LC) there is the Harwich Formation, a glauconic sand that represents the first material to be sedimented in the shallow sea (Tan *et al.*, 2003).

London Clay was a deep-water marine mud deposited in water depths of over 100 m, which could be considered a low energy marine environment. This fact allowed the formation of certain particles that are commonly found throughout LC, such as small shell fragments (commonly <5 mm in size) disseminated mica plates, glauconite grains and bioturbation. Pyrite may occur as small aggregates or discrete nodules (< 3 mm in diameter) and phosphatic and claystone nodules are quite common as well. When there is an intense appearance of some of the mentioned particles, it shows the deposition of LC was relatively slow. Very fine sand and silt dustings, parting and lenses are also frequent in the siltier clays, within the sandy clayey silts, thicker sand layers occur (Tan *et al.*, 2003).

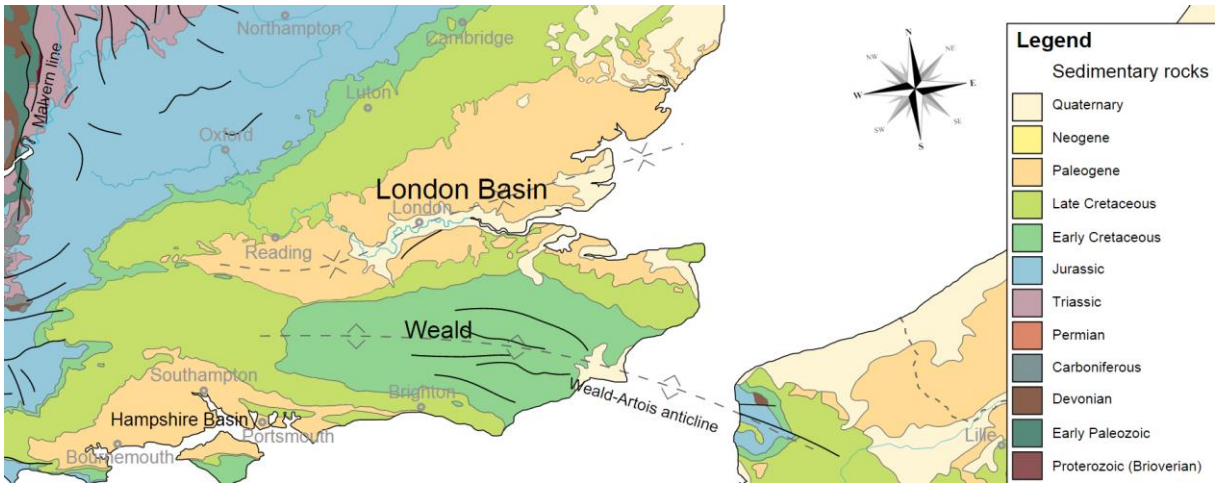

Fig. 2.1 - Geological map of southeast England, showing London and Hampshire Basin (Woudloper, 2009)

2.1.2. LITHOLOGICAL UNITS

In central London, where LC sedimentation was highly influenced by the sea level variations, its fall would be associated with a coarsening of the deposited material, for example. These consecutive regressions and transgressions of the sea level can be interpreted as cycles and according to King (1981), they provided the basis for the division of LC in lithological units. That author proposed 5 divisions in depth, from A to E, as shown in Fig. 2.2. In the same figure, one can notice that each cycle, or each unit, marks the base of an evident coarsening upward sequence, except on the A2 subdivision.

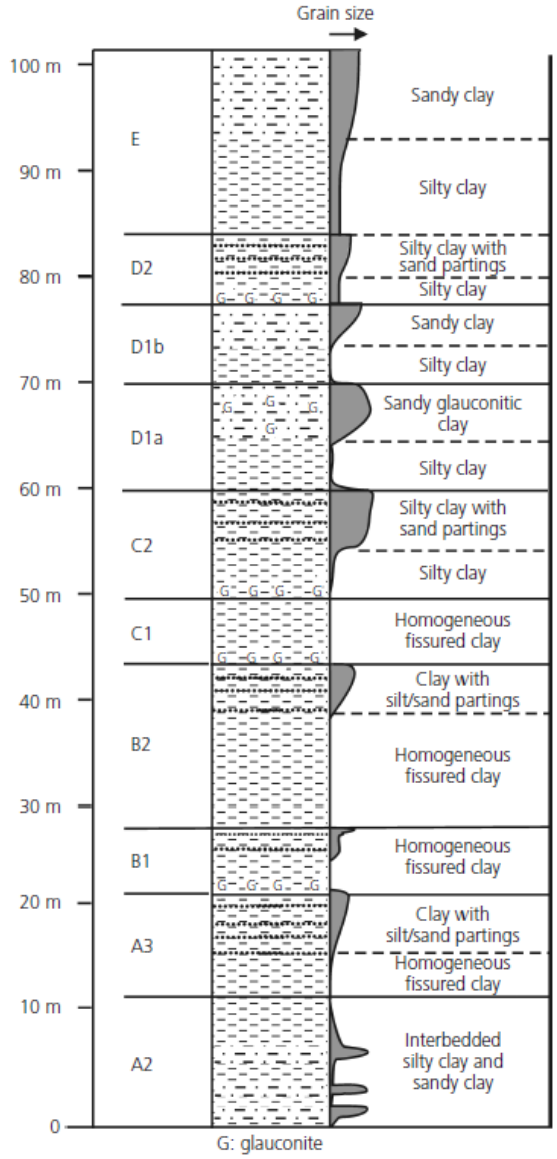

Fig. 2.2 - Stratigraphy sequence of LC proposed by King (1981) and adapted by Wright (2010)

The lowest unit, A2, is approximately 12 m thick and presents a high percentage of silt and occasional wood fragments and pyrite nodules, but does not contain claystones. Within this layer it can be noticed in Fig. 2.2 the several alternations of sandy and silty clays, which may reflect minor transgression-regressions of the sea.

Unit A3 also has an estimated 12m thickness and, close to its base, it can be found the first silty clay and claystone layers. Towards the top, silt and sand partings become more common in the silty clay. The boundary between the A and B units is marked by the presence of an approximately 1 m thick sandy clay (B1) which is glauconitic. Unit B2 comprises silty clays with weak silt and sand partings and numerous claystones (Tan *et al.*, 2003). The total thickness of unit B is about 25m.

All the other units (C1, C2, C3, D1, D2 and E) are recognized in the full sequence of LC. However, in Central London, due to erosion and further depositions, only the lower part of the sequence is preserved, from units B and downwards.

2.1.3. POST-DEPOSITIONAL PROCESSES AND EVENTS

As mentioned in the last section, LC "suffered" an erosion process, late in the Tertiary and Pleistocene times, which removed all the overlying deposits and much of the LC itself, mainly by the Thames Valley. By the end of this erosion process, that highly influenced the behaviour of LC, followed a deposition of gravel sheets along the Thames Valley and weathering. The top London Clay had been affected by desiccation, which had produced roughly sub-vertical discontinuities, by groundwater and clay in more significant depths, had been affect by ground freezing (Tan *et al.*, 2003).

In regions where the LC extends until the ground surface the top 9 m are found to be oxidated to a brown colour and beneath the topsoil, the clay is strongly weathered to a depth of about 1.5 m, presenting a granulated or fragmented texture. At greater depths there are only small reflects from weathering (Tan *et al.*, 2003). This weathering process according to Chandler, Apted (1988) may lead to a loss of effective cohesion, c', an apparent reduction in the Over Consolidation Ratio (OCR), increase in the water content and an intense fissuring.

2.1.4. HYDROGEOLOGY

Several references point out the existence of two main aquifers in the London Basin at different depths: a deeper one, which comprises the lower granular units of the Lambeth Group and whose water level goes until either the base of LC or the clays of Lambeth Group itself. The other, so called "upper aquifer", whose water table is in the Terrace Gravels, is recharged from surface precipitation and locally from the River Thames (Tan *et al.*, 2003).

Continuous extraction of water from the deeper aquifer through wells during the early 1900's caused relevant drops in water level leading to a state of underdrainage in the overlying clays. This caused a reduction of pore water pressure on those and increased the effective stresses. Water levels measured in 1967 show a dropdown of 60 m compare to the readings obtained in the 1850's. However, from 1967 to 1997 the water level has risen 48m and has continued to rise 1 or 2 m per year according to Simpson *et al.* (1989), which may cause ground settlements, damage large buildings and increase leakage into tunnels.

The presence of tunnels (mainly the ones acting as drains) can also enhance, or be the cause of local underdrainage. Fig. 2.3 shows some typical piezometric profiles from three sites across Central

London[1] where is clear the non-linearity of pore water pressure in depth. In addition, Fig. 2.4 shows the influence a draining tunnel can have in the piezometric profiles.

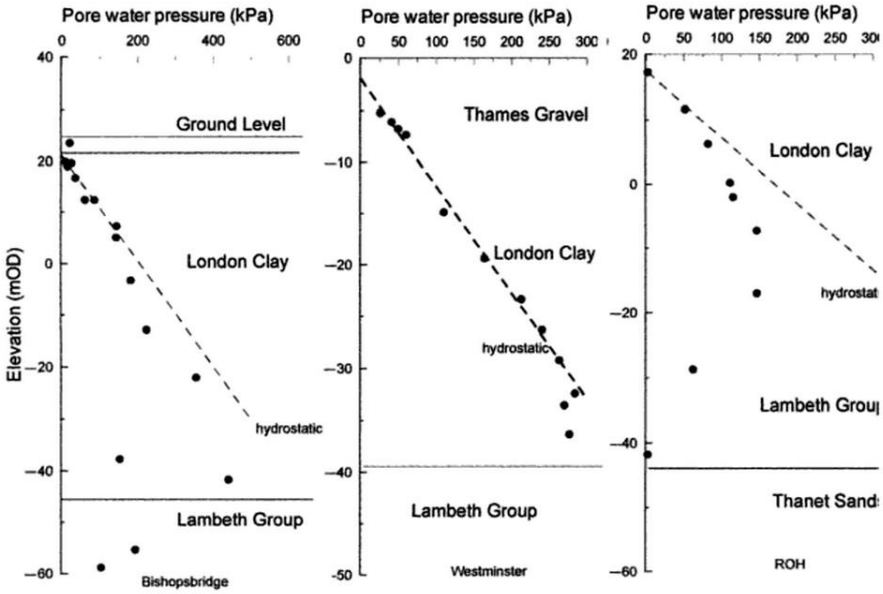

Fig. 2.3 – Typical Piezometric Profiles in Central London: Bishopbridge, Westminster and Royal Opera House (ROH) - (Tan *et al.*, 2003)

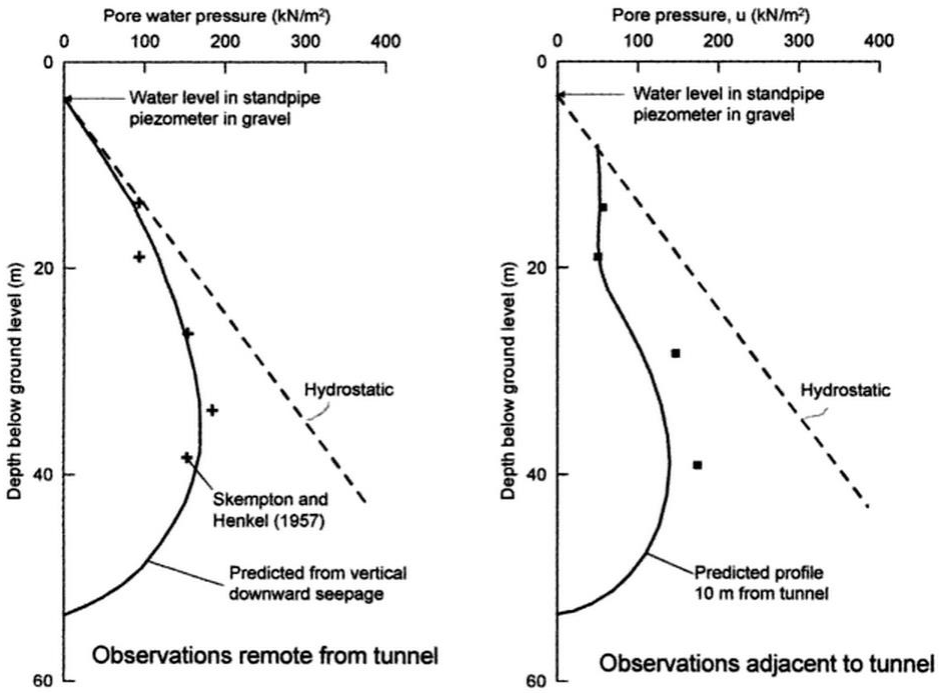

Fig. 2.4 – Effect of drainage to tunnel on piezometric profiles at Waterloo (Hight, Jardine, 1993)

[1] From this point of the present chapter several locations across Greater London will be referenced. Their location within London is presented in the Appendix I of this dissertation. That figure is, then, an essential element that should be consulted before proceeding to the next points.

2.1.5. MACROFABRIC

London Clay presents three principal natural discontinuity types whose presence may be relevant from an engineering point of view:

- Laminations – are characterized by a thin parting of more silty material with, in some cases, pieces of fossilized wood or a shell lying on the surface. These laminations correspond to what are now considered the boundaries between the different lithological units mentioned above.
- Joints – are defined as large fractures, mainly vertical, forming a series of intersecting curved surfaces.
- Fissures – are small fractures existing in clay and siltstone beds that do not cross the bed and the horizon within the bed (Gasparre, 2005).

2.2. GEOTECHNICAL CHARACTERIZATION OF LONDON CLAY

This sub-chapter will present a summarized characterization of the main geotechnical parameters of London Clay. The values of those parameters presented further will be used as reference in Chapter 5 when defining the LC parameters. For this characterization will be gathered results from laboratory and *insitu* tests, empirical expressions or some values established in engineering practice and used in similar projects to the case study. It must be said that looking for and describing the best laboratory or *insitu* tests that can best characterize LC parameters is out of the scope of this thesis, since the author only seeks to obtain reference values that can characterize this material

2.2.1. INDEX PROPERTIES – STRATIGRAPHY IDENTIFICATION

The following figures (from Fig. 2.6 to Fig. 2.9) present the variation in depth of the Liquid Limit (ω_L), Plasticity Index (PI) and Water Content (ω) obtained at Heathrow's Airport Terminal 5 (T5) and at other sites.

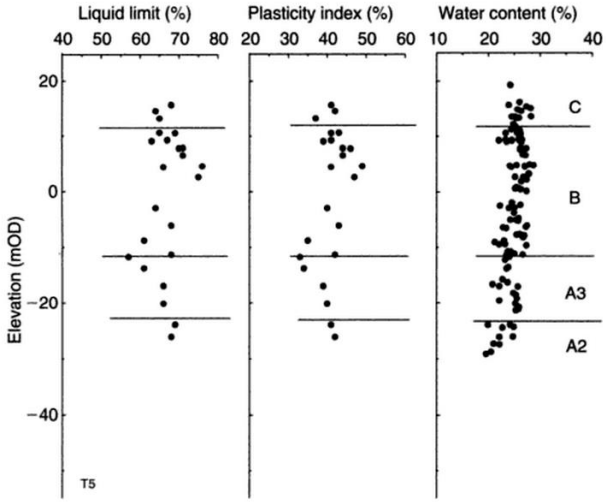

Fig. 2.5 – Index Properties at T5, (Tan *et al.*, 2003)

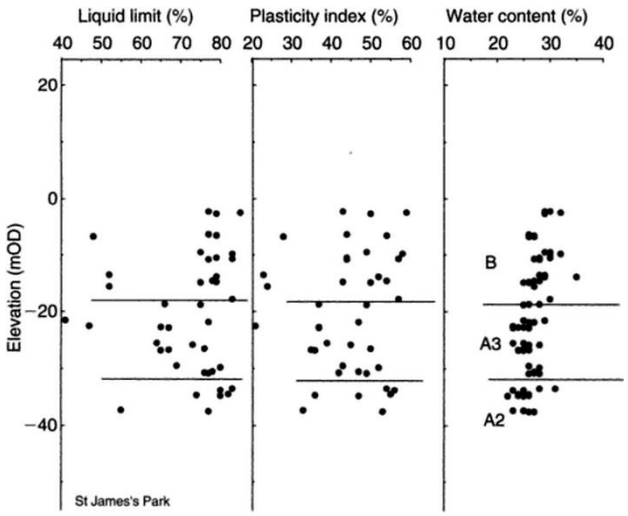

Fig. 2.6 – Index Properties at St. James's Park (Tan *et al.*, 2003)

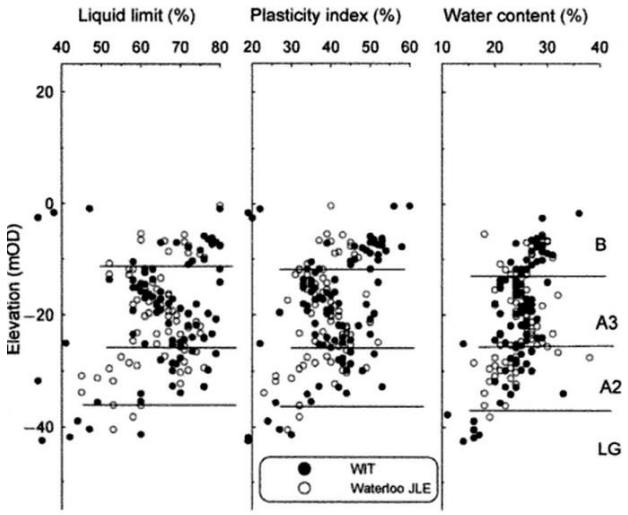

Fig. 2.7 – Index Properties at Waterloo (Tan *et al.*, 2003)

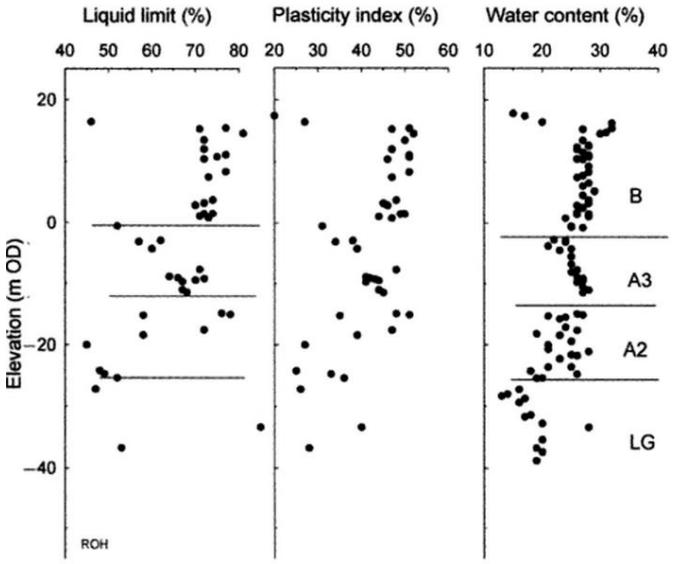

Fig. 2.8 – Index Properties at Royal Opera House, (Tan *et al.*, 2003)

From the previous figures, one can say that at T5, the clay is of high to very high plasticity considering the PI hovers around 40% reaching a maximum of 49% and a minimum of 33% and the ω_L varying from 65 to 70%. These values can only be representative for the west of the London Basin, since it is known that a proximity of the western margin of the depositional basin reflects lower plasticity than in the east due to higher thickness remotion of overlying sediments during erosion (Tan *et al.*, 2003).

Fig. 2.9 shows the data from T5 compared to other sites from the work of Bishop *et al.* (1965). In the latter, it is clear the decrease of PI from east to west (from Essex[2] to T5 – see Fig. 2.10), dropping from 65 to around 35%.

	W_L (%)	W_P (%)
Bradwell (Essex)	95	30
Waterloo (Central London)	77	27
Ashford Common	67	27
T5	65–70	22–28

Fig. 2.9 – Index Properties of London Clay (Bishop *et al.*, 1965)

[2] Essex is out of Central London, therefore, it is not represented in the map in Appendix I.

Fig. 2.10 – Bradwell (Essex) location

The patterns for the water content variation with depth were, then, used to identify lithological units where it was suggested that step changes in those values could represent unit boundaries. This correlation was first noticed by Standing, Burland (2000) in their ground investigations at St. James's Park in Central London, whose data is shown in Fig. 2.11. In the same figure data from other sites, including T5, are presented and it can be noticed the similar pattern and range of values within the same lithological unit. In Fig. 2.11 from left to right, first are presented only the values from St. James's Park, then by matching the unit boundaries are added the values from the Royal Opera House and Kennington and in the last plot are added the T5's.

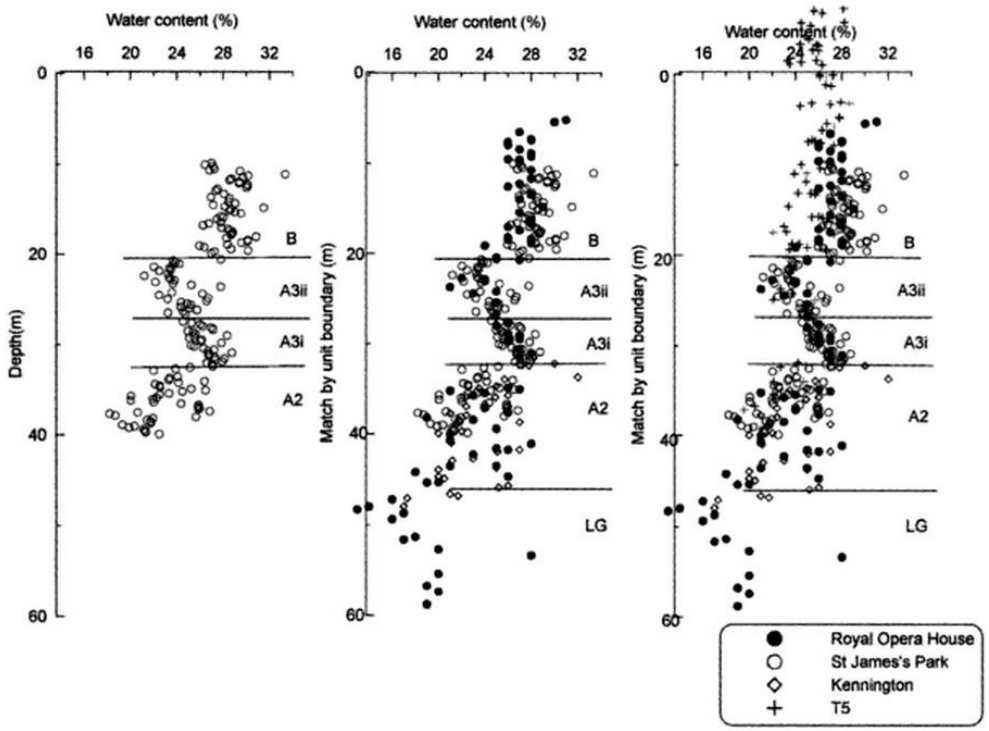

Fig. 2.11 – Index Properties and lithological units pattern correlation and comparison at several sites (Tan *et al.*, 2003)

The same pattern is also presented in Fig. 2.12 where the boundaries identified at St. James's Park are matched with the ones encountered at two ground investigations in Waterloo (Central London): Waterloo International Terminal (WIT) and Waterloo Jubilee Line extension (JLE) for the Tube.

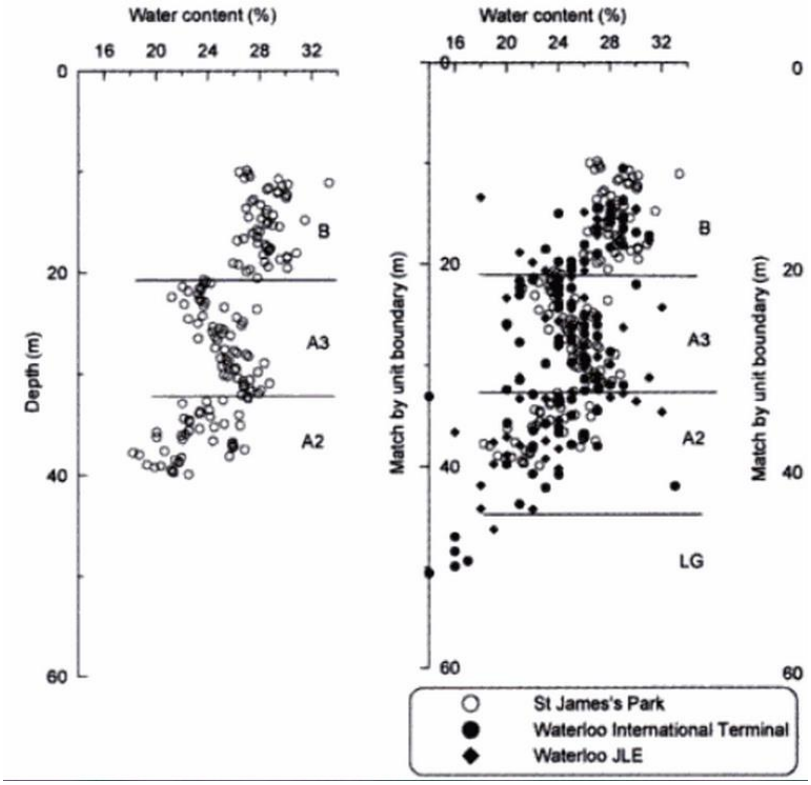

Fig. 2.12 - Index Properties and lithological units pattern correlation and comparison at Waterloo (Tan *et al.*, 2003)

These correlations between lithological units and water content not only show that this index can produce a good prediction for stratigraphy identification but also suggest the thickness of each unit is remarkably uniform across London and so it is possible to estimate the depth of the unit boundaries if the elevation of the LC base is known (Tan *et al.*, 2003). However, it is relevant to point out water content is a state parameter, and not an intrinsic soil property, which might be misleading when comparing sites with different geological history (Pantelidou, Simpson, 2007). There are, of course, other means of lithological identification commonly used as the Standard Penetration Test (SPT) or the Cone Penetration test (CPT), but would be out of scope of this thesis.

As a final note, the baseline report of case study only refers that the maximum LC Plasticity Index is 60%, which at least, corresponds the maximum values at other sites in London discussed in this point.

2.2.2. Geotechnical Parameters

2.2.2.1. Coefficient of Earth Pressure at Rest – K_0

Since the case study is a vertical structure subjected mainly to horizontal stresses, estimating K_0 becomes essential.

For normally consolidated (NC) soils, Jaky (1944) proposed a correlation between the effective friction angle, ϕ', and the coefficient of earth pressure at rest in that state ,K_{NC}, shown in expression (2.1). However, LC is known to be an overconsolidated (OC) soil and so, that expression cannot be applied for that matter, since the coefficient would have values higher than 1,0.

$$K_{NC} = 1 - \sin(\phi') \tag{2.1}$$

A model considering the overconsolidation ration (OCR) was, then, proposed by Mayne, Kulhawy (1982) where K_0, or K_{OC} can be related with OCR as shown in expression (2.2).

$$\frac{K_{OC}}{K_{NC}} = OCR^m \tag{2.2}$$

where *m* and *OCR* are defined as follows:

$$m = \sin(\phi') \tag{2.3}$$

$$OCR = \frac{\sigma'_p}{\sigma'_{v0}} \tag{2.4}$$

where, σ'_p is the effective pre-consolidation stress and σ'_{v0} is the effective vertical stress at rest.

However, the previous expression is not the most adequate for soils with a more complex stress history of loading and unloading. It also does not take into account effects such as creep (ageing) and cementation, which may lead to erroneous values of K_0

Other factor that influences the estimation of K_0 in depth within LC is the non-linearity shown in the hydrostatic pore-pressure line as mentioned previously. This reduction implied an increase of the effective vertical stress with lesser extent in the horizontal stress, which decreases K_0. Therefore, there is not, yet, a general-accepted expression to estimate an appropriate value of K_{OC}. Hight *et al.* (2003) even noted, "Still the most difficult parameter to determinate from London Clay is K_0". Having stated this, the approach for estimating values cannot just take into account all those factors.

Now, considering *insitu* test data, at Canon's Park, investigations obtained from a Marchetti dilatometer are presented in Fig. 2.13. From that figure, one can notice an average value of around 2. The estimations of this parameter are often made using the results from self-boring pressuremeter tests, although their interpretation remains controversial (Tan *et al.*, 2003).

Therefore, measurements of suction were carried out in laboratory. The variation of K_0 in depth obtained from these suction measurements is shown in Fig. 2.14. On that figure, samples from T5 site were extracted from two different locations, one containing an overlying gravel layer and the other without. Analysing the same figure it is clear that having the gravel removed reflected on a relatively higher OCR leading to higher values of K_0. It is also evident the difference in profiles by comparing two places located in the west of London (T5 and Ashford Common) and Central London (Paddington and Waterloo International Terminal), where in the first K_0 shows higher values than in the second, probably due to an uneven erosion process between the east and west of the London basin, as mentioned in 2.2.1. From Fig. 2.14 the author noted the average values of around 1.3 and 1.6 at Waterloo International Terminal (WIT) and Paddington, respectively. For the results at T5, the average is at least 2,0.

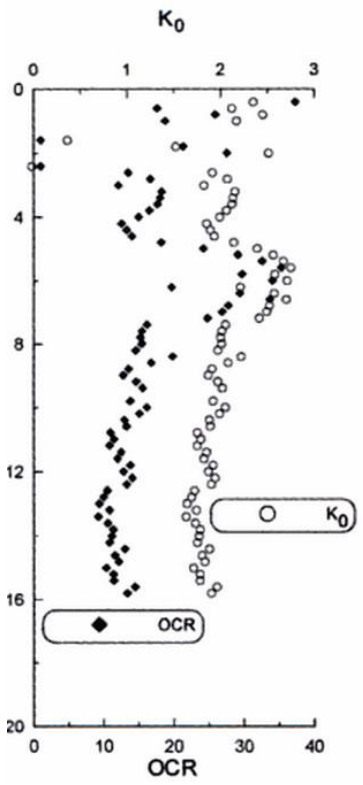

Fig. 2.13 – K_0 and OCR variation in depth at Canon's Park from Marchetti Dilatometer (Tan *et al.*, 2003)

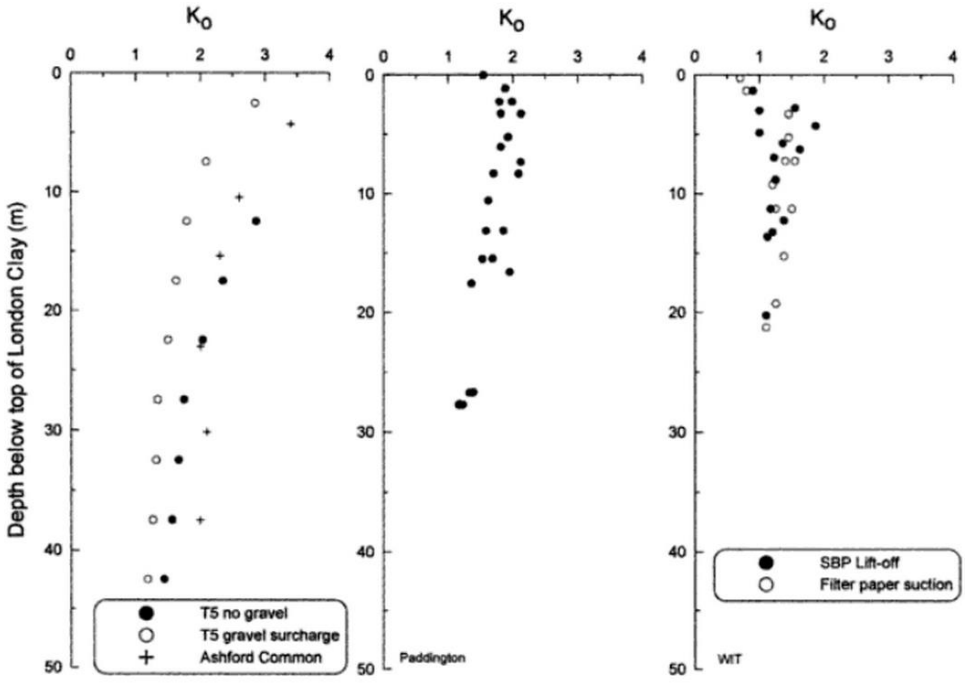

Fig. 2.14 – K_0 profiles in depth obtained at T5, Ashford Common, Paddington and WIT (Tan *et al.*, 2003)

One should have already noticed how this parameter can vary from different locations within London and in depth. Since it is necessary to input a value when modelling the case study in the numerical software it would be reasonable to consider only the values mentioned for the locations closer to the case study as: Waterloo, St. James Park, Royal Opera House or Westminster.

In addition, the reports provided to the author concerning the case study do not mention much about geotechnical parameters. So, considering the issue exposed, the author was provided with documents from an engineering company suggesting geotechnical parameters for the construction of a 36m deep shaft at Corsica Street, London – location also represented in the map of Appendix I. This construction intercepts a London Clay stratum between 3.4 and 32.2 m depth. Considering the case study, as it will be described in more detail in Chapter 4, is around 30 m deep and the shaft is involved in LC strata almost in its full depth, this construction could be a good reference. So, this reference will be continuously presented throughout the next points. As for K_0, considers the pair of expressions in (2.5), where z is the depth below ground level.

$$z<13m: 1+0.06(z-3) \qquad (2.5)$$
$$z>13m: 1.6-0.02(z-13)$$

Fig. 2.15 gathers the average values mentioned before (for the places considered relatively closer to the case study location) and the expression (2.5). The values start from around 5 m of depth, since that is the top of LC strata in the case study, as it will be described more carefully in Chapter 4.

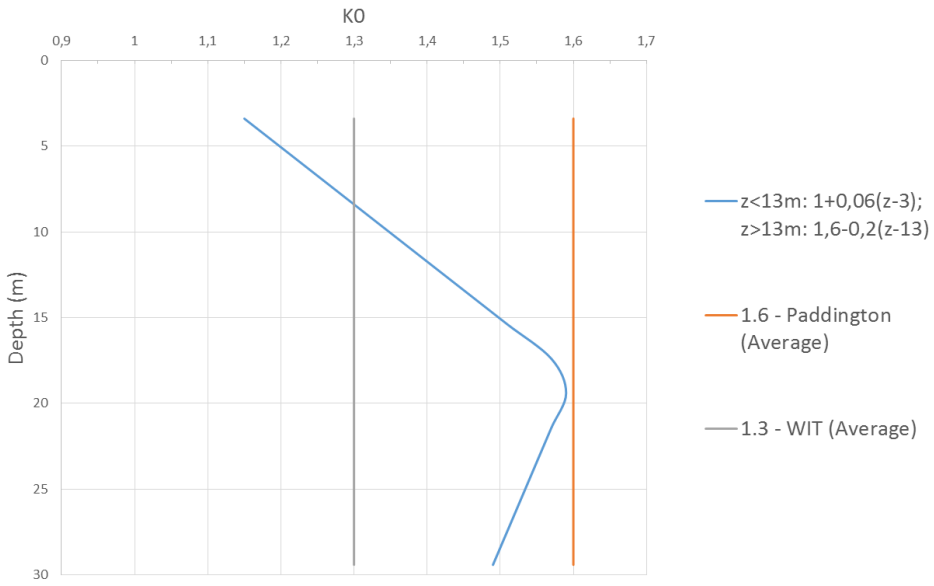

Fig. 2.15 - K_0 values comparison

2.2.2.2. Effective Cohesion (c') and Undrained Shear Strength (S_U or C_U)

Considering part of the construction of the case study was executed by employing a sequential excavation method, i.e., for a certain period of time the excavation face is unsupported (with null horizontal stresses), c' will play a key role on the horizontal displacements that will occur. If one considers an undrained analysis, the undrained strength will represent the failure boundary – see Fig. 2.16. So, it is evident the importance of both parameters for this study, however, clays have a typical undrained behaviour when loaded, there will be a main focus on the S_u in this point – Burland *et al.* (2001) suggests a range between 0-12 kPa; for a more specific case, the reference documents from Corsica Street Shaft suggest 2 kPa, for instance.

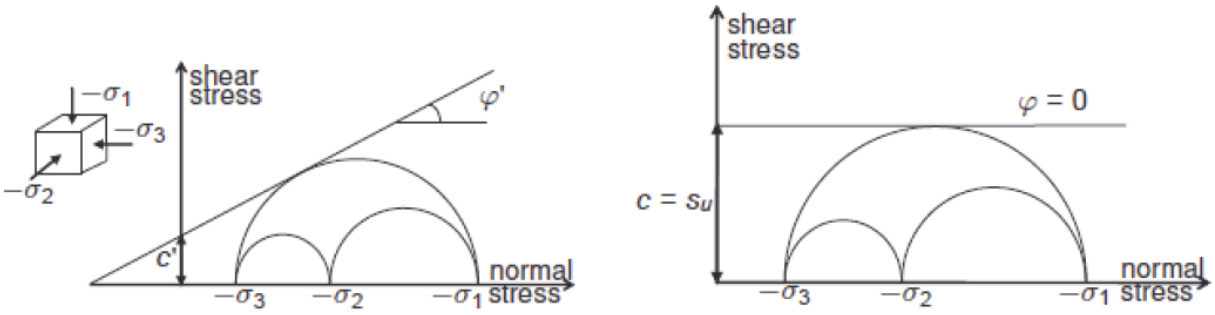

Fig. 2.16 - Drained (left) and undrained (right) failure envelope for Mohr-Coloumb model (from Midas GTS's User Manual)

Table 2.1 presents a "basic" reference for values of the undrained shear strength, being LC considered in several references as a "stiff to very stiff" clay (in Chapter 4, when describing LC at the case study's worksite, that classification will be used, for instance).

The undrained shear strength can be estimated by several ways: triaxial tests, vane tests, pressuremeter tests, CPT or even from the SPT - Terzaghi, Peck (1948) even suggest the expression of S_U for LC as $4{,}4.N_{60}$ (kPa).

Wright (2010) states that "a profile typically used for S_u of London Clay is $50+8z^3$ (kPa)", and that this parameter is also influenced by the effect of underdrainage, leading to strengthening of the material.

Table 2.1 – Estimation of values for Su (kPa) according to Stiffness

	S_u (kPa)	
Stiffness	(Terzaghi, Peck, 1948)	(Craig, 2004)
Very Soft	<12	<20
Soft	12-25	20-40
Firm	25-50	40-75
Stiff	50-100	75-150
Very Stiff	100-200	150-300
Hard	>200	>300

[3] Where z is the depth from below the top of LC strata;

Based on triaxial tests the document referring to the Corsica Street shaft suggests a distribution of 30+6z (kPa) (where z is the depth from the ground level). From the baseline reports of the case study there was an expression suggesting a minimum of 20+5z (kPa) (z [m]counting from ground level) and state as a maximum of around 450 kPa (this document does not make any reference regarding how the latter expression was obtained). Fig. 2.17 compares the previous expressions mentioned and one can notice that none of them surpasses the maximum value imposed by the case study's baseline report of 450 kPa and the extreme values of every expression are within the range of Table 2.1 for the classification of "stiff" to "very stiff".

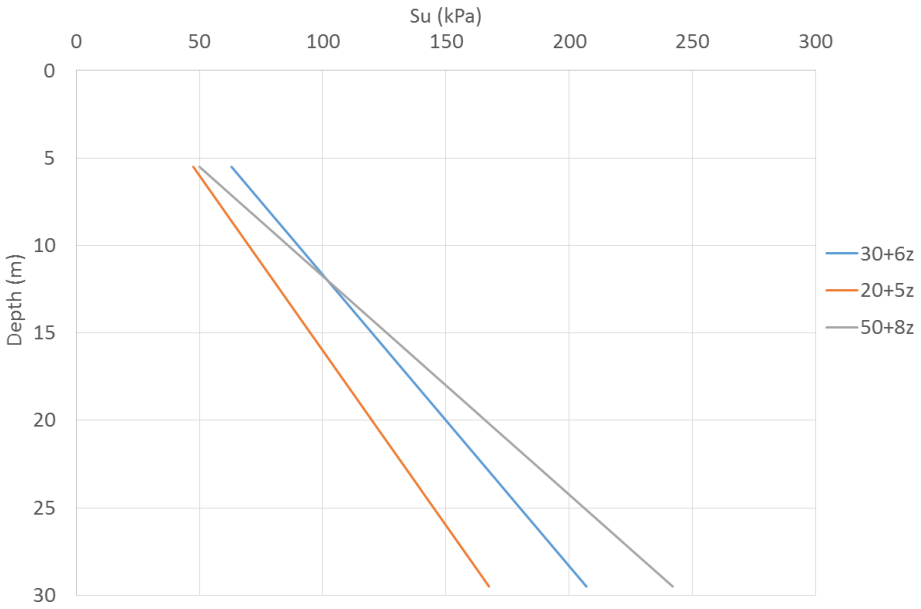

Fig. 2.17 - Comparison of different expressions representing S_u variation in depth

2.2.2.3. Stiffness – Shear Modulus (G) and Young's Modulus (E)

As Wright (2010) wrote, "soil stiffness is another difficult parameter to assess, as it is known to vary according to the amount of strain to which it was subjected". That author also presents typical profiles showing the variation of shear stiffness with strain in LC assuming G equal to E/3 for undrained conditions in Fig. 2.18 (meaning: Poisson's ratio, ν, equals 0.5 – see elastic expression 2.6). In that figure is also marked the strain range for tunnel construction in London Clay (note that the values of G are normalized for the mean effective stress *p'* – see expression 2.5)

$$p' = \frac{\sigma'_v + 2\sigma'_h}{3} \quad (2.5)$$

$$G = \frac{E}{2\times(1+\nu)} \quad (2.6)$$

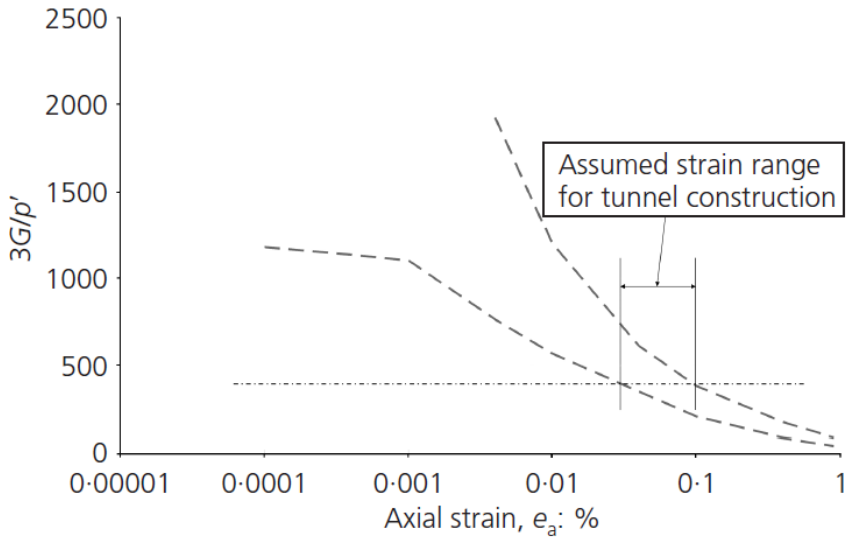

Fig. 2.18 - Variation of London Clay shear modulus in compression with strain (Wright, 2010)

Jardine *et al.* (1984) conducted several triaxial tests in clay (including LC) using local gauges to measure strain having obtained the following correlation presented in Fig. 2.19 (in this correlation the undrained Young's modulus (E_u) is normalized with the undrained shear strength). Analysing that figure and considering the strain range of Fig. 2.18 one can say that the ratio between those parameters could be around 500 and actually, Wright (2010) refers in his article that "for the initial assessment of tunnels, Tube Lines has taken the undrained stiffness for London Clay used in numerical modelling, Eu, to be 400Su". In order to backup that tendency, Fig. 2.20 shows another correlation of the undrained Young's modulus for a strain of around 0.1%, now relating the parameter with the plasticity index and the OCR. Now, if one look at the PI values presented in 2.2.1. will notice an average range between 30 to 60% (varying from site to site), which according to Fig. 2.20, may fit on the estimation given by Wright (2010), depending on ORC, of course.

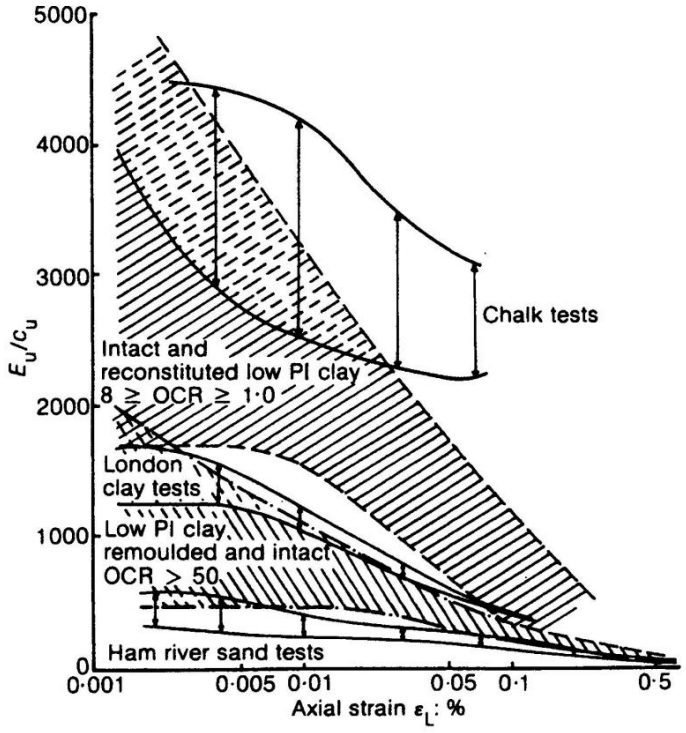

Fig. 2.19 - Correlation for undrained stiffness in clay (Jardine *et al.*, 1984)

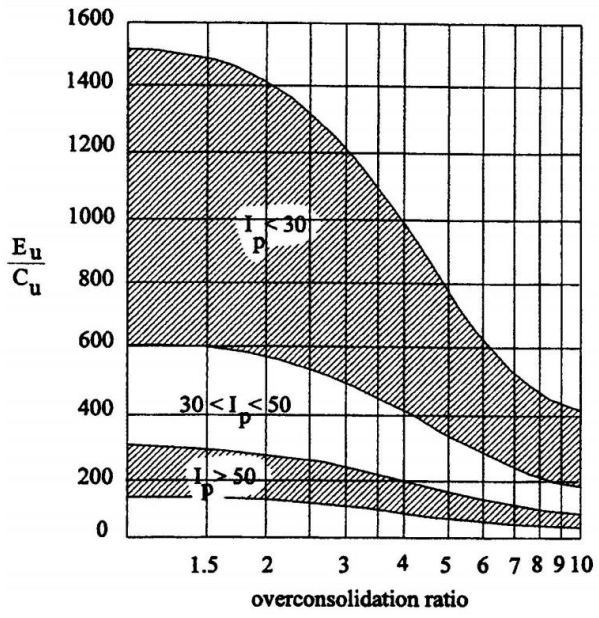

Fig. 2.20 - Correlation for undrained stiffness for strain values of around 0.1% (Duncan, Buchignani, 1976)

As already mentioned, London Clay due to the cycles of erosion-deposition is a highly overconsolidated soil and that can lead to an enhancement of its anisotropy properties. On the past decades, different authors subjected London Clay to compression triaxial tests in either undrained and drained conditions and for vertical and horizontal strains. The results of those are unanimous: the ratio between the horizontal and vertical Young's modulus would be around 2 (one can find more details in

the work of Atkinson (1973 and 1975). The reference for the Corsica Street shaft even considers $E'_{horizontal}$ as $0.8E'_{u}$ and $E'_{vertical}$ as $1.6\ E'_{horizontal}$.

2.2.2.4. Others

In Table 2.2 are presented others parameters whose definition is not so "controversial" and, or, with a relatively lower relevance for the structure's behaviour, since their variation range is relatively smaller.

Table 2.2 - Other London Clay parameters

Parameter	Range Values	Reference
Friction Angle (peak)	24-28º	(Burland *et al.*, 2001)
Unit Weight	18-21 kN/m^3	
Permeability	10^{-8}-10^{-10} m/s	
Poisson's Ratio	~0.20[4]	Corsica St. Shaft document

The author could not find any generalized value for the dilation angle (ψ). This is an important parameter that will have an impact on soil deformations, however, its value is dependent on the type of analysis one employs, if undrained with total stresses, the value becomes null, for instance.

2.3. FINAL NOTES

This was an important chapter that allowed the author to be acquainted with the main characteristics of London Clay and has here a reference that will allow him to support the choice of parameters used in the numerical analysis. Considering the knowledge of the author regarding this material was limited, London Clay turned out to be a complex material that possible may create difficulties during modelling, that will make the author apply certain "simplification measures" (targeting the materials anisotropy for stiffness or the variation with depth of K_0).

[4] For an undrained analysis, otherwise the value would become 0.50 so that the volume change is null.

3

Construction, Phenomenology and Design of Shafts

3.1. INTRODUCTION

Shafts are vertical structures excavated in either soil or rock and often present a circular, or elliptical, section so that the arching effect in soil\rock stresses is enhanced, making the structure work as a shell element (with hoop stresses) and the surrounding soil/rock load as a contributing factor to the structure's stability.

These structures represent a key component in urban tunnelling projects, functioning during construction works as a starting point for tunnel excavation and, or, as a breakthrough, as a way for supplying/extracting materials and equipment and as an intermediate access for the tunnel maintenance, or other purposes, during the tunnel lifetime. Their construction (as for tunnels as well) within an urban environment implies a careful decision making process regarding excavation sequences, groundwater control, structural lining design and a solid monitoring plan in order to avoid damaging the surrounding structures.

Shafts can be categorized according to the applied support methods and excavation techniques, and the choice for either one is primarily dependent of the ground conditions. The presence of rock or soil masses can lead to different solutions and even distinguishing cohesive from cohesionless soils might imply the application of different methods. There are of course obvious factors as time and budget that will influence the final decision, but those, despite being essential in the civil engineering industry, will not be discussed further in this work.

Considering that the case study of this work features a circular shaft within a soil, constructed firstly using a sinking caisson technique and then a sequential excavation, the following sub-chapter 3.2 will only refer to those methods in a general view – there are soil treatment procedures and some variations in techniques but will not be discussed in this work. Although, for further reading, a brief description of different methods can be found in Doig (2012) – Fig. 3.1 shows a diagram listing the different methods referred in that work.

In addition, since the numerical analysis presented in Chapter 5 is mainly concerned with the sequential excavation, where the shaft is constructed following a very similar procedure used in conventional tunnelling, sub-chapters 3.3 and 3.4 shall have that method as a basis.

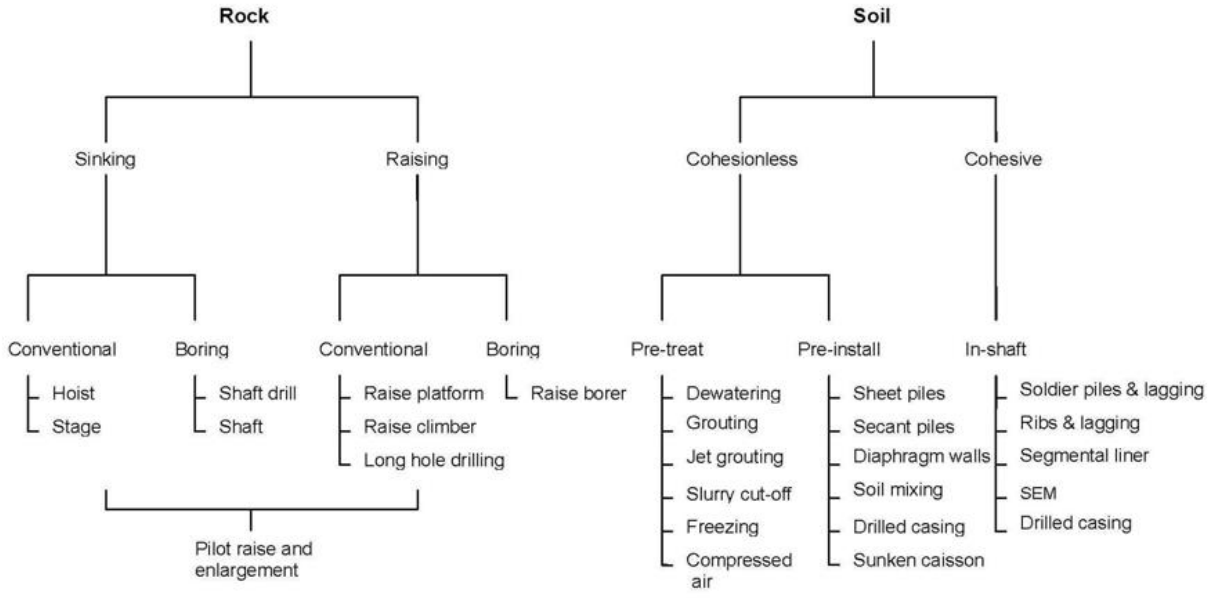

Fig. 3.1 - Different shaft excavation methods categorized by ground conditions (Doig, 2012)

3.2. CONSTRUCTION METHODS

3.2.1. CAISSON SINKING METHOD

Caisson sinking methods are generally applied in cohesionless soils where a vertical excavated face is difficult to achieve and/or where base stability is at risk due to water pressure (British Tunnelling Society and Institution of Civil Engineers, 2004). In this method, a precast concrete segmental lining is erected at the surface and sunk into position using kentledge or hydraulic jacks in order to make the piece self-weight overcome ground friction – this first segmental ring is provided with a steel cutting edge on its base. The excavation begins when there is structural support of two or three rings of height below the shaft's base.

In water-bearing strata, where dewatering within the shaft would cause basal instability, "wet caisson" sinking methods are applied and excavation is executed using a crane-mounted grab – long-reach excavators or air lifting pumps can also be used. In water-bearing strata where dewatering does not cause basal instability, but where sidewall stability is an issue, "dry caisson" methods are employed and a mechanical excavator may be used within the shaft (British Tunnelling Society and Institution of Civil Engineers, 2004). In either case, caisson sinking method features the following elements (Humes, 2012):

- In situ cast concrete collars – elements functioning as a guide ring to keep the caisson shaft vertical and in larger diameter shafts, acting a resistance element to the pressure from the hydraulic jacks;
- Hydraulic Jacks – are installed in order to steer and to add a vertical force to the ring's self-weight;
- Lubricant Fluid – the annulus between the shaft and the excavated ground should be filled with fluid (usually bentonite with additives) that acts as a lubricant;

- Bottom/choker ring – are designed to bolt the steel cutting edge to the shaft and provide perimeter between the shaft and excavated ground so that the fluid in the annulus above the ring is retained;
- All caisson units are provided with grout fittings allowing the exterior annulus to be filled with cementitious grout after installation.

Fig. 3.2 represents most of the elements mentioned above.

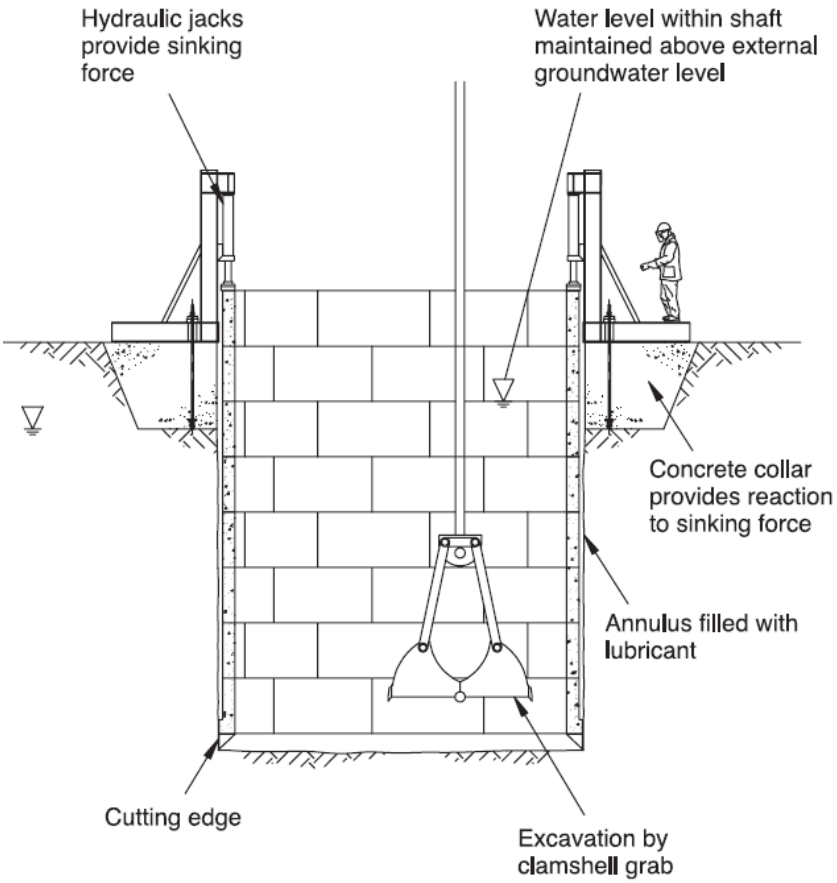

Fig. 3.2 – Elements features in the caisson sinking method, (British Tunnelling Society and Institution of Civil Engineers, 2004)

The installation process begins with the excavation of a circular area that is, at least, 0.8 m wider than the diameter of the shaft and a minimum 1.2 m deep, and positioning of the steel cutting edge on that area. Then, the bottom ring is installed on top of the cutting edge and the next ring is mounted on top of it. Next, a 50-60 mm thick polystyrene sheet is positioned surrounding the ring to create the annulus. The area between the completed bottom ring and the outer perimeter of the excavation is then filled with concrete to form the concrete collar, providing permanent support to the shaft excavation, lateral resistance to jacking forces and acting as a guide to shaft sinking. After the concrete collar has hardened the polystyrene can be dissolved using a chemical solvent. After the previous step, two more rings are built above ground level – it is important that one complete ring is always above ground, acting as a safety barrier during shaft construction. Then, the rings are sunk by excavation inside the shaft – if the soil is very soft the rings should sink under their own weight, otherwise pressure will need to be applied to the top ring using the hydraulic jacks. The grout socket assembly in each

segment can be used to introduce bentonite slurry into the annulus to lubricate and reduce ground friction while the rings are being pushed down. The process of excavating and building rings and pushing them down is repeated until the required depth is achieved. Finally, after completion of the shaft, the annulus is grouted from the bottom rings to the top (to avoid blocking the region) producing an intimate contact between the shaft and the ground. The steel cutting edge is lost at the end of the construction process.

Fig. 3.3 to Fig. 3.5 show a few steps described above.

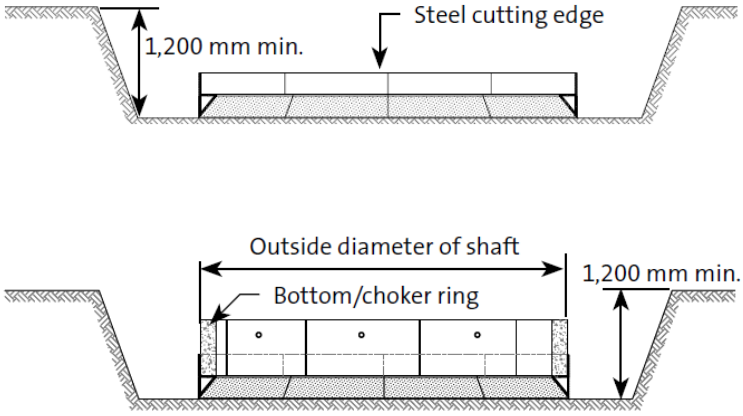

Fig. 3.3 – Caisson Sinking: excavation and positioning of cutting edge and bottom ring(Humes, 2012)

Fig. 3.4 – Caisson Sinking: Polystyrene surrounding the ring, (Humes, 2012)

Fig. 3.5 – Caisson Sinking: Ring being built on top of bottom ring, (Humes, 2012)

3.2.2. SEQUENTIAL EXCAVATION METHOD (SEM)

A shaft constructed employing a SEM is, basically, executed following a set of sequential steps of excavation/support application very similar to the principles of conventional tunnelling, being the main difference the construction's axis orientation. Therefore, this is a method where a relevant interaction exists between the excavated soil and the support, the latter being applied as soon as possible after excavation in order to maintain the soil resistance properties (Topa Gomes, 2008).

After soil treatment procedures and water level dropdown, the shaft construction begins with the large stiffness capping beam, an element that helps to control the beginning of excavation and offers a good resistance to the bending moments produced in the first few meters of construction. Despite the fact that shafts with circular section, or close to circular, are mainly subjected to hoop stresses, during the excavation of the first meters, bending moments assume a relevant role due to small deformations and loads that do not follow the axissymmetry of the shaft. Those loads may result from uneven positioning of materials and equipments at the worksite and even from the heterogeneity of the soil itself, hence the utility of a beam, stiffer than the general applied support to sustain those loads (Topa Gomes, 2008).

The construction proceeds with the excavation and application of support of the first ring. This process can either be done in the whole section or, for shafts presenting larger diameters, the work can be split into different segments, in some cases, occurring simultaneously. Fig. 3.6 and Fig. 3.7 show examples of these cases: the first from the geotechnical report from the case study at the MILE END circular shaft where the excavation was split into 4 sections; and the latter from an elliptical shaft executed for the construction of Salgueiros Metro Station in Porto referred to in Topa Gomes (2008), presenting 4 different excavation drives.

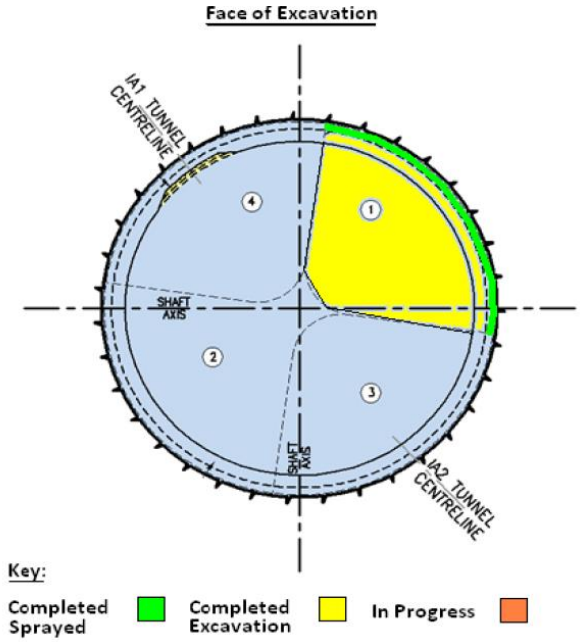

Fig. 3.6 - Excavation executed in different segments at MILE END, from Geotechnical Report

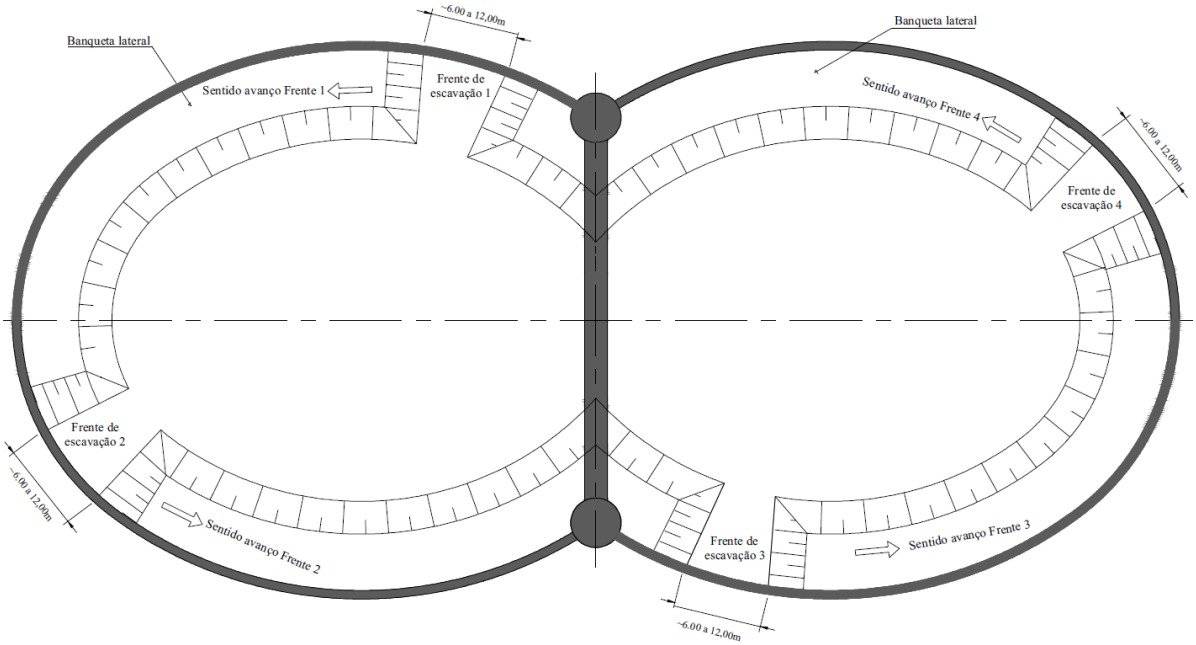

Fig. 3.7 - Excavation executed in different segments at Salgueiros Metro Station (Porto), (Topa Gomes, 2008)

The excavation height will depend on ground conditions, the shaft's cross section and even the necessity of limiting ground settlements and soil mass deformations on the excavated face. Nevertheless, the excavation depth for each ring should not be higher than around 2 m for practical purposes, both to avoid the ground movements mentioned before and regarding application of the shotcrete (also known as "sprayed concrete"), otherwise elevation mechanisms would have to be employed in the shaft for that purpose (Topa Gomes, 2008).

The employed support for these structures is usually shotcrete. Considering the circular shafts are mostly subjected to compressive stresses, concrete is generally a good option. However, the shotcrete can be combined either with steel reinforced fibres in its composition, or with steel reinforcements positioned on the face of excavation before spraying, for gaining resistance to loads of other nature. In both cases, the concrete should present good resistance properties during the first few hours after spraying so that further excavation can proceed within the shaft, so, the addition of additives on the concrete composition is advisable to accelerate its hardening (Topa Gomes, 2008).

The sequential steps of excavation-support are repeated until the required depth is achieved. In many cases, a secondary layer of shotcrete is applied on top of the first one, increasing the support stiffness and resistance. This second layer, usually cast in place with formwork, ensures the adequate durability of these structures.

The following Fig. 3.8 shows a scheme representing the excavation process and Fig. 3.9 a photo taken at the case study worksite showing the excavator and spraying equipment.

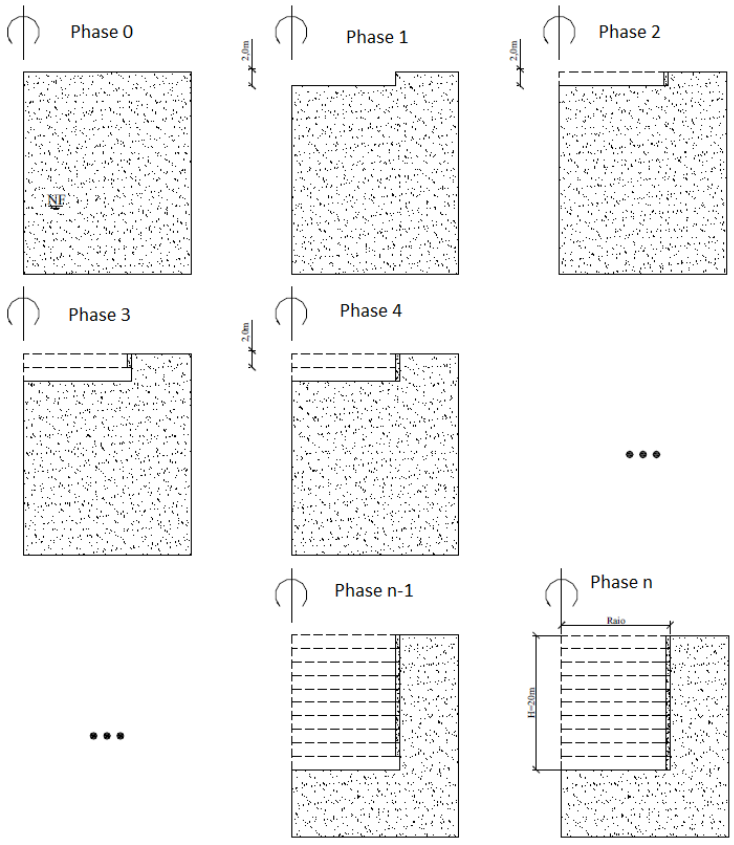

Fig. 3.8 – SEM: Sequential excavation-support steps (adapted from Topa Gomes (2008))

Fig. 3.9 – SEM: Application of shotcrete at the case study worksite, (photo from Progress Report)

Lowering the water level, if required, is an essential step before excavation proceeds to guarantee stability of the vertical excavated face, decreasing the hydrostatic loading on the primary lining support, avoiding rupture of the shaft base and water inflow. Some techniques to perform this step are the following:

- Auxiliary wells surrounding the shaft for cohesionless soils with relatively high permeability;
- As for cohesive soils with low permeability, the lowering of water table might not be mandatory, but the use of radial geo-drains installed perpendicularly to the shaft's vertical face is advisable for decreasing the hydrostatic load on the primary support;
- For heterogeneous soil masses where, for instance, a cohesionless and high permeability layer is located between two other "non-critical" layers (with higher cohesion and lower permeability) vacuum pumps can be employed for targeting a specific region to execute the water table dropdown (Campanhã, França, 2008)

3.3. PHENOMENOLOGY AND BEHAVIOUR OF SHAFTS DURING CONSTRUCTION

As mentioned in sub-chapter 3.1, shafts are structures that provide essential functions during most underground works. However, for large diameters shafts, the bibliographic references about their behaviour during construction are not much extensive

In order to study the behaviour and phenomenology of these structures, Topa Gomes (2008) worked on a numerical model of a shaft using a finite element analysis (FEM) software – *CODE_BRIGHT* (developed by the Ground, Cartography and Geophysics Engineering Department at Technical University of Catalonia) – where the sequential excavation-support process was simulated and, support/ground deformations and stresses were registered. In this model the shaft presents a circular section – allowing to perform an axisymmetric analysis – is excavated within the same soil layer, whose properties remain constant in its full depth (25m) and overlays in a ten times stiffer soil mass. Each ring was excavated in 2m lifts, making a total of 21 steps (counting with the in situ stage) and the support's thickness was constant in the shaft's full depth (0.30m) – this and other characteristics of the model can be observed in Fig. 3.10. The failure criterion used for this analysis was Mohr-Coloumb, the unit weight of the soil involving the shaft was assumed to be 18.2 kN/m^3, the shotcrete stiffness was 30 GPa and the water level was below the shaft's base. As for the finite element mesh employed, triangular elements with 1 Gaussian point were used across the model with the exception of the support and surrounding area with quadrilateral elements with 4 Gaussian points.

According to Topa Gomes (2008), the simplicity and theoretical approach of this model had the purpose to fully understand and register the shaft behaviour and the influence of certain parameters on the latter. Topa Gomes (2008) presents a thorough and extended work about the large diameter shaft behaviour and so, the following sections of this sub-chapter will only briefly present and comment some of those results obtained from that author's work. First, in 3.3.1 the behaviour of soil will be discussed regarding deformations and stress variations. Then, in 3.3.2, deformations and internal forces from the support and their variation in depth will be presented and following section 3.3.3 will discuss the variation of some geotechnical and support parameters and its influence in the structure. In the last section 3.3.4, a non-saturated situation will be considered. Note that these parametric studies are all based on the model represented in Fig. 3.10.

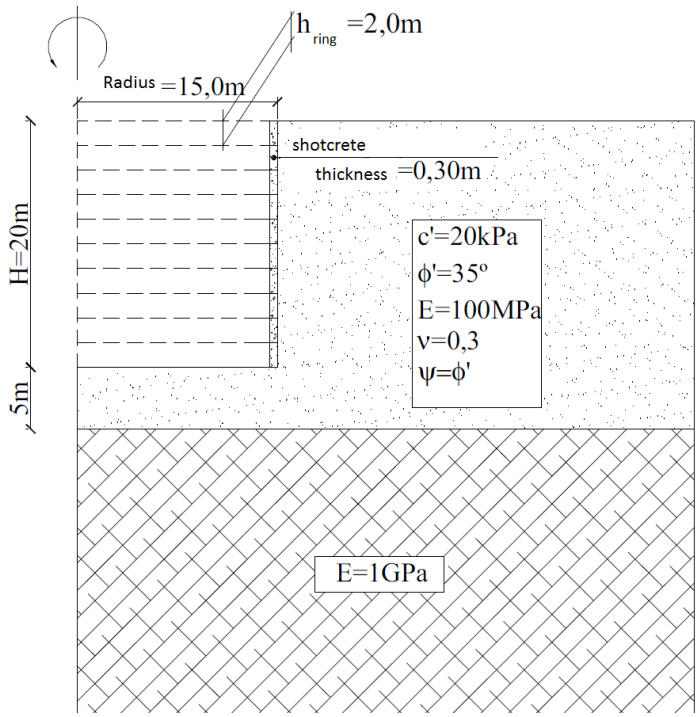

Fig. 3.10 – Shaft model used by Topa Gomes (2008) in *CODE_BRIGHT* (adapted from Topa Gomes (2008))

3.3.1. General Behaviour of Soil Mass

In this section, the deformations within the soil mass and stress variations in depth will be discussed. The discussion will not concern the actual values obtained (minima/maxima), but what they represent in the structure's typical behaviour.

3.3.1.1. Deformations and Displacements

The following Fig. 3.11 and Fig. 3.12 show the contour plot obtained from *CODE_BRIGHT* for horizontal and vertical deformations, respectively. It is clear the soil tends to move, horizontally, towards the excavation and its base moves vertically upwards.

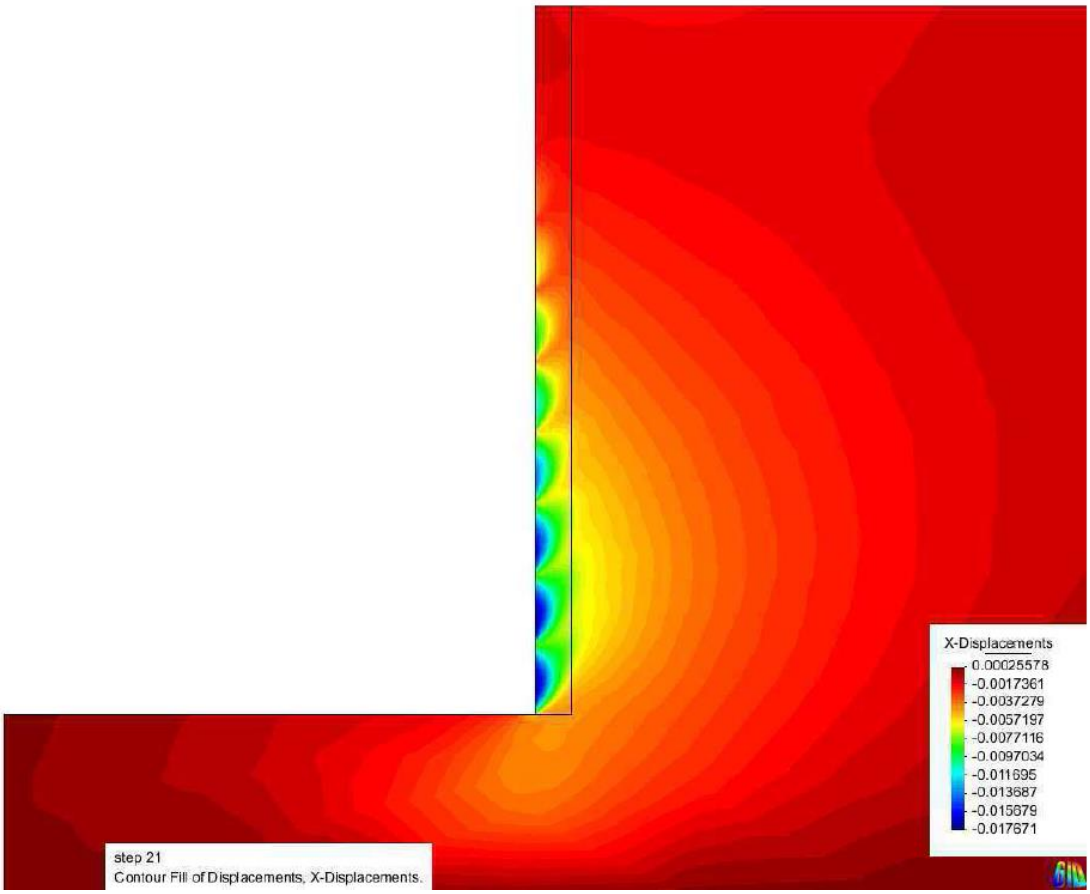

Fig. 3.11 – CODE_BRIGHT: Horizontal soil deformations [m] (Topa Gomes, 2008)

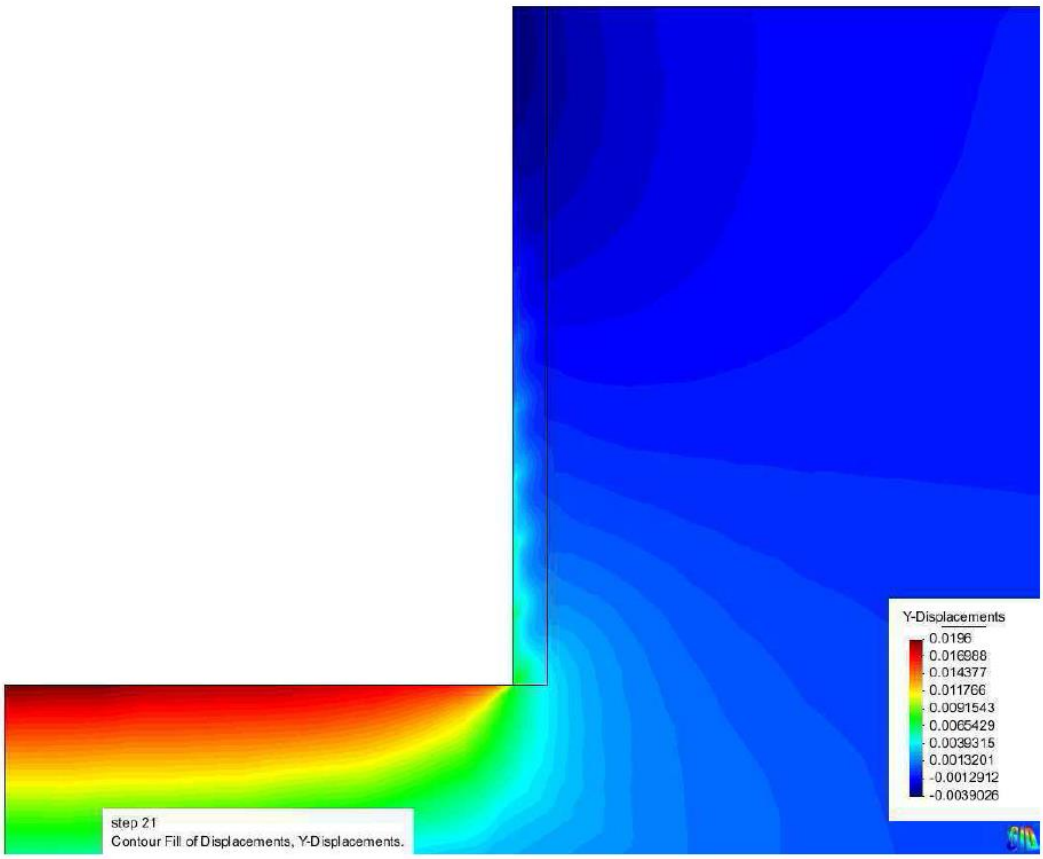

Fig. 3.12 - CODE_BRIGHT: Vertical soil deformations [m] (Topa Gomes, 2008)

As for the horizontal displacements, there is a growth of value in depth, mostly enhanced by soil's homogeneity chosen for this model. Fig. 3.11 already shows this behaviour if looking at the increasing area of the "coldest" colours for higher depths. For a better approach in the analysis of this behaviour, Topa Gomes (2008) presented a series of graphs for each ring excavation relating depth with horizontal displacement of soil behind the support – see Fig. 3.13. From that figure, the increase in horizontal displacements in depth is now clearer. Since for higher depths the stresses in soil are higher, the extraction of soil mass will reflect as a relatively higher unloading, causing, then, higher horizontal deformations, that is why in Fig. 3.13 the maximum value (approximately 1.8 cm) is located close to the base at around 17m in depth.

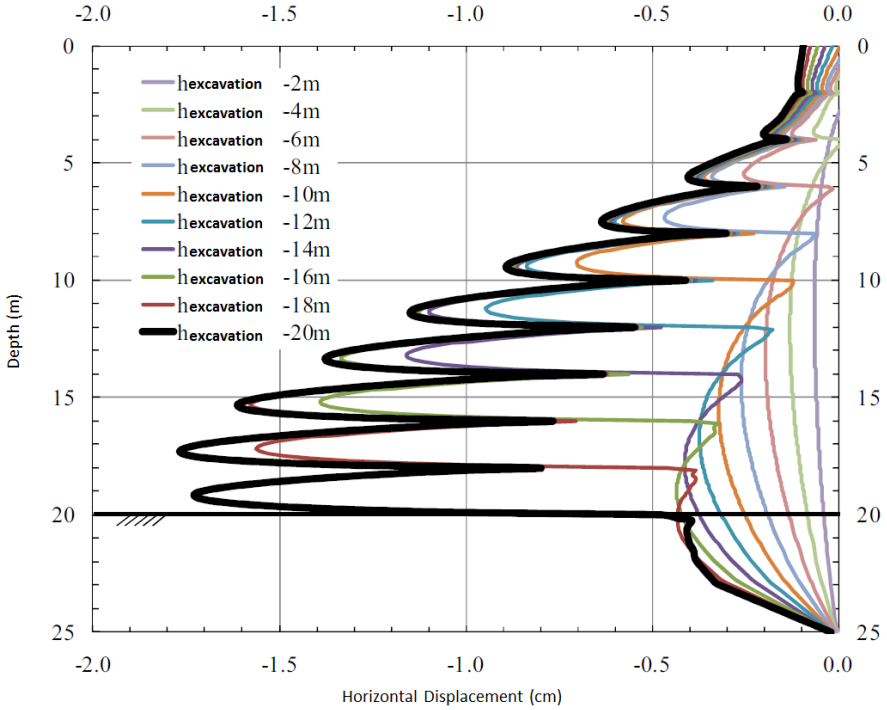

Fig. 3.13 - Effect of ring excavation on horizontal displacements with depth (adapted from Topa Gomes (2008))

Other evident phenomenon is the local variation of these deformations within the excavation of each ring, where the maximum is reached around its middle height. This effect can be explained by the fact that when a ring is excavated the open panel is only supported by the shotcrete, on the panel above, and the soil mass at the shaft's base, allowing the soil in the middle part to produce higher displacements. Fig. 3.14 shows this local effect in more detail with a graph reflecting the excavation evolution of a ring and relating it with horizontal deformations. In that figure, the ring located between 10 and 12m in depth had its mid-point (11m) and lower point (12m) analysed in terms of total and incremental displacements. Analysing the total displacements line for the point at 11m one can comment the following:

- First, as the excavation proceeds from 4 to 1 ring above that point, i.e., when the point is located below the base, the horizontal displacements tend to increase slowly. As the above panels are opened, there is an arching effect of stresses, distributing them to the support above the open panels and the soil at the excavation base, producing those slight horizontal deformations;
- Then, during the excavation of the analysed panel, the mid-point is completely exposed, producing, according to Topa Gomes (2008), around 70% of its total displacements in this case;

As for the point at 12m depth, it also shows the same slight increase of horizontal displacements when excavating the upper rings – actually, at this stage the growth is relatively higher than the mid-point due to a higher stress transfer to the soil towards the base. However, differently from the mid-point, during the 10-12m depth panel excavation, this point is at the frontier of the excavation base, and for the next panel opening, it has a support applied already. Therefore, the increase of the horizontal displacement is not so pronounced as the mid-point during the 10-12m

panel excavation, since it always presents some kind of "support". Nevertheless, 40% of the total displacements occur during that panel's opening (Topa Gomes, 2008).

Still, regarding Fig. 3.14, it is noticed for both points, the values of horizontal displacement stabilize after the excavation of the third ring below, which shows how localized the behaviour of shafts regarding this displacements is. Whereas in tunnels, the deformations at some point would still be influenced while excavating on further distances.

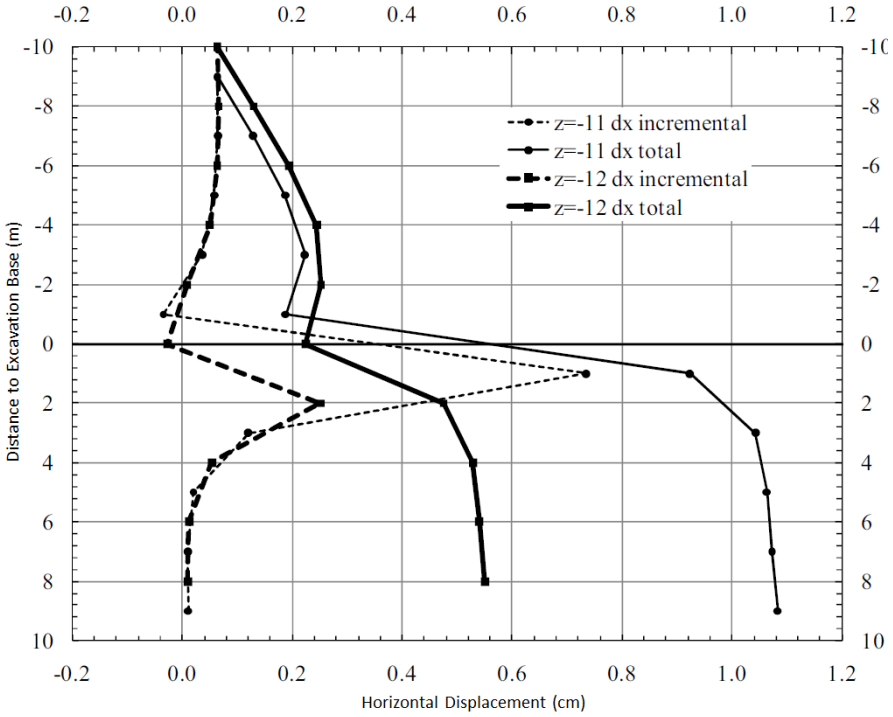

Fig. 3.14 – Horizontal displacements evolution with distance to excavation base (adapted from Topa Gomes (2008))

As it was mentioned above, while excavating a ring, at the open panel there is an arching effect that transfers stresses towards stiffer elements, which in these structures would be the shotcrete on the panel above and the soil itself on the base. This distribution towards the base makes the soil to behave similar to a compressed beam. Fig. 3.15 shows the generated incremental vectors for the last excavation step where it can be seen the upward movement at the base as it had been firstly seen in Fig. 3.12.

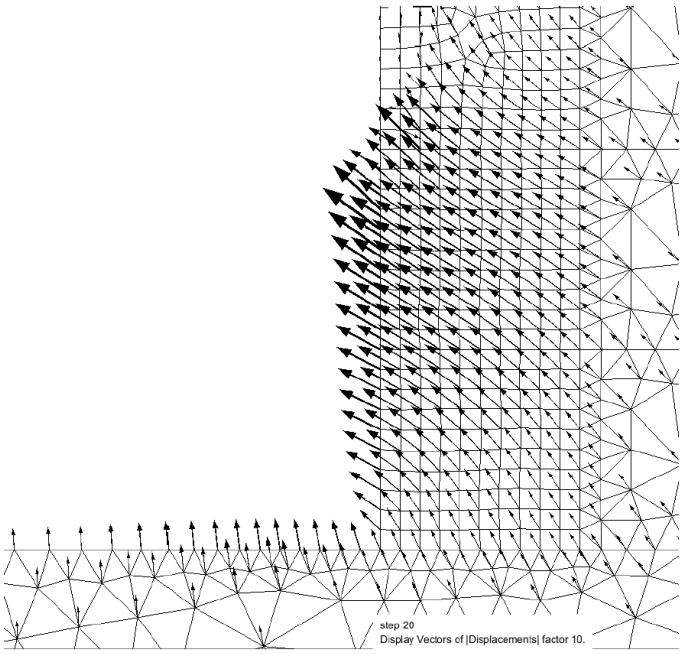

Fig. 3.15 – CODE_BRIGHT: Incremental Displacement vectors at final excavation phase (Topa Gomes, 2008)

The values obtained for displacements (vertical and horizontal) at ground level are represented in Fig. 3.16, varying with the distance from the support. Analysing the behaviour of the horizontal displacements, one can say it is similar to earth retaining structures: the maximum appears from 3m from the support, it is not a very pronounced value and from that point it decreases. As for the ground settlements, there is a maximum located just behind the support, and from that point until around 15 m there is a sudden variation of values. Further than 1 diameter (around 15 m) away from the support that variation is smoother. However, Topa Gomes (2008) warns that, for obtaining more realistic curves for ground settlements, a model that varies the deformability modulus in depth should be employed; otherwise, the points near the surface would present a higher stiffness that does not correspond to reality.

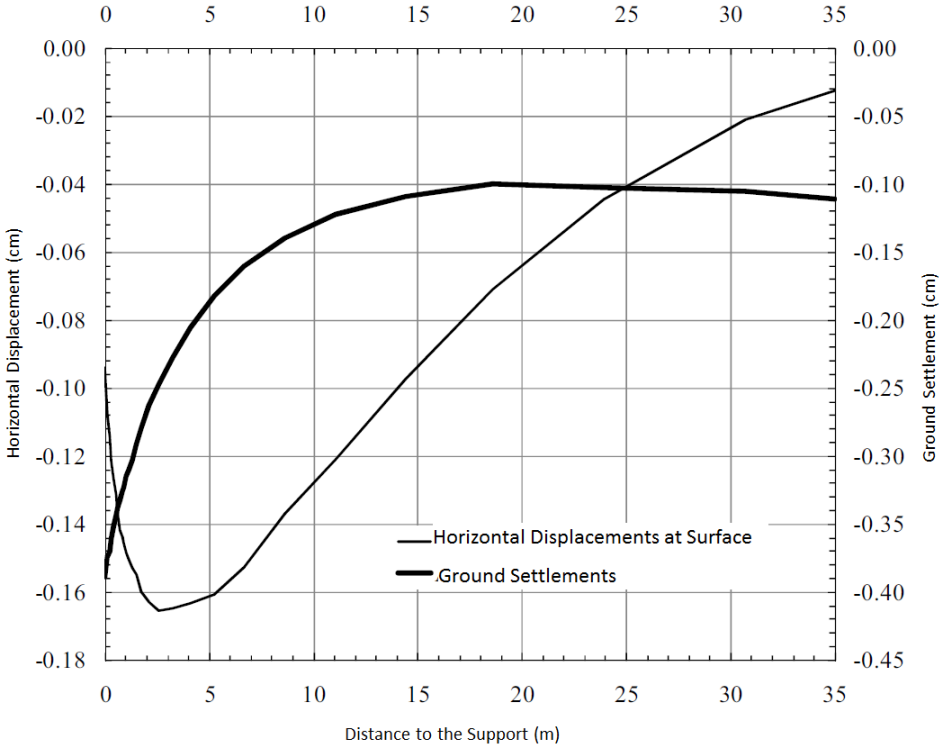

Fig. 3.16 – Displacements at ground level (adapted from Topa Gomes (2008))

3.3.1.2. Stress Variations During Excavation

The previous section focused only on the soil displacements, while the present section will approach the variations in stress during different stages of the shaft construction. Fig. 3.17 and Fig. 3.18 show the contour plot for effective horizontal and vertical stresses, respectively, for the last construction step and, as it was discussed for deformations, the biggest variations also occur quite near the excavation face. For distances of around 15 m from the support, is noticed that, for those two figures, the stresses already show to be very close to the in situ stresses.

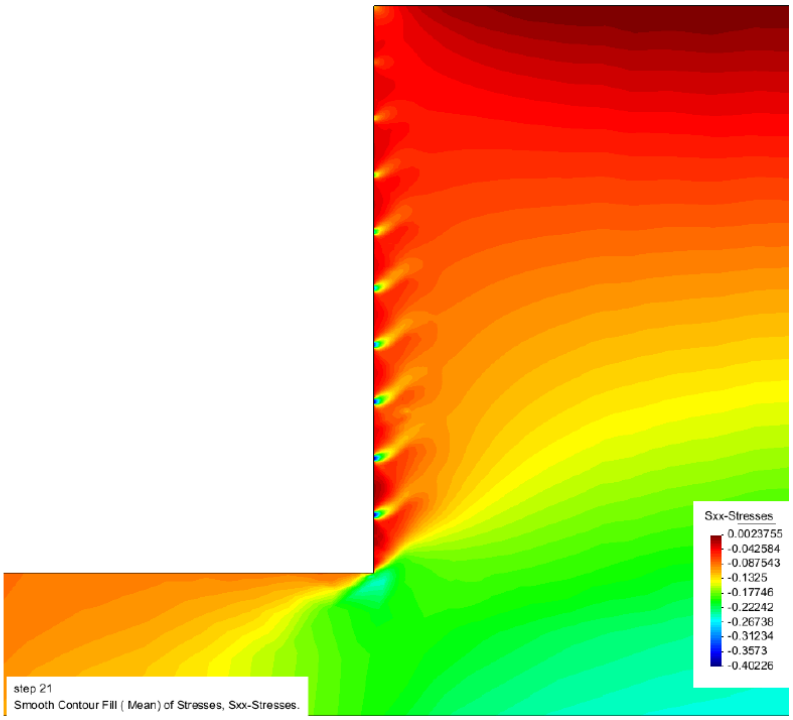

Fig. 3.17 – CODE_BRIGHT: Horizontal effective stresses [MPa] counter plot (Topa Gomes, 2008)

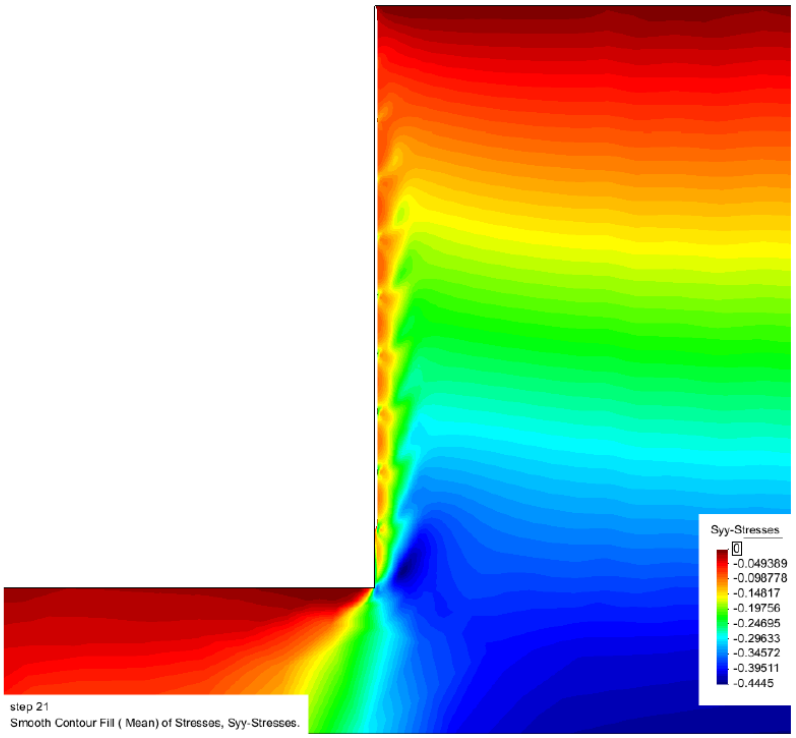

Fig. 3.18 – CODE_BRIGHT: Vertical effective stresses [MPa] counter plot (Topa Gomes, 2008)

The horizontal effective stresses in Fig. 3.17 show small regions within each ring where the values are considerably higher than the rest of the panel. This behaviour is discussed in detail in Fig. 3.19 where different lines representing the horizontal effective stress variation in depth for different distances

from the support are presented. The stress lines for the situation at rest ($K_0\gamma H$) and "limit" active state ($K_a\gamma H$) are also shown in that figure.

From Fig. 3.19, for the line representing the points just behind the support, it is interesting to notice that the "peak" stresses are located in the boundary points of the support applied in each ring, while lower values are for the points within each panel – representing, in a way, a "stress relief" for the unsupported region of the ring. This alternation between peaks and lower values clearly shows that arching effect already mentioned above, where, during the excavation of a ring, the stresses are transferred to stiffer elements. In addition, for that same line, it is important to mention that the lower values of effective horizontal stress tend to approximate to active state line ($K_a\gamma H$) - which justifies the deformations that occur for the unsupported points at the excavation face – while the peaks are higher than the stresses at rest state ($K_0\gamma H$), for the same reason. However, from a certain depth, the lower values are actually lower than the active state line and Topa Gomes (2008) justifies it by the fact that this line does not take into account the soil cohesion – a more developed explanation regarding this effect can be found in his work.

As for the other lines also in Fig. 3.19, represent the horizontal stresses for the distances of 2, 5 and 15 m from the support. What that figure shows is that, for higher distances there is a gradual approximation to the rest state line which, once again, reflects the idea that for a distance of around 15 m (equivalent to the shaft's radius – "1R") horizontal stresses remain practically "unchanged" from the state at rest, before construction.

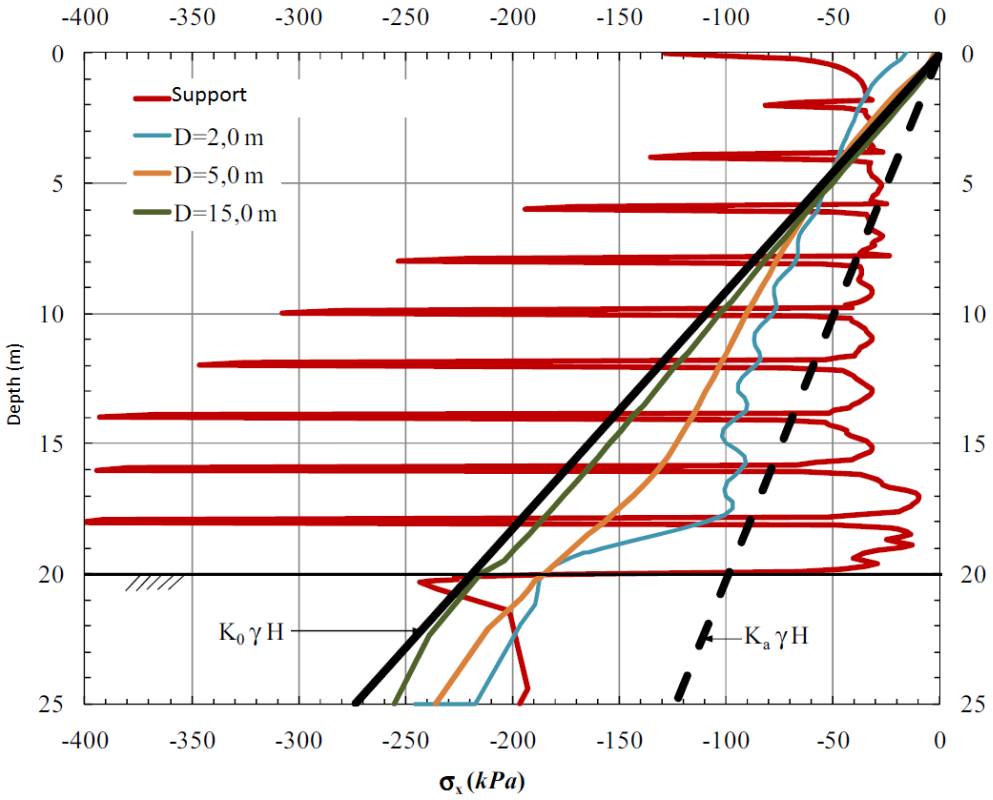

Fig. 3.19 – Evolution of horizontal stresses (σ_x) in depth for different distances from the support (adapted from Topa Gomes (2008))

A similar analysis was done in Fig. 3.20 for the vertical stresses, where the line for values at rest state is also represented (γH). Considering the distances from the support, the behaviour is quite similar to the one shown in Fig. 3.19, where for 1R distance the stress values are very close to at rest state and for the lower distance from the support, the line also presents a maximum-minimum peak variation but, with less impact than for horizontal stresses, though. A thorough analysis regarding stress variation can be found in the work of Topa Gomes (2008).

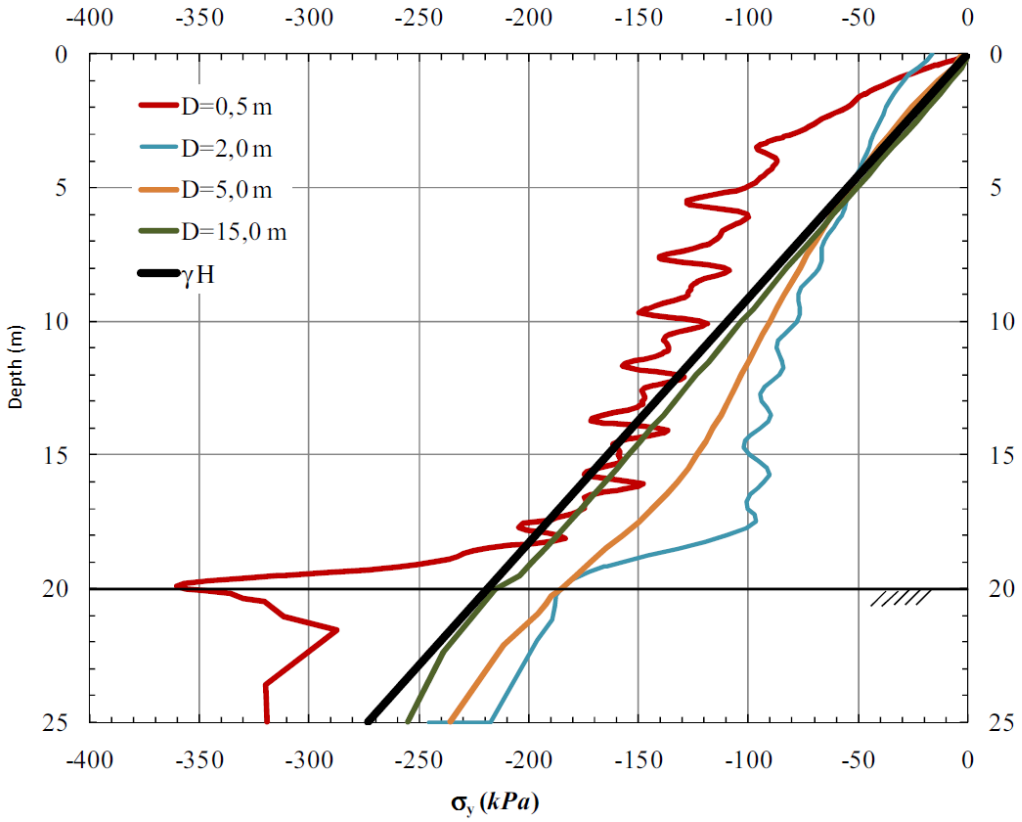

Fig. 3.20 – Evolution of vertical stresses σ_y in depth for different distances from the support (adapted from Topa Gomes (2008))

3.3.2. General Behaviour of Support

Section 3.3.1 discussed only the behaviour of the soil, its deformations and stress variations and the present will focus on the applied support where its displacements and internal forces will be briefly discussed.

Fig. 3.21 shows the variation in depth of the displacements registered on the concrete ring after its application on the excavation face. The first thing one can notice is the relatively lower magnitude of displacements comparing with Fig. 3.13, which means most of the horizontal displacements, in a shaft construction occur while the ring is unsupported – the higher value is just around 3.8 mm. These low values for displacements in the support can be explained by the structure high stiffness given by its axissymmetry and high hoop stiffness.

On Fig. 3.21, the line representing the displacements in depth presents a variation between peaks within each panel. For deeper rings, the maximum peaks tend to increase (effect, which is enhanced due to the homogeneity of the soil), while the minimum remain almost constant. This latter behaviour occurs due to the fact the arching effect in stresses is very localized and so, in each excavated ring the stresses are mostly transferred to the lower part of the support above the opened panel. This will be reflected in the hoop stresses, whose variation in depth presents a similar behaviour to deformations.

The first ring, between ground level and 2 m depth, is the only one, which does not follow the behaviour of all the others, mostly because, after the excavation of next ring, the arching effect has a relatively higher impact on the above support, since it's the only existing in the shaft by that time.

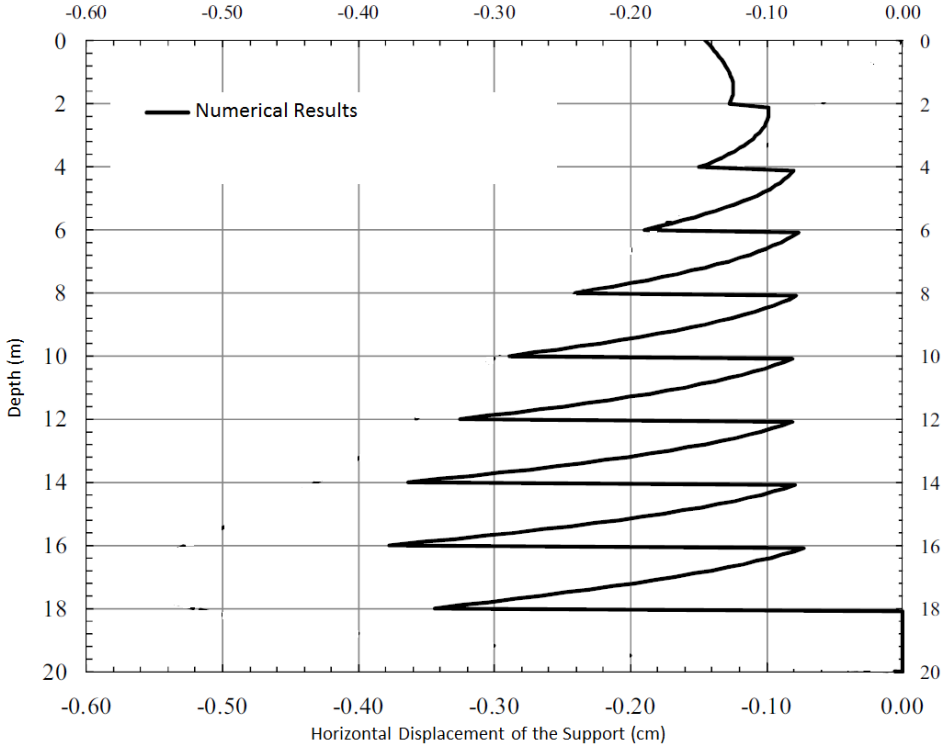

Fig. 3.21 – Variation in depth of the horizontal displacement of the support (adapted from Topa Gomes (2008))

Fig. 3.22, Fig. 3.23 and Fig. 3.24 show the variation in depth of the internal forces in the structure – hoop forces (N), vertical bending moments (M) and shear forces (T), respectively.

As already mentioned, the line representing the hoop forces in Fig. 3.22 is similar to the one that shows the deformations, with lower and almost constant values at the top of each concrete panel and peak values at the bottom. All the justifications mentioned for Fig. 3.21 apply also for the hoop forces. According to Topa Gomes (2008), the maximum value is 2451 kN.m/m at 16 m depth, which corresponds, considering the 30 cm thickness of the support, a compression of around 8.2 MPa.

As for bending moments, the variation in depth shows a clear increase for deeper rings, although within each ring, there is a peak value around their mid-height and relatively lower values at bottom level. At the bottom of each shotcrete ring, the circumferential stiffness is higher than the flexural stiffness, leading to an increase of hoop forces and a decrease of bending moments. Fig. 3.22 can actually be used to complement the analysis of Fig. 3.23, where at the bottom of each ring, every peak in hoop forces corresponds to a relatively lower value of bending moment. The maximum value is also reached at the ring between 14-16 m depth, as noticed for hoop forces.

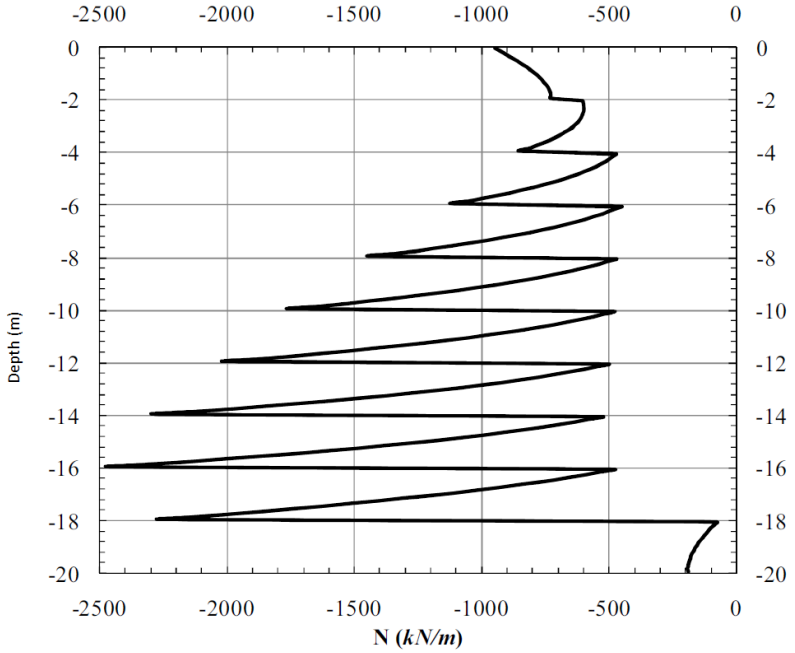

Fig. 3.22 – Hoop forces variation in depth (adapted from Topa Gomes (2008))[1]

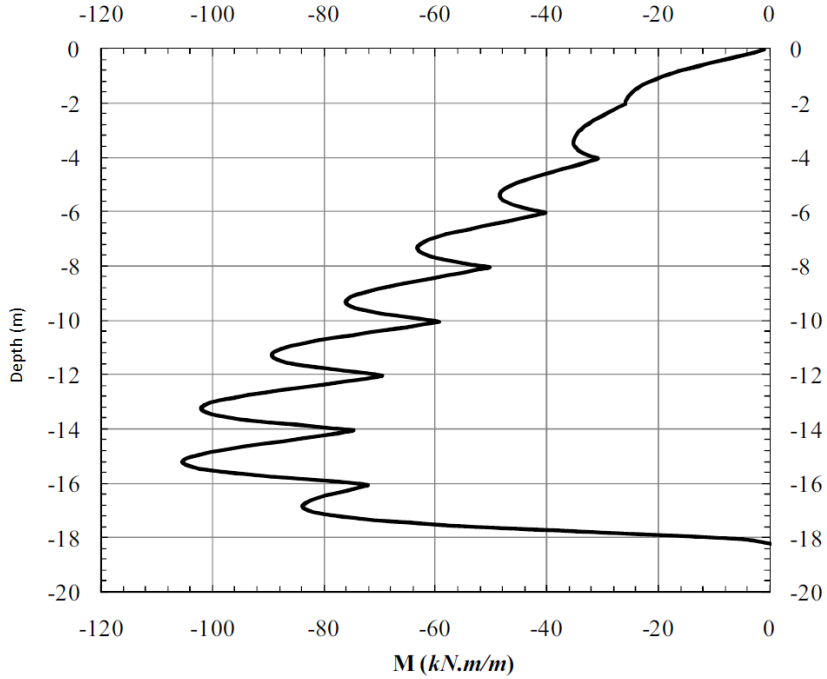

Fig. 3.23 – Bending Moments variation in depth (adapted from Topa Gomes (2008))

The shear force variation in depth is represented in Fig. 3.24, showing within each ring a variation between minimum and maximum peaks at the top and bottom level, respectively, where the second increases in depth. Once again, this is explained by the local arching effect: when a ring is excavated and unsupported the stresses tend to transfer to the supported panel above, mostly at his bottom.

[1] Note that compression was considered for negative values.

Contrarily to the other two cases, shear force reaches its maximum value at the bottom of the 16-18 m depth panel, and this value is actually quite higher, considering the almost constant growth of maximum peaks in depth. Let's say panel "X" is being analysed and is located at the shaft's final mid-depth. When "X" is excavated produces a stress distribution that leads to increase of shear forces at the above supported panel, mostly at its bottom. After the application of support in X, and excavation-support application of the ring just below, there's now a certain continuity of the support from the top of "X" until the below panel (at the shaft's base), and this continuity produces a redistribution in horizontal stresses from the support above "X", to "X" itself. This being said, it is now clear why there's such a pronounced shear force at the bottom of the 16-18 m depth panel. If the excavation-support application had proceeded to a new ring at 20-22 m depth, this maximum at -18 m would had been decreased, and would be distributed at the -20 m level as the new maximum.

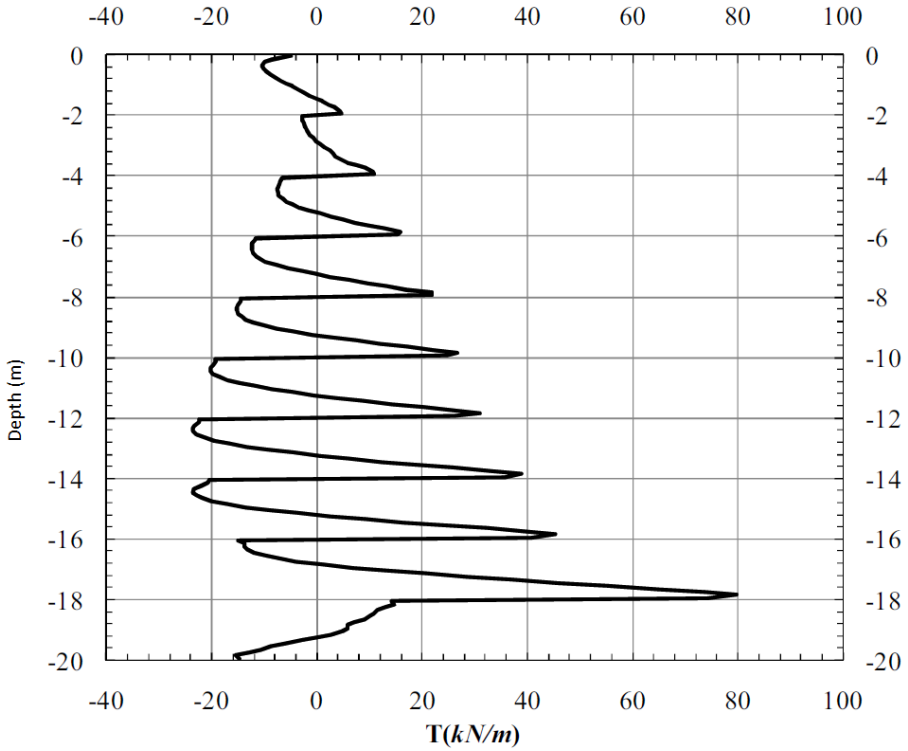

Fig. 3.24 – Shear forces variation in depth (adapted from Topa Gomes (2008))

3.3.3. PARAMETRIC STUDY

In his work, Topa Gomes (2008) presents an extended and thorough parametric study concerning the excavation geometry, support characteristics and strength and deformation parameters for the ground. All these parametric studies are based on the model discussed above and their results compared to the case presented in Fig. 3.10. Based on the work of Topa Gomes (2008), this section will focus only briefly on the parameters that can show variability in the case study, with the exception of the shotcrete layer thickness. Therefore, variations such as shaft's radius, depth and excavation height will be omitted, since those are constants for the analysed problem in Chapter 5. The points studied on this section are listed in Table 3.1. In each point the basic analysis will be used as comparison reference for internal forces and horizontal displacements just behind the support.

Table 3.1 – Parameters analysed

Group	Parameter	Variation Values
Support characteristics	t –Thickness	0.20, 0.30, 0.40, 0.50, 0.60 [m]
	E – Young's modulus	15, 20, 30 [GPa]
Soil resistance parameters	c' – Effective cohesion	10, 20, 50, 100, 500 [kPa]
	ϕ' – Friction angle	25, 30, 35, 40, 45 [º]
	K_0 – Coefficient of earth pressure at rest	0.4, 0.5, 0.6, 0.8, 1.0
Soil deformation parameters	E – Young's modulus	25, 50, 100, 200, 500 [MPa]
	ν – Poisson's coefficient	0.20, 0.30, 0.40, 0.49
	ψ – Dilation angle	0, 1/3ϕ', 2/3ϕ', ϕ' [º]

3.3.3.1. SUPPORT CHARACTERISTICS (T, E)

3.3.3.1.1. THICKNESS VARIATION

To study the impact the support's thickness had on the shaft's final deformations and internal forces, Topa Gomes (2008) studied the variation for 20, 30, 40, 50 and 60 cm. Since it is known, a high percentage of the final deformations occurs while the open panel is unsupported, increasing the support's thickness will not produce relevant changes in values. As for internal forces, however, the increase in thickness will obviously lead to an increase of circumferential and flexural stiffness, and this will reflect in higher values for internal forces.

Fig. 3.25 and Fig. 3.26 show the final horizontal deformations and internal forces considering the thickness variation. These two figures validate the comments made above:

- First in Fig. 3.25 there's a general decrease of horizontal displacements for bigger thicknesses. Changing the thickness from 20 to 60cm the maximum horizontal displacement drops only from 19 to 16 mm (a decrease of 15%). This clearly shows that increasing the thickness of the support shouldn't be a measure to contain deformations, but to sustain higher stresses.
- Then, in Fig. 3.26 there's an increase for all the analysed internal forces with greater relevance to the bending moments, where its maximum value gets almost 10 times bigger, when changing from the lowest to the highest thickness. Topa Gomes (2008) stated that while the hoop forces increase is directly proportional to thickness variation, bending moments increase is sensitively proportional to the thickness powered by 2, which explains such difference in results when varying this parameter.

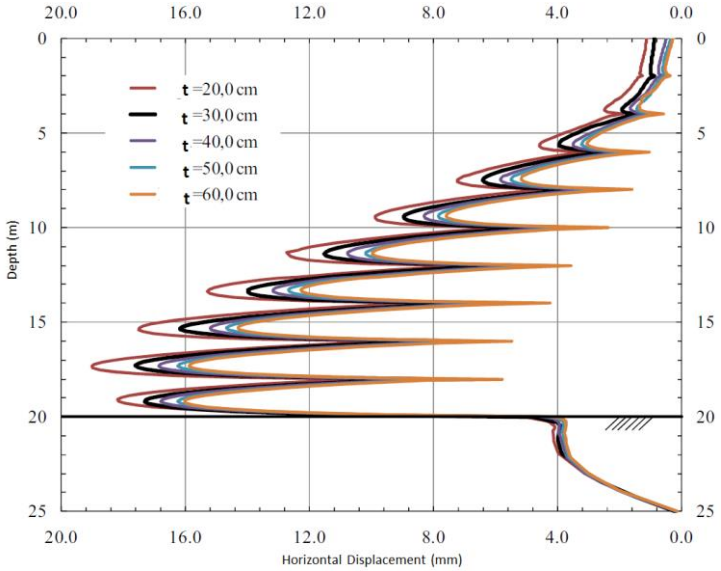

Fig. 3.25 – Thickness variation in the support: Horizontal displacements variation in depth (adapted from Topa Gomes (2008))

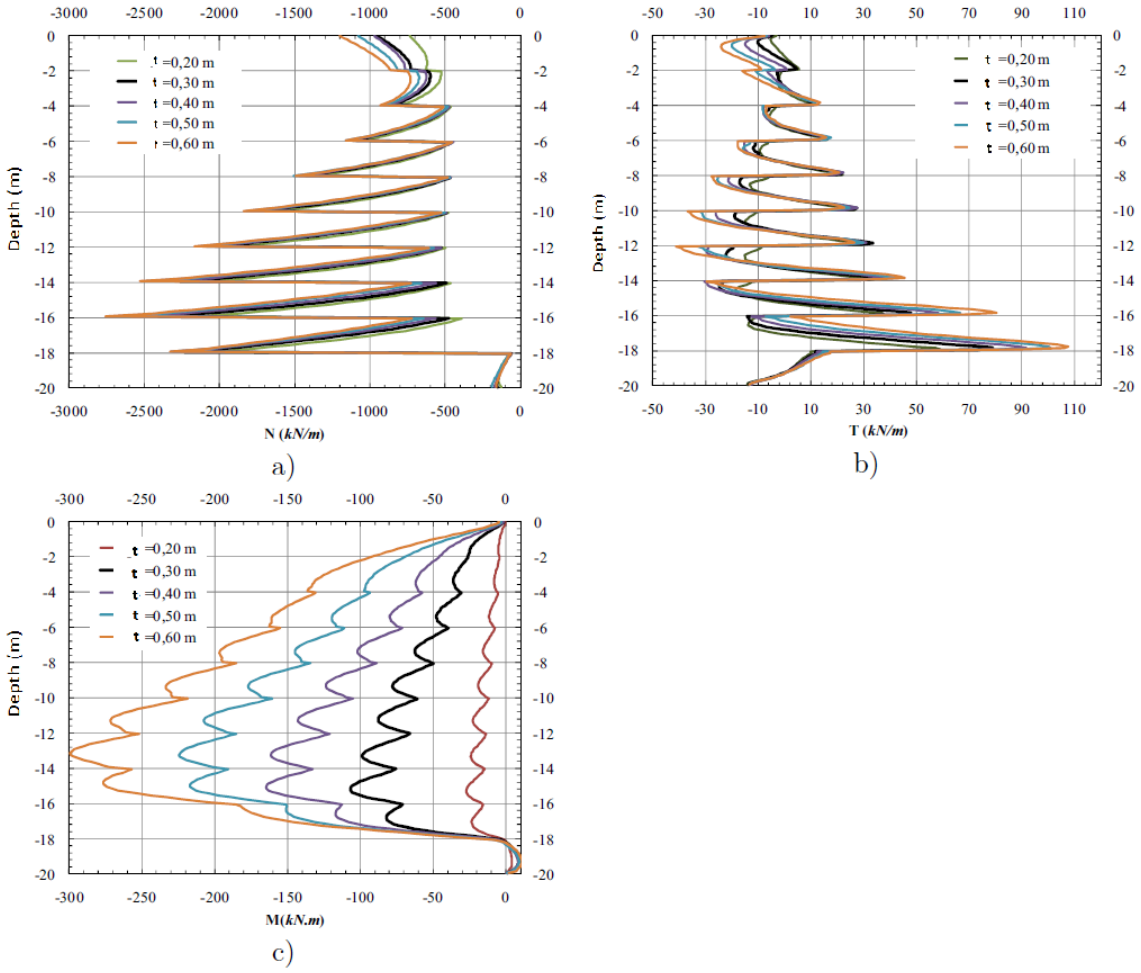

Fig. 3.26 – Thickness variation in the support: Variation in depth of: a) Hoop forces; b) Shear forces; c) Bending moments; (adapted from Topa Gomes (2008))

3.3.3.1.2. YOUNG'S MODULUS VARIATION - E

The Young's modulus of the shotcrete was also an object of this parametric study, considering cases for 15, 20 and 30 GPa. However, changing this parameter wouldn't produce many differences in behaviour from changing the support's thickness, since both procedures converge on the same idea, which is the increase of the structural stiffness. Therefore, Fig. 3.27 shows just a slight decrease of horizontal displacements (20mm to around 17mm) when changing from 15GPa to 30GPa. Concerning the internal forces, Fig. 3. 28, enhances the idea that varying the support's stiffness, the bending moments are the ones to suffer the higher variation, around 30%, while the shear force and hoop force around 20%, according to Topa Gomes (2008).

Sprayed concrete is a material whose resistance presents a time-dependent behaviour and, since the time it is sprayed on the open panels, it starts being loaded. Therefore, assuming a constant value for E, is not quite accurate to study the shaft's behaviour while varying this parameter. This issue will be a subjected to discussion on section 3.3.4 and analysed in Chapter 5. In order to have this effect into account, it is common in geotechnical engineering practice to assume half the value of E provided in current design codes. However, assuming lower values for E, leads to a reduction in the obtained stresses on the structural elements, making it a non-safe measure and so this practical method should be used carefully (Topa Gomes, 2008).

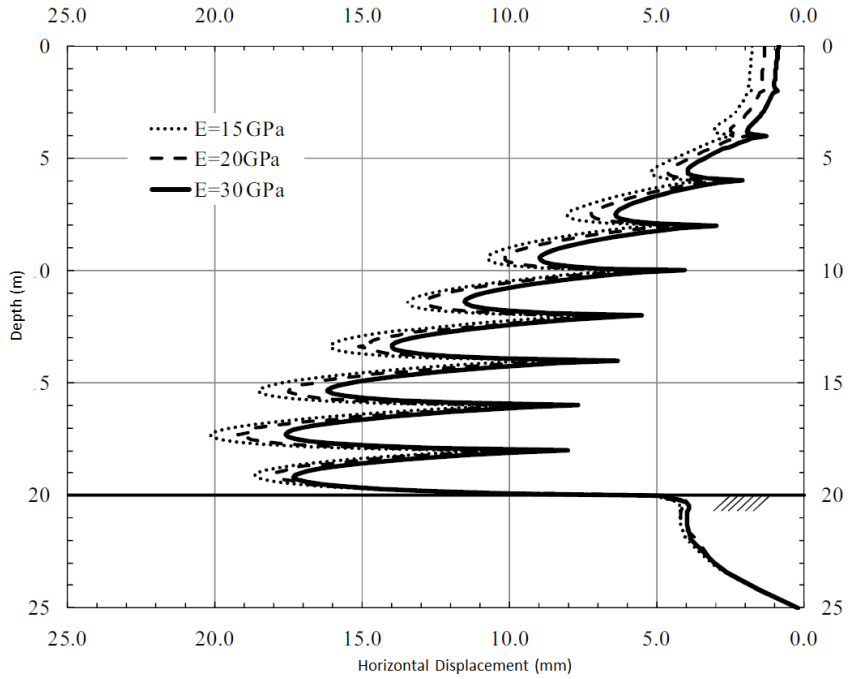

Fig. 3.27 – Young's Modulus variation in the support: Horizontal displacements variation in depth (adapted from Topa Gomes (2008))

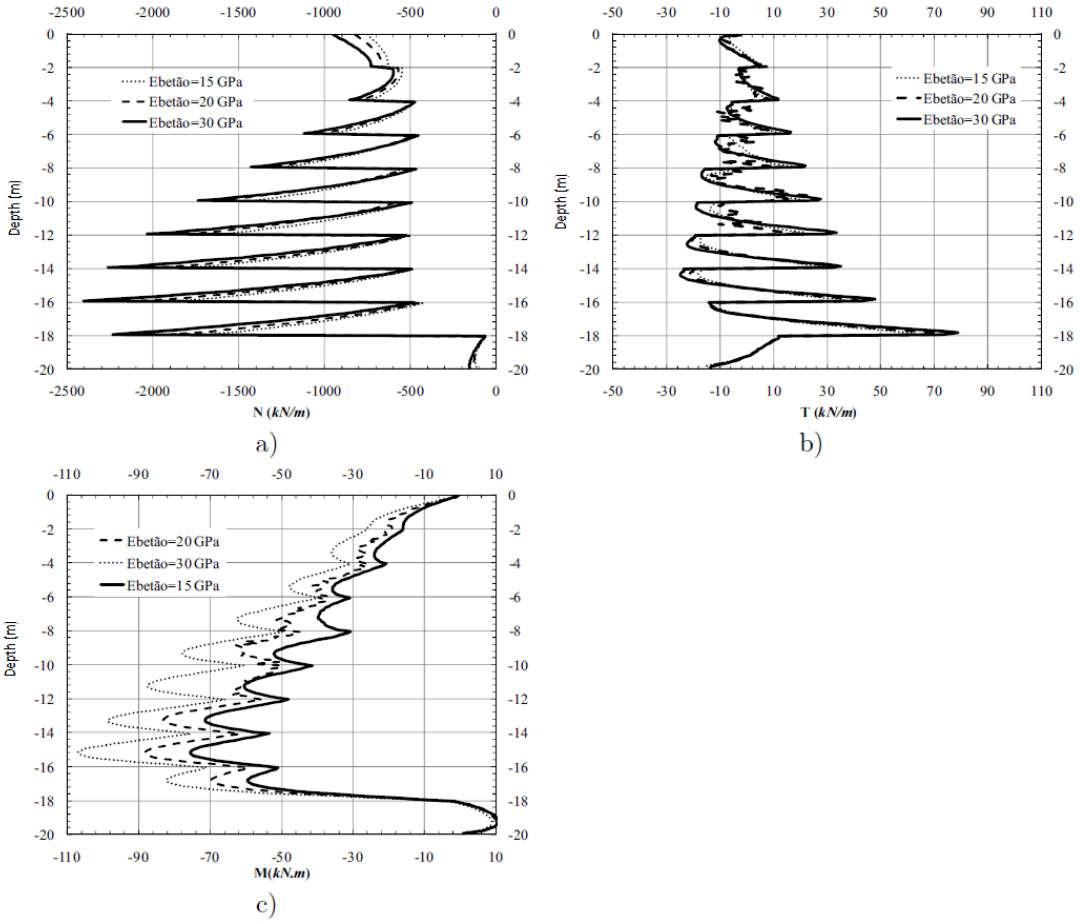

Fig. 3. 28 - Young's Modulus variation in the support: Variation in depth of: a) Hoop forces; b) Shear forces; c) Bending moments; (adapted from Topa Gomes (2008))

3.3.3.2. Soil Resistance Parameters

3.3.3.2.1. Cohesion – C'

In this point, the cohesion of soil was studied and compared for the values of 10, 20, 50, 100 and 500kPa.

When the soil is removed the horizontal stresses become null and the vertical remain almost constant, making those regions near the excavated face to surpass the yield surface and produce relevant plastic deformations. Then, vertical stresses are redistributed and decrease in value, making the points in those areas near the excavation face to turn back on their stress paths and "stay" on the yield limit. Having said this, it is clear now cohesion is going to be an essential parameter that can control directly those plastic deformations and the extension of area that suffer those deformations. In fact, soils whose particles interaction is merely frictional, with practically null cohesion, make impossible the construction of these structures when using a sequential excavation method.

Analysing Fig. 3.29, one can notice that when varying cohesion between the extreme values, the maximum displacement decreases for a bit less than half (from 20mm to around 8mm), which shows

the importance of cohesion discussed previously. In addition, every curve in that figure shows that only at each ring's mid-point, there are relevant variations in results, while at the top and below boundaries, the values are very similar from each other, which reveals how local the impact in varying cohesion is. This phenomenon is logical, considering that the upper and lower points in each panel are already supported either by the ground at the base or the shotcrete of the previous ring.

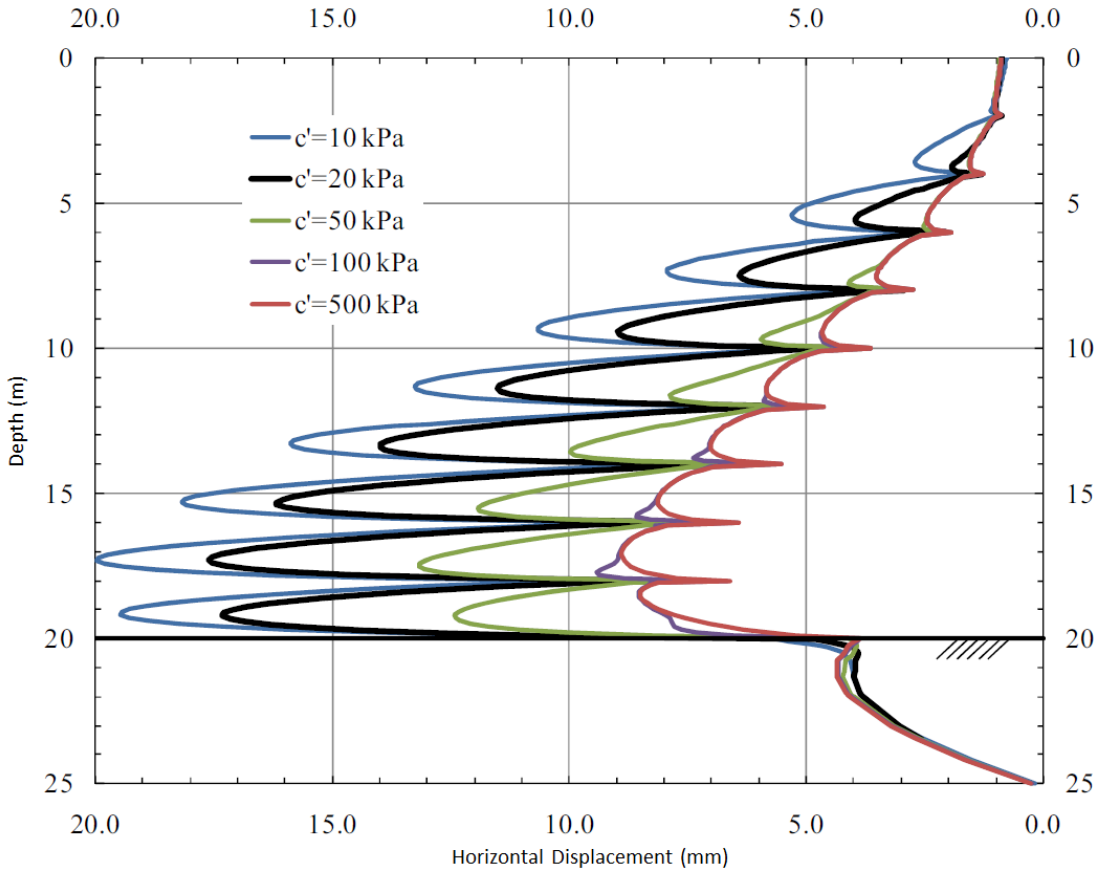

Fig. 3.29 – Cohesion variation in the soil: Horizontal displacements variation in depth (adapted from Topa Gomes (2008))

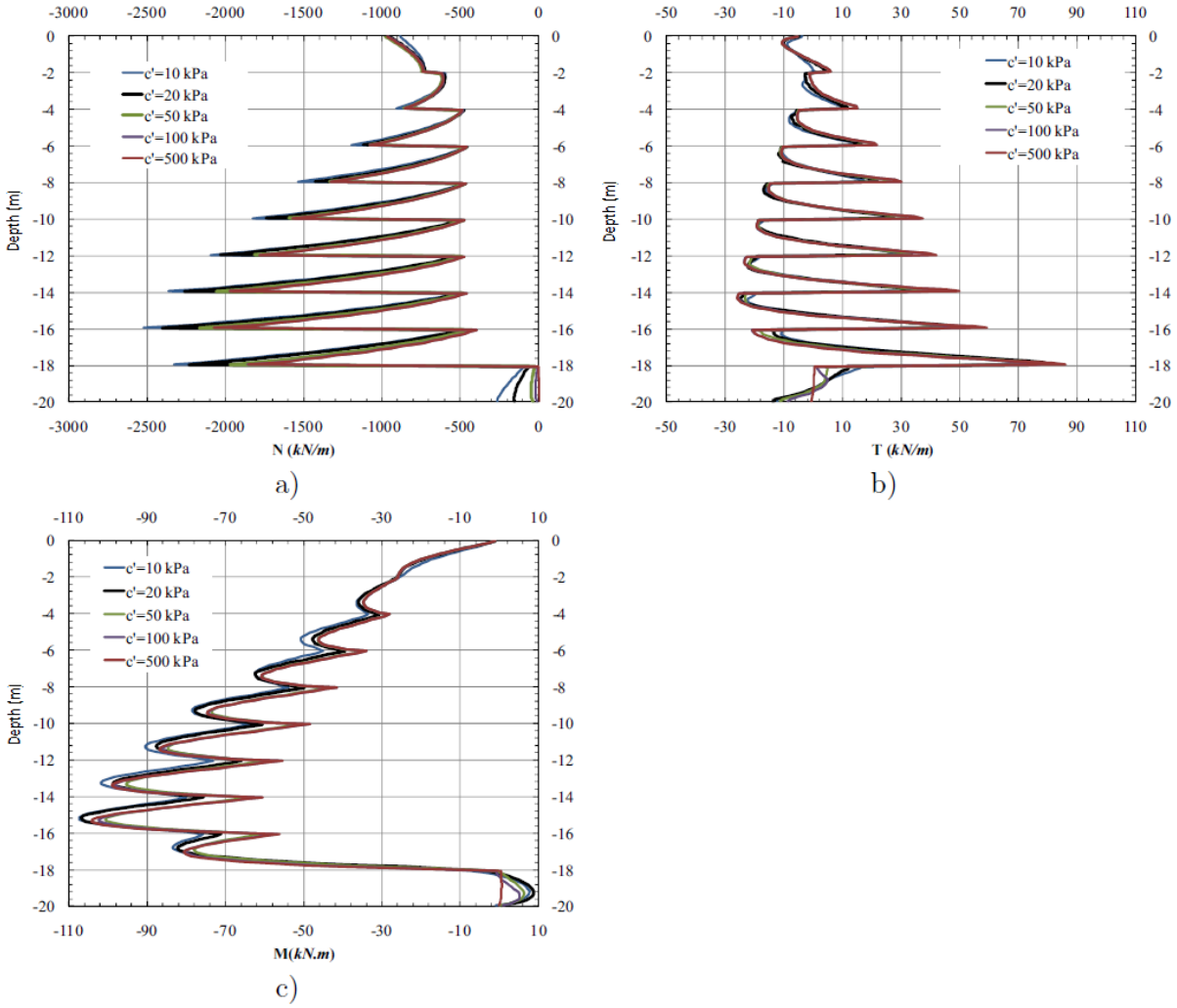

Fig. 3.30 – Cohesion variation in the soil: Variation in depth of: a) Hoop forces; b) Shear forces; c) Bending moments; (adapted from Topa Gomes (2008))

As it was mentioned a few times, most of the deformations occur while the panel is unsupported and so, the deformations "suffered" by the support are less relevant which implies the internal forces won't present significant differences in results. Topa Gomes (2008) refers a 5% decrease in values (for higher cohesion) for bending moments and shear forces, and around 20% for hoop stresses.

3.3.3.2.2. FRICTION ANGLE - ϕ

Being also a parameter that relates to the soil's resistance, varying the friction angle should produce similar results when in last section cohesion was changed.

Varying this parameter in 5º increments from 25 to 45º, the horizontal displacements shown in Fig. 3.31 also decrease at its mid-point, with less impact on the boundaries of each ring. As for the internal forces shown in Fig. 3.32, the same behaviour is presented when changing cohesion, only the hoop stresses show an increase, but no more than 20%. Despite the behaviour similarities with cohesion, when increasing the friction angle, the impact on decreasing horizontal displacements had a lower

impact because, first, even for the maximum value of ϕ'there are still plastic deformations, but less significant, which does not occur when cohesion is 500 kPa. Secondly, cohesion is a parameter that allows a variation of values much larger than for the friction angle, and so can have a stronger impact in results.

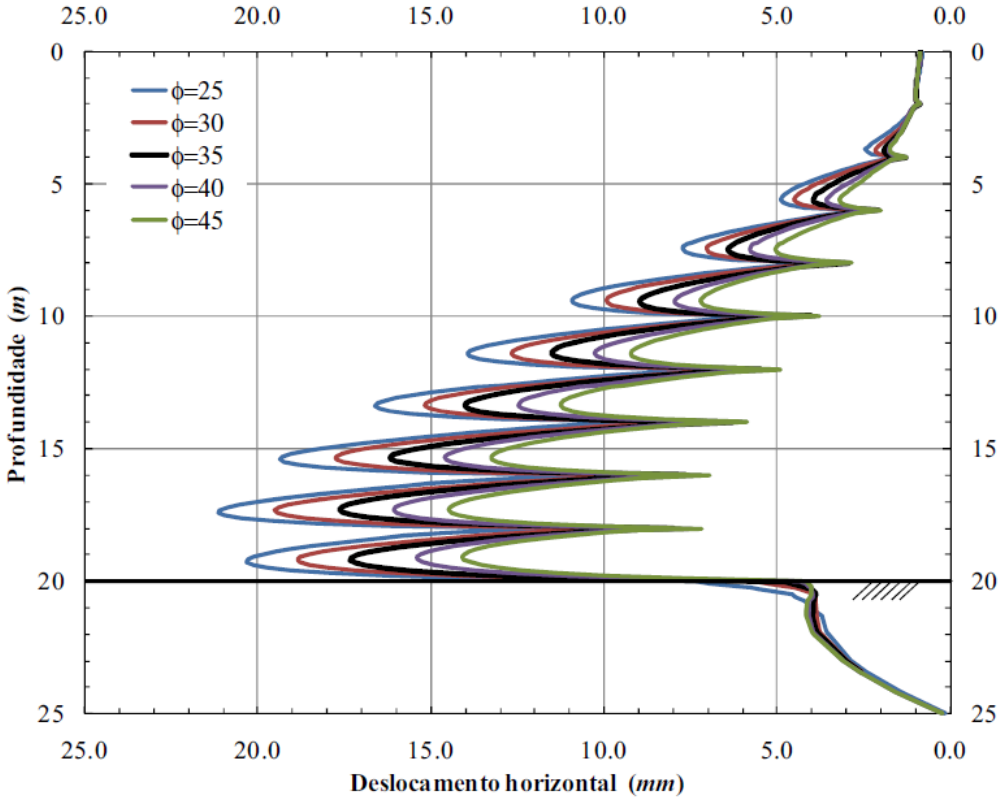

Fig. 3.31 – Friction angle variation in the soil: Horizontal displacements variation in depth (adapted from Topa Gomes (2008))

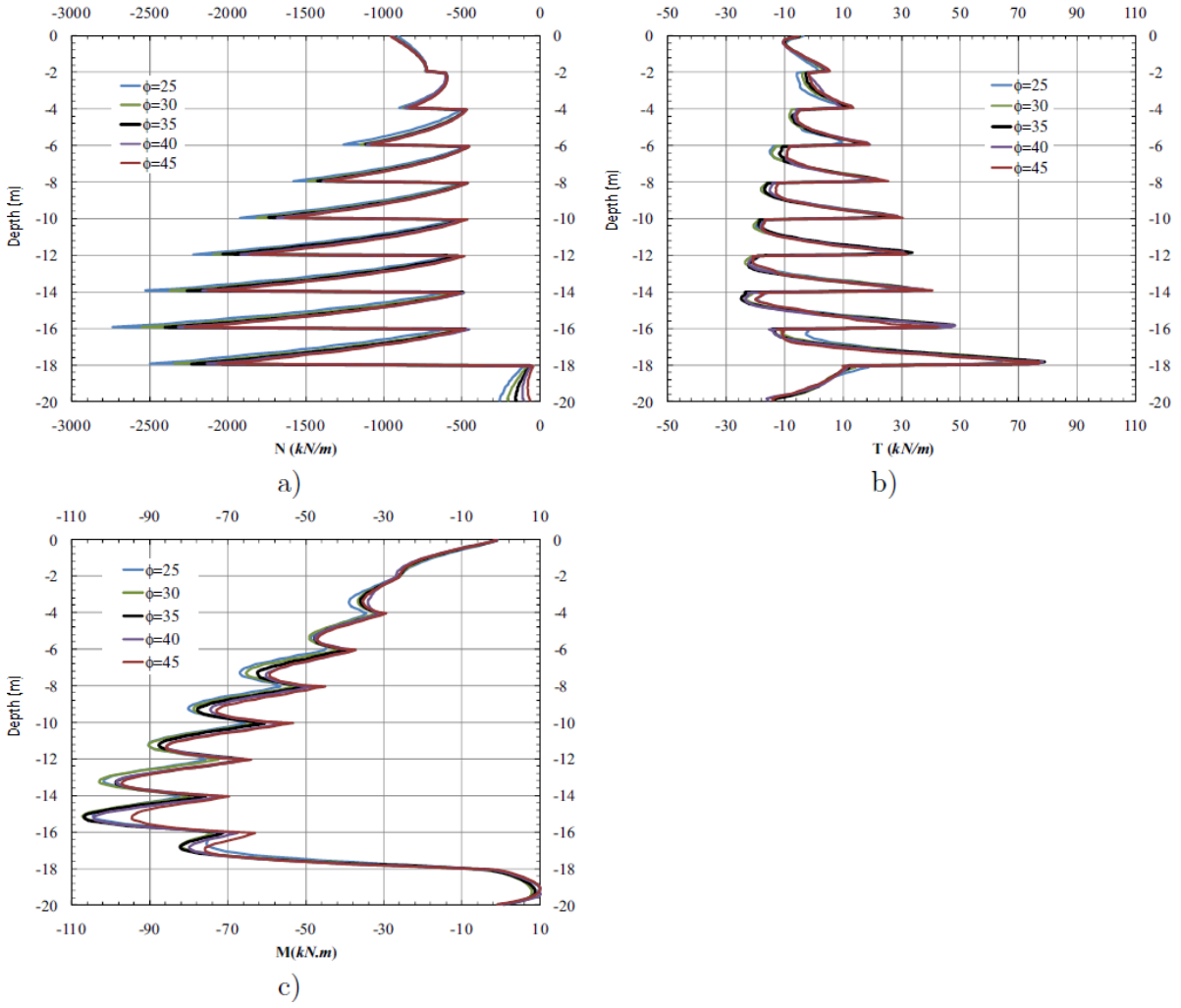

Fig. 3.32 – Friction angle variation in soil: Variation in depth of: a) Hoop forces; b) Shear forces; c) Bending moments; (adapted from Topa Gomes (2008))

3.3.3.2.3. COEFFICIENT OF EARTH PRESSURE AT REST – K_0

This parameter is not actually a resistance parameter of soil; it was included in this in this section, because it controls the amplitude of horizontal stress unloaded while the soil is removed, which has an important impact in the shaft's final displacements (Topa Gomes, 2008).

The cases studied in this point were for K_0 equal of 0.4, 0.5, 0.6, 0.8 and 1.0.

Analysing the horizontal displacements in depth for each case in Fig. 3.33, one can verify an increase of displacements for higher K_0, as it was expected. As it has been discussed in every case, the larger changes in values always occurs at the mid-point of each ring, however, in this case, the curves also increase significantly their values on the upper and lower points, showing the alteration of K_0 doesn't produce such a local effect in soil as the others parameters already discussed. The maximum variation in values is of 60% (Topa Gomes, 2008).

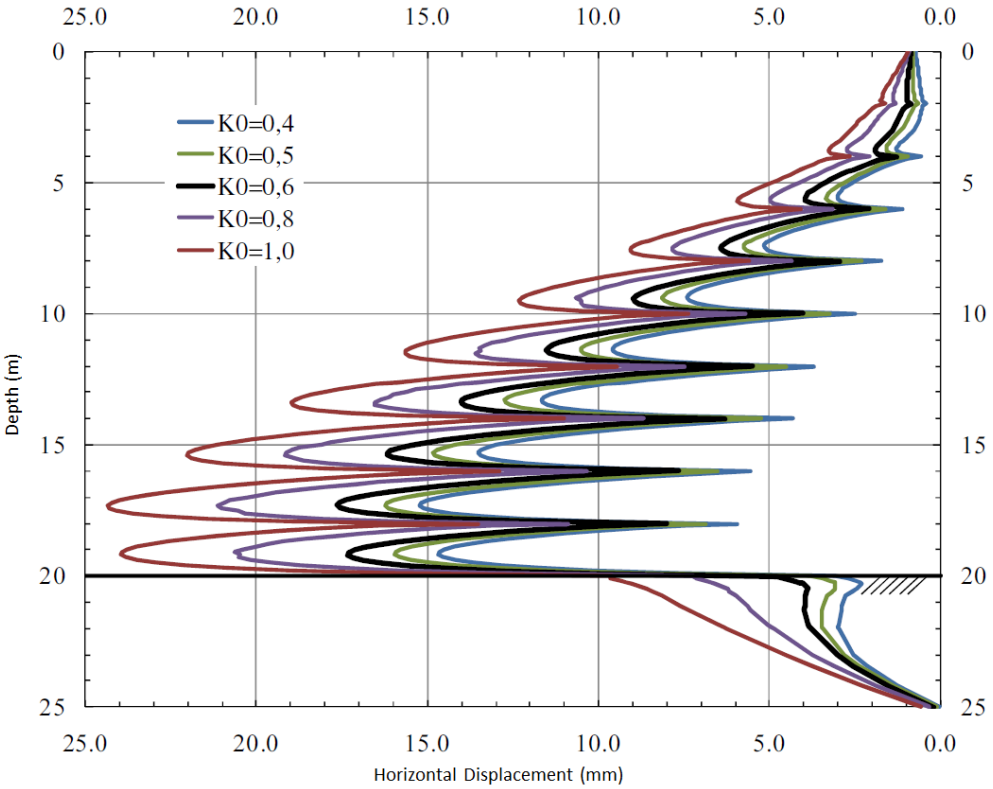

Fig. 3.33 – K_0 variation in the soil: Horizontal displacements variation in depth (adapted from Topa Gomes (2008))

Regarding the internal forces, presented in Fig. 3.34, varying K_0 between the extreme values (from 0.4 to 1.0) reflected in increasing forces: according to Topa Gomes (2008) there was a 30, 29, 58% increase for bending moments, shear forces and hoop forces, respectively, which are relevant differences. The fact that horizontal displacements and internal forces suffered significant changes in value shows how important this parameter is when used for designing purposes.

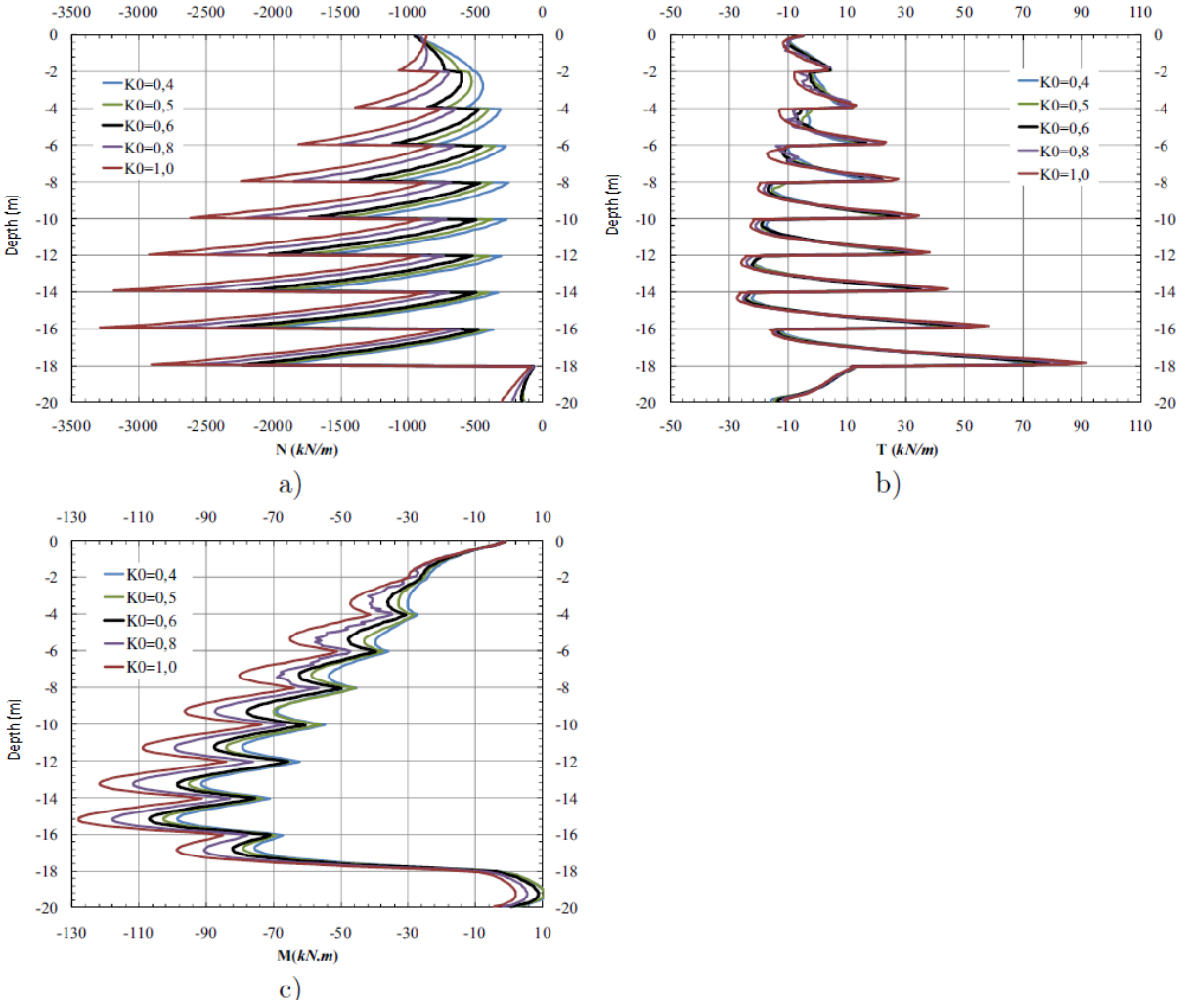

Fig. 3.34 - K_0 variation in the soil: Variation in depth of: a) Hoop forces; b) Shear forces; c) Bending moments; (adapted from Topa Gomes (2008))

3.3.3.3. Soil Deformation Parameters

As mentioned in the beginning of this chapter Mohr-Coloumb was the model chosen in the numerical analysis to characterize the soil's behaviour. In this model, when the soil is loaded it suffers elastic deformations, controlled by E and ν, and when it reaches the yielding point it has a perfect plastic behaviour commanded by the dilation angle, ψ. This is why these parameters are analysed in the following sections.

3.3.3.3.1. Poisson's Coefficient - ν

This is not a parameter with a wide range of values and so its influence on deformations won't be so pronounced. In addition, being a parameter only related with elastic deformations, its variation won't have relevant impact on the areas where points achieve and surpass the yielding surface. Fig. 3.35 shows exactly that, Topa Gomes (2008) stated that changing ν from 0.2 to 0.49 increases only 1.5mm at their maximum horizontal displacements. The fact that the biggest variations in displacements occur, not at the mid-points of each ring, but at their top and lower points justifies what was written

above. Points at mid-height of a ring tend to produce plastic deformations since they're completely unsupported, and so changing ν has little influence, and the contrary happens at the lower and upper points.

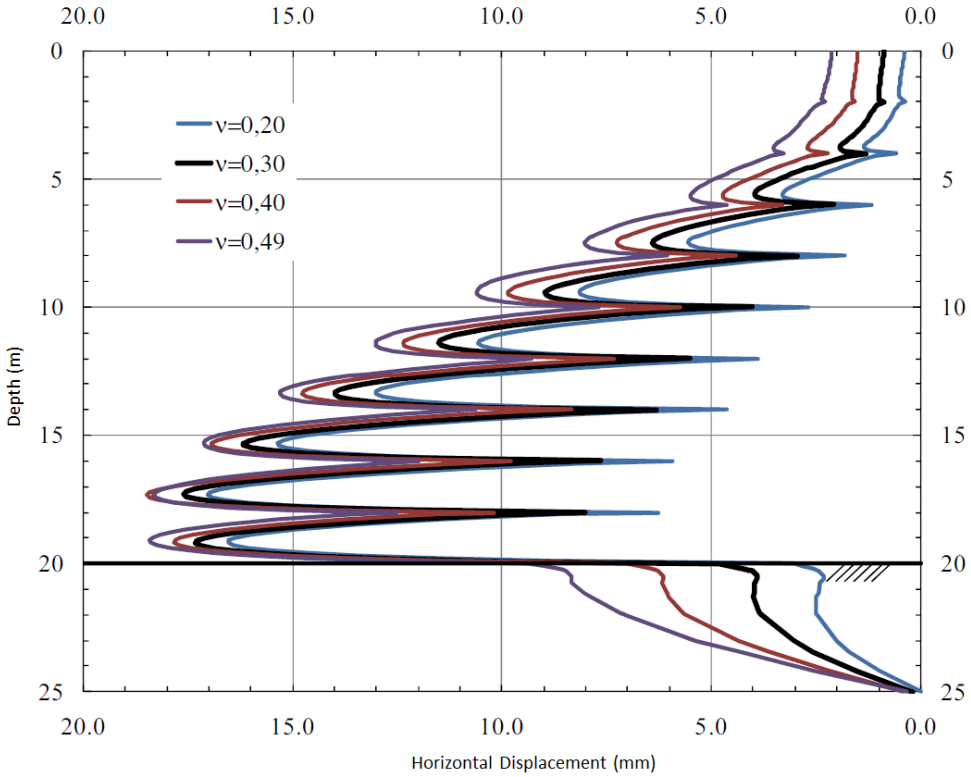

Fig. 3.35 - ν variation in the soil: Horizontal displacements variation in depth (adapted from Topa Gomes (2008))

Like the all the other cases, when there is a reduction in deformations, there's an increase of internal forces, and according to Topa Gomes (2008) this increase is around 30% for the 3 kinds of forces, which, then, makes this parameter relevant when designing this structures.

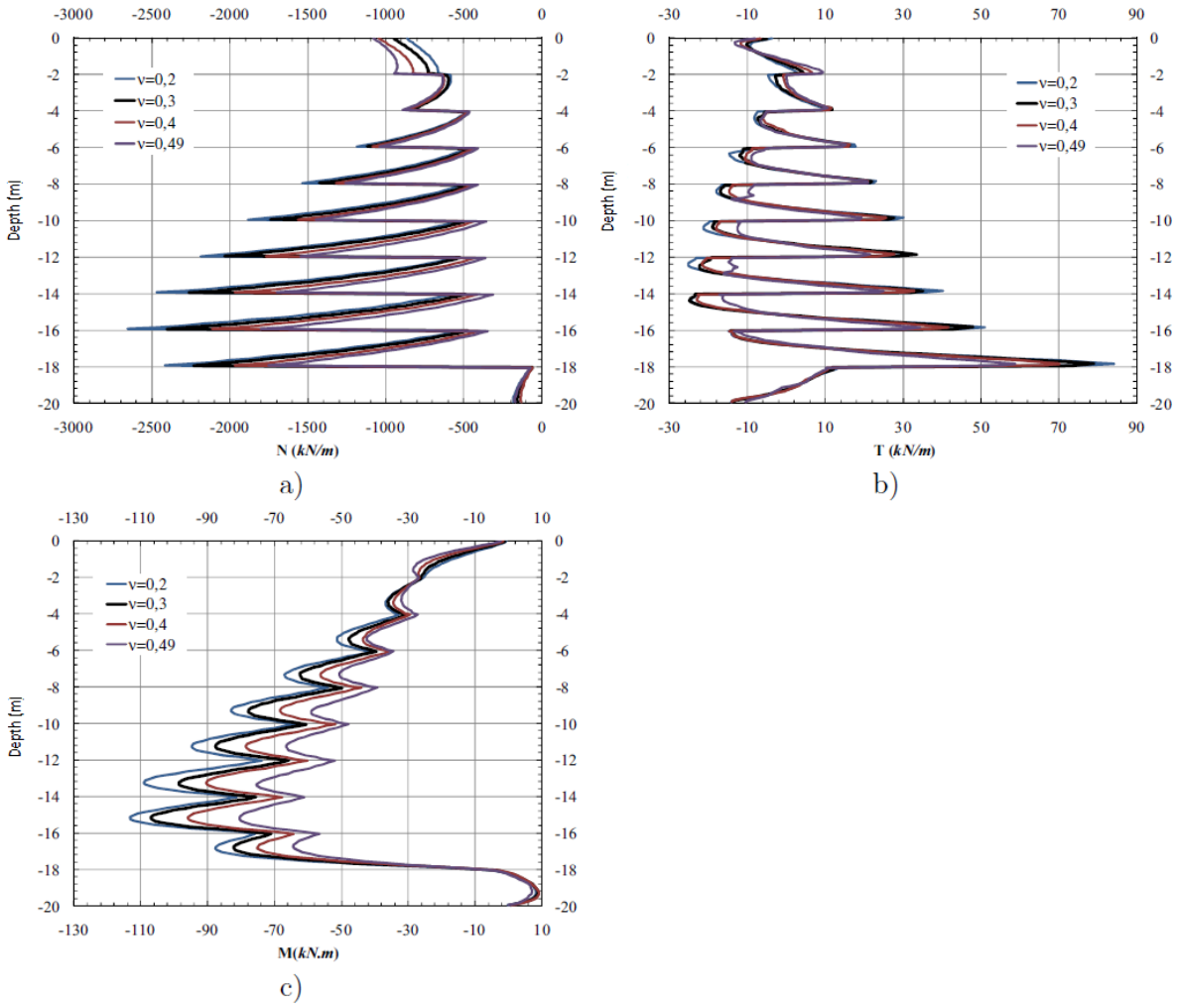

Fig. 3.36 - ν variation in the soil: Variation in depth of: a) Hoop forces; b) Shear forces; c) Bending moments; (adapted from Topa Gomes (2008))

3.3.3.3.2. YOUNG'S MODULUS - E

Like ν, the Young's modulus of the soil is also an elastic parameter and so, its influence in final deformations at "first sight" should be limited, considering the greater horizontal displacements occur in points that surpassed the yield surface and present a plastic behaviour. However, the soil having a higher E, when the plastic deformations occur, the decrease of vertical stresses to reach the equilibrium is relatively smaller, making the plasticized points to "turn back" within the yield surface without achieving higher plastic deformations. This makes the stiffness in soil to be a parameter that, then, can control the magnitude of those plastic deformations. Fig. 3.37 and Fig. 3.38 show a variation for 25, 50, 100, 200 and 500 MPa for E.

Regarding the horizontal displacements in Fig. 3.37, comparing to all other cases studies, turned out to be the most relevant, notice the difference of maximum displacements when varying E from 25MPa to 500 MPa is of around 40 to 7.5 mm. Despite the high differences between extreme values of E, one should keep in mind, that a 500 MPa for E, the soil is almost presenting the same stiffness as rock.

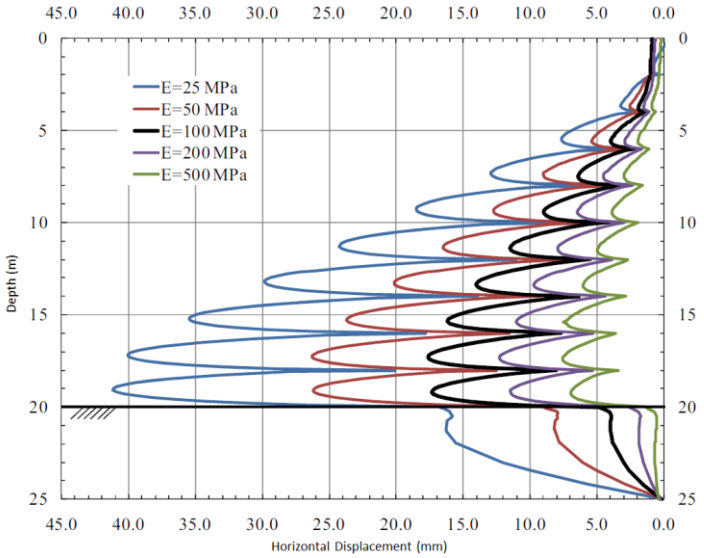

Fig. 3.37 - E variation in the soil: Horizontal displacements variation in depth (adapted from Topa Gomes (2008))

As for internal forces, Fig. 3.38 shows a general behaviour of decreasing forces for bigger values of E, since the deformations that influence those forces are lower. Analysing the lines in that figure, one can notice the differences are significant.

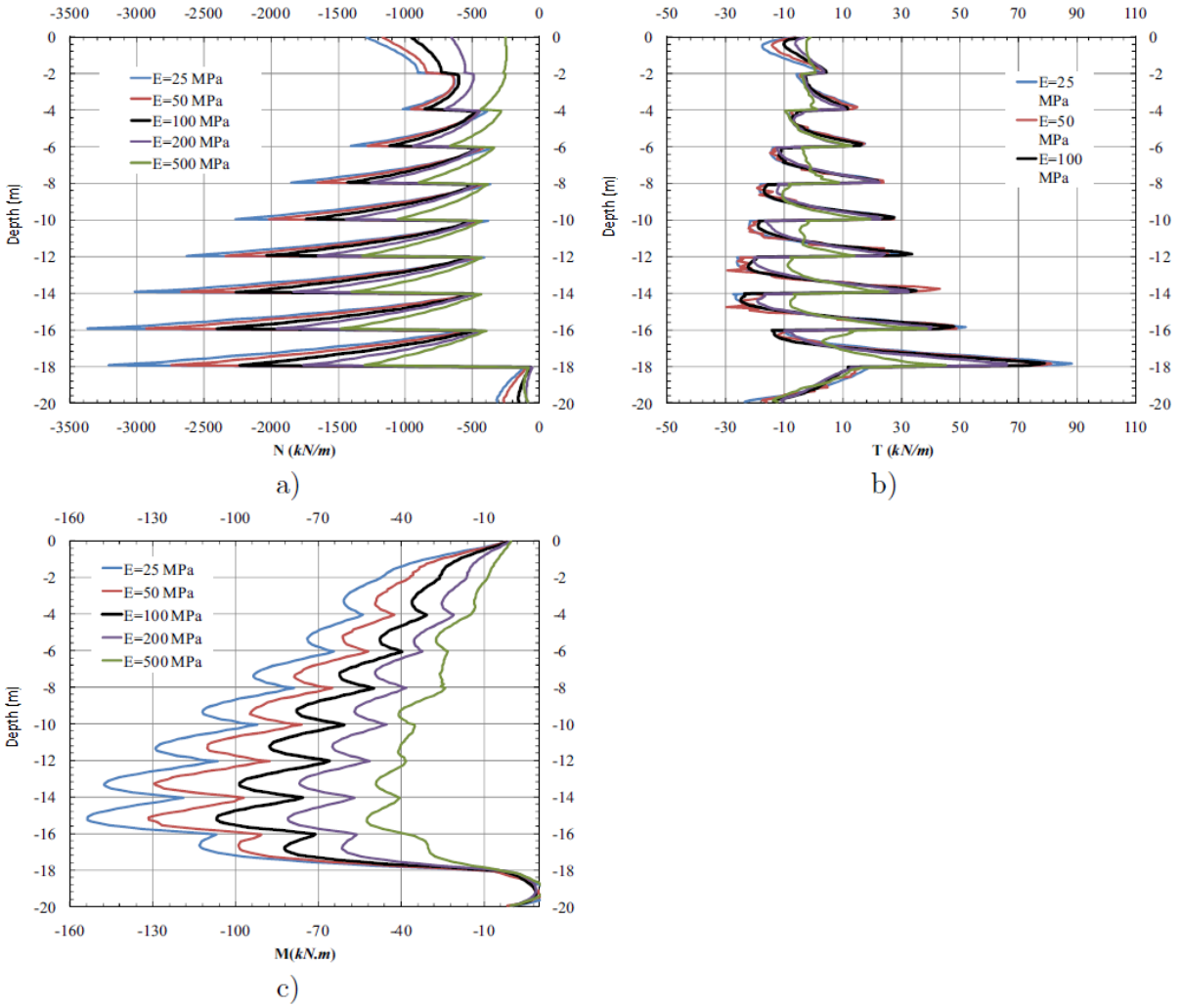

Fig. 3.38 - E variation in the soil: Variation in depth of: a) Hoop forces; b) Shear forces; c) Bending moments; (adapted from Topa Gomes (2008))

This analysis for the variation of E in soil, as the one made in 3.3.1 and 3.3.2, had considered this parameter as a constant in the soil's full depth for practical purposes (and to enhance the main general characteristics of shafts constructed with the SEM). However, considering that E as a constant value in depth for this model, does not fully represent the actual behaviour of soils. As discussed in Chapter 2, this parameter tends to increase for greater depths. This will, of course, influence the results showed in the last two previous figures. For elevations closer to the surface and, then, for lower values of E, the deformations should be relatively higher than for a case where E would be constant in full depth. For higher depths, the contrary would occur – higher E, and lower deformations. This behaviour would lead to relatively more "uniform" deformations and internal forces in depth, which would be essential and more economical when designing the structure. It is also important to point out that having a lower E near the surface would produce relatively higher settlements on the ground. For a more detailed discussion regarding this subject, one should read Topa Gomes (2008) work, where all this sub-chapter is based on.

3.3.3.3.3. DILATION ANGLE - ψ

Contrarily to the soil's E and ν, the dilation angle influences the plastic deformations and its magnitude on those deformations is as high as more extended are the plasticized areas of soil. To study the variation of ν, Topa Gomes (2008) analysed horizontal deformations and internal forces (see Fig. 3.39 and Fig. 3.40, respectively) for cases of ν being: 0, 1/3ϕ', 2/3ϕ' and ϕ' - where ϕ' is the value used on the basic analysis referred in 3.3.1 and 3.3.2 (ϕ' = 35º) – the latter case corresponds to an associated flow rule.

Fig. 3.39 shows that for increasing ψ, the deformations tend to be higher, mostly by the mid-height of each ring, where most of plastic deformations occur. In addition, the lines for lower depths show very similar values in all the four cases, while for deeper elevations tend to diverge, which makes sense, considering closer the surface and for lower stresses in soil elastic deformations are more dominant. According to Topa Gomes (2008) between extreme values, there is a 20% difference in maximum horizontal displacements.

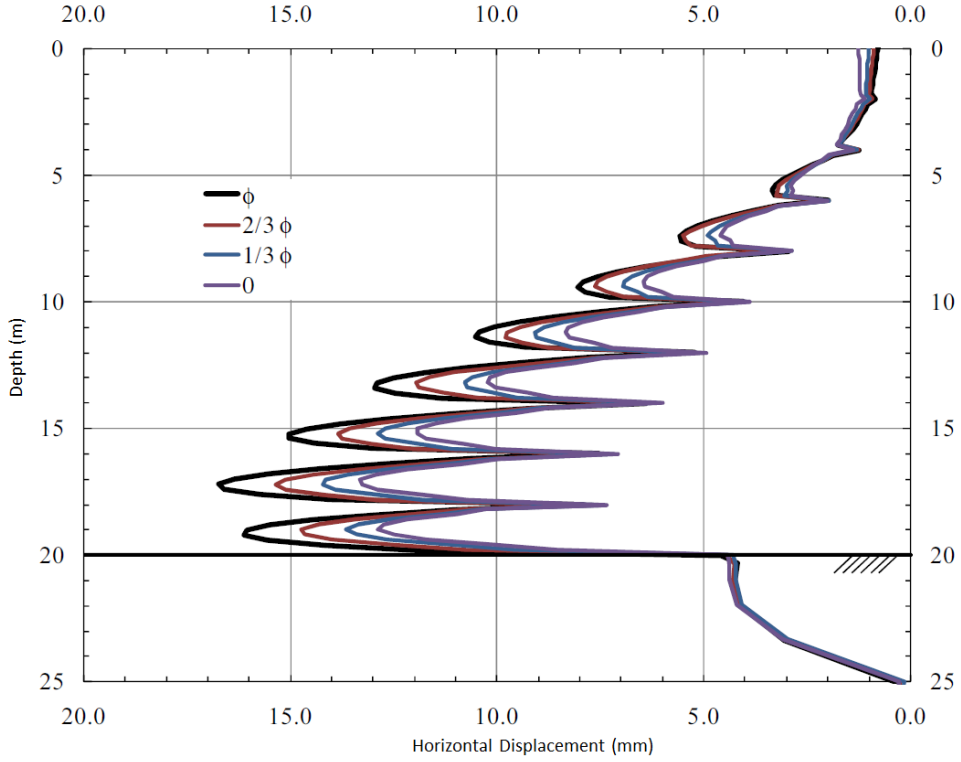

Fig. 3.39 - ψ variation in the soil: Horizontal displacements variation in depth (adapted from Topa Gomes (2008))

As for the internal forces in Fig. 3.40, when increasing the dilation angle, there were increasing forces: 37%, 25% and 10 % for shear forces, bending moments and hoop forces, respectively – which for the first two, the variation is fairly relevant when designing.

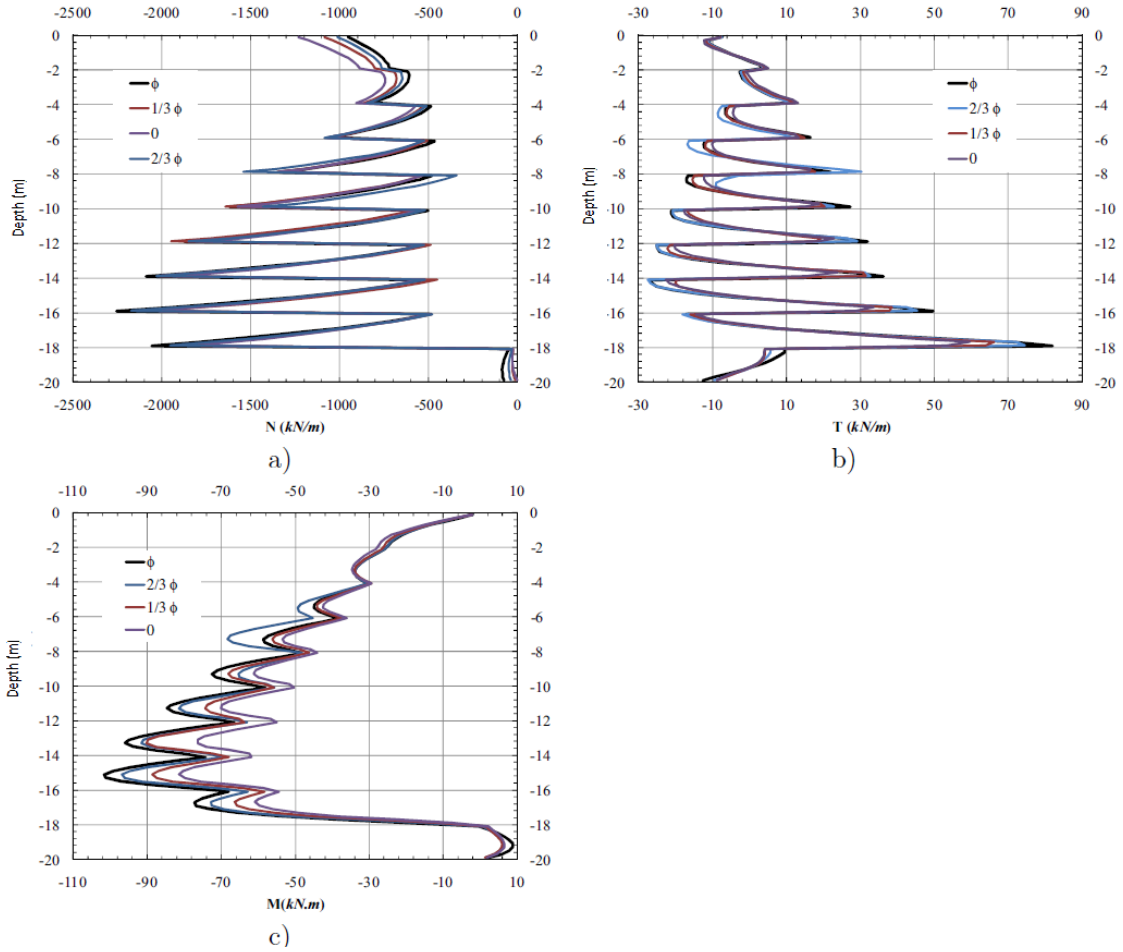

Fig. 3.40 - ψ variation in the soil: Variation in depth of: a) Hoop forces; b) Shear forces; c) Bending moments; (adapted from Topa Gomes (2008))

3.3.4. The Influence of the Water Level Dropdown - Suction

As mentioned before, it is common procedure to lower the water level before the construction of shafts using the SEM, but that decrease implies that the soil mass above phreatic level will be unsaturated and so, with negative pore pressures – suction. This negative values will, then, work, even if just temporarily, as an increment of the soil's resistance (c') and deformability parameters (E) parameters, providing an important stability factor when the excavation face is unsupported.

Fredlund et al. (1978) adapted Mohr-Coloumb failure criteria in order to include the suction effect, presented in expression 3.1.

$$\tau = c' + (\sigma - u_a) \cdot \tan \phi' + (u_a - u_w) \cdot tan\phi^b \quad (3.1)$$

Where ϕ^b is the angle indicating the rate of increase of shear strength relative to suction, $(u_a - u_w)$, and $(\sigma - u_a)$ is the net normal stress normal stress; u_a and u_w are the air and water pore pressure, respectively.

For the case discussed in this chapter, Topa Gomes (2008) simulated a water level variation from the ground level shaft's base, making the soil passing from a saturated to an unsaturated condition. The

same author proceeded to triaxial tests in unsaturated soil conditions (in residual granite soils from Porto) and obtained a value of ϕ^b around 14º, which was used for this analysis. Considering that value, next Fig. 3.41 shows the values of suction and equivalent value of cohesion, or strength, $(c' + (u_a - u_w) \cdot tan\phi^b)$, where the later increases for higher negative pore pressures.

In the same triaxial tests Topa Gomes (2008) found a relation of suction and E, and concluded there was a slight increase of the latter for higher values of suction and that relation was around 0.78% for each 1kPa of suction – also represented in Fig. 3.41.

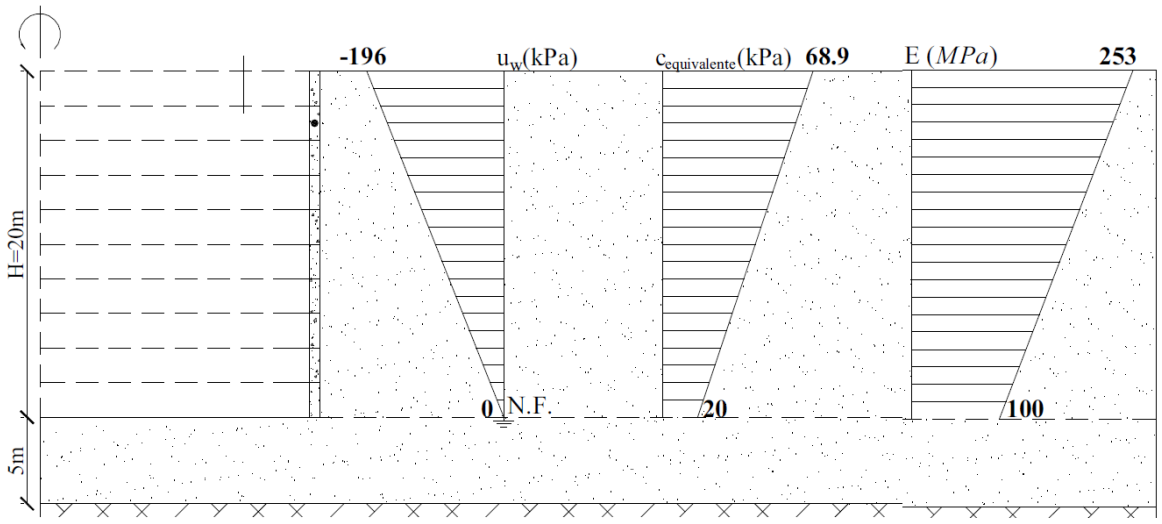

Fig. 3.41 – Suction influence: suction variation in depth, equivalent strength and E for ϕ^b =14º (adapted from Topa Gomes (2008))

The analysis in CODE_BRIGHT was solved and compared for 4 cases: the basic analysis referred in 3.3.1, but now for a saturated condition; 2 cases considering the isolated effect of either equivalent strength or increase of Young's Modulus ("resistance" and "deformability" cases, respectively); and a final case combining the two previous cases.

As it had been done in previous sections, Fig. 3.42 presents the variation in depth of the horizontal displacements behind the support for the 4 mentioned cases. Analysing that figure, it is clear that the influence of suction improves the soil characteristics in either case by reducing its horizontal displacements. It is interesting to notice that for higher elevations the "resistance case" produces lower deformations than the influence of E isolated while for deeper elevations results the contrary, where the influence of suction decreases and the values tend to get closer to ones from the basic analysis. When considering the effect of suction only for the "deformability case" the reduction of horizontal displacements is constant in depth (Topa Gomes, 2008). Finally, considering the combination of the two previous cases, the deformations are always lower than the other 2 cases with the exception of the two deepest panels where the "resistance" case shows values very close to this case. This shows that for lower values of suction, i.e., for lower elevations, the influence on resistance (equivalent strength) is practically null, while the influence on the deformability parameter is still relevant.

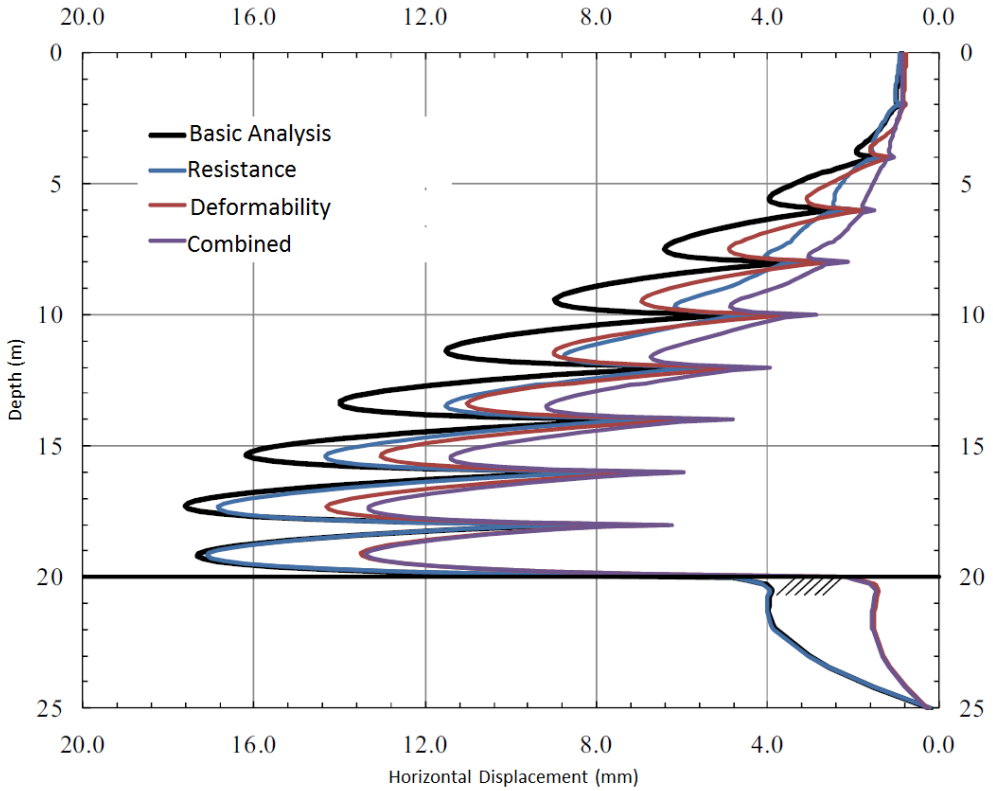

Fig. 3.42 – Suction influence: Horizontal displacements variation in depth (adapted from Topa Gomes (2008))

As for the influence on the internal forces, the variation in depth for hoop, shear forces and bending moments is shown in Fig. 3.43. The effect of suction on the deformability characteristics continues to be more influent than resistance, since when considering that isolated case the maximum values of hoop forces and bending moments decrease around 15% and shear forces 10%. Whereas, considering the isolated case of suction influencing resistance that decrease of internal forces from the basic analysis are less than 5%, according to Topa Gomes (2008).

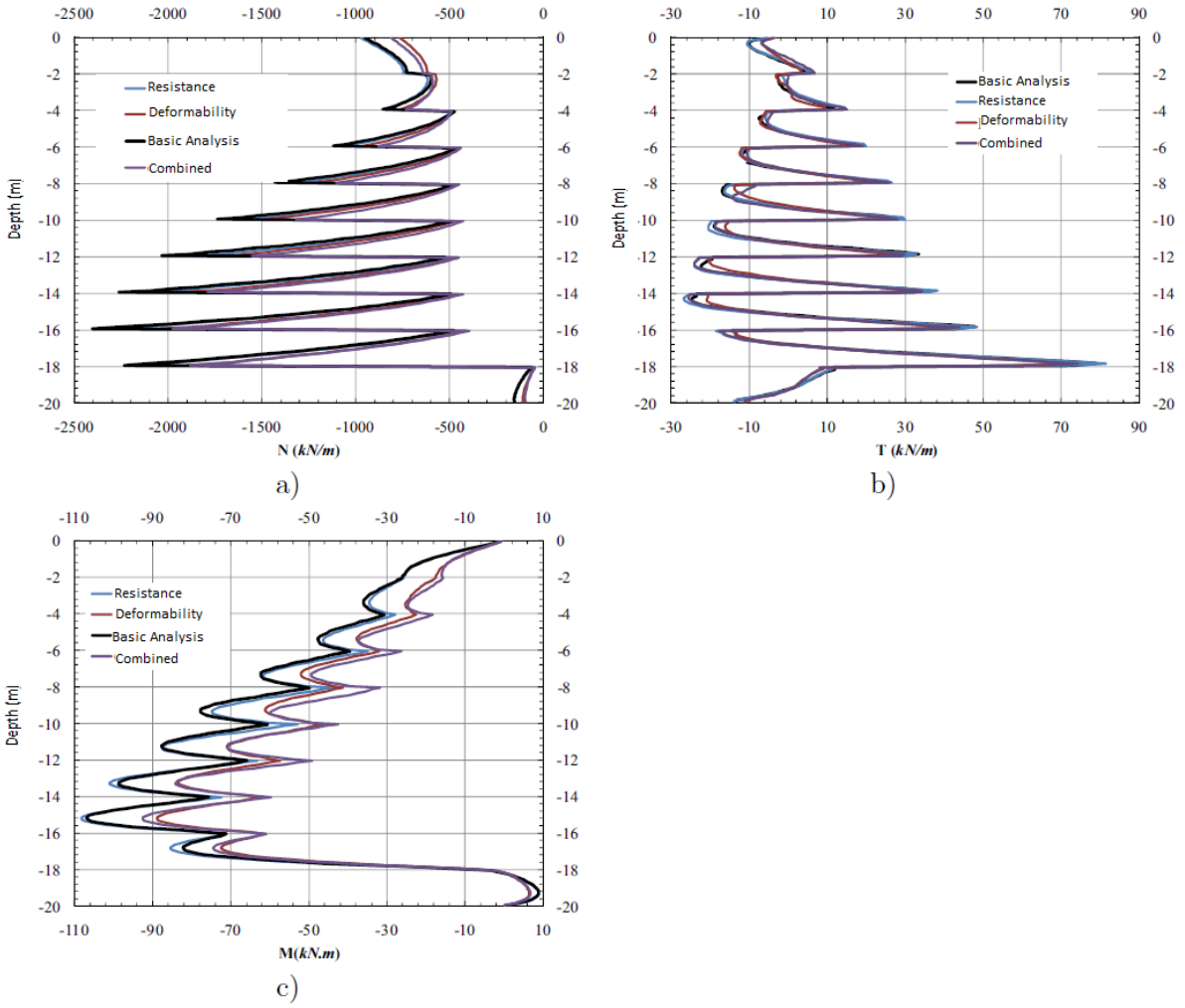

Fig. 3.43 – Suction influence: Variation in depth of: a) Hoop forces; b) Shear forces; c) Bending moments; (adapted from Topa Gomes (2008))

3.4. SUPPORT (SHOTCRETE) AND DESIGN OF SHAFTS

As it was already mentioned throughout this dissertation, circular shafts with large diameters constructed with sequential excavation method are the main subject of this project. Until nowadays (2014) there are not yet specific or standard directions regarding the design of these structures. So, in practice, testing the quality and suitability of a solution regarding the shaft's full depth, geometry, thickness of the support and construction methods, like excavation height or water pumping, for instance, is an iterative procedure by performing numerical analysis using software that usually uses the Finite Elements Method.

For an engineer when designing this support, in a simple approach, one has to balance the class of resistance with its thickness so that the choice is suitable in terms of safety and economics. There are several elastic theories and empirical expressions that correlate the lining thickness with its load (mainly hoop stresses), but all of them are regarding mine shafts interacting with rock masses, where the loads are relatively higher than in soil and then, the support is generally considered thicker – some of those theories and expressions are summarized in Guler (2013).

Table 3.2 – Elastic and empirical expressions for determining support's thickness in mining shafts (Guler, 2013)

Expression	Parameters
for an elastic model: $t_c = r\left(\sqrt{\frac{f_c}{f_c - 2p_{sc\,max}}} - 1\right)$	$p_{sc\,max}$ – max. support pressure on shotcrete/concrete f_c – uniaxial compressive strength of shotcrete/concrete t_c – thickness of shotcrete/concrete r – shaft's radius
considering plasticity: $t_c = r\left(\sqrt{\frac{f_c}{f_c - \sqrt{3}p_{sc\,max}}} - 1\right)$	(same as above)
empirical expressions: $t_c = \frac{p_o r}{f_c}$ $t_c = r\left(e^{2.04 p_o / f_c} - 1\right)$	p_o – radial pressure[2]

As it will be described in more detail in Chapter 4, the shaft subjected to study in this dissertation has steel reinforced shotcrete as its support from mid-depth to its base while the rest is constituted of precast concrete segments until the surface. In this specific case, differently from the precast concrete, the shotcrete presents a time-dependent behaviour regarding its resistance properties. From the moment when it is applied on the open excavation face its strength (and therefore, its stiffness) increases as time passes by, this process is commonly known as "hardening". However, when referring to shotcrete, and not conventional concrete, the support is loaded since from its early strength age, and that is why is a common procedure to mix additives to its composition in order to increase the hardenings rate. This time-dependent behaviour will influence final deformations, settlements and its internal forces and so, deserves to be considered and discussed in more detail.

3.4.1. YOUNG'S MODULUS (E) ESTIMATION

As discussed in the parametric study in 3.3.3, E is an essential concrete parameter since its value can influence deformations and internal forces when loaded. Usually the estimation of E is done based on uniaxial compressive strength values obtained from laboratory tests, making it possible for one to use simplified empirical expressions provided in codes and guidelines and get an estimation of E. However, most literature references that provide those expressions concern only conventional concrete and, despite the fact some studies attempt to propose other expressions, its extrapolations are not feasible, since differences regarding type of equipment used for spraying and the material's

[2] In Guler (2013) one can also find several expressions for p_o

composition, due to the inclusion of accelerators or bigger aggregates, are not considered (Globardes *et al.*, 2013). Therefore, there are not yet available expressions in the technical literature for sprayed concrete and the analysis for the best one is out of the scope of this dissertation.

The work of Globardes *et al.* (2013) discusses the practical application of some empirical expressions in different codes (being one of them the Eurocode), compares them to laboratory results and attempts to input factors on those expressions so that can best fit the lab results – the results from this author's work should be considered in further studies. However, the main point of this dissertation is more concerned on inputting a time-depend behaviour on the numerical model of the structural member and check its influence and not to seek the best hardening curve for the support. Therefore, for simplicity, the expressions presented in the "Eurocode 2: Design of concrete structures" (EC2) will be used in this work. In that code, the variation of the mean compressive strength in time is shown in expression 3.1 and the Young's modulus in 3.3.

$$f_{cm}(t) = \beta_{cc}(t) \times f_{cm} \quad (3.1)$$

Where, $\beta_{cc}(t)$ is defined as follows in expression 3.2:

$$\beta_{cc}(t) = exp\left\{s\left[1 - \left(\frac{28}{t}\right)^{1/2}\right]\right\} \quad (3.2)$$

And,

$$E_{cm}(t) = \left(\frac{f_{cm}(t)}{f_{cm}}\right)^{0.3} \times E_{cm} \quad (3.3)$$

- t is the age of concrete in days;
- f_{cm} is the concrete's mean compressive strength at 28 days and according to table 3.1 of EC2 is obtained as: $f_{cm} = 8 + f_{ck}$ [MPa] where f_{ck} is the characteristic compressive strength of concrete for cylindrical cores
- s is a coefficient which depends on the type of cement:

  = 0,20 for cement of strength Classes CEM 42,5 R, CEM 52,5 Nand CEM 52,5 R (Class R) ;

  = 0,25 for cement of strength Classes CEM 32,5 R, CEM 42,5 N (Class N) ;

  = 0,38 for cement of strength Classes CEM 32,5 N (Class S);
- $\beta_{cc}(t)$ is a coefficient which depends of the age of the concrete;
- E_{cm} is the average Young's modulus for the age of 28days and is defines as $22.[(f_{cm}/10)]^{0.3}$ [GPa]

The "European Specification of Sprayed Concrete" already presents a certain guidance regarding the material's composition, test methods failure modes and others. From that specification Uotinen (2011) gathers in an article the main resistance characteristics for shotcrete. Those are listed in Fig. 3.44.

Class ($f_{ck}/f_{ck,cube}$) [MPa]	Unreinforced compressive strength ($f_{c,pl}$)	Unreinforced tensile (or shear*) strength ($f_{ct,pl}/f_{cv,pl}$)	Fibre reinforced compressive strength (f_c)	Fibre reinforced tensile (or shear*) strength (f_{ct}/f_{cv})	Elastic modulus (Young's modulus) (E_{cm})
C8/10	5.4	0.50	6.8	0.84	25.3
C12/15	8.2	0.66	10.2	1.10	27.1
C16/20	10.9	0.80	13.6	1.33	28.6
C20/25	13.6	0.93	17.0	1.55	30.0
C25/30	17.0	1.08	21.3	1.80	31.5
C28/35	19.0	1.16	23.8	1.94	32.3
C30/37	20.4	1.22	25.5	2.03	32.8
C32/40	21.8	1.27	27.2	2.12	33.3
C35/45	23.8	1.35	29.8	2.25	34.1
C40/50	27.2	1.47	34.0	2.46	35.2
C45/55	30.6	1.59	28.3	2.66	36.3
C50/60	34.0	1.71	42.5	2.85	37.3

Fig. 3.44 – Table gathering shotcrete resistance characteristics from Uotinen (2011) work

3.5. FINAL NOTES

Throughout the present chapter were discussed essential points that will sustain the analyses further performed in Chapter 5 and so, deserve some final remarks.

This chapter's content had the potential to be much more extended either regarding construction methods or parametric studies based on Topa Gomes (2008), but it was essential to stick to what was specifically related to the case study.

The construction of large diameter shafts instead of other common earth retaining structures is relatively recent and the references about their design and behaviour are limited. That implicated to perform numerical analysis simulating the construction process in order to study the soil mass and its support's behaviour, as it was presented in 3.3 based on Topa Gomes (2008) work. From that analysis one learned that the changes in deformations and stresses are generally local – behind the excavation face – which constitutes a major difference from tunnels construction. In addition, a parametric analysis was discussed and showed how important it is to obtain reliable soil parameters when performing a numerical analysis, since their variation (mainly, the soil Young's modulus and K_0) can lead to relevant different results in deformations and internal forces of the support and so, the structure's design. This variation in parameters was also induced by simulating the decrease of the phreatic level and turned out to enhance the resistance and deformability properties of the soil, due to

suction. For a structure whose construction method implies the opening of vertical unsupported panels, the considering the effect of suction is most relevant.

Nowadays, large diameter shafts are structures, which are not yet covered specifically by standard codes, and the available design methods are practically reduced to numerical analysis performed in software, employing the finite element method. The most common support for these structures is the application of shotcrete and there is already some guidance regarding its main resistance characteristics. However, estimating its Young's modulus does not yet gather consensus, due to its "special properties" that differentiate from ordinary concrete. Therefore, in Chapter 5, one will employ the expressions from Eurocode 2, for simplicity.

4

Characterization of the Case Study

4.1. Main Context

The shaft recently built in Mile End Park and its connecting galleries are part of the Cross-rail project in London. In a brief reference, the Cross-rail is a new London rail link project, which will enable the introduction of new and improved rail journeys through and into London from the southeast of England. The project includes the construction of 7 central stations and 42 km of new tunnels, providing interchange with London Underground, National Rail and bus services.

Fig 4.1 shows an overview of the Cross-rail project within Greater London, where the reddish lines represent the routes in tunnel and the dots, the stations.

Fig. 4.1 – Cross-rail routes within Greater London (image from context report provided to the author)

The case study in this work is located in the eastern tunnels more precisely in the TBM tunnel drive Z (Pudding Mill Lane to Stepney Green), as shown in Fig 4.2. From Fig. 4.1 one can see this tunnel drive represented by the red line connecting Stratford to Whitechapel. In the eastern tunnels, unlike the

western ones, the shafts and adits were constructed before the arrival of the tunnel-boring machine (TBM).

Fig. 4.2 – TBM Tunnel Drives (image adapted from case study context report)

The context report of this project states that "intermediate shafts between stations on the tunnelled section of the Cross-rail route are required to provide one or more of the following features:

- Emergency intervention points (EIPs), located at a maximum spacing of approximately 1 km, to be used by the emergency services to access the tunnels – the shafts will include lifts or hoists and stairs, with a parking area provided at the surface for emergency services;
- Escape facilities, consisting of lifts and stairs to allow for passenger evacuation, with a place of safety provided at the surface; and ventilation facilities, containing ventilation fans used to reduce temperatures in the tunnel and to provide forced ventilation for smoke control during emergencies;"

In the same report, it is written that at Mile End Park a circular vent, escape and EIP shaft will be constructed (including fire-fighting lift). The shaft will be located at the south east corner of Mile End Park and adjacent to the proposed site is Burdett Road (A1205) and the "London to Tilbury" viaduct. Fig 4.3 shows the map representing the location of the work site, its surroundings and the future tunnel routes.

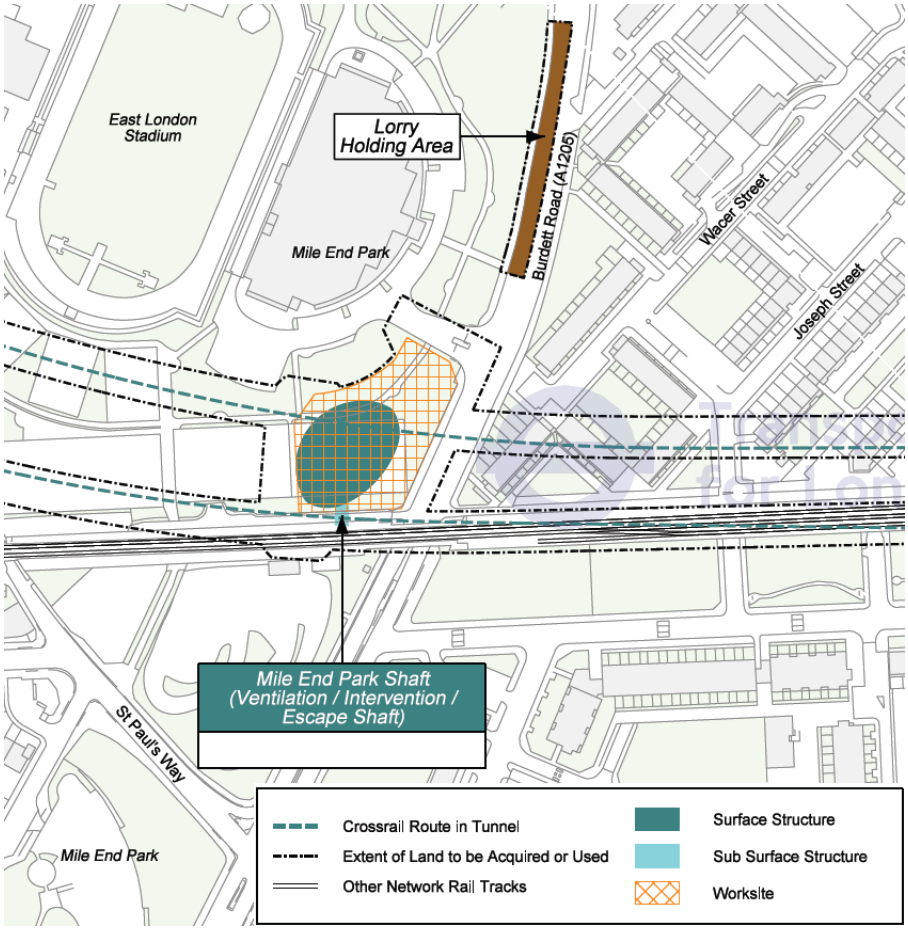

Fig. 4.3 – Map of MILE END work site (image from construction context report)

4.2. SHAFT CONSTRUCTION

At Mile End Park, a 29.94 m deep shaft and two adits entailing 22.8 m of tunnel were constructed. After excavation, the TBM will excavate two tunnels whose axis will pass by each adit's axis perpendicularly.

On the first 15.65 m of depth, a 300 mm thick pre-cast segmental lining of 11.37 m of diameter was sunk as a wet caisson. In this case, the pre-cast concrete rings, which were around 1 m height, were sunk using "8no. jacks" with maximum of 20 tonne force and a 9 tonne excavator was used to remove the soil within the shaft. Where water was encountered within The River Terrace Deposits and London Clay excavation, an 80 tonne crane with rope grab was used for excavation – see Fig. 4.4. Also in that figure, one can see the hydraulic jacks at the picture above and the interior of the shaft after completion of caisson sinking.

Fig. 4.4 – Wet caisson sinking at the worksite: Crane and grab (set of photos from progress report)

For the remaining 14,29m, the soil was firstly excavated in a single 1,5m lift using four equal segments, while the remainder was excavated with 1m full profile lifts. A primary 300mm lining of fibre-reinforced shotcrete (SC) was applied after a full profile was excavated and then a secondary lining of 300mm of the same material, performing a thick final layer support of 600mm and diameter of 12,1m. As mentioned in Chapter 3, the strength class of shotcrete used was C32/40 MPa and the reports from the worksite mentioned "CEM I" as the type of cement in its composition and 52.5N as its strength class.

According to the images from the construction progress reports, the second 300 mm layer of shotcrete was applied around 1 or 2 rings above the excavation base. Prior to the SC lining (SCL) works a dewatering process from the ground was executed through dewatering wells and vacuum pumps, lowering the water levels below the shaft base. The adits were excavated in full face in 1m advances using an excavator and sprayed with a 300mm of fibre-reinforced shotcrete.

Therefore, the shaft subjected to study consists in a mix of two construction methods (briefly described in Chapter 3), which will have a direct influence on its behaviour, leading to some differences from the one described in the previous chapter, where only the conventional excavation was considered. This factor should always be taken in consideration when analysing results and comparing the structure and soil behaviour.

4.3. GEOTECHNICAL AND GEOLOGICAL CONTEXT

A summary of the stratigraphy encountered in MILE END is represented in Fig. 4.5, along with a representation of the shaft, adits and support applied. In the next sections of this sub-chapter a brief description of the site geological conditions will be presented based on reports from CROSS-RAIL that followed the excavation process.

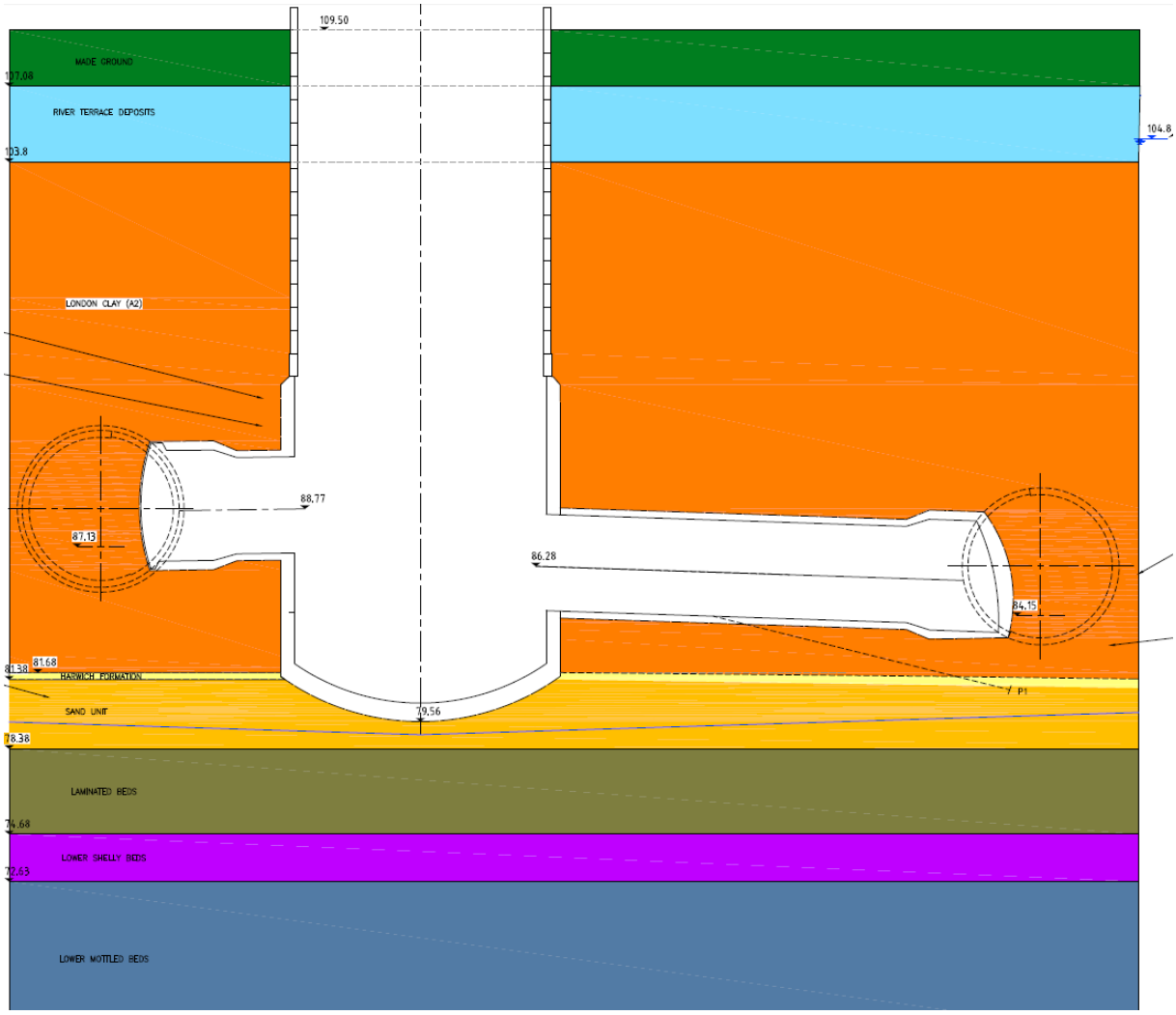

Fig. 4.5 – Representation of the Shaft, Adits and Stratigraphy at the Worksite (from Progress reports provided)

4.3.1. GEOLOGICAL DESCRIPTION

The following table presents the different formations encountered at the site. Resulting from 43 geotechnical logs recording ground conditions during the shotcrete lining works (SCL).

Table 4.1 – Stratigraphy's base elevations

Formation	Elevation of Stratum Base (m PD)[1]
Made Ground	107.5
River Terrace Deposits	104.1
London Clay (A2)	81.9
Harwich Formation	81.5
Sand Unit (Woolwich Formation)	Seen at 79.5 (shaft bottom)

According to the Fig. 4.5, the ground level is at 109.50m PD.

4.3.1.1 SUPERFICIAL DEPOSITS

Made Ground encountered between ground level and 107.5m, is highly anisotropic, although it is in general comprised of sandy gravelly clay and gravelly sand. The sand is fine to coarse and gravel is comprised of angular to rounded brick.

River Terrace Deposits encountered at the site comprised clayey very gravelly fine to coarse sand. The elevation of the boundary between this layer and London Clay varies ±0.4m due to erosion phenomena.
On this interface, water was encountered at ±104.8 m due to the accumulation from the upper aquifer. During excavation, this aquifer was isolated by the pre-cast concrete rings sunk at 9.3 m from the London Clay top surface.

4.3.1.2 LONDON CLAY

As it can be noticed from the previous table and image, the London Clay layer is the thickest and involves the majority of the shaft and adits.

The unweathered clay encountered at the site varies from stiff to very stiff, fissured, dark grey, sandy clay. The sand found within the clay is fine. The fissures are closely spaced, sub-horizontal and sub-vertical, planar smooth and occasionally polished. The clay at the site belonged entirely to the A2 division, defined in chapter 2, and occasionally presents partings of gravel sized pockets of fine sand as shown in Fig. 4.6.

[1] PD – Project Datum – to avoid dealing with negative elevations, the ordnance datum (sea level) is added by 100.

Fig. 4.6 – Sand Parting within London Clay (photo from the provided case study's Geotechnical report)

The undrained shear strength (Su) was stiff (75 to 150kPa) to very stiff (150-300kPa) and this transition was located at approximately the level 89.9 m PD. As depth increased, block size also increased reflecting increasing undrained shear strength. During excavation within the clay, no water flow from the excavated faces was observed.

4.3.1.3 HARWICH FORMATION

This layer was found with a total thickness of less than 0.4 m and is comprised of dark grey clayey sand with sub-rounded to rounded flint gravel. Its low thickness can be verified in Fig. 4.7

No water seeped from the Harwich Formation verifying the success of the dewatering plan (referred in section 4.3.2)

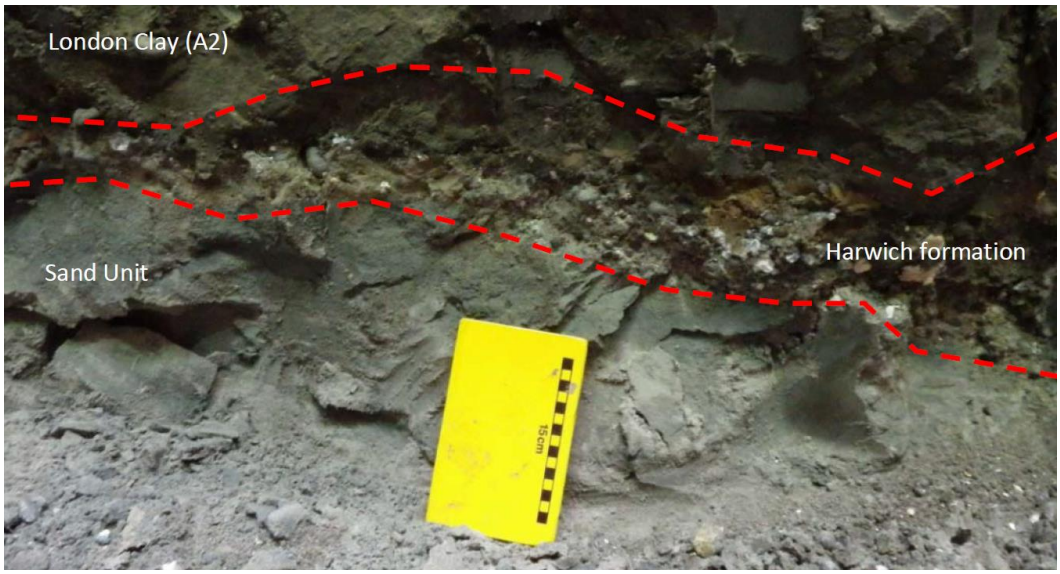

Fig. 4.7 – Harwich Formation and its boundaries (from the provided case study's Geotechnical report)

4.3.1.4. SAND UNIT (WOOLWICH FORMATION)

Bellow the Harwich Formation there is a sand unit, which is a channelized deposit and due to its grey unoxidised colour can be classified as part of the Laminated Beds. This layer is grey, medium to fine sand and occasionally clayey. No stability issues were encountered within the sand due to its dewatered state.

4.3.1.5 DISCONTINUITIES AND FAULTS

Considering the high undrained shear strength encountered within the LC in short-term excavation, the stability of the material is governed by its discontinuities and so it was relevant to consider their properties and anticipate their behaviour.

The fissures registered, according to the description from the report, are "medium to closely spaced, tight, slightly smooth to planar with no evident fill, weathering or moisture. Fissures were predominantly sub-vertical and sub-horizontal". Table 4.2 presents the orientations of the major discontinuity sets.

Table 4.2 – Discontinuity sets within London Clay

ID	Orientation (Dip/Dip direction)
1	86/267
2	03/042
3	81/334
4	72/019
5	74/019

From the previous table it is clear that the orientation of discontinuities is mainly sub-horizontal and sub-vertical resulting in blocks daylighting within the shaft. This "blocky" nature of the ground lead to some minor over-excavation, since the fissures' length were generally less than 1m. Neither faults nor shearzones were observed within the shaft and the adits.

4.3.2. HYDROGEOLOGY

There are three aquifers within the excavation site, the Upper, the Intermediate and the Lower Aquifer, named according to their water level.

The Upper Aquifer is located between the superficial deposits and London Clay and during excavation was intersected at 104m PD and no dewatering was undertaken due to the water caisson sinking method applied in that region.

The Intermediate one is found within the Harwich Formation above the Mid Lambeth Group. Since the latter contains discontinuous sand channels within the Upper Mottled Beds and sand units within the Laminated Beds, the Lambeth Group is more permeable than the London Clay and so, it was

important to control the water level above the Mid Lambeth Group as the stability of the adit invert and shaft base could be compromised.

As the shaft base was located within a sand unit, the dewatering process lowered the water level from 91m to 78m PD, so that they would be below the shaft base.

Fig. 4. 8 shows the water level drawdown measured by the three piezometers installed. As it can be noticed the water level decreased to the desired level in about a week, showing the influence of relatively higher permeability from strata bellow the London Clay.

The lower aquifer, consists of the Thanet Sands and Chalk formations, which are not represented, in Fig. 4.5. The shaft-dewatering target of 79m PD is above the piezometric profile of the lower aquifer and so works undertaken had little effect.

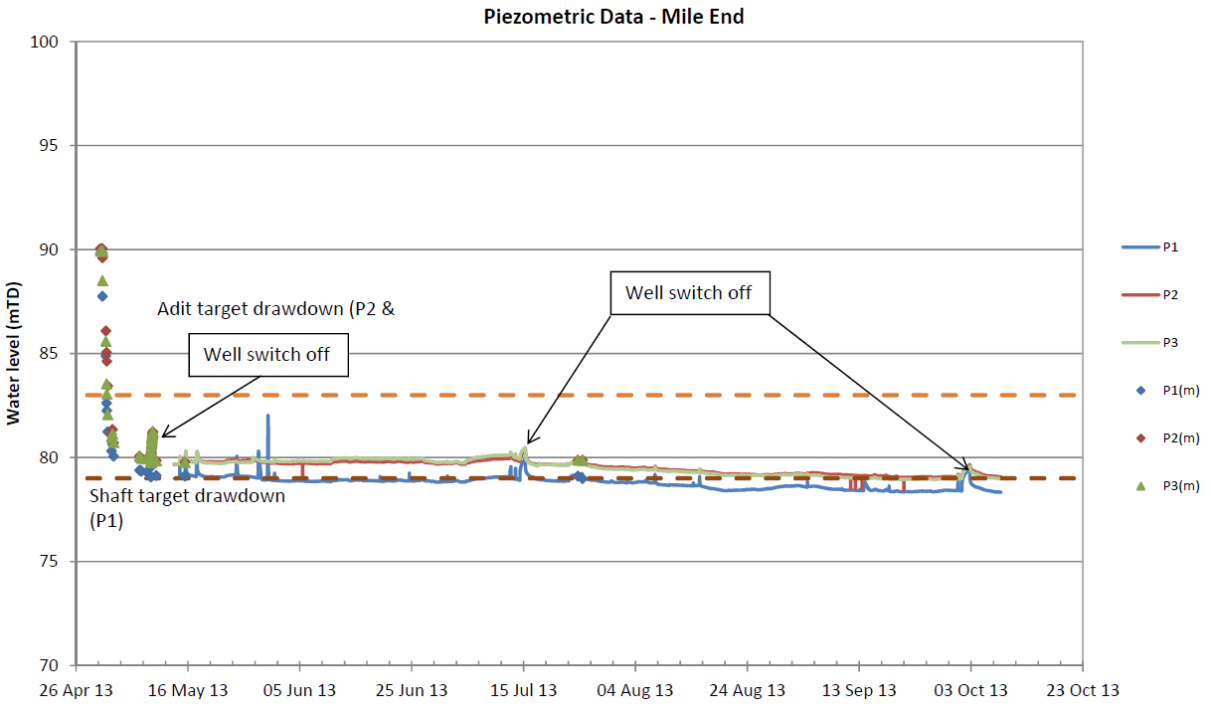

Fig. 4. 8 - Piezometric Data showing the water level drawdown, from Geotechnical Report

4.4. MONITORING PLAN AND DATA ANALYSIS

During underground construction, different phenomena occur due to excavation such as vertical and horizontal displacements at the ground level, drawdown of water level, variation of stresses in the soil mass and installed support, radial displacements along the lining of the excavation among others (these, are applied to either tunnels or shafts). Since in geotechnical works engineers have to deal with natural materials, which, despite having their resistance and state parameters tested in situ or/and in laboratory, are still associated to a degree of uncertainty regarding their behaviour throughout excavation. Therefore, those phenomena must be registered, studied and controlled, not only to keep safety, productivity and integrity of the construction itself, but also to avoid damage to the surrounding structures (especially if the works are taking place in highly developed urban areas).Hence, it is essential to set a monitoring plan that defines the instruments, their position, quantities to be measured and frequency.

This sub-chapter will present and discuss the monitoring data of the shaft obtained from the worksite, based on provided monitoring reports to the author. Since the numerical analysis performed in Chapter 5 will focus only on the shaft excavation and support construction, i.e., not considering the adits excavation, the in situ data discussed on the following sections will not go much further than the shaft completion date.

In Table 4.3 are presented the instruments installed and quantities measured in the Mile End case (or at least, the ones whose data was provided to the author).

Table 4.3 – Instruments used for the monitoring plan

Instrument	Number	Quantity	Unit	Notes[2]
Piezometer	3	Water Level	m	P1,P2,P3;
Inclinometer	2	Deflection/Horizontal Displacement within strata	mm	I1,I2;
Extensometer	2	Vertical Displacement within strata	mm	E1,E2;
Monitoring Points	-	Lining Convergence	mm	CB1/8
Monitoring Points	-	Ground Settlements	mm	A1-1/17; A2-1/7;

The viaduct that exists nearby was also a monitoring target, but due to lack of data, it is not going to be considered in this study. In addition, considering the position of the extensometers, their main purpose was to study the behaviour of soil due to the adits excavation and so, will not be considered in this discussion.

[2] This is the notation used in Fig. 4.9 obtained from one of the reports from the monitoring plan.

In Fig. 4.9, one can verify the position of the piezometers, inclinometers, extensometers and monitoring points for ground settlements.

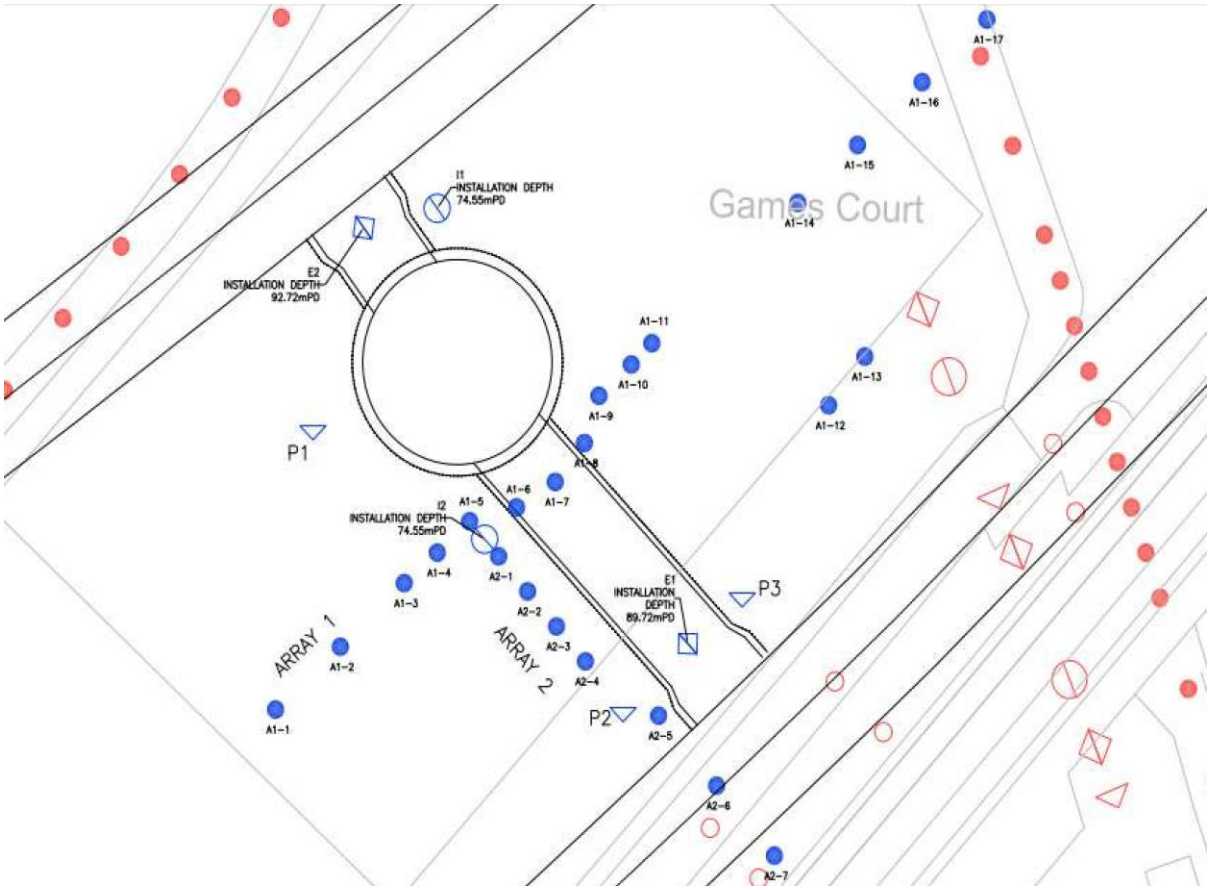

Fig. 4.9 – Location of monitoring plan instruments (from Monitoring Report)

It must be said that all the measurements and data to which the author had access are from the reports following the works from the beginning of SCL works, and so one cannot justify either missing or "odd" results from those.

Before passing to the next sections where measurements data will be presented, it might be important to summarize in the following Table 4.4 the construction sequence according to time, so that we can relate some result variations to the project different stages.

Table 4.4 – Dates from main construction stages

Date	Description
26/04/2013	Starts the dewatering process
17/06/2013	Starts the SCL works
22/07/2013	Shaft is completed
14/08/2013	Starts the excavation of the eastbound adit (IA1)
23/08 to 6/09/2013	Starts the excavation of the westbound adit (IA2)
28/08/2013	IA1 is completed
23/09/2013	IA2 is completed

4.4.1. Lining Convergence

In the shaft, sets of monitoring points were installed at three levels (8 points per level) on the support surface: 93.50, 89.78 and 86.16m PD, which shall be called, first, second and third monitoring sections, respectively.

At each level, the eight monitoring points have the following distribution, shown in Fig. 4.10.

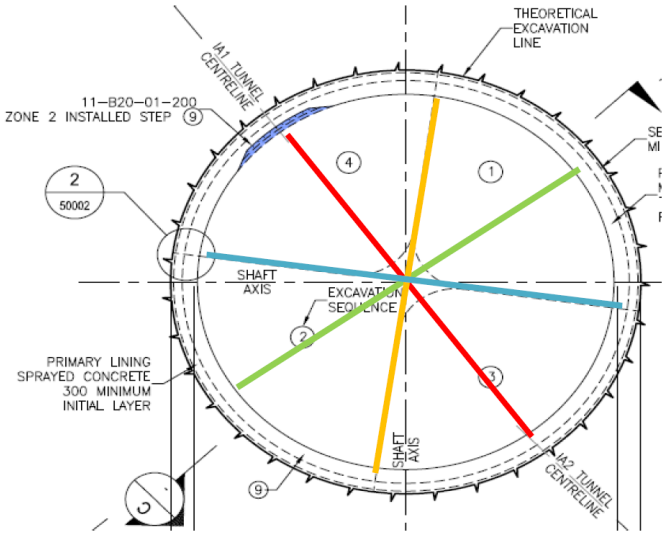

Fig. 4.10 – Distribution of monitoring points for lining convergence (from the monitoring report)

From every monitoring point, the coordinates (easting, northings and elevation) are measured, and from those results, the convergence is then calculated by comparing the distance between two opposite points at a certain date and the first registered value.

The graphs in Fig. 4.11 and Fig. 4.12 were obtained from the provided monitoring reports and present the evolution of lining convergence throughout time, from the beginning of SCL works until the end of adits construction.

In a monitoring plan, it is common practice to define limit values for a certain quantity that represents different degrees of warning. Generally these limit values are defined as a percentage of the values predicted during design. When those are surpassed, measures are taken to stabilize or invert the values and so, those limits are called "trigger values", since, in a way, they trigger an intervention. The trigger values adopted for the lining convergence are 10mm for "Green" (1st), 15mm for "Amber" (2nd) and 20mm for "Red" (3rd) warning. None of the case study reports provided to the author specifies how those trigger values were defined and what measures would be taken if crossed.

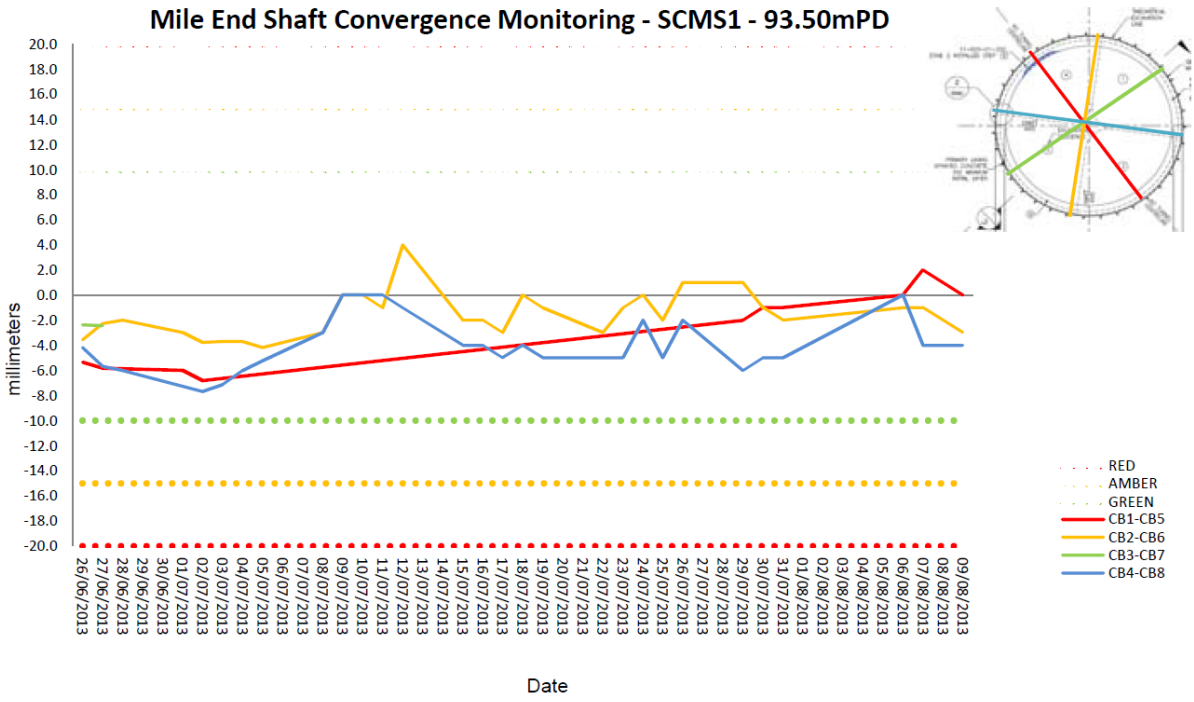

Fig. 4.11 – Convergence monitoring at 93.50m PD during SLC works, from Monitoring Report

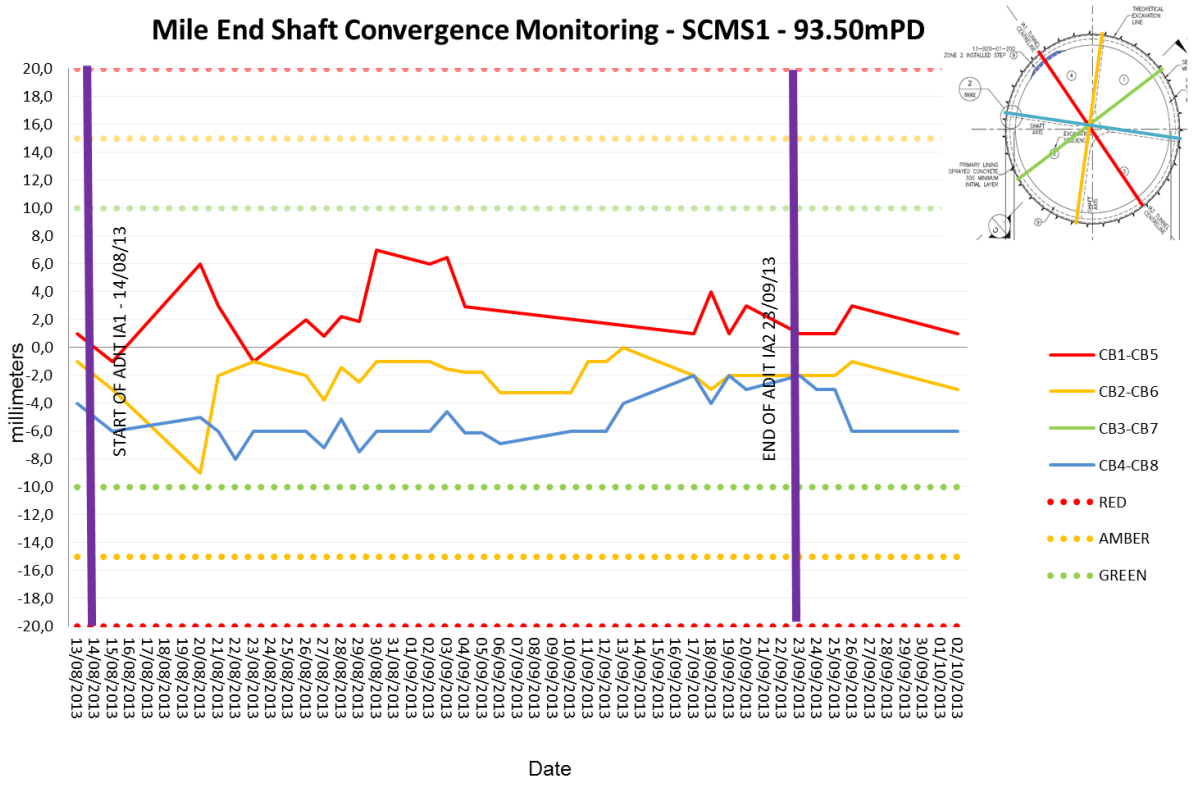

Fig. 4.12 - Convergence monitoring at 93.50m PD during Adits construction, from Monitoring Report

The values from the two previous figures show a certain oscillation, which can be explained by the high sensitivity of the monitoring devices to exterior conditions, as wind or temperature variation, for example, or even, to the vertical displacements the support may suffer, considering each pair of MP is not exactly at the same elevation. For practical purposes these values were processed so that only a mean value from each level was considered. In addition, the "suspicious" values, like sudden dilations, have not been considered on the average calculation. Table 4.5 summarizes some dates and shotcrete application evolution, as a complement for the data analysis.

Table 4.5 – Temporal evolution of support lining application

Dates	Excavation Base Level (m PD)	SC Application Level (m PD)	
		1st Layer	2nd Layer
27/06/13	90.86	90.86	-
5/07/13	89.86	89.86	92.86
11/07/13	86.86	86.86	88.86
15/07/13	~84.00	85.20	86.86
18/07/13	79.60	~83.00	85.20
25/07/13	79.60	81.40	82.00

Ideally, the chosen dates from the table above should be related with the excavation and application of support of the segmental rings following the MP, but the data provided to the author regarding time-construction progress does not achieve that level of accuracy. Figures from the progress report for the considered dates can be found in the Appendix II of this dissertation.

The next three figures (from Fig. 4.13 to Fig. 4.15) present the average convergence values throughout time for the three MP's.

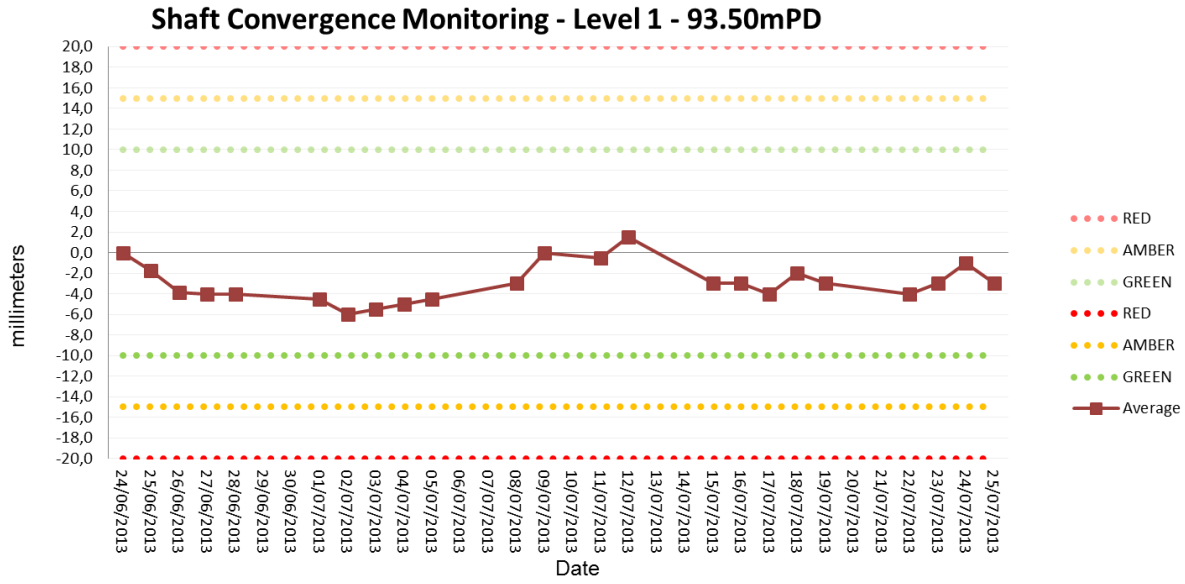

Fig. 4.13 - Lining Convergence, average values from MP - 93.50m PD

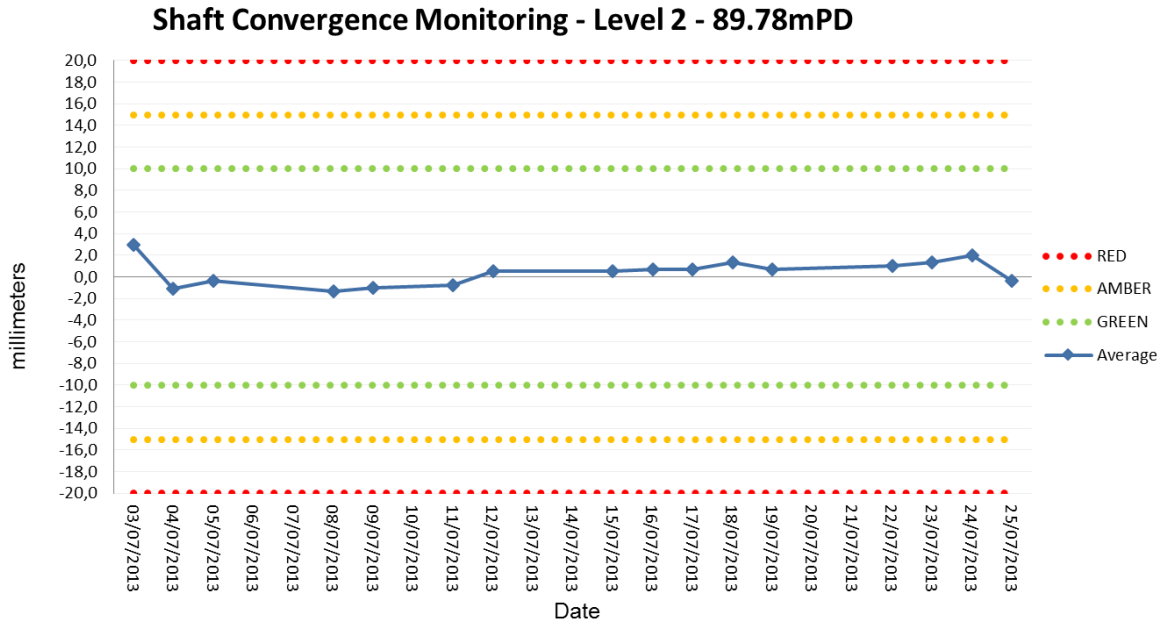

Fig. 4.14 - Lining Convergence, average values from MP – 89.78m PD

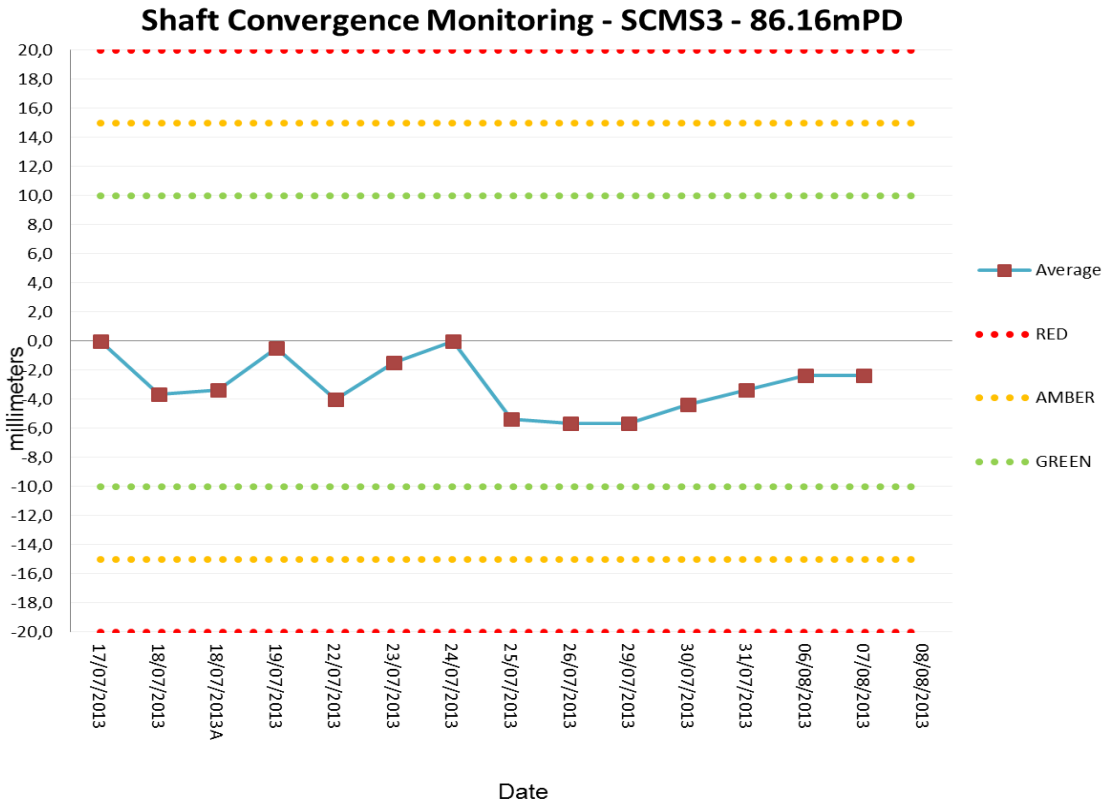

Fig. 4.15 - Lining Convergence, average values from MP – 86.16m PD

Analysing the previous figures, one can verify that, even using the average, eliminating some highly dispersive values, an oscillation is present throughout time. Therefore, the use of these values for further comparisons during the numerical analysis should be taken carefully and with criticism. Apart from this point, the order of magnitude of these values are in conformity to what was stated in Chapter 3 – practically all horizontal displacement occurs before the application of the support – since by the end of the excavation the convergence is no more than 2 mm.

4.4.2 HORIZONTAL DISPLACEMENTS BEHIND SUPPORT

Two inclinometers were positioned in opposite sides of the shaft and registered the strata horizontal deflection throughout its whole depth, as seen in Fig. 4.16. Both devices were positioned between 2 to 3,5 meters from the support (I1 and I2, respectively)

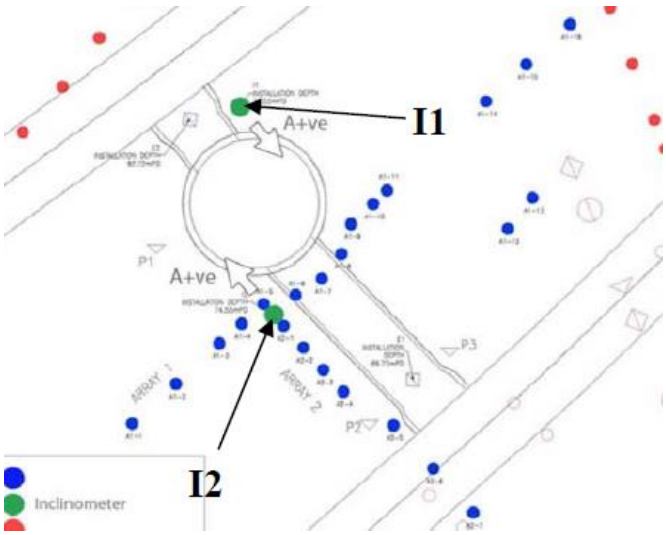

Fig. 4.16 – Inclinometers position (from the Monitoring Report)

Unfortunately, the data from the Monitoring Report provided only deflection values after the shaft excavation was finished, and so it is not possible to analyse its behaviour during excavation and support application, as it will be done in Chapter 5 in the numerical analysis. The data from both inclinometers is presented in Fig. 4.17 and Fig. 4.18. Once again, the shaft depth is very close to 30 m.

Since there is a lack of data during the excavation progress, only the deflection maximum values towards the shaft will be highlighted and used for further comparison: where for I1 it was registered 5.6mm at 26m depth and for I2 5.4mm at around 20m. Both figures also present maximum values for the opposite direction very near the shaft base. As for the variation in depth of horizontal displacements, one can notice some similarities with the several figures presented in Chapter 3 from 15m depth, where the shaft was built with a sequential excavation technique. Those similarities are clearer in Fig. 4.17 where from that depth is evident the increase of deflection.

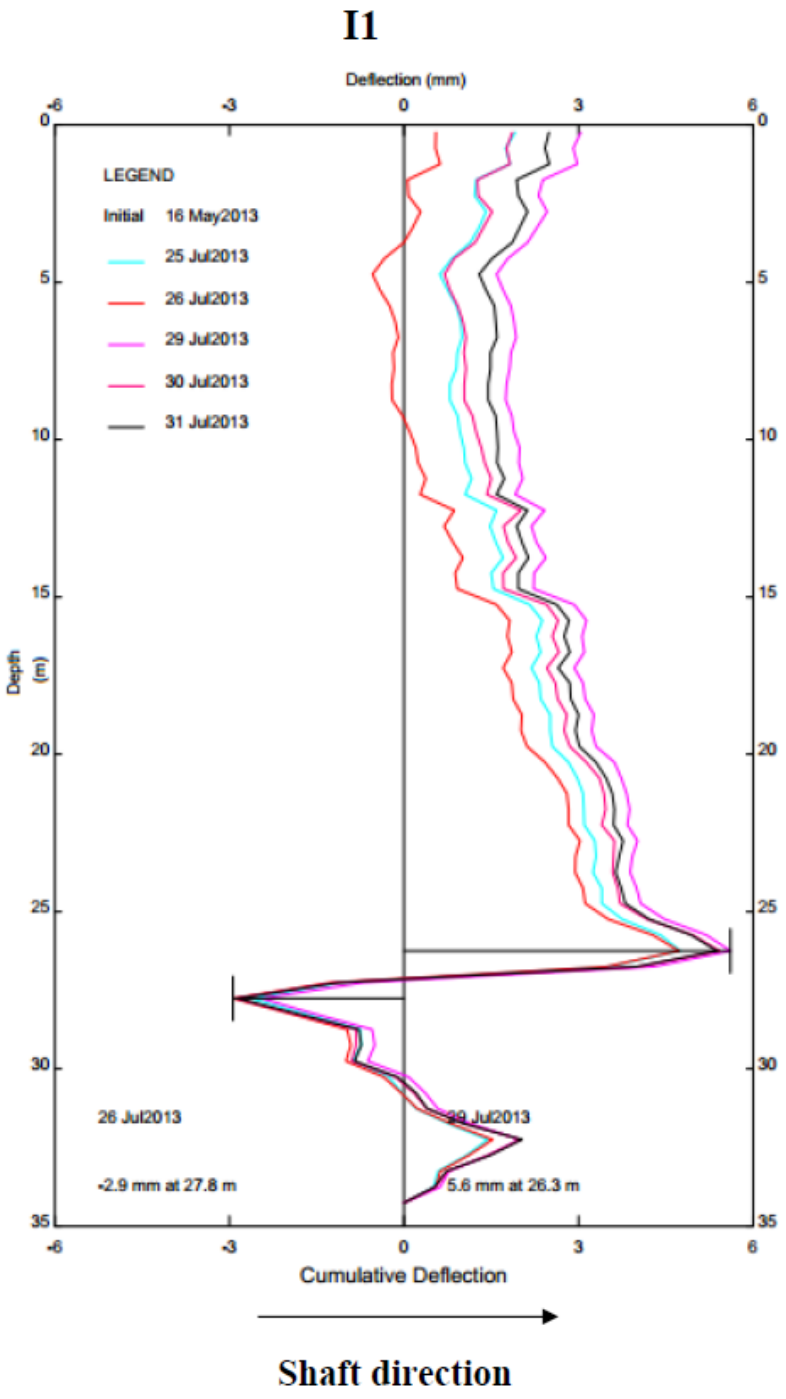

Fig. 4.17 – Deflection from I1 (from the Monitoring Report)

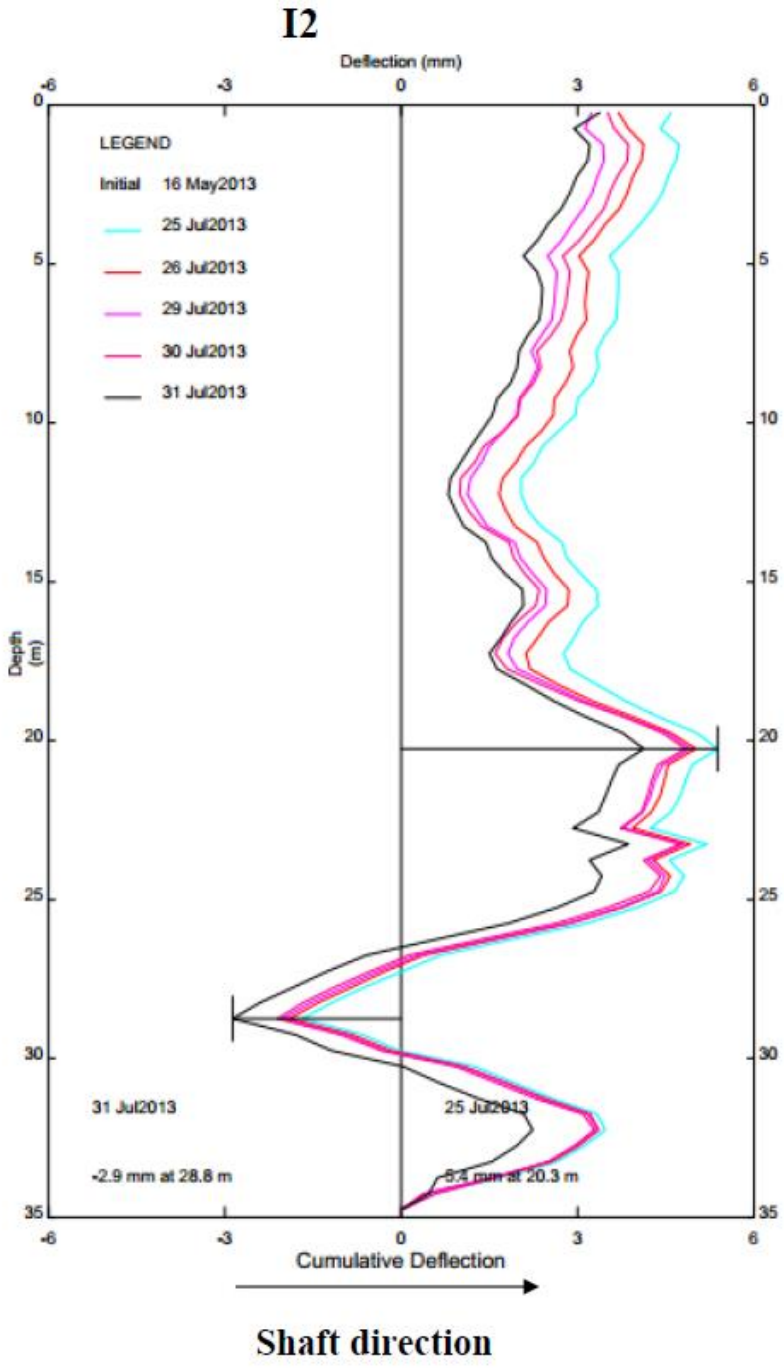

Fig. 4.18 – Deflection from I2 (from the Monitoring Report)

4.4.3. Ground Settlements

The monitoring points were positioned in two lines: Array 1 (A1) and Array 2 (A2), as showed in Fig. 4.9. Despite the fact there is data almost on a daily basis, this work will only focus around the highlighted dates shown in Table 4.4.

Considering the alignments A1 and A2 where MP's were positioned it is clear that the first had the main purpose of studying the vertical settlements on the adits transversal section produced by I2, and the latter the settlements produced by the shaft. Nevertheless, considering the shaft axissymmetry, the ground settlements, in theory, should be the same for equal distances from its axis and so, the data from A1 will be processed so that a similar graph from A2 data is obtained.

Once again, this dissertation will only focus on the behaviour of the shaft excavation and will not consider the adits influence.

4.4.3.1 Data Before SCL Works

Fig. 4.19 and Fig. 4.20 show the graphs obtained directly from the Monitoring Reports and considering the dates shown, the values should already reflect the effect of the water level dropdown and shaft construction with caisson sinking until around 15m depth. For this case, there are also trigger, or warning, values represented by the colours green, amber and red, where the latter, nearer the shaft represents a limit between 1.2 to 1.4 cm.

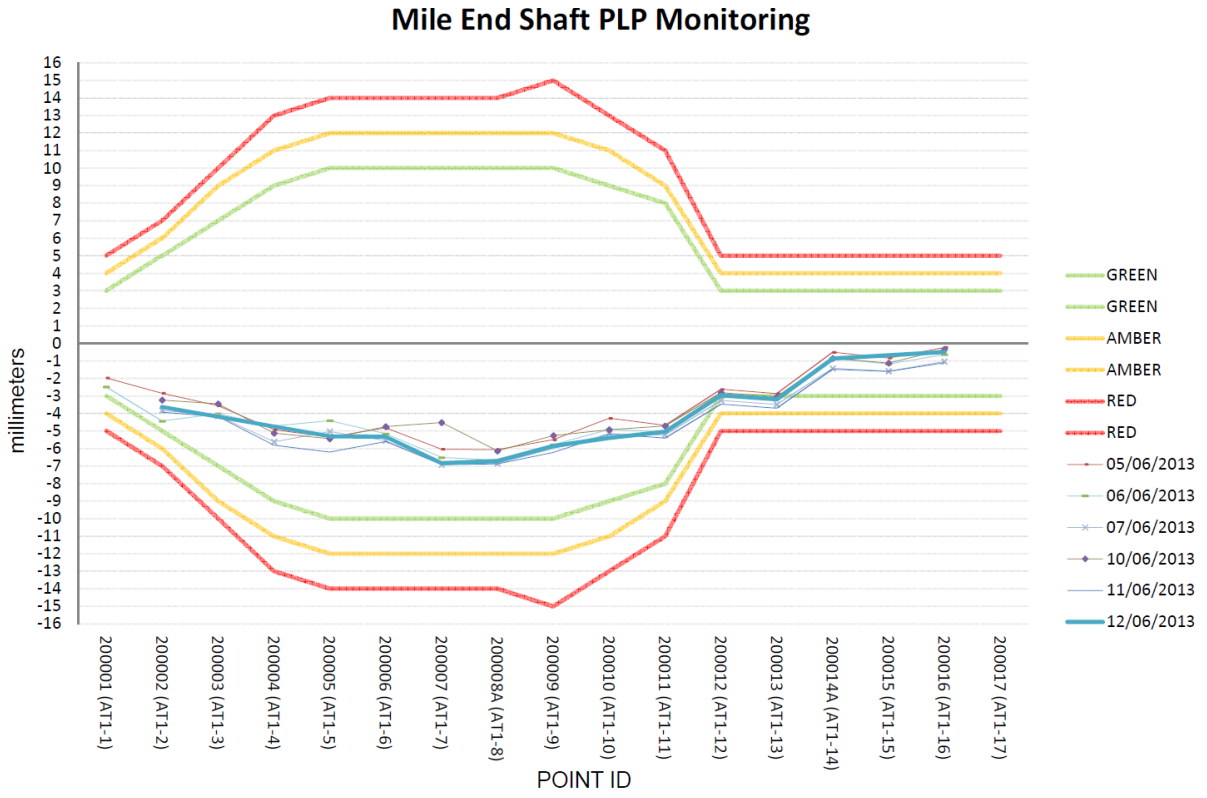

Fig. 4.19 – Ground Settlements from A1 – Before SCL works (from the Monitoring Report)

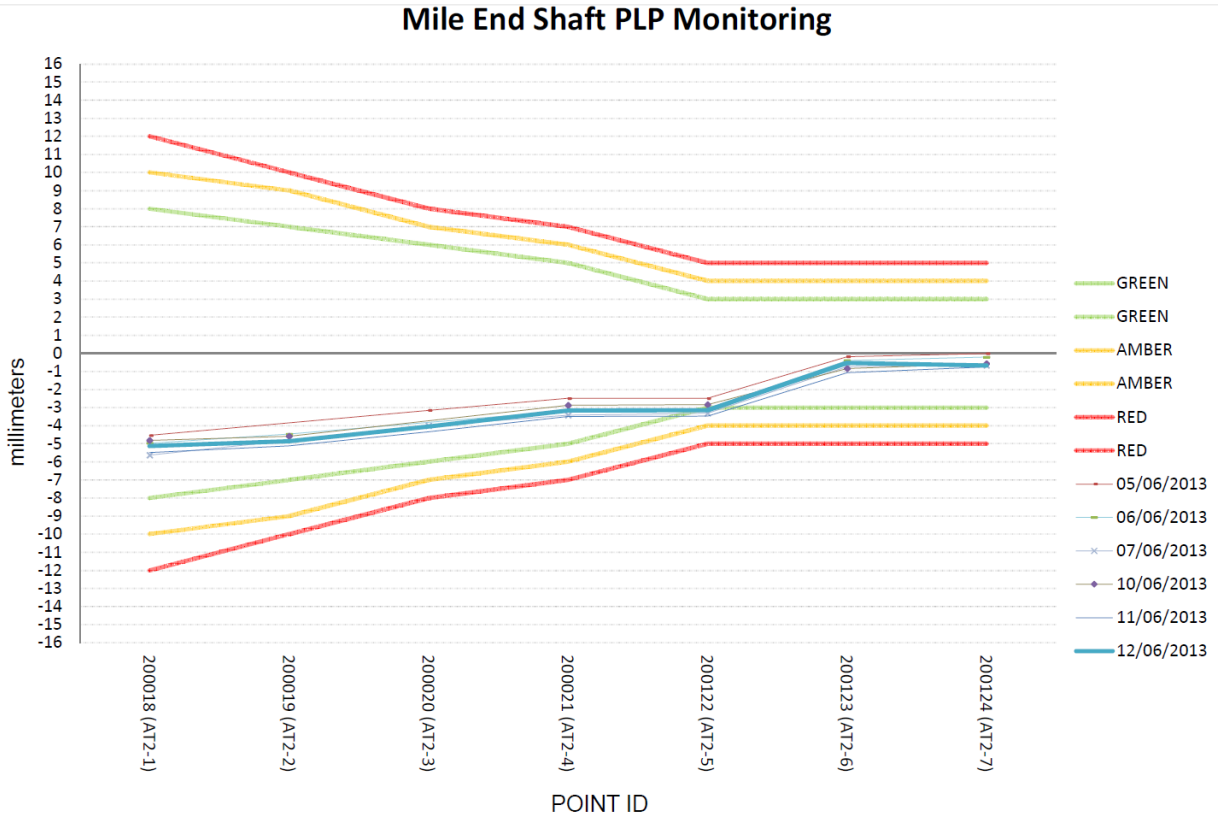

Fig. 4.20 – Ground Settlements from A2 – Before SCL Works (from the Monitoring Report)

The graph from Fig. 4.19 was then changed for a representation as shown in Fig. 4.20, and the data from the latter added on this new graph. For this purpose, and since the author was only provided with images in PDF format, firstly the monitoring points distance from the shaft excavation face were measured radially "by hand", which may lead to a certain error. Then, the ground settlements from A1 and A2 were "picked" directly from the figure, which can also produce slight deviations[3]. All the images from the monitoring plan report used in this process are presented in Appendix III of this dissertation.

Table 4.6 presents the measured distances for the MP's and the ground settlements measured "by hand".

[3] In each graph only the later dates will be considered for the analysis.

Table 4.6 – MP's Radial Distances to Shaft Excavation Face and Measured Ground Settlements

		Ground Settlements (mm)				
MP ID	Distance ~ (m)	12/06/2013	24/06/2013	09/07/2013	17/07/2013	25/07/2013
A1-5	2,8	-4,5	-7,0	-10,0	-12,0	-12,0
A1-6	3,0	-5,0	-6,5	-9,0	-10,5	-10,5
A1-7	3,0	-6,0	-8,0	-11,0	-12,5	-13,0
A1-8	3,0	-6,0	-7,5	-11,0	-12,5	-13,0
A1-9	3,0	-5,0	-6,5	-9,0	-11,5	-12,0
A1-10	3,0	-4,5	-6,5	-8,5	-11,0	-12,0
A1-4	4,6	-5,0	-6,0	-7,0	-9,5	-10,0
A1-11	5,2	-6,0	-5,5	-7,5	-9,0	-8,5
A2-1	5,2	-5,0	-6,0	-8,0	-10,0	-10,5
A1-3	6,8	-4,0	-4,5	-6,0	-7,0	-8,0
A2-2	7,5	-4,5	-6,0	-7,5	-9,5	-9,5
A2-3	9,8	-4,0	-4,0	-7,0	-8,0	-8,5
A1-2	11,4	-3,8	-4,0	-6,0	-7,5	
A2-4	12,1	-3,0	-3,5	-5,0	-6,5	-7,0
A1-12	14,8			-5,5	-6,5	-6,0
A1-14	14,8	-3,0	-3,5	-3,5	-4,0	-5,0
A1-1	15,9	-3,5	-4,0	-	-	-
A1-13	16,5	-1,0	-1,5	-6,5	-7,5	-7,0
A2-5	16,6	-3,5	-3,5	-5,0	-5,5	-6,5
A1-15	18,9	-0,7	-1,5	-2,0	-4,0	-4,0
A2-6	21,6	-0,5	-1,0	-2,0	-3,0	-3,0
A1-16	23,9	-0,5		-1,5	-1,5	-3,0
A2-7	26,2	-1,0	-0,5	-1,0	-2,0	-1,5
A1-17	29,6	-	-	-	-	-

So, the graph from Fig. 4.19, after the process mentioned above, turns into Fig. 4.21.

MPs with approximately the same distance from the shaft face present slightly different values of settlement and for that reason a continuous line connecting all the points could not be drawn.

From the analysis of Fig. 4.21 is noted that the effects of the water level decrease of the intermediate aquifer and the first 15m of supported excavation had little impact on ground settlements, considering that the nearest MPs only register settlements of around 5mm.

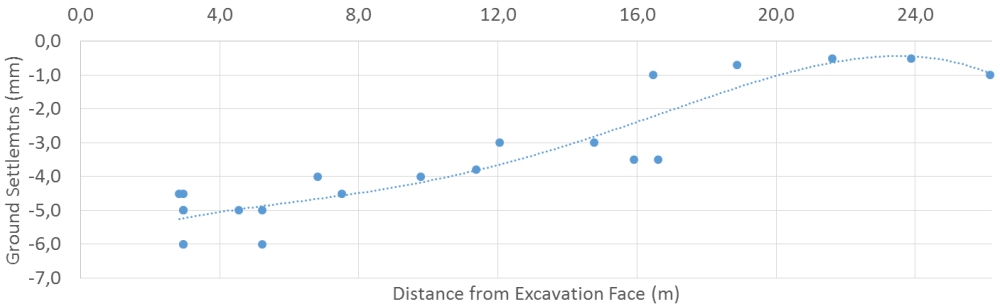

Fig. 4.21 - Ground Settlements from A1 – Before SCL works (12/06/13)

4.4.3.2 DURING SCL WORKS

As for the data during SCL works, the same process described in the previous section was also used.

Fig. 4.22 to Fig. 4. 25 present the ground settlements for the excavation evolution for the dates stated in Table 4.6. The dates related to those figures are close to the ones referred in Table 4.4.

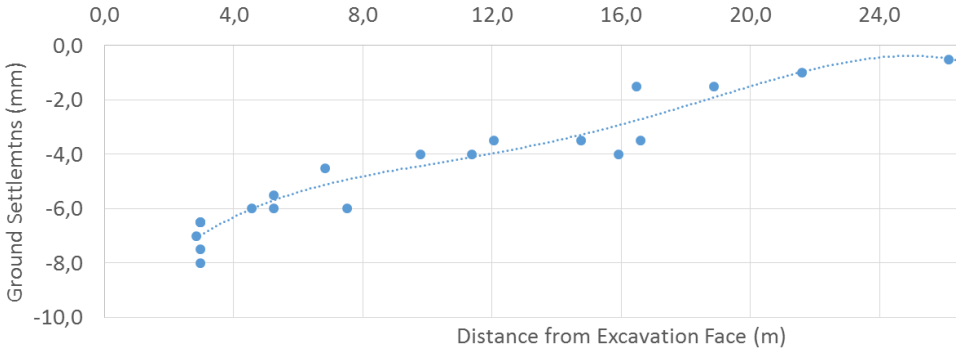

Fig. 4.22 – Ground Settlements during SCL works from A1 and A2 for 24/06/2013

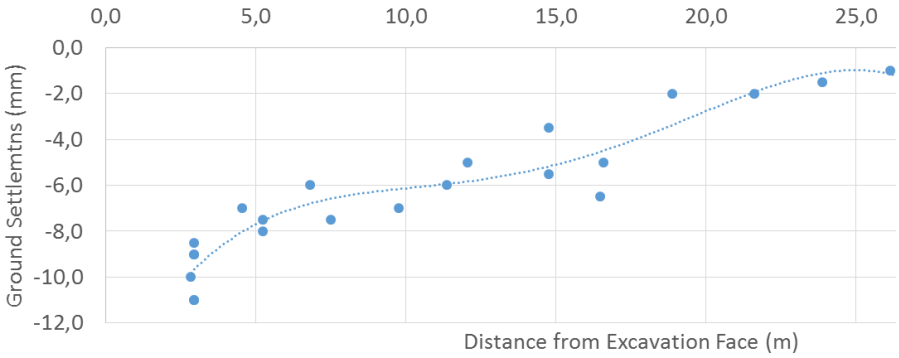

Fig. 4. 23 - Ground Settlements during SCL works from A1 and A2, for 9/07/2013

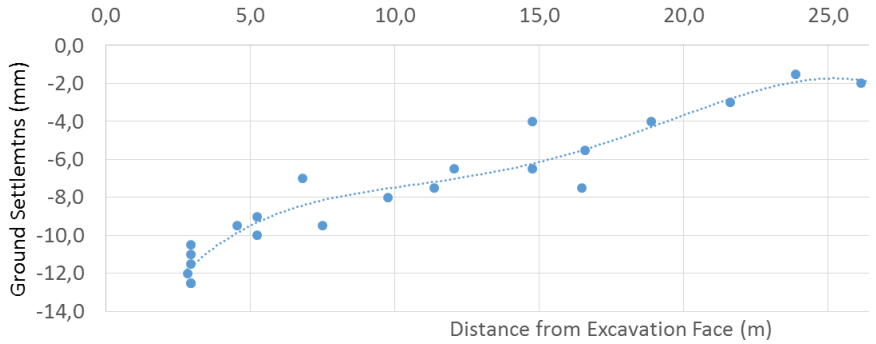

Fig. 4. 24 - Ground Settlements during SCL works from A1 and A2, for 17/07/2013

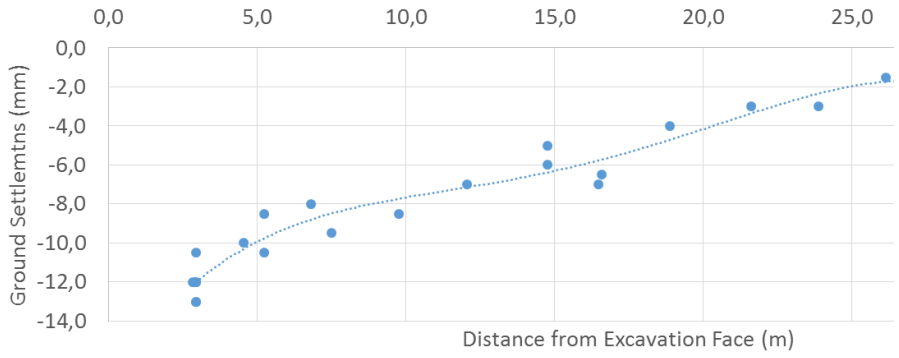

Fig. 4. 25 - Ground Settlements during SCL works from A1 and A2, for 25/07/2013

Analysing the ground settlement evolution in the previous set of figures and in Fig. 4. 26, the final values from the MPs closer to the shaft's face (around 3 m) show a maximum vertical displacement of around -12 mm. and minimum of 2 mm (25 m away from the shaft, corresponding near to 2 diameters of distance from the support). It is, then, evident the effect that the sequential excavation method has on the ground settlements. The maximum of this quantity, just behind the excavation face, suffers an increase in value of almost 2,7 times its initial value, before the SEM started. This maximum actually

surpasses the “Red Warning” limit represented in Fig. 4.20, of 12 mm, meaning intervention measures had to be taken. These measures, if taken, were not specified in any of the documents provided to the author.

Each graph did not show that sudden curve of settlements within 1D of distance described in Chapter 3 when discussing the general behaviour of a large diameter circular shaft. That may be explained with the fact that the example studied in that chapter was only theoretical, considering only one type of soil comprising the shaft full depth, its construction only employed the SEM and did not consider the water level dropdown. Although, by the time the shaft is practically fully constructed the trend lines tend to increase their inclination between 3 to 10m of distance from the excavation face, which can reflect the influence of the SEM employed.

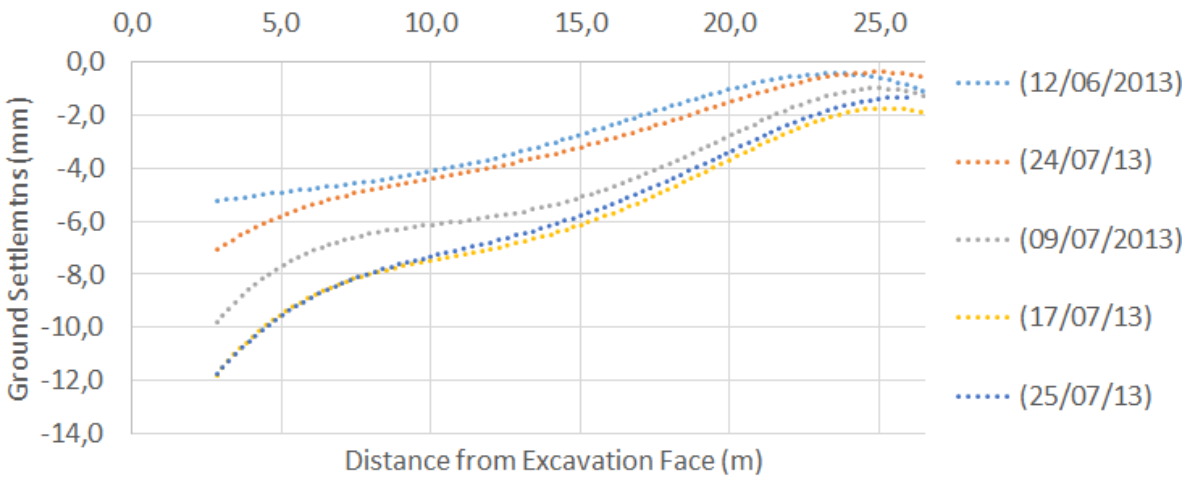

Fig. 4. 26 - Set of Ground Settlements from A1 and A2, for all analysed dates

4.4.4. SUPPORT – SHOTCRETE: HARDENING

According to the information obtained from documents regarding the construction, the material used as support had different samples subjected to laboratory compressive tests between 10min to 1 day after application and on site from 1 day to 90 days. To obtain the evolution of the compressive strength with time were used the average values for each sample, which are listed in Table 4.7 and represented in Fig. 4.27. Despite it was not stated in the reports, it was assumed that the samples tested had a cubic shape.

Table 4.7 – Mean compressive strength values from the Monitoring Report

Time		Mean Compressive Strength
"Description"	Hours	MPa
10min	0,17	0,31
20min	0,33	0,43
30min	0,50	0,52
40min	0,67	0,69
1hr	1,00	0,73
2hr	2,00	2,35
3hr	3,00	4,19
6hr	6,00	11,59
1d	24,00	48,00
3d	72,00	56,40
7d	168,00	59,30
28d	672,00	66,00
90d	2160,00	74,30

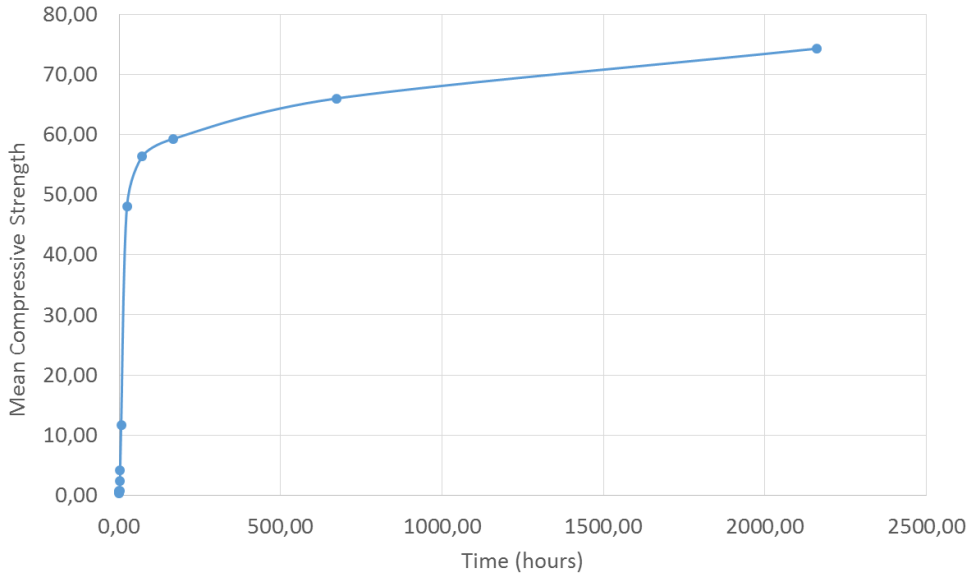

Fig. 4.27 – Evolution of mean compressive strength in time from the Monitoring Report

Using the expressions presented in sub-chapter 3.4 from the Eurocode 2 (EC2) and considering for f_{cm} (28d) the values listed in Table 4.7 and E_{cm} (28d) as 33.33 GPa, then one can obtain the Young's modulus variation in time represented in Fig. 4.28. As it can be noticed, by the end of the first day the material already achieves around 75% of its final stiffness, which stands around 34.2 GPa.

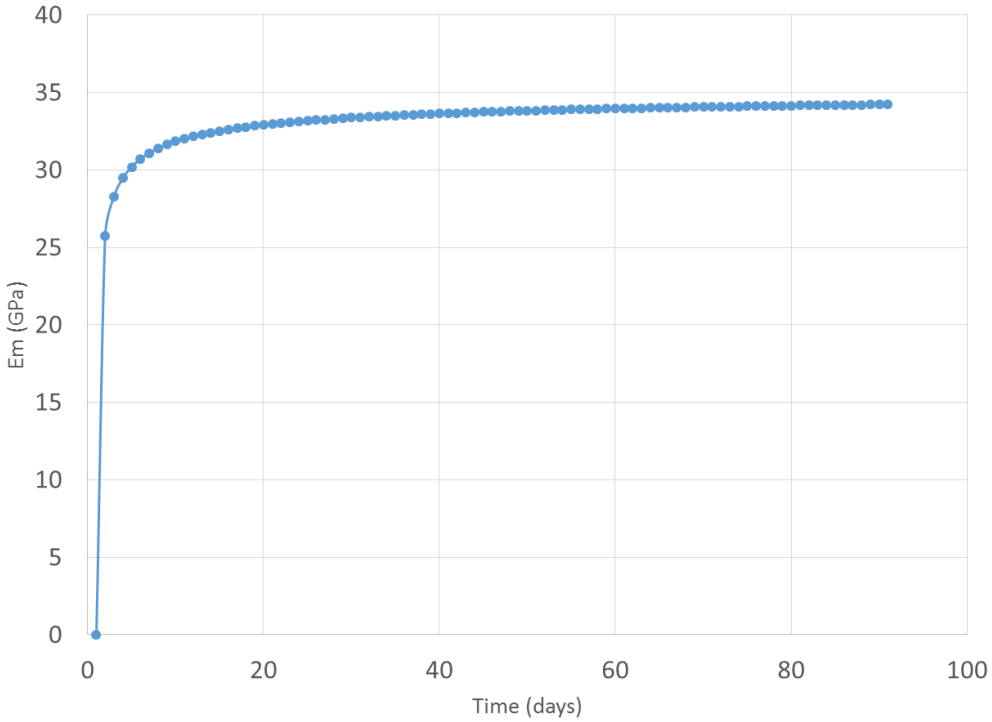

Fig. 4.28 - Young's Modulus variation in time, considering an EC2 expression

4.5. FINAL NOTES

The present chapter was essential to understand the context and characterization of the case study. The reports provided to the author regarding this construction played an essential role for the chapter development, although in some cases they either lack some data or the content was not so clear, as it was mentioned previously.

The shaft geometry, surrounding strata and construction process description in this chapter provides a good base for the author to define a quite similar model to the reality when using the software Midas GTS NX. However, for practical purposes, some simplifications will have to be done on that model, as it will be described in the next chapter.

One should keep in mind that the study presented in Chapter 3 regarding the behaviour of circular shafts is an important reference for this dissertation. However, as it was described in 4.2 the structure studied in this dissertation had half of its height excavated after the support application, contrarily to the case study in Chapter 3 where a sequential excavation method was employed in full depth. This will obviously lead to some different results and so, the comparisons between cases regarding their behaviour should be done with caution.

From the monitoring reports was possible to obtain values that can be used as reference for the results obtained in the numerical analysis of Chapter 5. Of course, one should already expect that a difference between those values and the numerical analysis results will exist.

As for the support, the data obtained from the reports allowed one to estimated an Young's modulus evolution in time, which will be necessary for studying the impact of the hardening process of the material in the behaviour of the case study structure.

5
Numerical Analysis

5.1. INTRODUCTION

The previous chapters allowed one to be acquainted with the main London Clay properties and design parameters, understand the basic phenomenology of shafts constructed with the sequential excavation method and to become acquainted with the case study – its geometry, construction methods, geological characterization and monitoring plan. Now, the present chapter will present and discuss a numerical analysis of the case study performed with the MIDAS GTS NX software (from this point, the latter will be referred simply as "Midas").

Midas is a software relatively recent both in the market (especially in Europe) and practically unknown to the author and both academic's frame of Faculty of Engineering of University of Porto and University College London. Having said this, and adding the fact that the references regarding this software are practically no more than its tutorials and user manuals, it was felt relevant to proceed to its validation prior to the purposed numerical analysis of the case study. This validation will be performed by comparing the axisymmetric model presented and discussed in Chapter 3 (see Fig. 3.10) and will attempt to capture the general behaviour rather than just obtaining very similar results – one should expect that different software often present different solver algorithms, leading to different results.

After this validation, the numerical analysis of the case study will be performed and divided into two major parts. Similarly to what was done in Chapter 3, firstly, a basic (or "baseline") analysis is performed following the failure criteria of Mohr-Coloumb. Then follows a parametric study including other factors in the shaft construction as the water level dropdown and the hardening of the shotcrete, for instance. In this second part, there will also be an attempt to compare the results obtained to the ones provided in the monitoring plan.

After Chapter 3 and 4, one can tell there is a special focus in this thesis on analysing numerically the sequential excavation method of the case study. However, one is already aware the construction in study presents around 15 m (from a total of 30 m) of its depth where another method was employed – wet caisson sinking method – whereas contrarily to the SEM the support is applied prior to the excavation. This will obviously lead to a different behaviour in both the soil and the support, which will be briefly characterized. In addition, the impact of having employed this method for practically half the construction of the structure will be studied and discussed.

5.2. MIDAS GTS NX VALIDATION

There was an attempt to make the model presented in Chapter 3 to be most similar: triangular elements were used in most areas, combined with quadrilaterals on the support. The main difference between the model in CODE_BRIGHT and Midas was the use of quadrilateral elements in an area that extends a

few meters behind the support and at the shaft base. The main reason for this change was to create a more uniform mesh in these areas where most stress and deformations variations occur in the soil so that more stable results could be obtained. Fig. 5.1 and Fig. 5.2 show screenshots taken from Midas representing the mesh used in this validation analysis in a general and detailed view, respectively.

This analysis and further discussion of results will be firstly focused on the general behaviour of the structure (variations in deformations, stresses and internal forces on shotcrete) and then, will include the effect of suction, implying to input a variation of parameters in depth (effective cohesion and Young's modulus).

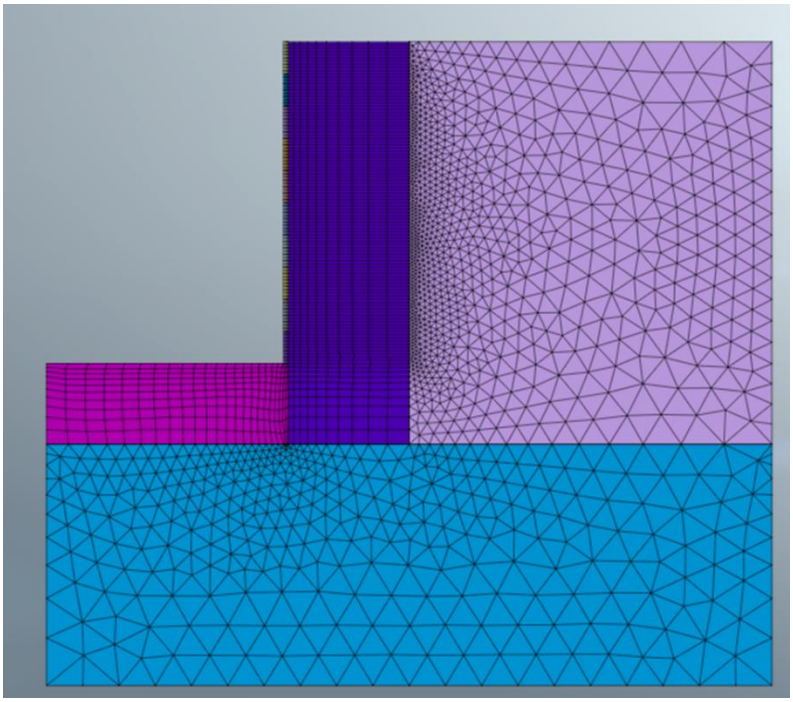

Fig. 5.1 - Midas validation: General view of the used mesh

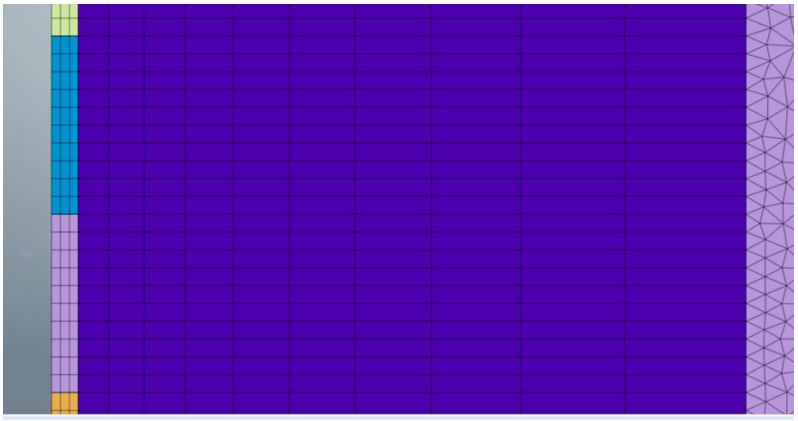

Fig. 5.2 - Midas validation: Detail of the mesh used for the support and area behind it

5.2.1. General Behaviour

5.2.1.1. Soil Deformations

Fig. 5.3 Fig. 5.4 present the contour plot for horizontal (Tx) and vertical displacements (Ty) respectively[1]. In the first, one can notice an increase of values for higher depths and the existence of a variation within each panel where higher values exist by their mid-height (this behaviour is more evident for higher depths), where the soil is completely unsupported. As for vertical displacements, there is a relevant upward displacement at the shaft base of around 1,8 cm, as expected. On the ground level, the contour plot shows higher settlements nearer the excavation face that tend to decrease for further distances. Fig. 5.5 shows the vectors representing the total displacement at the corner between the shaft base and excavation face, where one can notice the upward movement at the base and the soil mass movement towards the excavation on the vertical face.

The general behaviour of the model in Midas shows a very similar representation to the one in CODE_BRIGHT, although the results tend to be higher in the first.

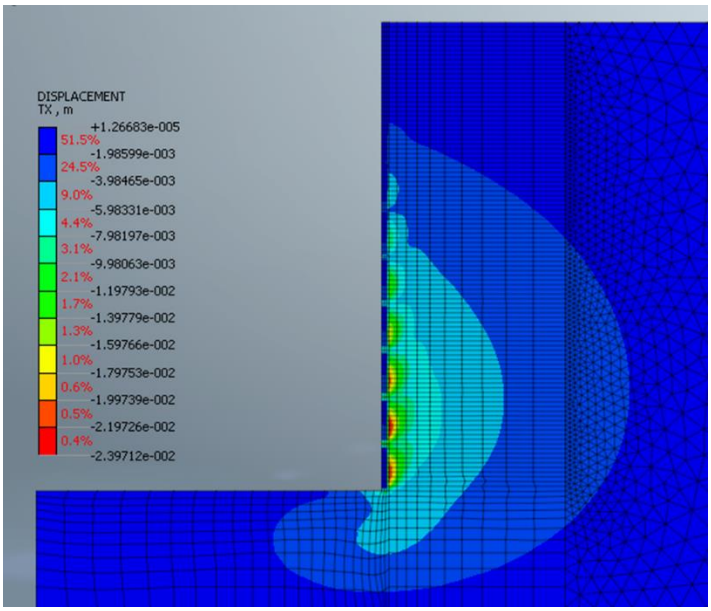

Fig. 5.3 - Midas validation: Horizontal displacements contour plot

[1] It must be clarified Midas considers a global axis XY, where X (horizontal) is positive from left to right, and Y (vertical) from bottom to top, which makes most of the horizontal displacements at the excavation face negative, for instance. The same applies for stresses.

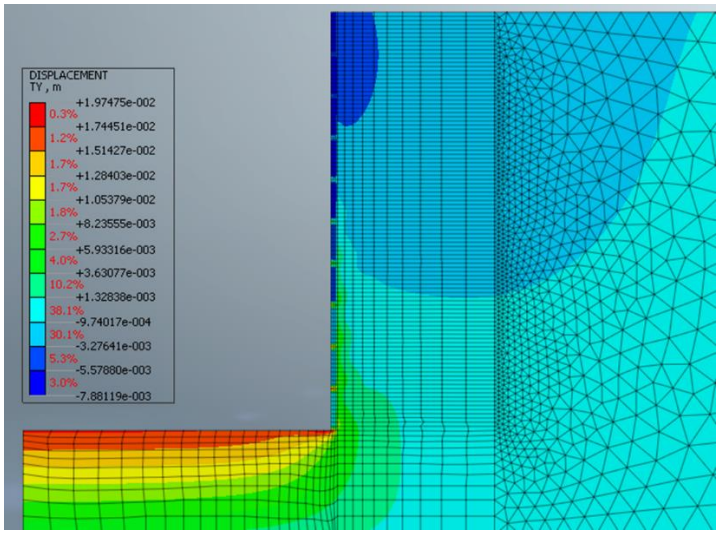

Fig. 5.4 - Midas validation: Vertical displacements contour plot

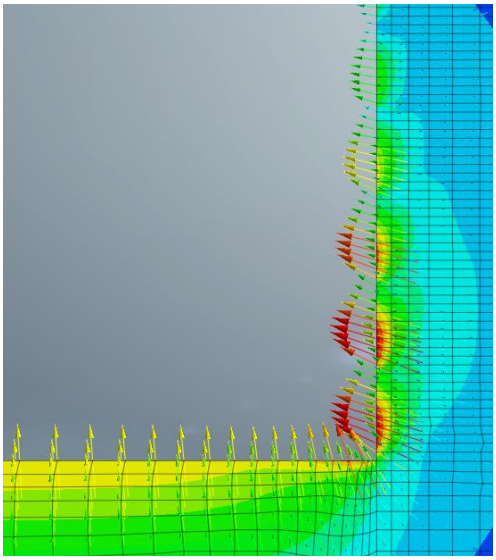

Fig. 5.5 - Midas validation: Vectors for total displacements

Fig. 5.6 enhances what has just been said regarding horizontal displacements. The latter shows different lines each one representing the horizontal displacements variation in depth for each excavation stage. In the final stage, one can notice the general increase of displacements in depth, whereas within each panel there is the kind of "parabolic" variation, achieving a maximum value at the mid-point and minima at the bottom and top points, which was verified and discussed in Chapter 3.

Comparing the influence of the excavation of one panel on the others above, one can verify that its influence extends, practically, to no more than its first “neighbouring” panel above.

The maximum value reached was around 2,2 cm in the 16-18m panel, consisting in a 0,5 cm difference from the model in Code Bright.

Despite the differences in both programmes regarding solver algorithms that can lead to some different results, there is another important factor: CODE_BRIGHT can provide the values obtained at the Gauss Points; Midas, in the other hand, only gives results at the nodes after an interpolation process at the Gauss points. The amplitude of this factor will depend if the variation of values for small increments of depth is significant or not. Looking at the geometry of the line representing the excavation at 20m depth one can suggest there might be an influence of that factor, but relatively lower, considering other cases that will be presented further.

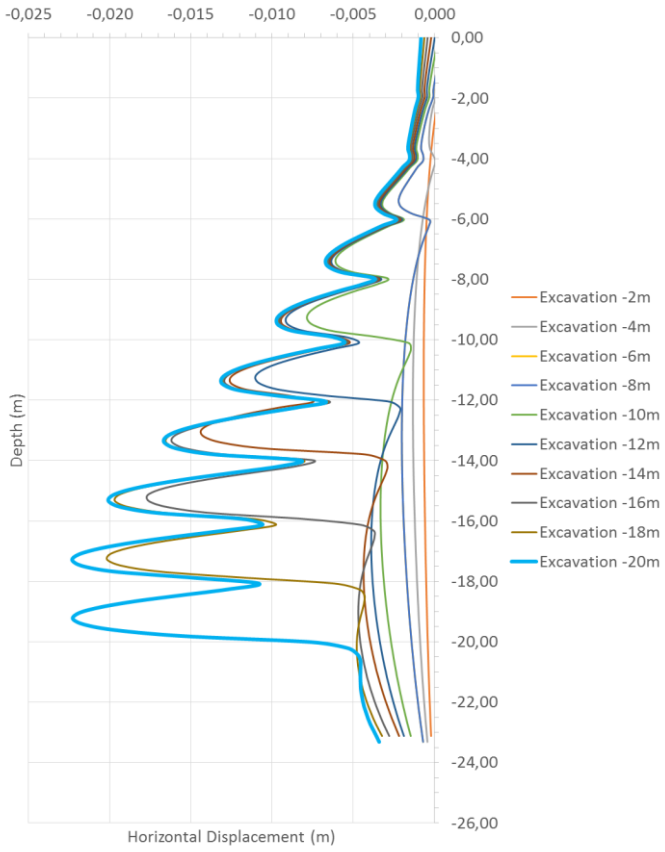

Fig. 5.6 - Midas validation: Horizontal displacements variation in depth for different excavation stages

Fig. 5.7 shows the horizontal and vertical displacements (or settlements) at the ground level. The behaviour is similar to the case in Chapter 3: Just behind the support, the ground settlements reach their maximum and for further distances the values tend to decrease towards zero; there is a sudden decrease from the maximum to around the distance of 1 radius (1R) from the support and then a slower variation from that point. The magnitude of values for the horizontal displacements are relatively smaller, the maximum reaches less than 2 mm. The values obtained in Midas are practically the same as in Code Bright.

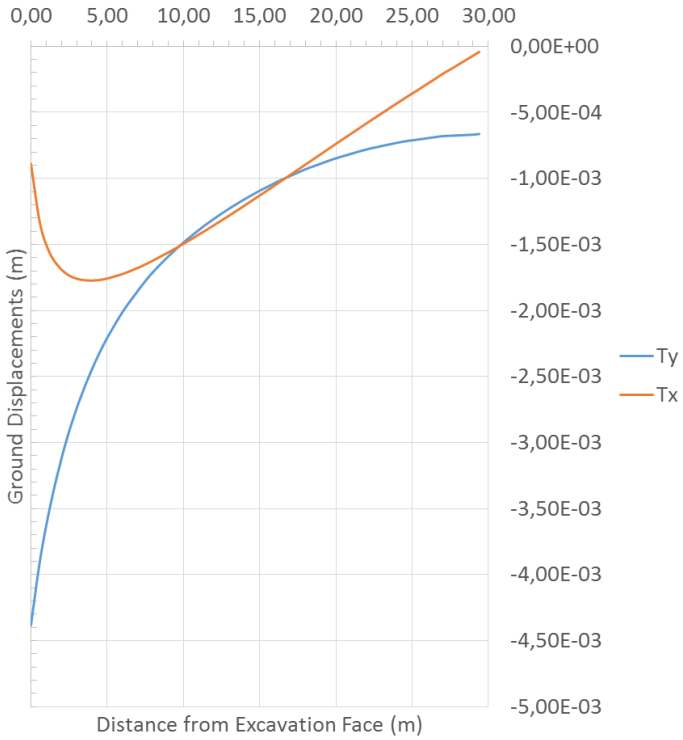

Fig. 5.7 - Midas validation: Horizontal and vertical displacements at ground level

5.2.1.2. Soil Stresses

The horizontal stresses contour plot is represented in Fig. 5.8. One can notice the higher values concentrated on the top and bottom points of each panel which validates the arching effect mentioned in Chapter 3. One can notice this effect extends also to the shaft's base. As for the vertical stresses – see Fig. 5.9 – there is a decrease in values on the shaft's base due to unloading and just behind the support due to stress distribution.

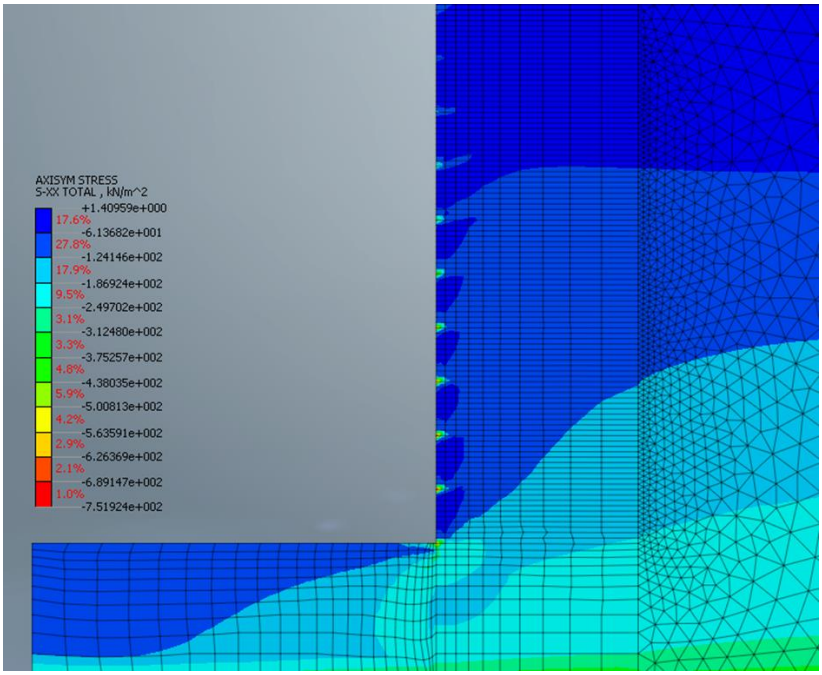

Fig. 5.8 – Midas validation: Effective horizontal stresses contour plot

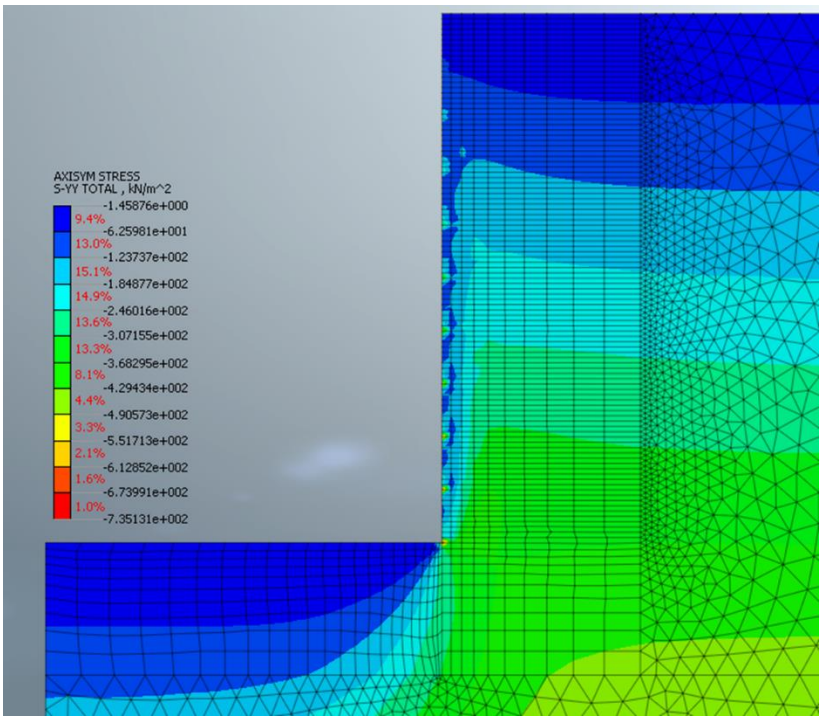

Fig. 5.9 – Midas validation: Effective vertical stresses contour plot

The horizontal stresses variation in depth presented in Fig. 5.10 is for the excavation of the last panel. For the line representing stresses just behind the support the behaviour of the horizontal stresses matches what was described in Chapter 3. Due to arching effect, the horizontal stresses are transferred to where the soil is supported, on top where is by the shotcrete and below, by the soil itself at the shaft base.

In the same figure are also represented the values for different distances from the support (2, 5 and 15 m), the horizontal stresses at rest (line "k_0") and in the active state (line k_a). One can notice that for increasing distance from the support, the lines tend to get closer to the values at rest. For 15 m from the support, the stresses are practically the same as at rest, which shows how local the variations in stresses are in these structures. This behaviour was already pointed out in the CODE_BRIGHT model in Chapter 3. Therefore, generally the model in Midas follows the expected phenomenon, but, if one analyses the values in more detail, one will notice a maximum of around 630 kPa just behind the support, whereas in the model of CODE_BRIGHT was around 400 kPa. This relevant difference might be due to that interpolation issue mentioned in 5.2.1.1, where the values are only displayed for the nodes after interpolation at the Gaussian points. One can notice that the line representing the horizontal stresses just behind the support presents a very high variation of stresses for very small increments of depth by the bottom of each panel. For example: from the results obtained in Midas for the ring -14/-16 m in depth, close to the bottom an increment of 20 cm presents a growth in stresses close to 400kPa. Therefore, this issue turns out to have an important relevance in results.

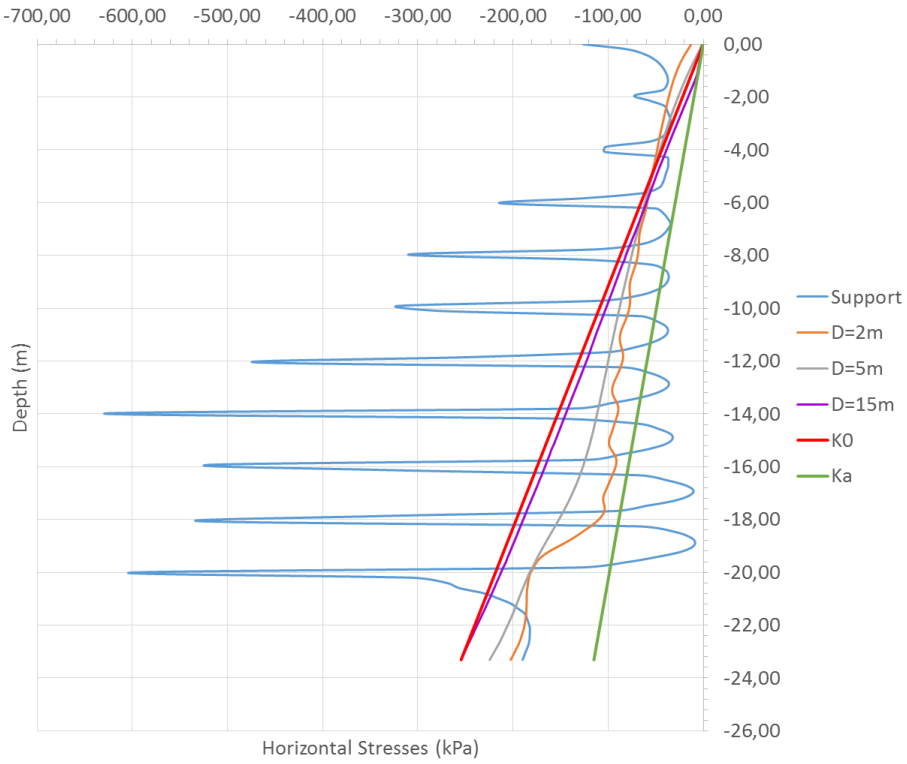

Fig. 5.10 – Midas validation: Effective horizontal stress variation in depth for different distances from the support

As mentioned when referring to Fig. 5.9 the vertical stresses suffer a decrease in value by the mid-point of each panel and an increase in depth at the bottom and top, that can be noticed in Fig. 5.11. In the latter, are represented the variation in depth of vertical stresses for different distances from the support and for the case "at rest". This behaviour is extremely localized so that for 2 m of distance the line is practically coincident with the line representing the stresses at rest.

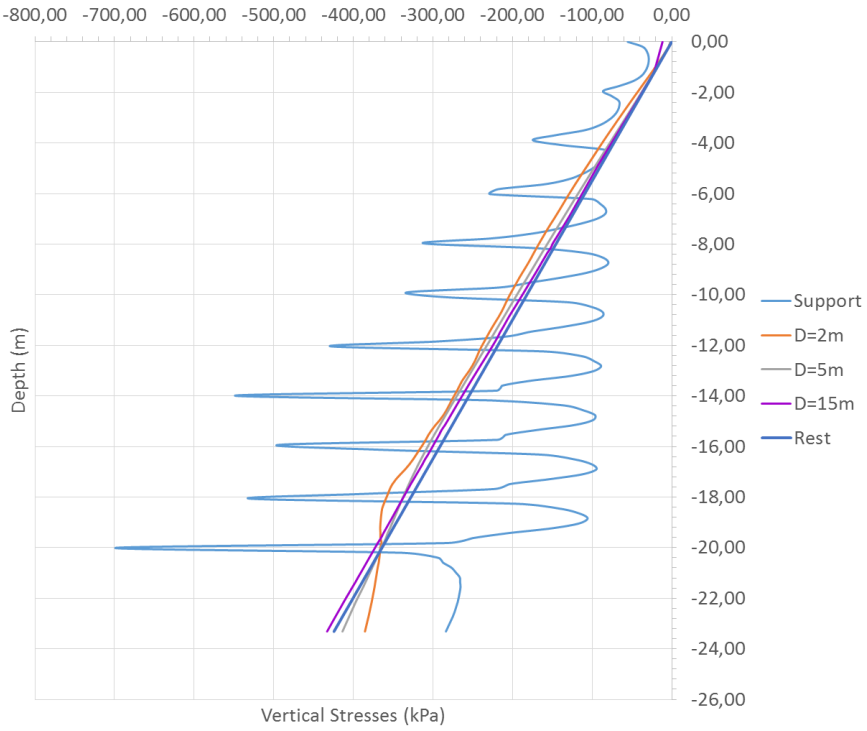

Fig. 5.11 - Midas validation: Effective vertical stress variation in depth for different distances from the support

5.2.1.3. SUPPORT INTERNAL FORCES

Contrarily to displacements and stresses, Midas does not provide directly the internal forces to the user since it was used a "solid element" for the support, instead of a shell (or "zero-thickness) element. Ideally, in order to calculate the internal forces one should pick the stress values for the set of nodes of the support at the same depth and calculate coming from the variation. This procedure was done for bending moments, due to this case's simplicity – there was practically a linear variation for each set of nodes at the same depth. However, for hoop and shear forces the process was not so simple and so, for practical purposes the author considered the average values of the set of nodes.

Fig. 5.12, Fig. 5.13 and Fig. 5.14 present the hoop forces, bending moments and shear forces variation in depth, respectively. In general, all the representations in those figures show a very similar behaviour to the ones presented in Chapter 3:

- The hoop forces vary almost linearly within each panel, achieving a maximum at the bottom and a minimum at the top, which is practically constant in every panel. However, the maximum values within each panel are considerably lower relatively to the model in CODE_BRIGHT, where the maximum achieved almost 2500 kN/m whereas in Midas doesn't exceed 1700 kN/m;
- The bending moments present variation within each panel, reaching a maximum at around their mid-point, as expected. The values shown are slightly lower than the analysis in CODE_BRIGHT;
- Finally, the line representing the shear forces variation in depth also presents a fairly similar "shape" to the one obtained in CODE_BRIGHT, although, its values are relatively higher. Actually, since at the bottom of each panel there is an enormous increase of values for very

small increments of depth, this might be another case whose results were influenced by the interpolation issue already mentioned in 5.2.1.2;

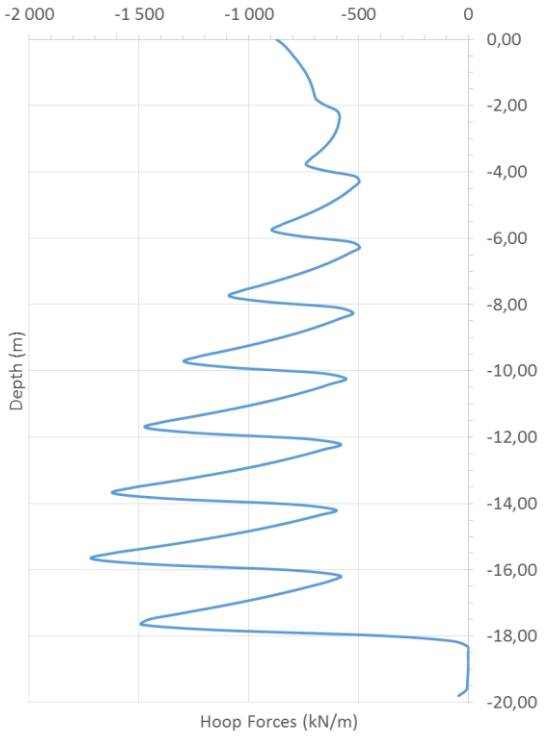

Fig. 5.12 - Midas validation: Hoop Forces variation in depth

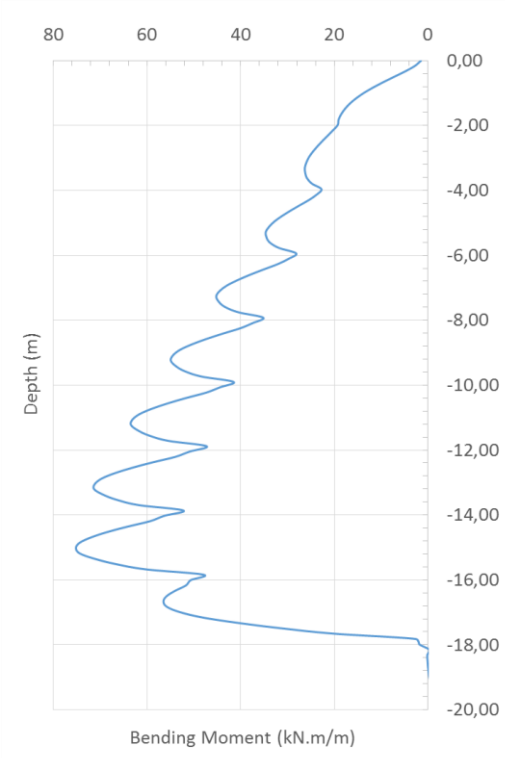

Fig. 5.13 - Midas validation: Bending moments variation in depth

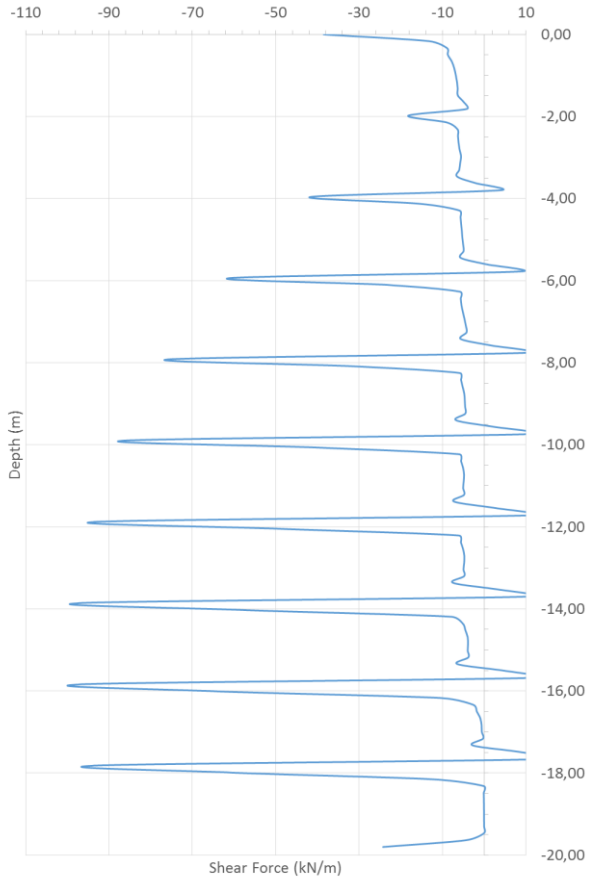

Fig. 5.14 - Midas validation: Shear forces variation in depth

5.2.2. UNSATURATED CONDITION

The suction effect is a point that was included in this validation since it deals with parameters variation in depth. In his analysis, Topa Gomes (2008) included the suction effect on the soil in, let us say, a "mechanical approach", since that author simulated it by increasing either Young's modulus or cohesion (or both) for increasing negative pore water pressure.

That analysis was also included in this validation and its effect on horizontal displacements is presented in Fig. 5.15 – in that figure are also presented the results for the basic analysis represented in Fig. 5.6.

The increase of the values of c' and E considered is the same shown in 3.3.4. The main behaviour of those three lines looks reasonable since increasing in depth E and c' (or combining them) actually decreased horizontal displacements. As discussed from the results in CODE_BRIGHT, for the resistance (c') case for the lower rings closer to the base, the results tend to approach the baseline values. On the other hand, E' shows some sort of "uniform" trend in depth, which shows higher relevance than c' (mostly because the range of values is greater than the latter and it was already confirmed E alongside k_0 are the most influential parameters). In addition, as previously discussed, closer to the shaft's base E has values closer to the one which combines both resistance and deformability, where the results are lower than any other case, as expected.

As it has being noticed, despite the behaviour is similar to what was discussed in Chapter 3, the values are still generally higher, which might be understandable, considering the causes already mentioned.

Midas, as most geotechnical software in the market, already provides a feature that allows the user to define the water retention curve (water content-suction). Therefore, besides the "mechanical approach" to simulate suction, it was also included in this validation an analysis where the soil was actually defined with an unsaturated condition. For that purpose the Van Genuchten (1980) equation with 4 variables was used and those values were determined by Topa Gomes (2008) based on laboratory test data for residual soil. The results obtained are also included in Fig. 5.15, represented by the "Unsaturated" line. Generally, the values for this case are lower than the baseline, as expected, and for increasing depth the values tend to approximate that line, opposed to what was noticed when combining the effect of increasing c' and E. Other particularity of this case is that for lower depths the horizontal displacements values are actually positive, with lower magnitude, though (less than 5 mm). In addition to this particular analysis Fig. 5.16 shows the pore water pressures variation in depth - one can confirm the phreatic level position at the shaft's base for 0 kPa and the suction value at the top; and in Fig. 5.17 is presented the water retention curve based Van Genuchten (1980) equation, where for decreasing water content there is an increase of negative pore water pressure (suction).

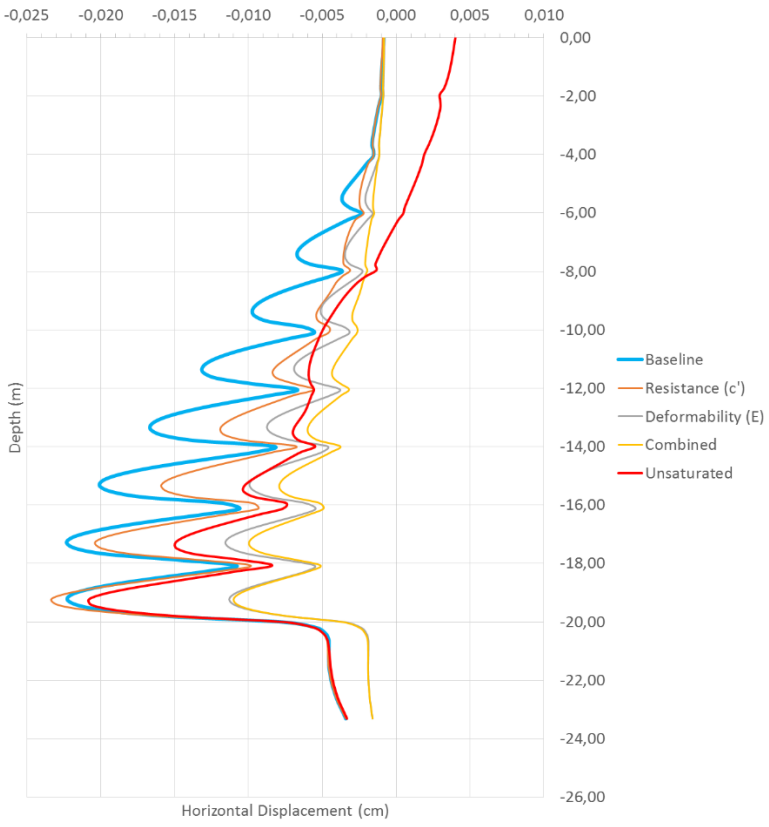

Fig. 5.15 - Midas validation: Horizontal displacements variation in depth considering suction

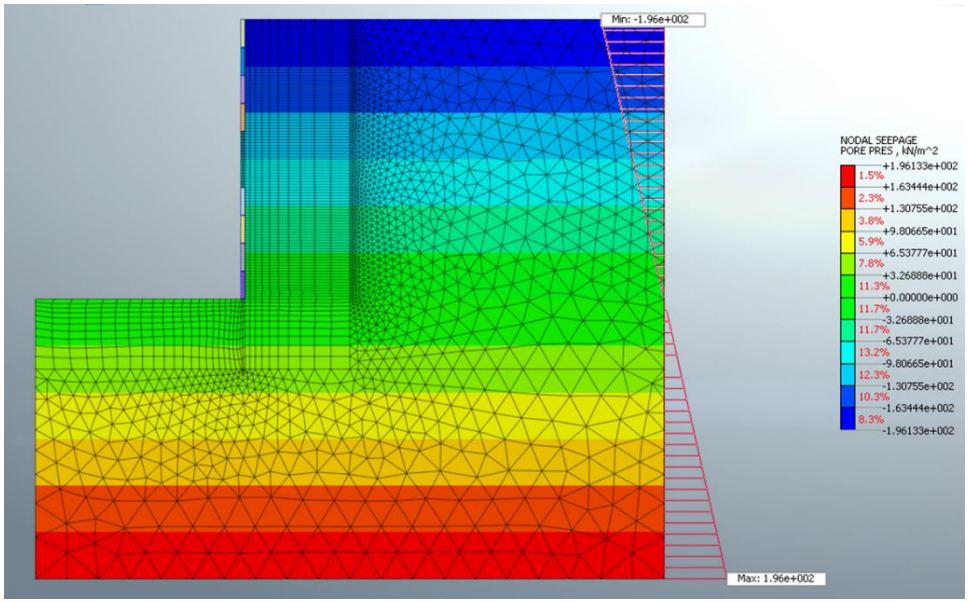

Fig. 5.16 – Midas validation: Pore water pressures considering unsaturated condition

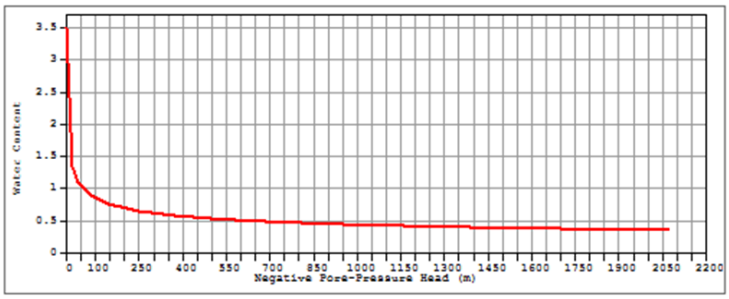

Fig. 5.17 - Midas validation: Water retention curve used for unsaturated condition using Van Genuchten (1980) expression

5.3. THE CASE STUDY – NUMERICAL ANALYSIS

The following sections will present and discuss the numerical analysis for the case study. The study case model is considerably more complex than the model dealt in 5.2. The previous model discussed in that sub-chapter and in Chapter 3 was of a "simple nature", since the structure crossed the same homogenous soil; the support only included one layer at the excavation face and at shaft base was not even considered. Having said this, it was felt relevant to introduce a few notes describing the model.

In the numerical analysis of the case study there will be a main focus on analysing the displacements of the structure and of the surrounding soil mass mostly because, that was practically all the data the author was provided from the monitoring point in order to compare results.

5.3.1. INITIAL NOTES

5.3.1.1. GEOMETRY

The geometry of the shaft itself, as described previously, has a diameter approximately 12 m and around 30 m of depth. The precast concrete lining has 0,30m of thickness and the shotcrete, counting with the 2 layers, is 0,60 m thick. The support at the shaft's base in the cross section view is circumferential with a radius of around 2,8m (the reports related to the case study provided to the author does not provide a direct value of this radius, so one had to calculated it based on scaled images). The model is represented in Fig. 5.18.

The model extends horizontally around 38 m from the excavation face. It is true that from the discussion made in Chapter 3 and confirmed in 5.2, the main variations in soil for these kind of constructions occur relatively near the structure compared to tunnels, but it was the choice of the author to extend that vertical boundary until the position of the last monitoring point for ground settlements was reached. As for the lower boundary it was extended to a few more meters than 1D.

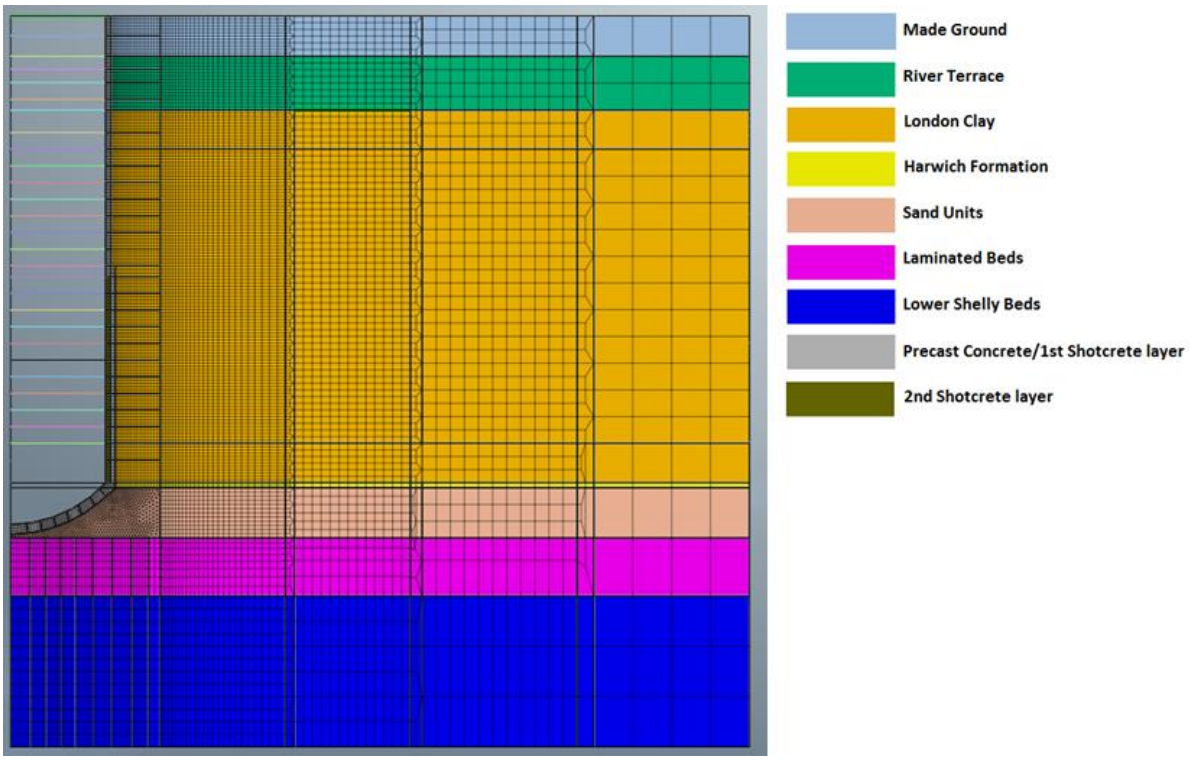

Fig. 5.18 – Case study: Geometry of the numerical model

5.3.1.2. MESH AND ELEMENTS

The author opted to use 4-node quadrilateral elements in practically the whole model, except at the shaft base due to its curved geometry, where only triangular elements were employed (mixing quadrilateral and triangular elements was something the author avoided since a few references warn it may cause numerical instability when running the model).

The smallest elements of the mesh were placed at the shaft's base and behind the excavation face, since one knows already those are the areas where the main variations occur in the soil. As the distance from those areas increase, the elements size also increases as well, and so, the author had to use "transitional columns" - see Fig. 5.18 - those columns, constituted by quadrilateral elements, allowed an increase of height without employing a mix of triangles and quadrilaterals.

Finally it should be said that the support was modelled with regular elements of 0,10x0,20 m (width x height). Therefore, the support was modelled by employing a "solid element", as done in the model of Chapter 3 and 5.2, and not a "shell element". Despite the second provides great advantages like, when using it the software calculates directly its internal forces , it might introduce some numerical problems as poor convergence or unstable integration points (Potts, Zdravkovic, 2001)

Midas provides an option that seeks for, what it calls, “poor elements” that can lead to unstable or “odd” results. This classification is done having in consideration some parameters as the “aspect ratio”, the “skew angle” or “warpage” and others – their definition can be easily found in the user’s manual of Midas (User’s manual, Chapter 4, p.275). Fig. 5.19 shows the location of those elements in the model (in the Harwich Formation close to the support) and, although, one can notice their number is practically null, they are located within a “critical area”.

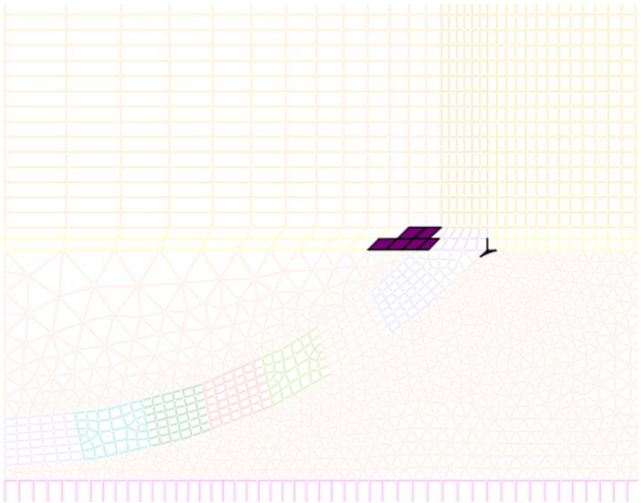

Fig. 5.19 - Case study: "Poor elements" represented by the “dark” colour

5.3.1.3. CONSTRUCTION SIMULATION

Every excavation lift was executed, in average, for every 1 m of depth, as it was mentioned in chapter 4. The horizontal lines crossing the shaft of Fig. 5.18 represent every excavation stage.

The first part of this construction was made by sinking the precast concrete rings into the soil. This construction method was simulated by starting to replace the material at the specified meshes from soil to concrete (see Fig. 5.20). Despite the reports from the construction site did not refer the height of the precast rings, the author assumed it to be around 1 m, so that it would coincide with each excavation

stage. In this model, every excavation stage was executed when the support had already been sunk two rings below (which would consist of around 2 m below the base). This sequence is represented in Fig. 5.20: by the remotion of the amount of soil framed by the rectangle (in that same figure), the support for the next 2 rings is already installed (pointed by the 2 arrows on the right), i.e., the soil material on those two small meshes had already been replaced by concrete. Of course, this simulation is not the most realistic regarding the precast concrete rings penetration, that would be by , maybe, employing a dynamic analysis similar to the case when diving a pile.

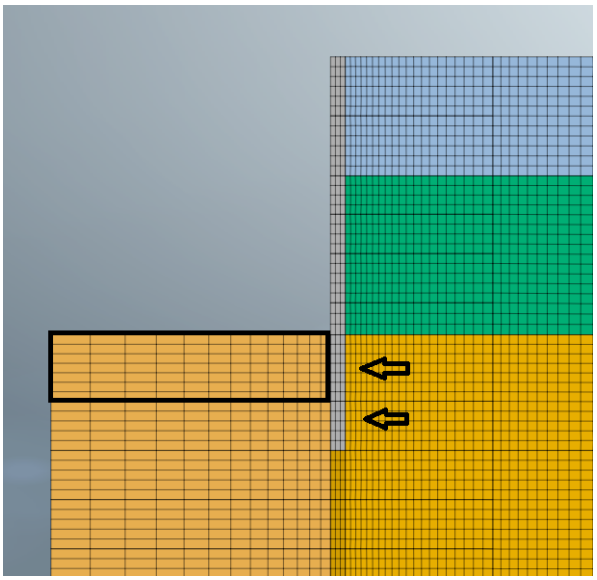

Fig. 5.20 - Case study: Construction simulation for caisson sinking

The second part of the construction was performed with the sequential excavation method which simply removes the soil in one stage and applies the support in the following stage; the process is, then, repeated. As for the application of the second layer of shotcrete, it was considered it was installed two rings above the one last excavated – see Fig. 5.21. For practical reasons the shaft's base for being round, the whole 3 m of depth of soil were removed at once, in the same stage – the set of images in Fig. 5.22 show the simulation adopted for the construction at the base. The fact that the whole 3 m of soil are removed in the same stage, is something that might influence the results, mainly on the vertical displacements in that area, since a relatively large amount of soil is being removed leading to a higher unloading. Both shotcrete and precast concrete rings follow an elastic behaviour and share the same value of Young's modulus of 34.2 GPa, as estimated in 4.4.4 from the expressions of Eurocode 2.

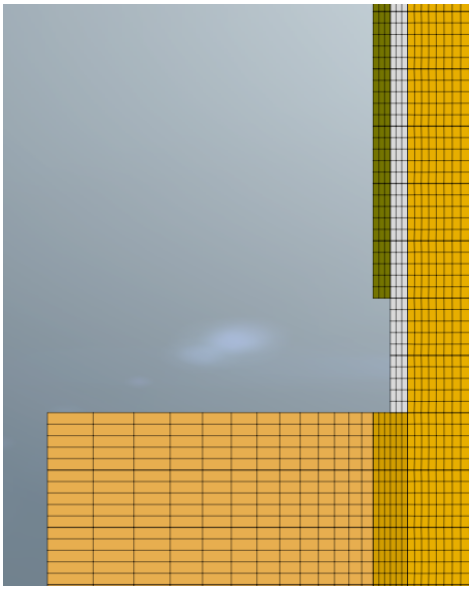

Fig. 5.21 - Case study: Construction simulation for sequential excavation – application of the 2nd shotcrete layer

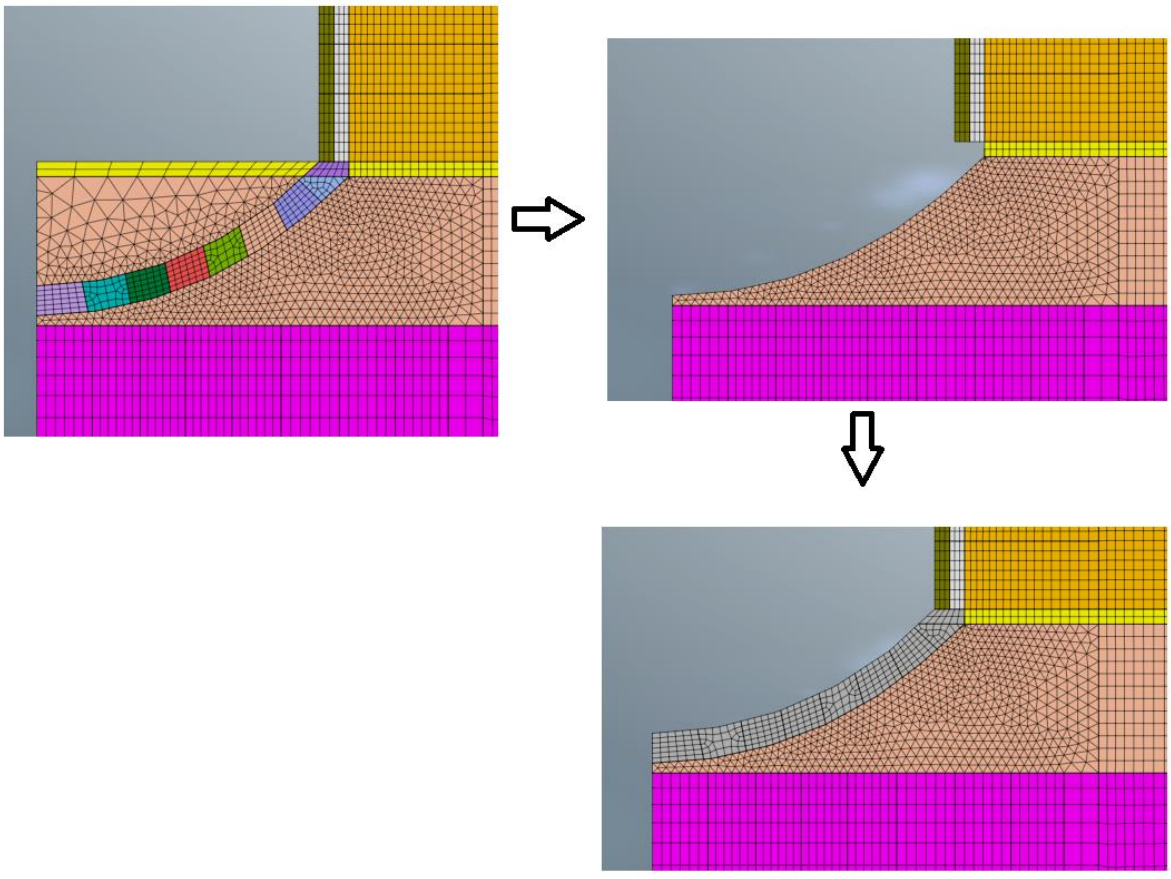

Fig. 5.22 – Case study: Simulation of final construction sequence at the shaft base

5.3.2. BASELINE ANALYSIS

This analysis is going to present and discuss the general behaviour of the soil and structure during construction. Being a "baseline" (or basic) analysis, it is not going to incorporate all the features regarding the construction, like the water level dropdown or the shotcrete hardening, for instance[2]. Those are going to be included only in the further parametric analysis and then, compared with results from the basic analysis, so that one can study their influence on the structure and soil.

Considering the structure was constructed with two different methods whose main difference is the presence or absence of concrete by the time of excavation, those 2 parts shall be discussed, in a first approach, separately. The first part of the structure, built with the precast rings of concrete will be mentioned as "PC" and the other, built with shotcrete, as "SC". Throughout the next points there is going to be an attempt to characterize the behaviour of PC in more detail than the SC, since the behaviour of the first is still "unknown" in the content of this dissertation.

5.3.2.1. SOIL PARAMETERS

As it was mentioned previously, the failure model chosen for this analysis is Mohr-Coloumb, which is the most simple and practical model used in geotechnical engineering. However, its simplicity does not quite represent thoroughly the soil real behaviour, since its failure envelope is linear, which means it does not consider a variation of strength and deformability parameters for increasing confining pressure. Still, this model will be employed for this analysis since for a certain range of confining pressure, it can be accurate.

The parameters used for the London Clay were based on the values presented and discussed in Chapter 2. All the other materials had their geotechnical parameters based on the data from the Corsica St. Shaft. Table 5.1 summarizes the parameters used for this analysis. Regarding those, it is important to clear out that:

- The values provided regarding the effective cohesion (c') are quite low which brings convergence issues in a numerical analysis. From here, one has two options: either increase cohesion considering the effect of suction, or considers an undrained analysis using the undrained strength with a "null friction angle". The second option was chosen considering that the effect of suction will be discussed separately.
- Having stated above that an undrained analysis will be undertaken, i.e., no volume change occur, automatically the dilation angle considered was null and Poisson's ratio becomes 0.50 (for avoiding numerical issues, the input values has to be lower than 0.50, so it was considered 0.495)
- The value input in Midas for Young's modulus is for undrained stiffness.
- The expression used for London Clay's undrained strength was presented in Chapter 2 and it is from the study case "Baseline Reports". As it was said in that chapter, this expression represents a minimum of values for the undrained strength at the case study's location, which is a conservative approach taken by the author that could lead, for instance, to higher deformations on the soil.

[2] The presence of the upper aquifer that should load the structure with hydrostatic pressure was not considered in this analysis;

Table 5.1 - Baseline analysis: Soil parameters for Mohr-Coloumb model

	Strata						
Parameter	Made Ground	River Terrace	London Clay	Harwich Formation	Sand Units	Laminated Beds	Lower Shelly Beds
E_u – Young's Modulus [MPa]	9.6	9.6	$400.S_u$	96	79.2	96	72
ν – Poisson's Ratio	0.495	0.495	0.495	0.495	0.495	0.495	0.495
γ - Self-Weight [kN/m^3]	20	20	19	19	20	20	21
K_0 – Coefficient of Earth Pressure at Rest	0.66	0.66	1.3	1.2	1	1.2	1.2
S_u – Undrained Strength [kPa]	50	50	$20+5z$[3]	300	-	300	150
ϕ' – Peak Friction Angle [º]	20	20	25	26	36	30	30
ψ - Dilation Angle [º]	0	0	0	0	0	0	0
c' – effective cohesion	0	0	2	0	0	0	0

[3] Where z is the depth from below ground level and not below top of London Clay's top.

5.3.2.1. General Behaviour

5.3.2.1.1. Precast Concrete Lining

Fig. 5.23 presents a couple of images representing the contour plot for horizontal and vertical displacements just behind the support for the part of the structure built with the precast rings (PC). Considering the bigger displacement variations occurred for higher depths, mainly where the shaft was constructed by the sequential excavation method the contour plot in that figure is not much representative. However, from the colour scheme one can tell the displacements in both vertical and horizontal directions are quite small. A more detailed analysis will be presented further.

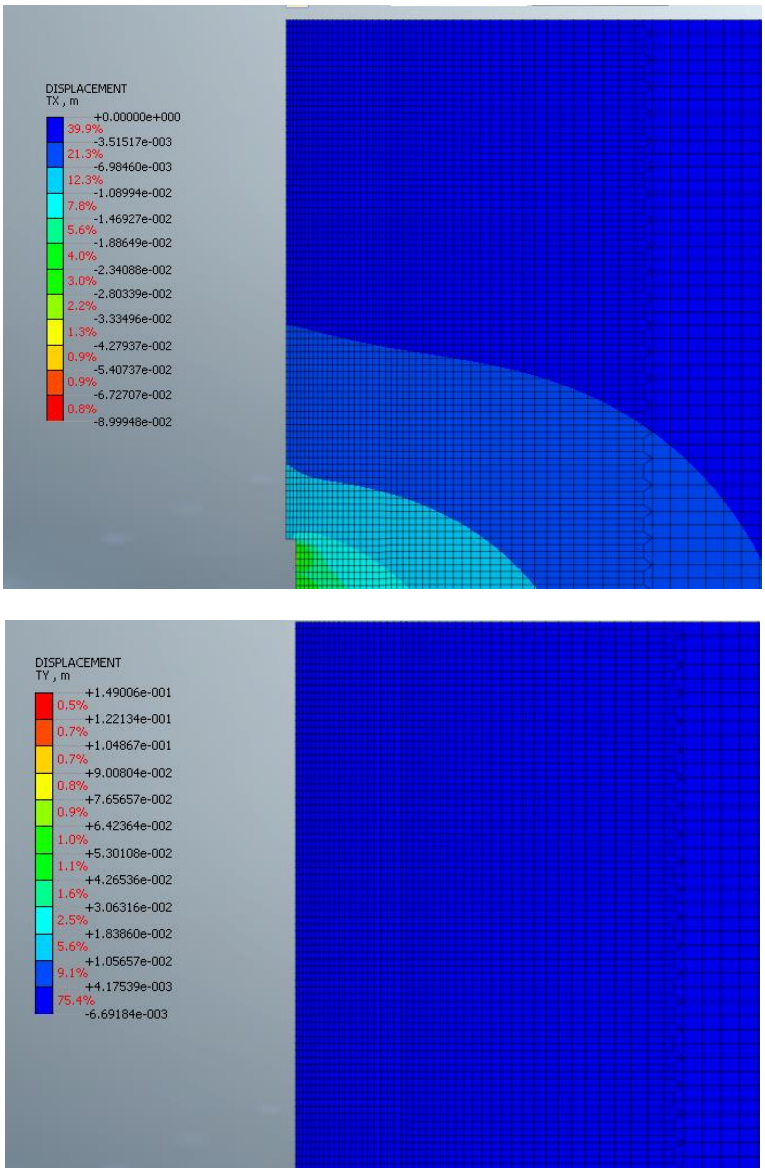

Fig. 5.23 - Baseline analysis: Horizontal (top) and vertical (below) displacements for PC

The set of images on Fig. 5.24 represent the contour plot of PC for horizontal and vertical stress. Both images on that figure do not allow one to discuss the variation in stresses in detail, since it is not so evident in those contour plots. Actually, considering the plot uniformity in XX direction, it seems the stresses are very close to the values at rest.

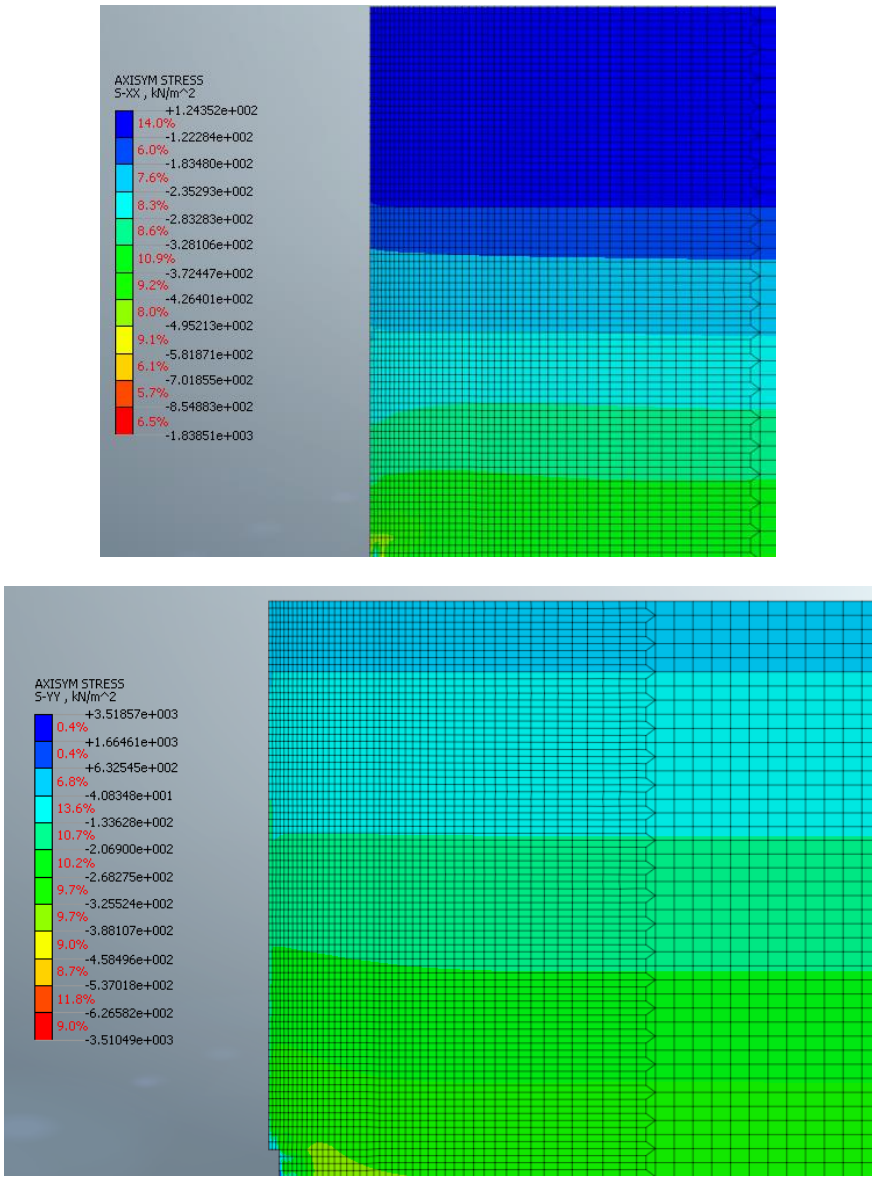

Fig. 5.24 - Baseline Analysis: Horizontal (top) and vertical (below) effective stresses for PC

5.3.2.1.2. SHOTCRETE LINING

As for the displacements on the sequential excavation method one can notice in Fig. 5.25 that generally, the soil mass presents the same behaviour captured previously in Chaper 3 and 5.2. Horizontal displacements directed towards the shaft and increasing in depth, with higher values, within each panel, by the mid-points – achieving a maxiumum of 3.7 cm at a depth of around -28 m; and an upward movement at the shaft base. It is worth mentioning, since the shaft base is not flat as the other cases discussed before, it still presents a relvant value for horizontal displacement, achieving an almost "unpractical" value of 9 cm, although one has to bear in mind that for the simulation of the construction of the base, the author removed around 3 m height of soil on the same stage (for practical purposes), which doesn't correspond to what was done at the worksite.

As for vertical displacements, it is clear the upwards movement due to unloading. The maximum value of vertical displacement at the base has also that "unpractical" magnitude referred above of around 15 cm due to the same reasons mentioned above.

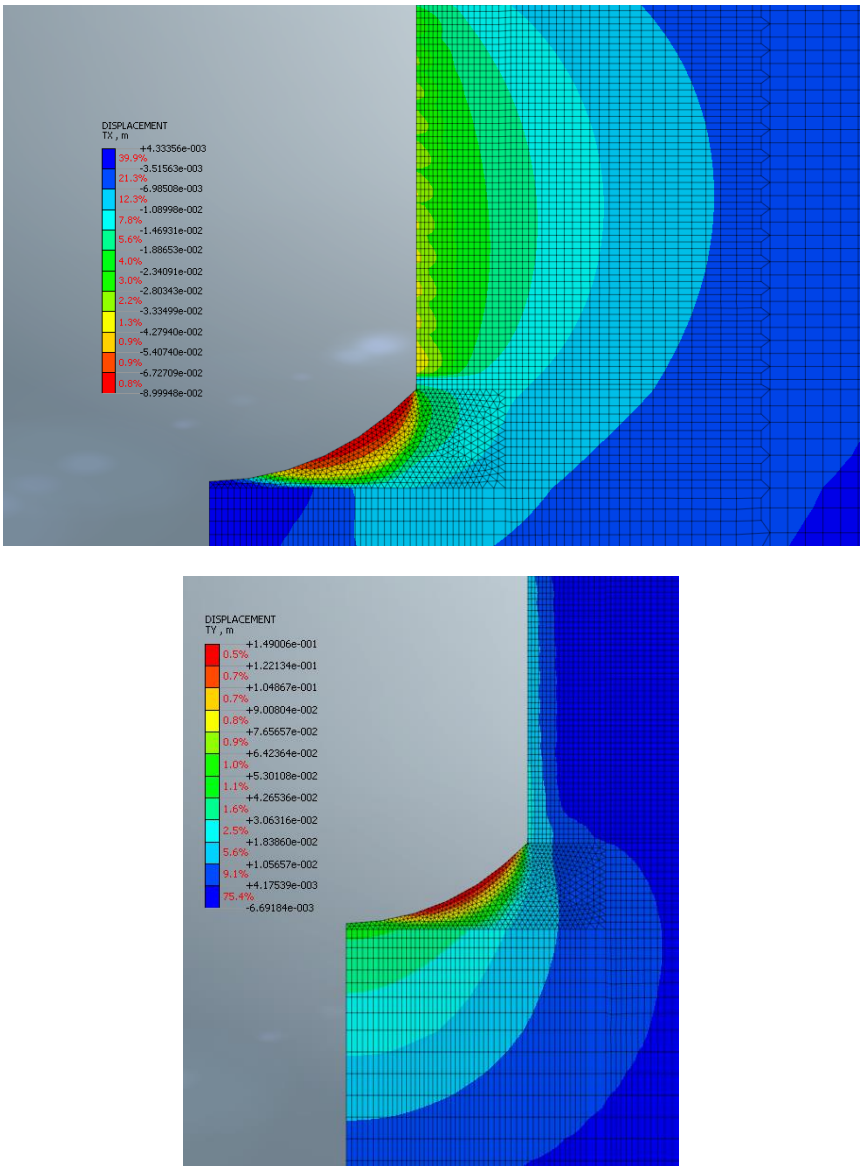

Fig. 5.25 - Baseline analysis: Horizontal (top) and vertical (below) displacements at SC

In the SC part, the horizontal stresses in Fig. 5.26 seem to follow the behaviour mentioned previously also, with higher values located on the top and lower boundaries of the support. As for the vertical stresses, there is the evident unloading at the base and, despite not being so clear, some lower values by the mid-points at the shaft face, due to stress redistribution.

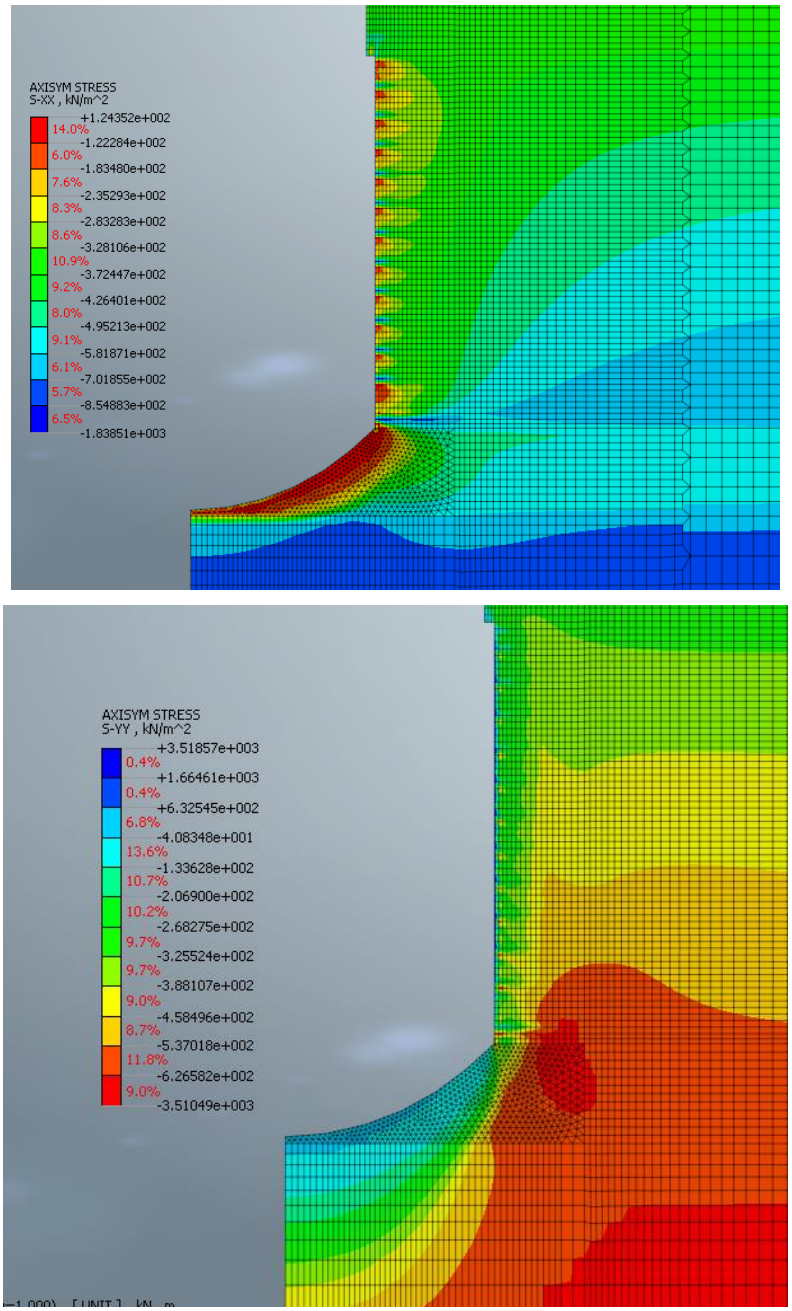

Fig. 5.26 - Baseline analysis: Baseline Analysis: Horizontal (top) and vertical (below) effective stresses for SC

5.3.2.2. SOIL DEFORMATIONS

Starting with PC horizontal displacement variation in depth, represented at several excavation stages in Fig. 5.27, generally, one can tell that the displacements increase in depth for every stage, although, looking at magnitude of results for the final excavation stage, the maximum displacement is no more than 8 mm.

Actually, this "final" line has sudden changes of shape in depth that reflect the passage to a different soil: at around -2,50 m from Made Ground to River Terrace and at -5,5 m from River Terrace to London Clay.

Let us take the stage where the soil is removed until the elevation of -10m, for example: when removing the soil mass that existed between -9 and -10 m, it was already explained that the support was already installed until -11m. What seems to happen is that the line reaches a maximum value at around -12,50m, i.e., 1,50 m below the last element of support. This difference in behaviour from the sequential excavation method is clear, since there is not an "open panel" in every phase of construction. Therefore, during one excavation stage, the deformations in soil are relatively lower due to the existence of the support, which is generally much stiffer than the soil. This maximum value reached a few meters below the base, seems similar to the deformation noticed in Fig. 3.13 of Chapter 3, when discussing the impact one excavation phase has below the shaft base. One can argue that for the late excavation stages (from around -14 m) they seem to behave differently from what was described about reaching a maximum a few meters below the base. That is due to the fact that those areas below the base are not represented in Fig. 5.27, since from -15,65 m other construction method is used, since from there starts the sequential excavation method, otherwise that maximum would have been noticed.

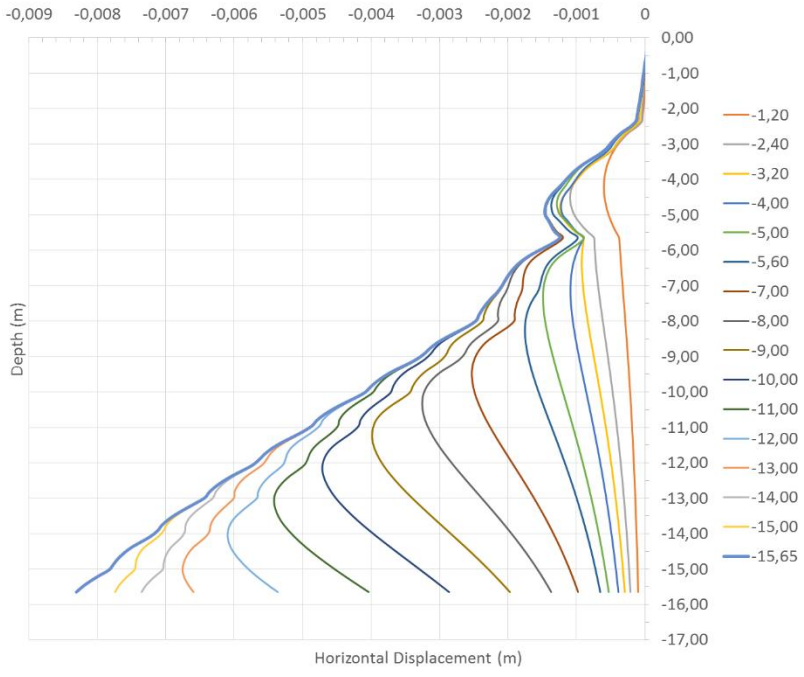

Fig. 5.27 - Baseline analysis: Horizontal displacements variation in depth for different excavation stages for PC lining

In order to analyse the influence that the second part of the construction (SC) has on the first one, the deformations behind the precast support on both final stages of each part are presented in the next figure. It is clear that the influence is practically null, so, during construction with the sequential excavation method on the second part of structure (-15,65 to -28 m) the horizontal displacements remain practically the same on the first part.

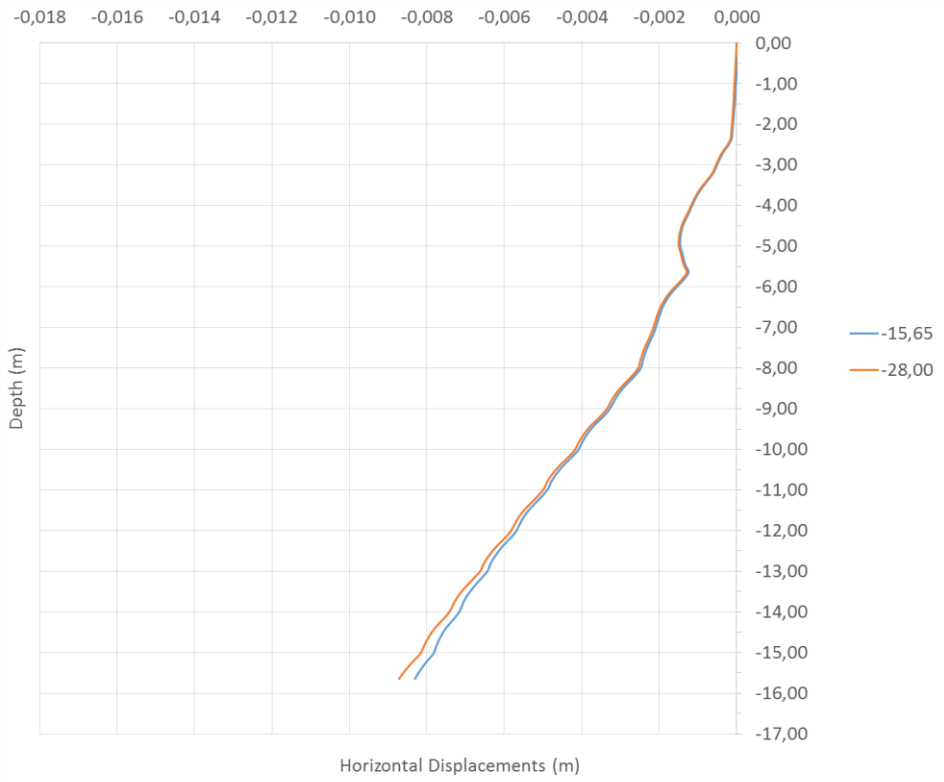

Fig. 5.28 - Baseline Analysis: Horizontal displacements at PC for final stages at PC and SC

The displacements for the SC part, only for the final excavating stage, are presented in Fig. 5.29 – in this figure, and further ones of the same kind, will only show results until 28 m depth so that those “unpractical” results at the round base are excluded from this analysis. The displacements tend to increase in depth and, still, is verified a variation within each panel, where by mid-height is reached a maximum. However, comparing this plot with the one presented in 5.2, this one seems more “uniform", i.e., the difference between maximum and minimum values within each panel doesn't seem to increase for higher depths. This might be explained with the fact that for this "baseline" analysis the author already considered an increasing Young's modulus and “cohesion” (undrained strength) for higher depths within the London Clay.

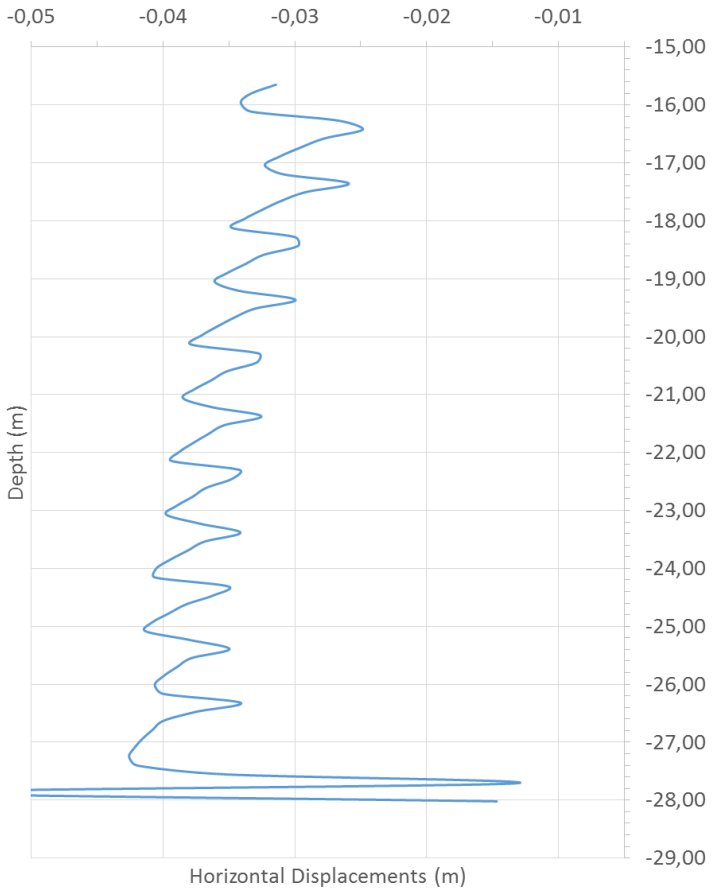

Fig. 5.29 – Baseline analysis: Horizontal displacements variation in depth for SC lining

Finally, the ground displacements are presented in Fig. 5.30. Analysing the variation of both vertical and horizontal displacements in that figure once can tell the behaviour of the latter is quite close to the one presented in the model studied in CODE_BRIGHT by Topa Gomes (2008) and in the validation of Midas in 5.2. As for the vertical displacements, the graph shows to what seems an "odd" shape, however, if one looks at the magnitude of those settlements one will notice the maximum value is even lower than 1 mm, which makes the thing practically null. This might reflect the influence of having part of the construction sequence where the support is installed prior to the soil's removal.

The maximum value for horizontal displacements is around 1.5 mm, reached at around 10 m from the support.

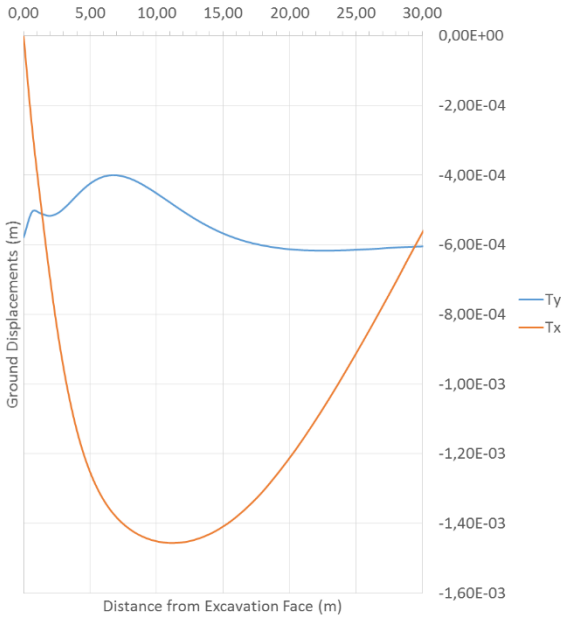

Fig. 5.30 - Baseline analysis: Horizontal (Tx) and vertical (Ty) displacements at ground level

5.3.2.3. Soil Stresses For The Precast Concrete Area

As mentioned in the beginning of the present sub-chapter 5.3, the focus of this numerical analysis of the study case are the displacements at the ground and just behind the support, but it is also important to characterize the behaviour of soil when the structure was built with the wet caisson sinking method. Therefore, this point will just briefly focus only on the effective stresses variation in depth for that part of the structure.

In point 5.3.2.1 the contour plots representing the stresses for PC weren't quite clear about the soil's behaviour and so, the stresses for the state "at rest" (before construction) were compared for the results after the final stage in Fig. 5.31 and Fig. 5.32. The first represents the stress variation in depth for horizontal stresses and the second for vertical stresses. The evident conclusion for both figures is that throughout construction there is not practically a variation in stresses. This might be explained by the fact that, first, by the time the soil is removed at one stage there is already a support preventing relevant deformations and so, preventing a stress redistribution or an arching effect like in the sequential method. Second, it might be the simulation itself used to reproduce the penetration of the precast rings, which consists, basically, in replacing the soil material of a specific area of the mesh for the support – as it was said before, this method might not be the best to model the construction method.

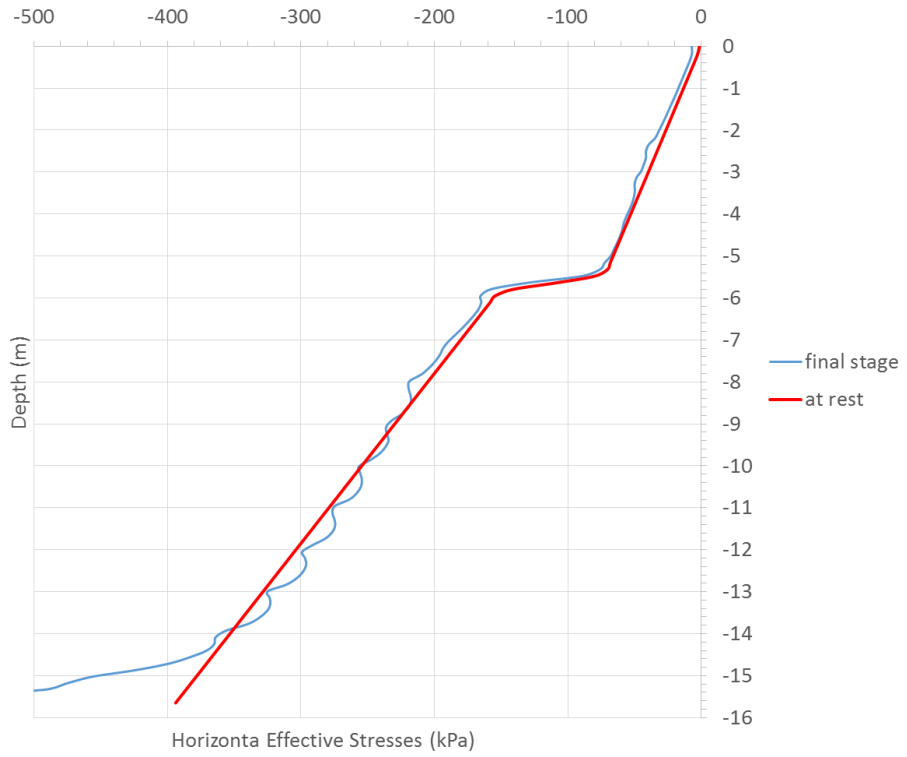

Fig. 5.31 - Baseline analysis: Horizontal effective stress variation in depth behind the support for PC

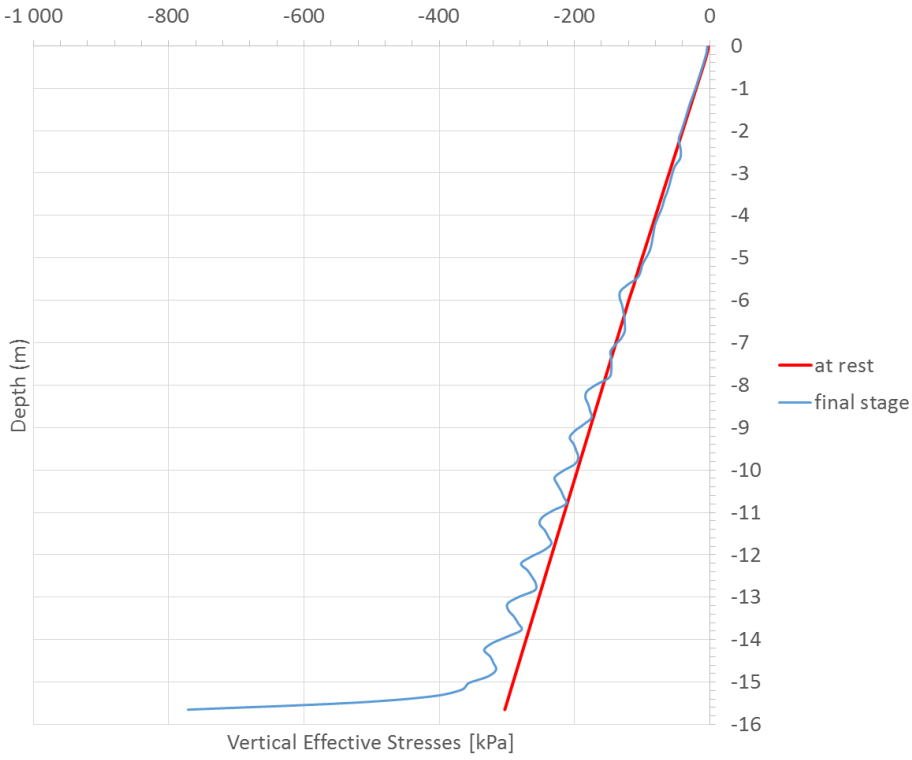

Fig. 5.32 - Baseline analysis: Vertical effective stress variation in depth behind the support for PC

5.3.2.4. Internal Forces On The Precast Lining

Since a brief characterization of the behaviour of the construction part, built with the wet caisson sinking method, has been carried out throughout this baseline analysis, hoop forces and bending moments are presented in Fig. 5.33 and Fig. 5.34, respectively.

It is curious to notice that both representations show a certain similarity with the theoretical (elastic) solution for shafts described by Topa Gomes (2008), based on Timoshenko, Woinowsky-Krieger (1959) studies. Those similarities are enhanced by the low values of bending moments in depth (no more than 10 kN.m/m until around 11 m of depth) and the shape of the hoop forces variation line that, in a way, shows a certain resemblance with the line representing horizontal displacements in Fig. 5.27. In that solution, the shaft is considered as a cylindrical deposit subjected to a linear axisymmetrical load from the exterior. This model, does not consider the excavation-application of support sequence. Instead, the "deposit" presents as fully "excavated" within its interior. Considering the caisson sinking method employed in this first part of the case study has the support installed prior to excavation that might be the reason for such similarity in behaviour.

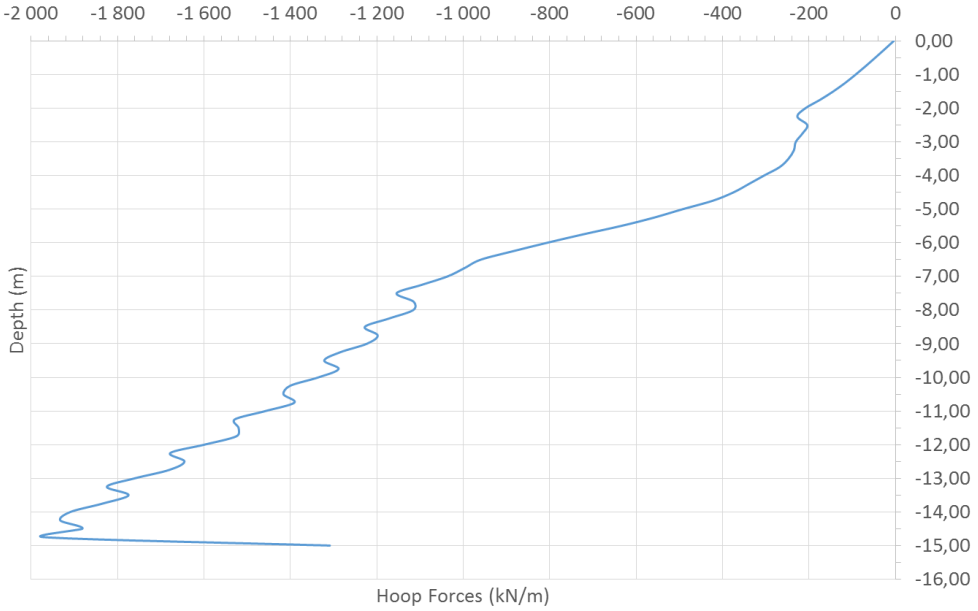

Fig. 5.33 - Baseline Analysis: Hoop forces variation in depth at PC

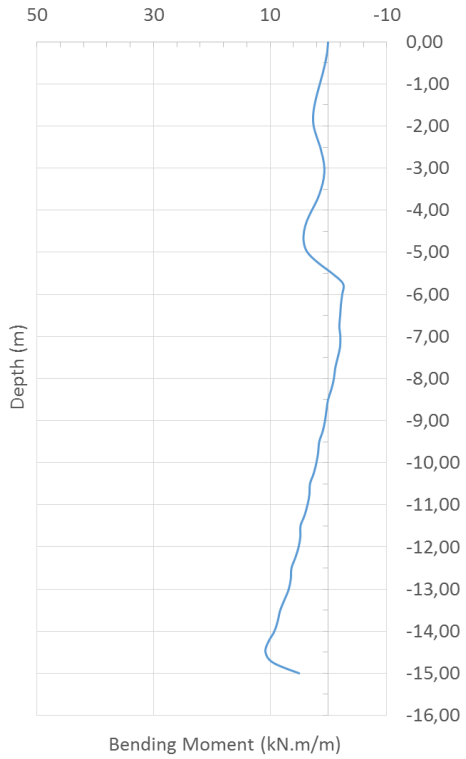

Fig. 5.34 - Baseline Analysis: Bending moment variation in depth at PC

5.3.3. Parametric Analysis

Despite being called "parametric analysis" this section won't present results regarding variations of parameters. Instead, will first consider the situation where the sequential excavation method is employed at the structure's full depth, in order to check the influence on using the caisson sinking method in the first part. Then, the effect of water level dropdown will be included to the baseline analysis and in the next point the effect of the shotcrete hardening. In addition, the Modified Cam-Clay model will replace Mohr-Coulomb's in a separate analysis. These analyses will be studied and compared with the baseline case only in the perspective of horizontal displacements and ground settlements (when felt necessary) due to time restriction for the completion of this work.

5.3.3.1. Shotcrete Lining in Full Depth

Fig. 5.35 presents a graph comparing the variation in depth for the horizontal displacements just behind the support for the baseline analysis and this case. Analysing that figure the most obvious change in behaviour was obviously between 0 to 15 m of depth, where the construction method was replaced. In that area, not only the maximum increases from around 0.8 cm to 2.8 cm, but the whole shape of the line changes, incorporating that characteristic behaviour often described for sequential excavation method. The difference between maximums of the 2 lines clearly shows the impact the construction process may have on final displacements.

As for the second part of the structure (from 15 m of depth), the behaviour is similar to the baseline. Although the results of this new case start to be considerably different (between -15 to around -21 m), there's a tendency of approximation of both lines for increasing depth. This approximation might be due to the fact in this model an increase in both strength and deformability parameters for higher depths, making the variation of horizontal displacements more "uniform". From the characterization of the shaft's phenomenology presented in Chapter 3 one should know already that when removing the soil at higher depths (where the stresses at rest were higher) there's a higher unloading that leads to higher displacements. However, in this case, higher unloading is, in a way, balanced by increasing resistance and deformability parameters, leading then to this "uniformity".

As for ground settlements – see Fig. 5.36 – the line representing the values for this case "Shotcrete – full depth" shows now a very similar behaviour to the Midas validation, reaching a maximum just behind the support of almost 1.6 cm, which is natural, considering the increase of horizontal displacements. From that maximum point until a distance of around 10 m (almost the distance of the shaft's diameter) there's a sudden variation in values. From those 10 m of distance, there's, then, a slower variation until reaching practically 0. Fig. 5.36 reflects once again in this case, how influent is the "absence" of the caisson sinking method between 0-15 m of depth. This also shows, the sequential excavation method, despite being a fast and economic procedure, might not be the best if controlling deformations would be a primary goal.

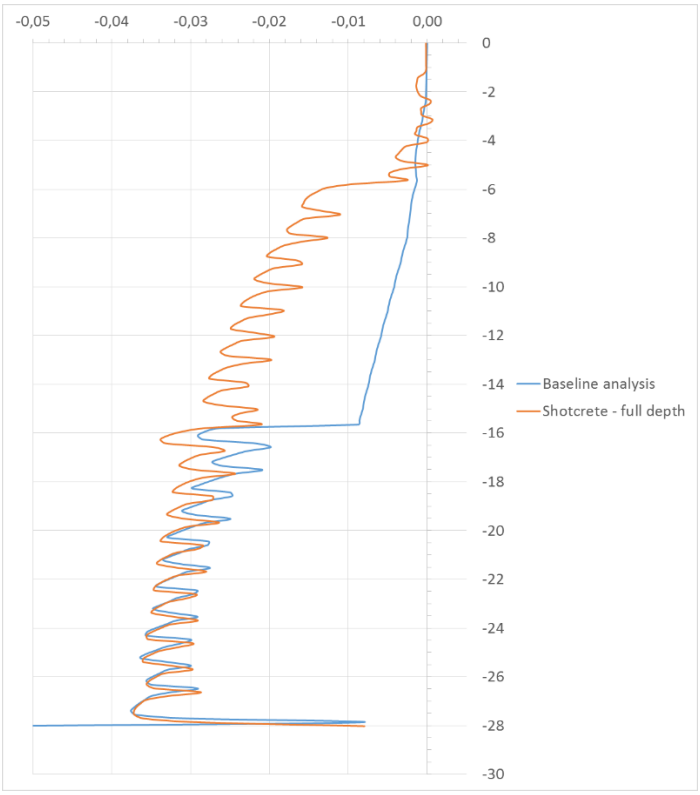

Fig. 5.35 - Parametric analysis: variation of horizontal displacements in depth for the case “Shotcrete Lining in Full Depth”

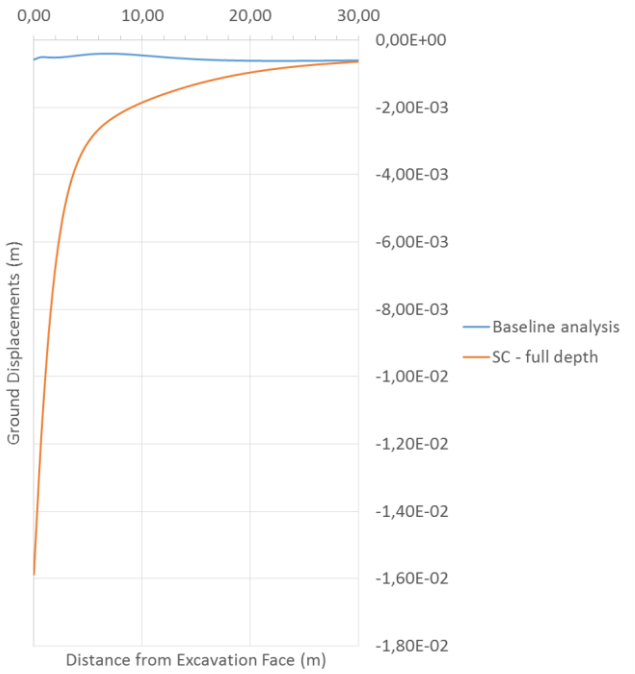

Fig. 5.36 - Parametric analysis: ground settlements for the case “Shotcrete Lining in Full Depth”

5.3.3.2. ADDING THE INFLUENCE OF SUCTION

The simulation of the effect of suction in the soil mass was done in two different ways, similarly to the 5.2 validation. The first one was by using Fredlund *et al.* (1978) expression define in Chapter 3. The negative pore water pressure was estimated and then multiplied by $\tan(\phi^b)$ in order to obtain the "equivalent" cohesion (in this analysis there's only going to be an increment cohesion, Despite the soil used in the model of CODE_BRIGHT is different from the case study, the value used for ϕ^b was the same (14º). In this simulation there's only going to be considered an increment o c'. Fig. 5.37 shows the graphic representation of negative pore water pressure (suction), undrained strength (values considered in baseline case) and c' equivalent within the London Clay strata.

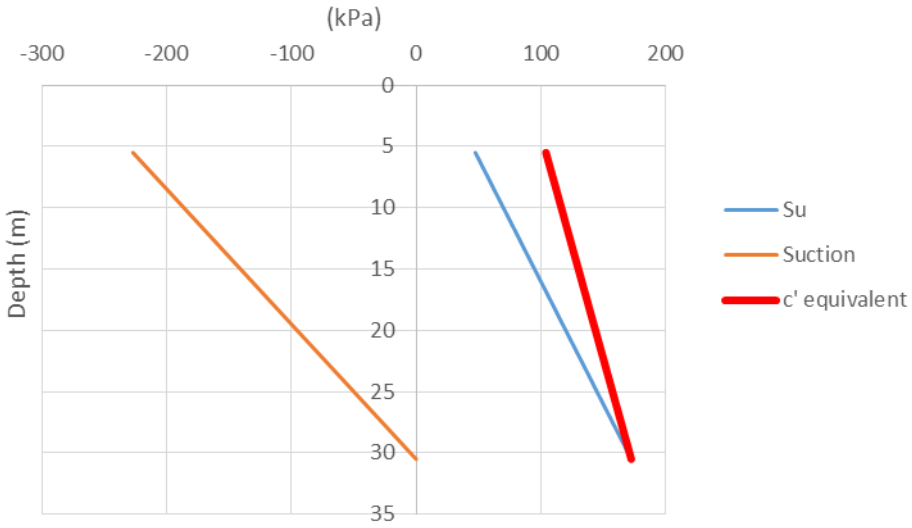

Fig. 5.37 – Parametric analysis: variation of S_u, suction and c' equivalent in depth within LC when simulating suction

There was also an attempt to simulate the unsaturated condition by defining a water retention curve by using Van Genuchten (1980) expression referred in 5.2. For that purpose the author was able to find curve-fitting parameters for a clayey soil in Yang, You (2013). The image representing the curve and showing the parameters shown in the following figure.

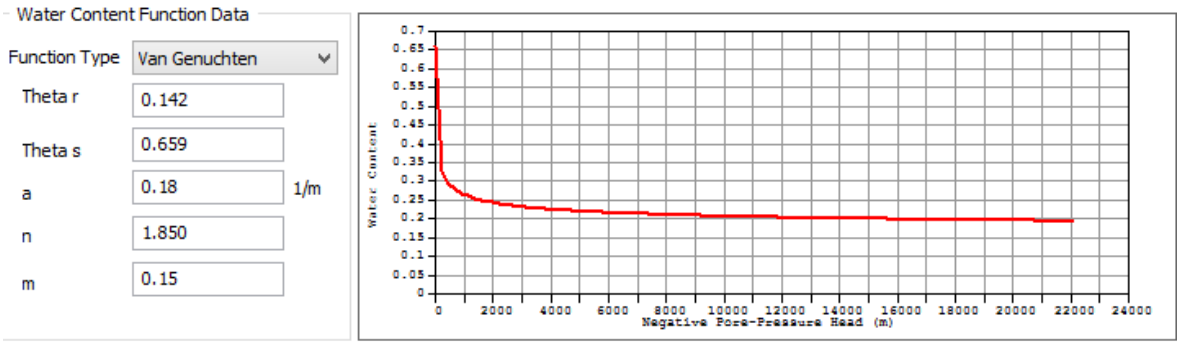

Fig. 5.38 - Parametric analysis: water retention curve using Van Genuchten (1980) function (screenshot from Midas GTS NX)

Fig. 5.39 presents the results obtained for this case. Unfortunately, both simulations were unsuccessful. For the case where the unsaturated condition was simulated by inputting a value of "c' equivalent" the outcome was what the author called before, "unpractical". The magnitude of horizontal displacements was completely out of proportion.

Considering now the case where the water-retention curve was defined, the values for horizontal displacements in Fig. 5.39 turned out to be higher than the baseline case, which is not coherent. The fact one introduced an unsaturated situation within the soil mass, should have strengthened it, inducing it to suffer lower deformations. The validation made done in 5.2. didn't follow this "odd" behaviour for both cases, which makes it harder to find a plausible explanation.

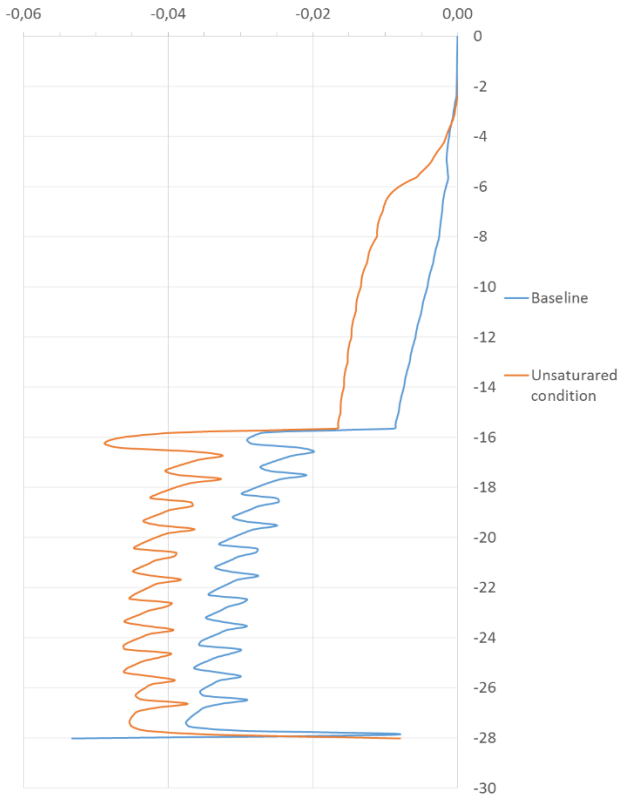

Fig. 5.39 - Parametric analysis: variation of horizontal displacements in depth when adding the suction effect

5.3.3.3. SIMULATING SHOTCRETE HARDENING

Midas allows the users to associate a material with a time-depending behaviour and, complementarily, when simulating a construction sequence, one can chose to associate each stage to either load steps or time steps. Since the author had information regarding the hardening process of the shotcrete used at the case study's site, one felt it would be interesting to attempt to recreate this time-depending behaviour and check its influence on the structure. Of course, one could simulate that behaviour by simply replacing the shotcrete's mesh set for other with better properties. However, in order to get a more accurate time-depending behaviour one would have to proceed to several mesh substitutions, which would be no easy task considering the complexity of this model.

Firstly, using the "elastic modulus function", the author defined the curve representing the shotcrete's hardening evolution – Fig. 5.40.

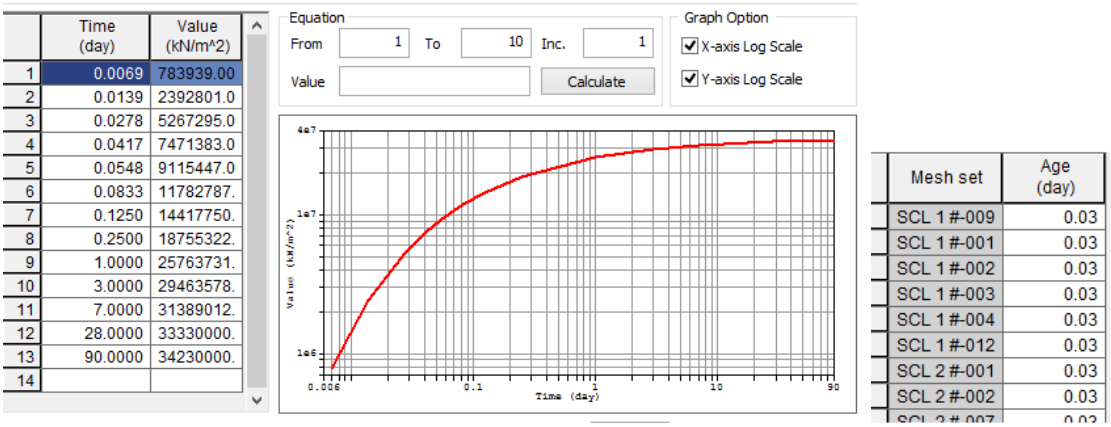

Fig. 5.40 – Parametric analysis: shotcrete's hardening evolution curve (screenshot from Midas GTS NX)

Then, it was considered that every construction stage would represent 1 day-step, meaning that, for instance, the soil's remotion at certain construction stage would represent 1 day, and the further shotcrete application would be executed during the next 24h.

Finally, before running the analysis, the user must define from which point of the "hardening-curve" the time-depending behaviour starts. In other words, the user can choose a starting point in time so that, by the time of its application its deformability parameter is different from 0. In order to avoid possible numerical problems during analysis, the author considered a starting point of 40minutes (around 0.03 days), meaning that, when the shotcrete is applied it will start to harden from a Young's modulus of around 5.3 GPa.

The results of the analysis are as follows in Fig. 5.41. From 0 to 15 m of depth, one was already expecting the lines to be completely coincident, since between that depth the simulation is exactly the same as the baseline. The values from the two cases are also extremely close for the shotcrete lining part. From these results, one can come up with two possibilities for such coincident results: first, would be the confirmation that shotcrete is, in fact, a good material to use during shafts and tunnels constructions, acting almost promptly as a primary support after spraying. The later possibility, however, lacks of some more intensive study and it would be interesting, specially, to analyse its internal forces throughout its hardening process (unfortunately, cannot prolong the length of this dissertation to include those studies). The second possibility is that, including time-dependent behaviour (specially in an element functioning

as a support) is a recent feature of Midas GTS NX and even its User Manual doesn't, yet refer how does the process works. It is not entirely clear if the starting time for the hardening process is coincident with the "first day" of the first construction stage. Meaning that by that shotcrete starts hardening even before it is activated, making it practically at its full strength by the time it is installed.

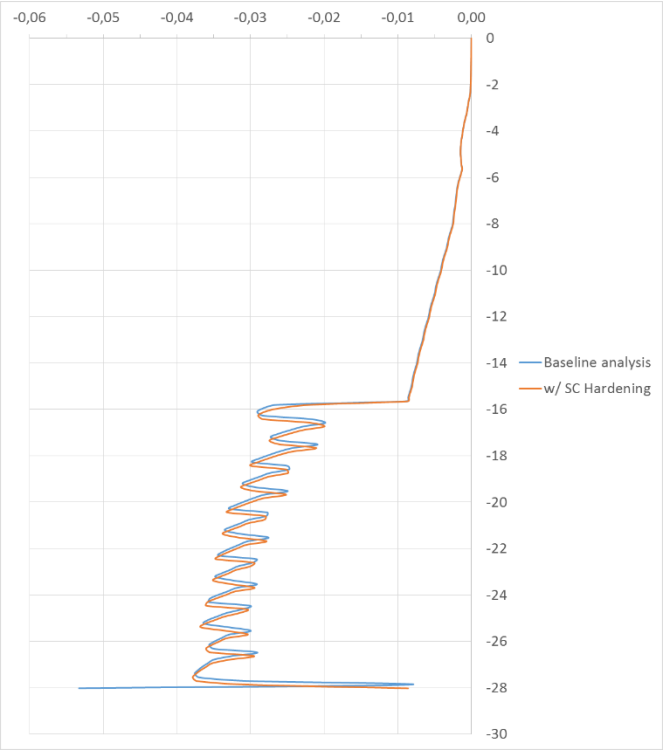

Fig. 5.41 - Parametric analysis: variation of horizontal displacements in depth when considering the SC hardening evolution

5.3.3.4. MODIFIED CAM-CLAY

Before completing this parametric analysis, it would be interesting to try running Midas with a different soil model, more specifically, one that would incorporate elasto-hardening behaviour (i.e., for increasing pressure, the stiffness increases), which Mohr-Coulomb's perfect elasto-plastic model doesn't cover. The model chosen was the Modified Cam-Clay and its input parameters are as follow in Fig. 5.42. The values of "Lambda", "k" and "M" were obtained from a numerical analysis of a tunnel in London clay made by Masín, Herle (2005). As for the overconsolidation ratio, the author did an estimation based on the expression (2.2.) of Chapter 2, considering $\phi'=25^{o}$ and $K_{OC}=1.3$, obtaining a value of around 7. This estimation of the OCR might not be the best procedure.[4]

Since this model incorporates the hardening of the soil for increasing pressures, the user can only input a constant parameter for stiffness. So, the author Young's modulus average value from the expression used in the baseline analysis (recall Table 5.1).

[4] Note that only London Clay was changed to the Cam-Clay model, all the other materials kept with Mohr-Coloumb;

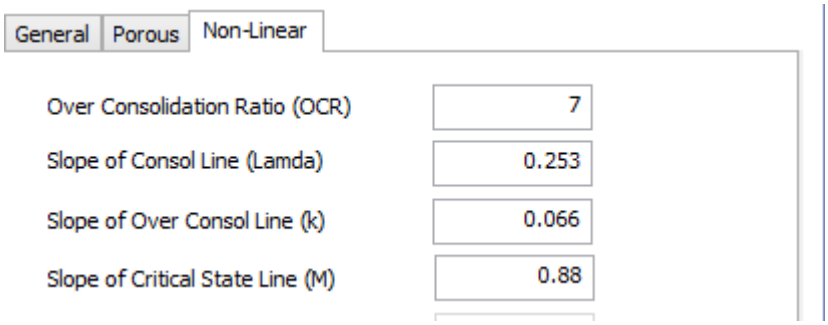

Fig. 5.42 – Parametric analysis: input parameters used from Masín, Herle (2005)

The horizontal displacements and ground settlements are presented in Fig. 5.43 and Fig. 5.44, respectively. At first sight, the maximum values within each panel for the SC part doesn't vary so significantly, with the exception of the last ring. But it is interesting to notice that the results from the Modified Cam-Clay model lose that "uniform" shape in depth, i.e., the variation between minimums and maximum within a penal can achieve a significant value of around 1.50 cm. This is due to the fact the deformability parameter (E) is not increasing in depth in this model. On the other hand, this model also "improves" E for higher stresses points, but those would have first to reach the model's yield surface, because within it, the soil behaves as purely elastic, just like Mohr-Coulomb's.

As for ground settlements, there's a considerable change by comparing to the baseline case, where for the Cam-Clay model, the vertical settlement achieves a maximum of around 4.2 cm.

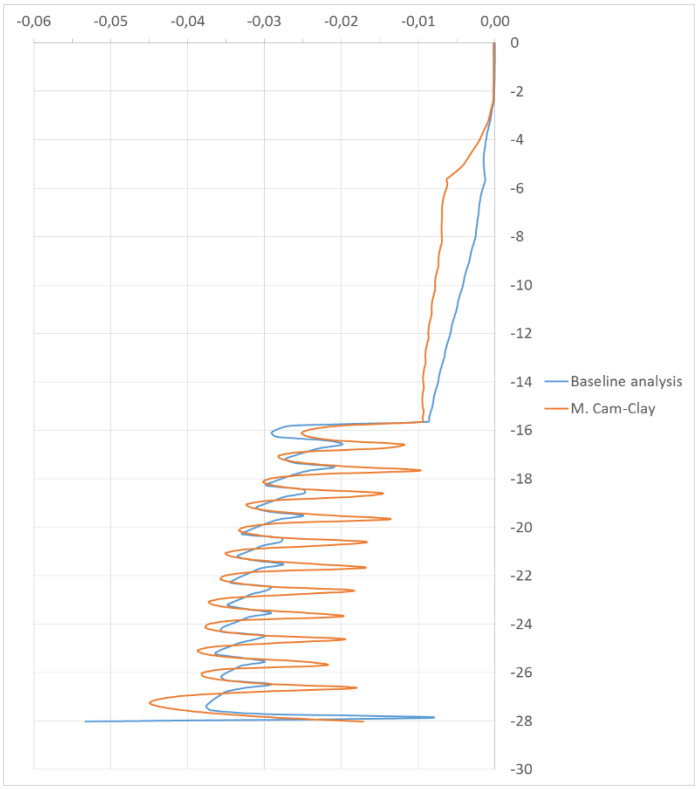

Fig. 5.43 - Parametric analysis: variation of horizontal displacements in depth when considering the Modified Cam-Clay model

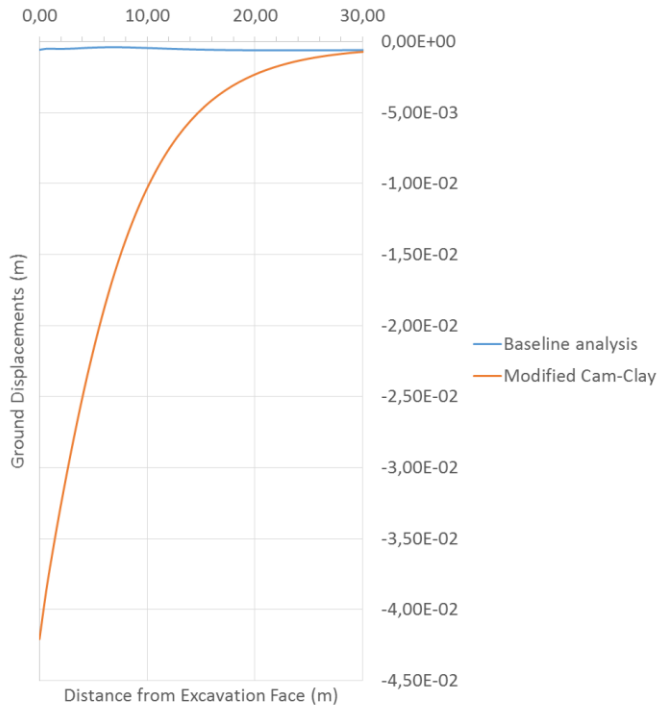

Fig. 5.44 - Parametric analysis: ground settlements when considering the Modified Cam-clay model

5.4. FINAL NOTES

The present chapter presented the proposed numerical analysis for the case study. The analysis had, as its base, Midas GTS NX. Being a recent software in the market, it was subjected to a validation by comparison to the model used in CODE_BRIGHT presented in Chapter 3. The results from that validation were generally satisfactory, the author's primary intention wasn't to achieve coincident results, but rather to validate the structure's behaviour and get "coherent" results. There are always differences between software, either at generating elements or running different solvers, and so, comparing results should be a task taken with care.

The analysis of the case study started with some careful initial notes that in different aspects attempted to simplify what was already a relatively complex model. Some of those choices didn't work out so well, mainly, considering the full excavation of the whole round shaft at one stage, that lead to what the author called "unpractical" results. Regarding the parameters chosen (specially for London Clay) the choices made are, of course, subjected to discussion, although they were based on the references of Chapter 2.

From the baseline analysis, without considering those "unpractical" results, the values obtained were fairly good. Considering the structure's full depth is around 30 m, achieving a maximum value around 3.7 cm a positive point. There was also an attempt to characterize briefly the behaviour of the structure for the part constructed with the caisson sinking method, which the author gave the possibility it reassembles to an elastic shell model described in Topa Gomes (2008) work.

The parametric analysis was the section where the author felt more difficulties. Despite the interesting results regarding the case where the model was simulated as built with only with the sequential excavation method, "unpractical" and incoherent values were obtained when simulating the water level

dropdown at the shaft's base. This would be an important and interesting analysis since it was a procedure done during the shaft's construction. The causes that lead to those results are not clear yet, but it could be an error made but the author himself while working with the software (since this analysis was done successfully during Midas validation) or an error on the model.

The attempt to simulate the shotcrete's hardening during the construction progress wasn't so successful as well. Despite the results were plausible, the software' references are not clear about using that feature. There was an initial attempt in this chapter to add up the effect of the water level dropdown and the shotcrete hardening to the baseline case and compare the results to the ones obtained from the monitoring plan presented in Chapter 4. However, due to the results issue described above, that comparison didn't feel pertinent.

In the end, the Modified Cam-Clay model was introduced and one got fairly interesting results. This is relatively more complex soil model and it should be considered in a more extensive study.

6
Conclusion

6.1. Conclusions and Dissertation Review

In the beginning of this dissertation the main goal was to perform numerical analysis of a circular shaft recently built in London that crosses a thick London Clay strata. From that point the author proposed other goals that would give a more structured shape to this thesis as it was: characterization of London Clay, study of circular shafts phenomenology, construction methods and design, and thorough characterization of the construction based on documents provided to the author. Generally speaking all those points met their purposed goals, although one can point out some difficulties during the process.

In Chapter 2 the geotechnical characterization in 2.2 was an essential point that allowed the author be acquainted with referenced values that could be used in the numerical analysis. However, fully characterize London Clay and finding reliable parameters that could be used in Chapter 5 was no easy task. The author recognizes that the characterization wasn't the most complete an accurate. It would have been interesting, for instance, to have presented expressions that, based on tests data could estimate some geotechnical parameters.

Chapter 3 allowed one to understand the two construction processes used in the case study and the way these structures behave during their construction. There was an attempt to study the large diameter shaft's design, but being structures not so commonly used, their design relies on numerical analysis based on the finite elements method. In the end, the behaviour of shotcrete during its hardening was studied in the perspective of finding the best expressions that could estimate its Young's modulus evolution in time so that it could be simulated in the numerical analysis. It turns out, there aren't yet commonly accepted expressions for shotcrete, and so the author opted to use the Eurocode 2 expressions.

Chapter 4 was based on the information provided by documents from the construction of the case study. Some of the data from the monitoring plan was processed and discussed, as the lining convergence or ground settlements, for instance. From these values, one could already start to relate the shaft's behaviour discussed in Chapter 5 with those results.

Finally, Chapter 5 was the one that presented more adversities to the author, since he had to learn how to use Midas GTS NX from scratch and that software, recent in the market, doesn't provide so many references. The validation, based on the comparison of results from other software, CODE_BRIGHT, produced good results when speaking about getting coherent structural behaviour, because there were some numerical issues that would cause a deviation of values, mainly at the shotcrete internal forces. The parametric analysis was also marked by some adversities since it wasn't possible to simulate correctly the water level dropdown.

This dissertation attempted to approach different aspects of the case study, although did it only briefly for each of those. This thesis, in a way, turned out to be "generalist" since there was an intention to fully analyse the problem, however due to limited time to finalize this thesis it wasn't possible to focus on every aspect in detail.

6.2. PROPOSITION FOR FURTHER STUDIES

Having this subject a certain degree of complexity it would be interesting if one would pick one of the several aspects "introduced" in this thesis and developed a more focused and detailed study. For example, one could simply focus only on a parametric analysis changing the values of some relevant geotechnical parameters of London Clay and check their influence and differences on the precast lining and the shotcrete lining, something that was not done in this thesis.

Midas GTS NX was the software proposed to perfume the numerical analysis, but as it was mentioned, presented some issues that prevented some simulations, so it would be interesting to model the case study in a different and better known numerical software. In addition, performing a whole numerical analysis (basic and parametric analysis) with a more complex soil model that considers a non-linear elasticity like the Modified Cam-Clay would be worth studying.

Other aspect worth studying more in more detail would be the behaviour of London Clay regarding its unsaturated condition due to the water level dropdown.

Finally, it must be said that while using Midas GTS NX no interface elements were used between the soil and the structural elements. By employing these elements the numerical analysis would present a more realistic approach to reality. Therefore, a further work regarding this case study including this elements in the analysis would be most pertinent and interesting.

7
Bibliographic References

Bishop, A. W., Webb, D. L., Lewin, P. P. (1965). *Undisterbed Samples of London Clay from the Ashford Common Shaft: Strength-Effective Stress Relationships*. Géotechnique. Vol. 15. p. 1-31.

Boháč, J., Mašín, D., Malát, R., Novák, V., Rott, J. (2013). *Methods of determination of K0 in overconsolidated clay*. Charles University in Prague, Faculty of Science, Albertov 6, 12843 Praha 2, Czech Republic.

British Tunnelling Society and Institution of Civil Engineers, I. (2004). *Tunnel Lining Design Guide*. Thomas Telford, London.

Campanhã, C. A., França, P. T. (2008). *Poços de Grande Diâmetro*. Brazil.

Chandler, R. J., Apted, J. P. (1988). *The effect of weathering on the strength of London Clay*. Journal of Engineering Geology and Hydrogeology. Vol. 21. p. 59-68.

Craig, C. (1996). *Advances in Site Investigation Practice.* Thomas Telford, Institution of Civil Engineers (UK).

Craig, R. F. (2004). *Craig's Soil Mechanichs.* Spon Press, London and New York.

Doig, P. J. (2012). *Shaft Construction for Civil Engineering Projects*. London.

European Commitee for Standarisation. (2002). *Eurocode 2, Design of concrete strucutes. Part1: General Rules for buildings*. Bruxelles, Belgique.

Fredlund, D. G., Morgenstern, N. R., Widger, R. A. (1978). *Shear strength of unsaturated soils*. Can. Geotech. n.º 15 p. 313-321.

Gasparre, A. (2005). *Advanced Laboratory Characterisation of London Clay*. Imperial College London, London.

Globardes, I., Cavalaro, S. H., Aguado, A., Garcia, T. (2013). *Estimation of the modulus of elasticity for sprayed concrete*. Elsevier.

Guler, E. (2013). *A methodology for lining design of circluar mine shafts in different rock masses*. Middle East Tecnhical University.

Hight, D. W., Jardine, R. J. (1993). *Small-strain stiffness and strength characteristics of hard London Tertiary clays*. Geotecnhical Engineering of Hard Soils-Soft Rocks. p. 533-552.

Humes. (2012). *Segmental and One Piece Shafts - Installation Guide*.

Jaky, J. (1944). *The coefficient of earth pressure at rest*. Journal of the Society of Hungarian Architects and Engineers. Vol. 78. n.º 22 p. 355-358.

Journal, T. (2013).

King, C. (1981). *The Stratigraphy of the London Clay and Associated Deposits.* Backhuys, Rotterdam, the Netherlands.

Matos Fernandes, M. (2006). *Mecânica dos Solos - Conceitos e Princípios Fundamentais.* FEUP Edições, Faculdade de Engeharia da Universidade do Porto.

Matos Fernandes, M. (2011). *Mecânica dos Solos, Introdução à Engenharia Geotécnica.* FEUP Edições, Faculdade de Engenharia da Universidade do Porto.

Mayne, P. W., Kulhawy, F. H. (1982). *K0 –OCR relationships in soil*. Journal of Geotechnical Engineering. Vol. 108. n.º GT6 p. 851-872.

Pantelidou, H., Simpson, B. (2007). *Geotechnical variation of London Clay across central London*. Géotechnique. Vol. 57. n.º 1 p. 101-112.

Potts, D. M., Zdravkovic, L. (2001). *Finite element analysis in geotechnical engineering - Application.* Thomas Telford Publishing, London.

Simpson, B., Blower, T., Craig, R. N., Wilkinson, W. B. (1989). *The Engineering implications of rising groundwater in the deep aquifer beneath London.* Construction Industry Research & Information Assoc, London.

Standing, J. R., Burland, J. B. (2000). *Ground Characterisation to Explain JLEP Tunneling Volume Losses in the Westminster Area*. LUL.

Survey, B. G. (2004). *Geology of London, Special Memoir.* Keyworth, Nottingham.

Tan, T. S., Phoon, K. K., Hight, D. W., Leroueil, S. (2003). *Characterisation and Engineering Properties of Natural Soils.* Swets & Zeitlinger, Netherlands.

Terzaghi, K., Peck, R. B. (1948). *Soil Mechanichs in Engineering Practice.* John Wilei and Sons, New York.

Timoshenko, S., Woinowsky-Krieger, S. (1959). *Theory of Plastes and Shells.* 2nd edition. McGraw-Hill International Editions,

Topa Gomes, A. (2008). *Poços Elípticos pelo Método de Escavação Sequencial na Vertical - O Caso do Metro do Porto*. Faculdade de Engenharia da Universidade do Porto - FEUP, Porto.

Uotinen, L. (2011). *Design of shotcrete rock reinforcement in hard rock according to Eurocode*.

Webb, D. L. (1964). *The Mechanical Properties of Undisturbed Samples of London Clay and Perre Shale*. University of London.

Wright, P. J. (2010). *Validation of soil parameters for deep tube tunnel assessment*. ICE Publishing.

Ymsiri, S. (2002). *Pre-Failure Deformation Characteristics of Soils: Anisotropy and Soil Fabric*. University of Cambridge.

Appendix I

In Appendix I, one will find the map of Greater London representing the locations of the several places referred in Chapter 2.

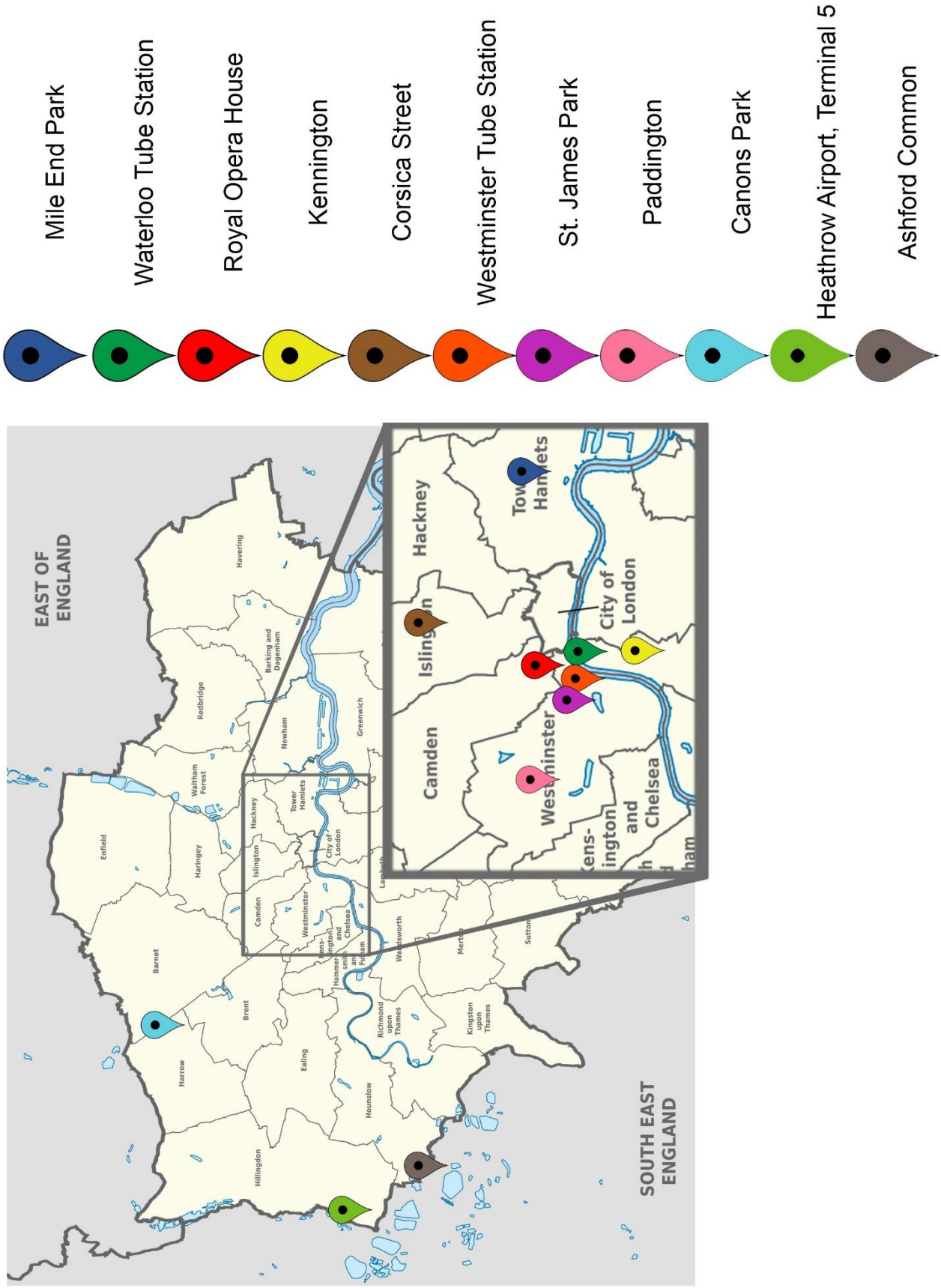

Fig. AI.1 – Representation of the several places across Central London referred in Chapter 2

Appendix II

In this appendix are presented figures from the case study's progress reports provided to the author. The following figures show the progression of construction when employing the sequential excavation method and are related with the dates referred in Chapter 4.

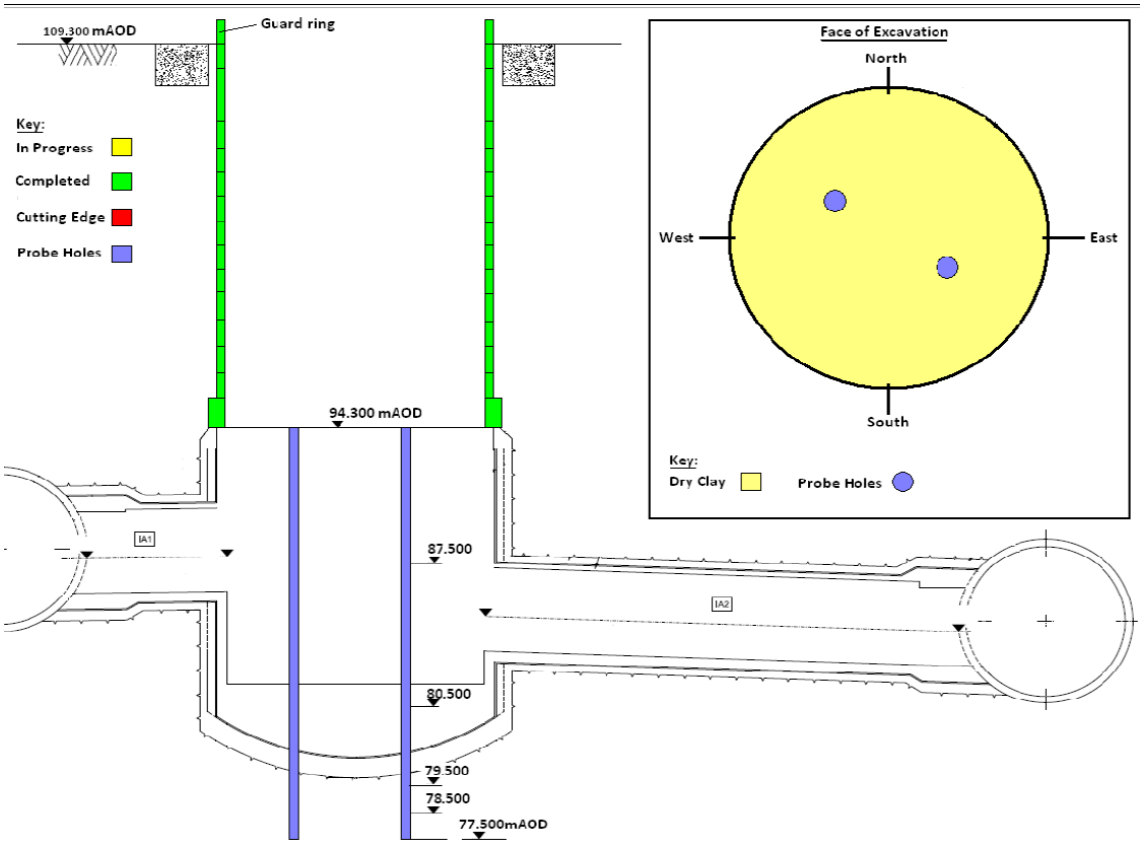

Figure AII.1 - 12/06/2013

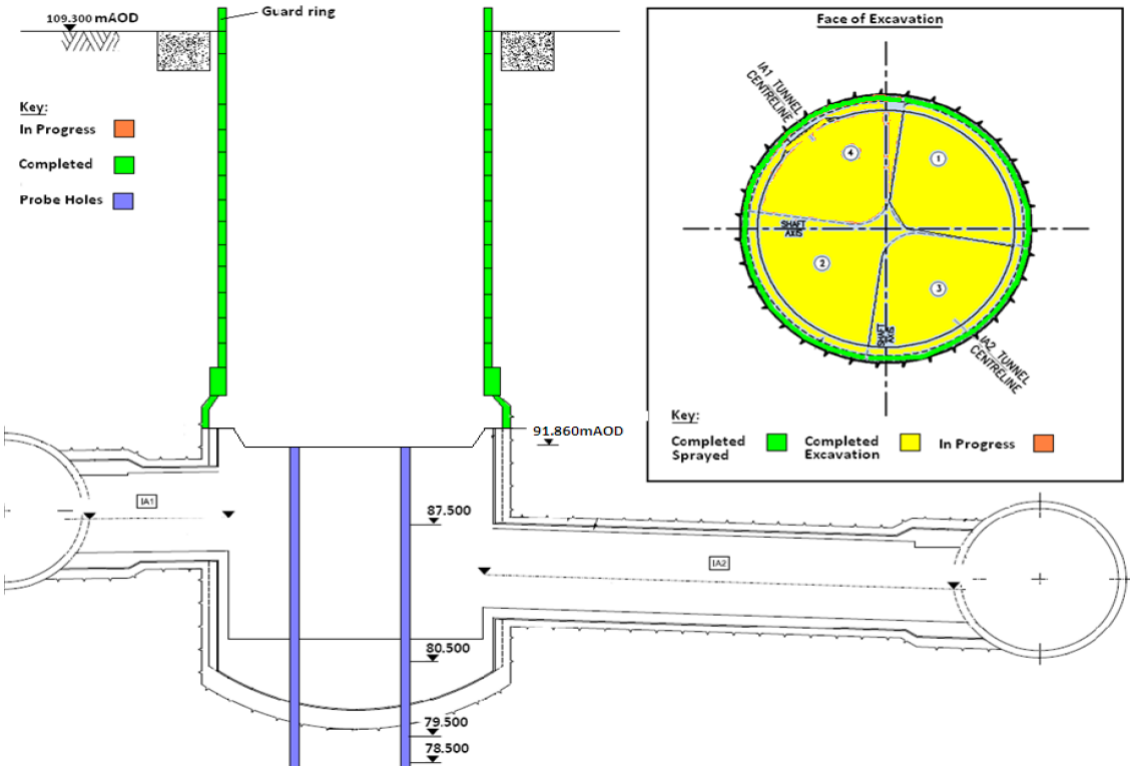

Figure AII.2 - 24/06/2013

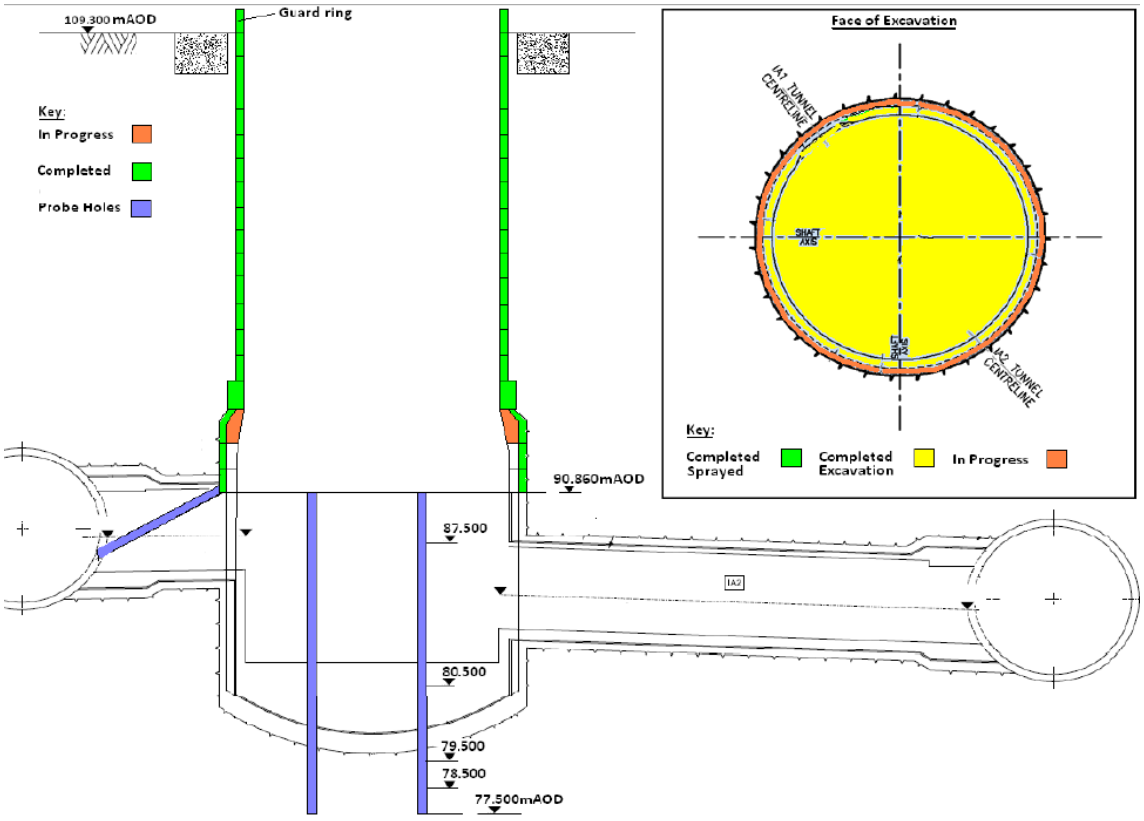

Figure AII.3 – 27/06/2013

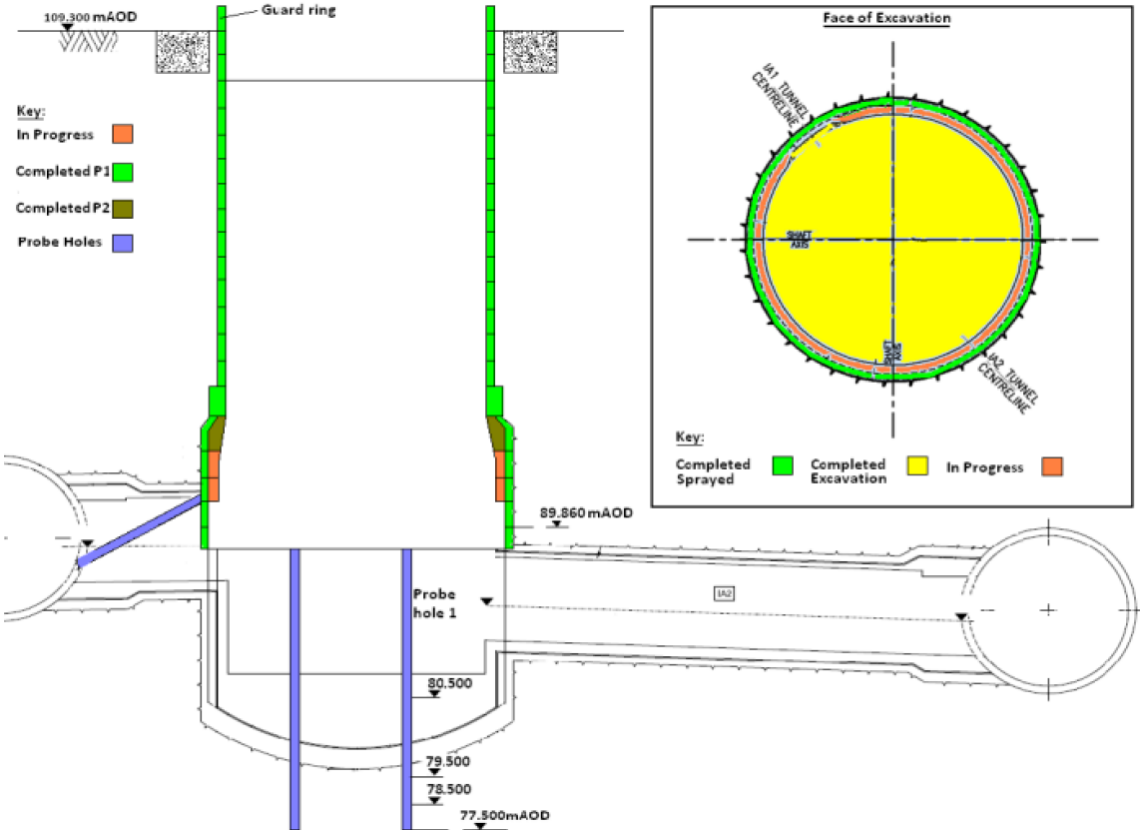

Figure AII.4 – 5/07/2013

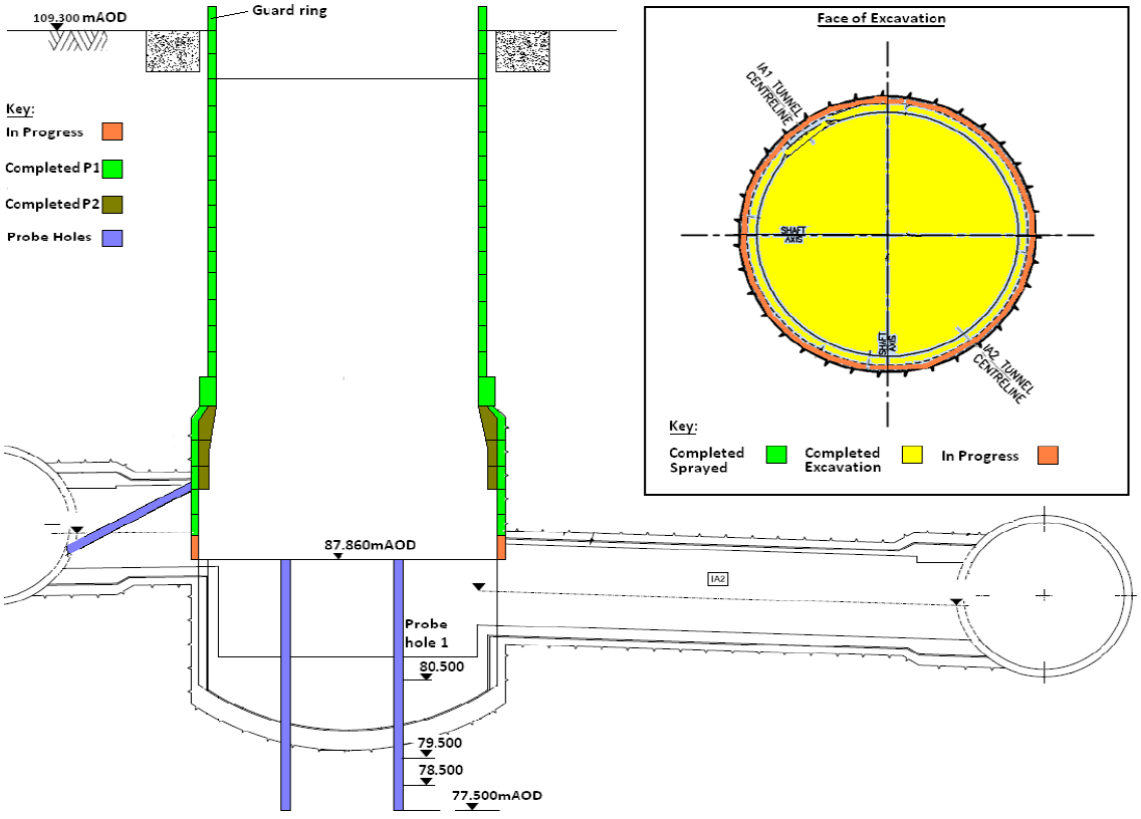

Figure AII.5 - 9/07/2013

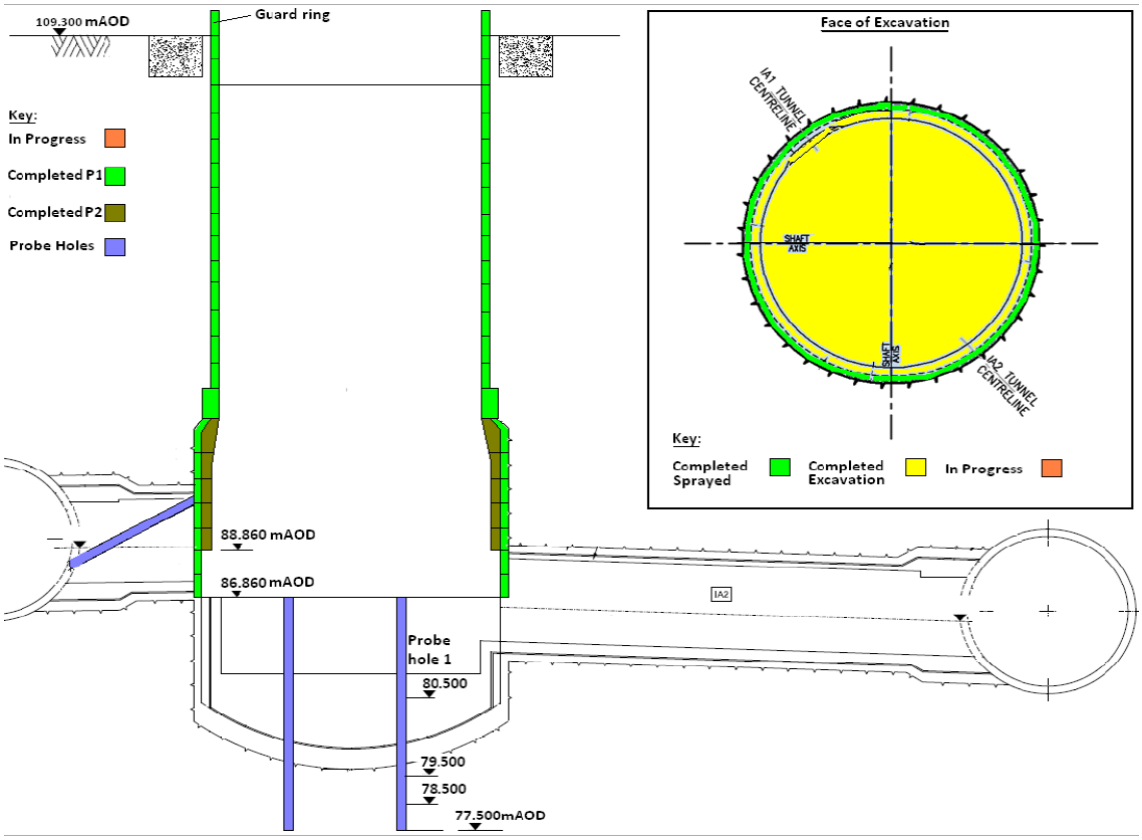

Figure AII.6 - 11/07/2013

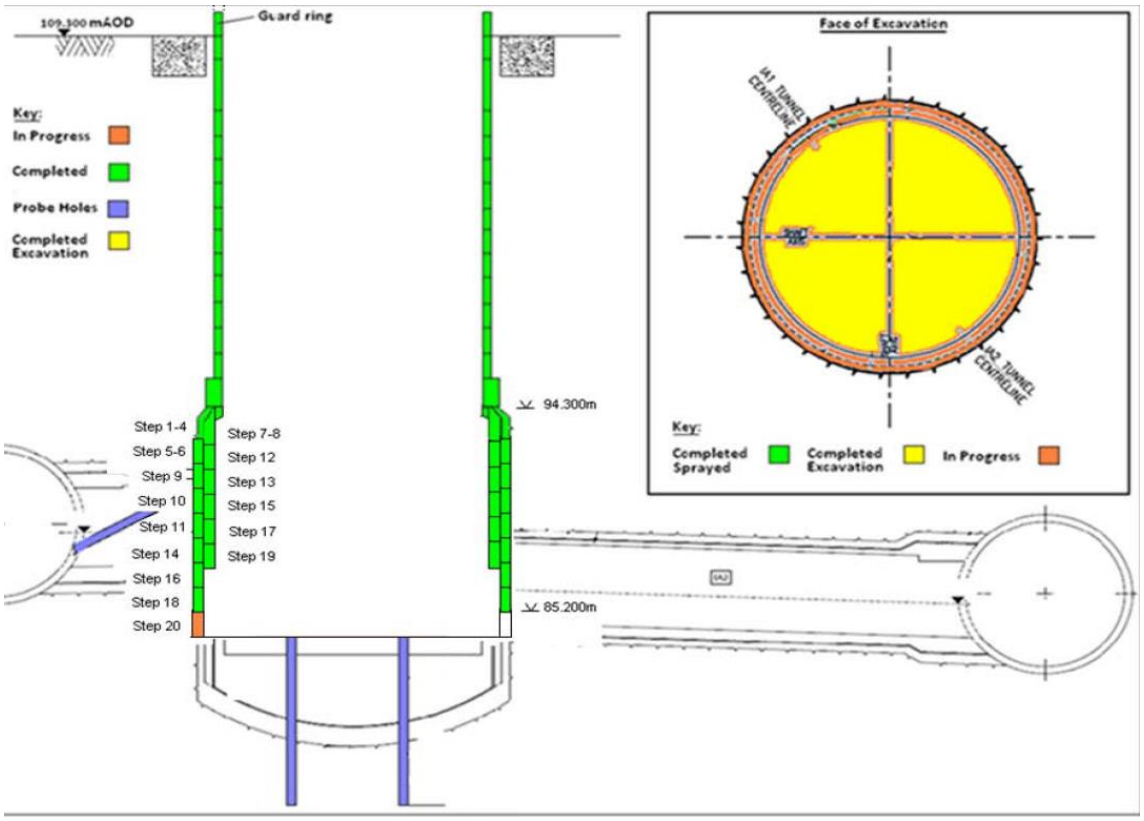

Figure AII.7 - 15/07/2013

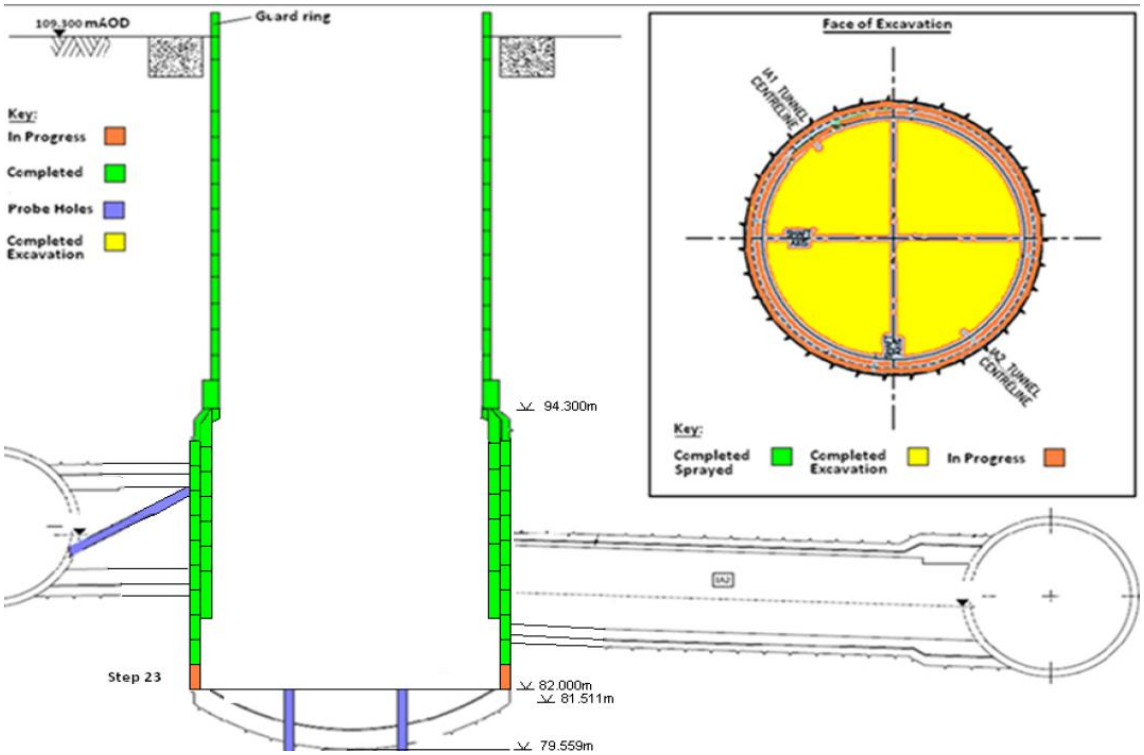

Figure AII.8 - 18/07/2013

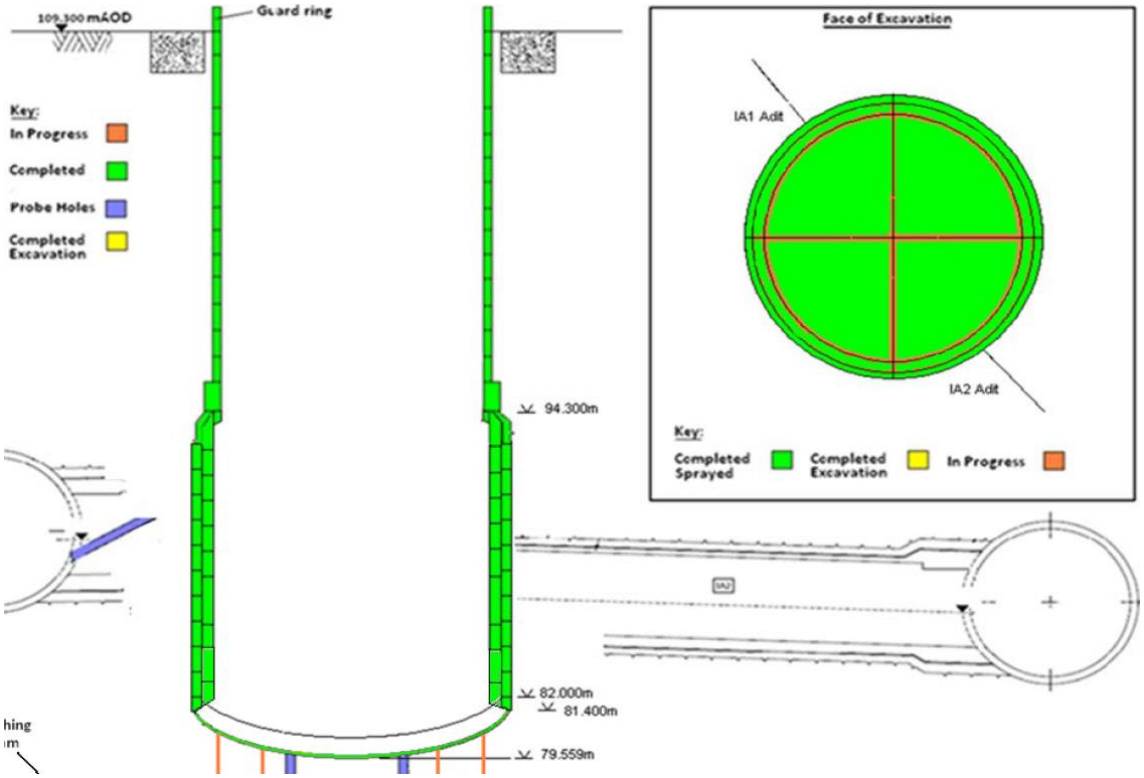

Figure AII.9 - 25/07/2013

Appendix III

In this appendix are presented figures from the case study's monitoring report whose values were used to produce the ground settlements graphs shown in Chapter 4.

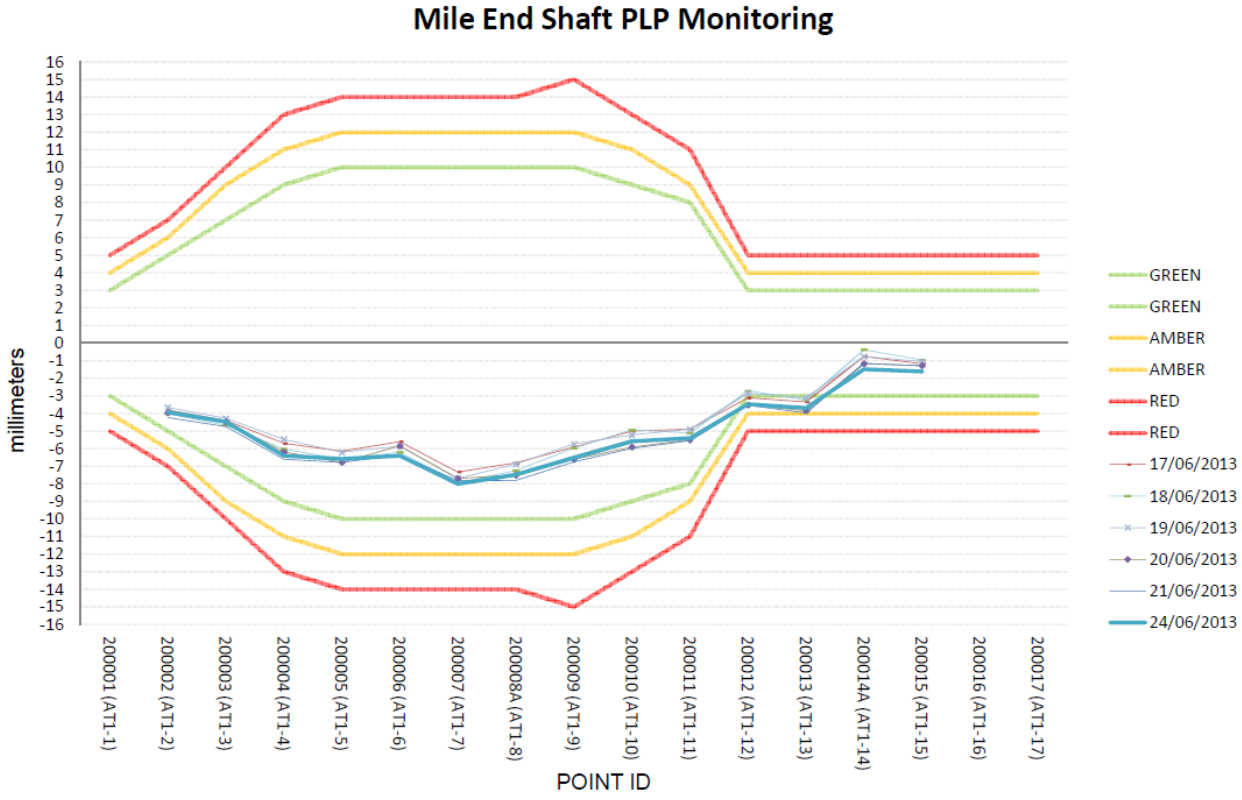

Figure AIII.1 - 24/06/2013

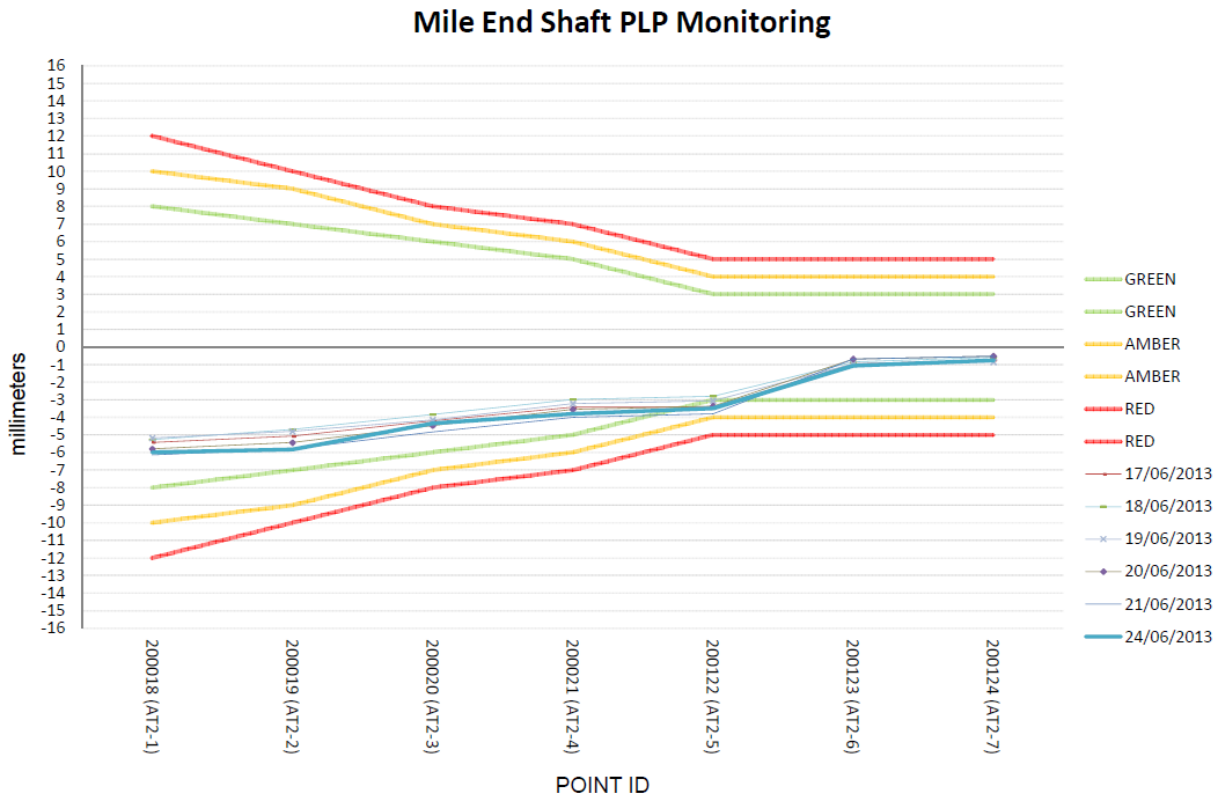

Figure AIII.2 - 24/06/2013 A2

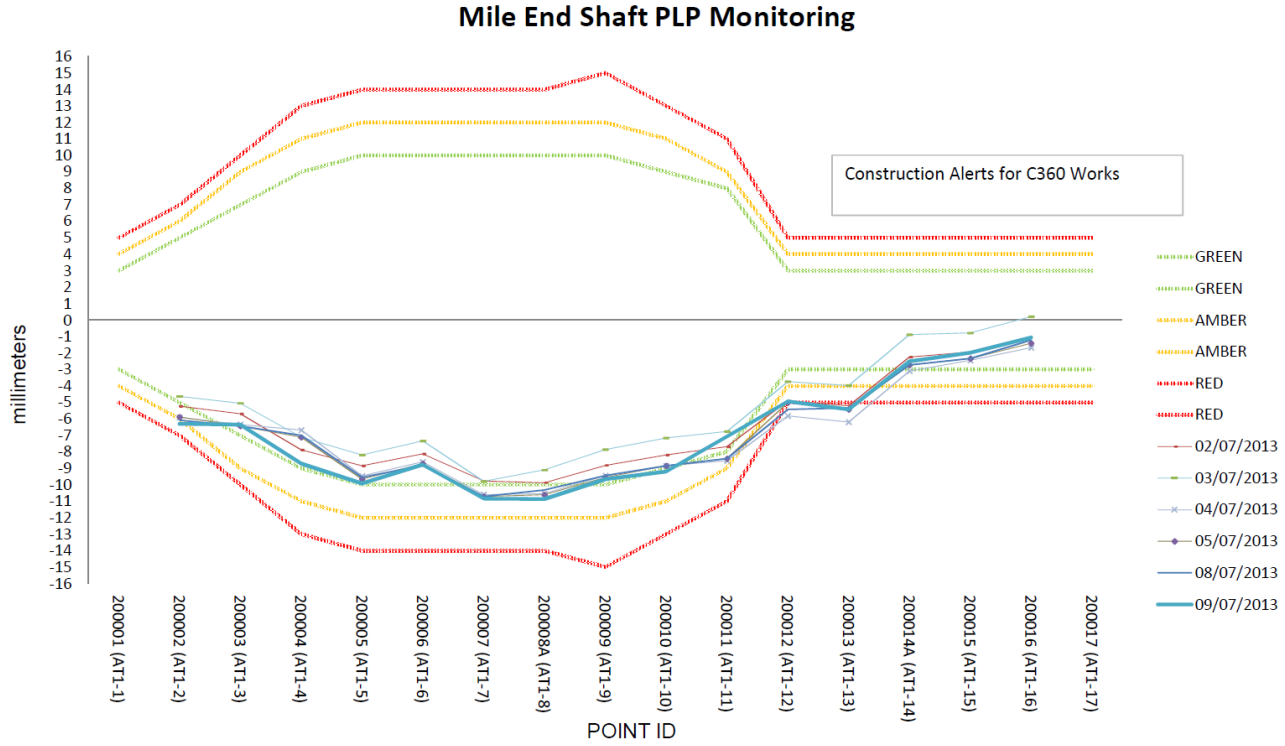

Figure AIII.3 – 9/07/2013

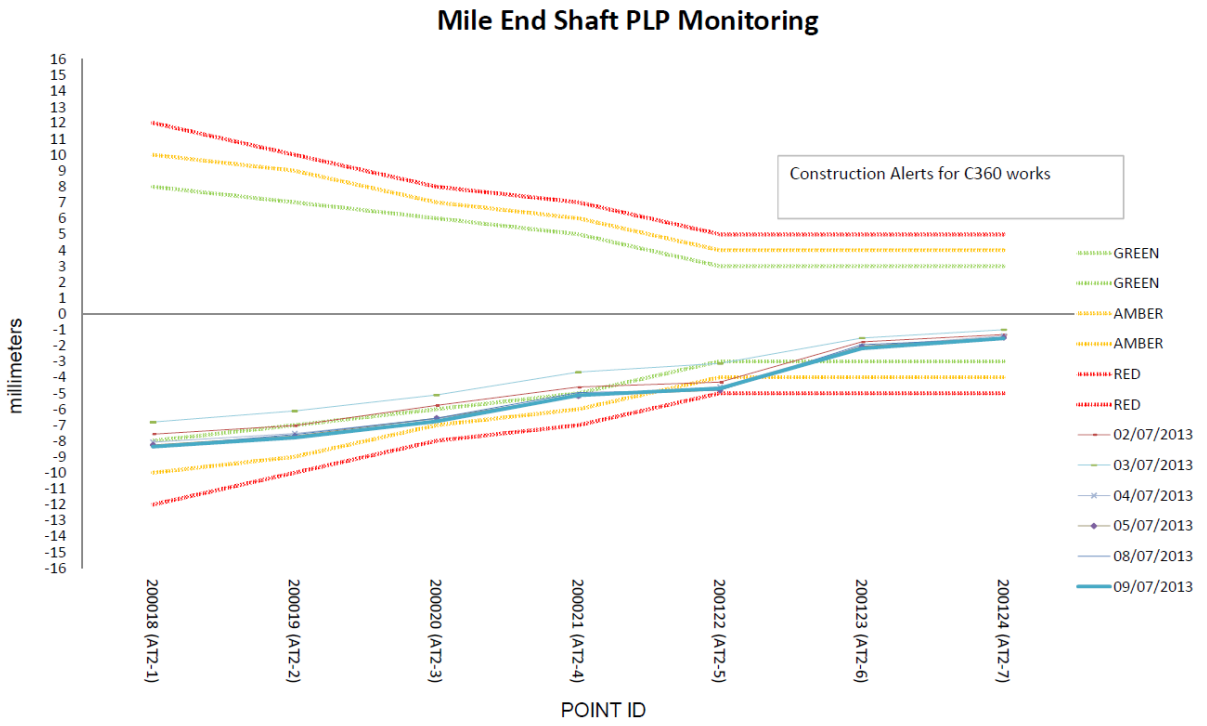

Figure AIII.4 - 9/07/2013 A2

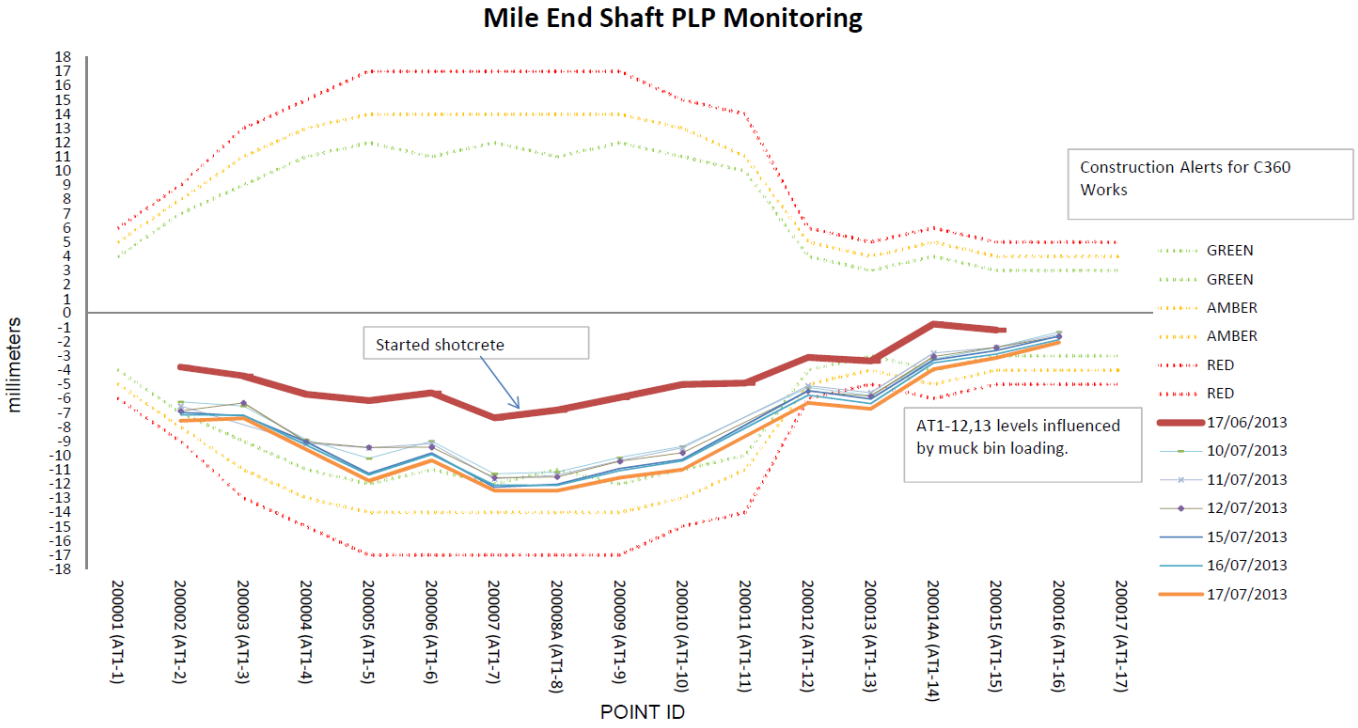

Figure AIII.5 - 17/07/2013

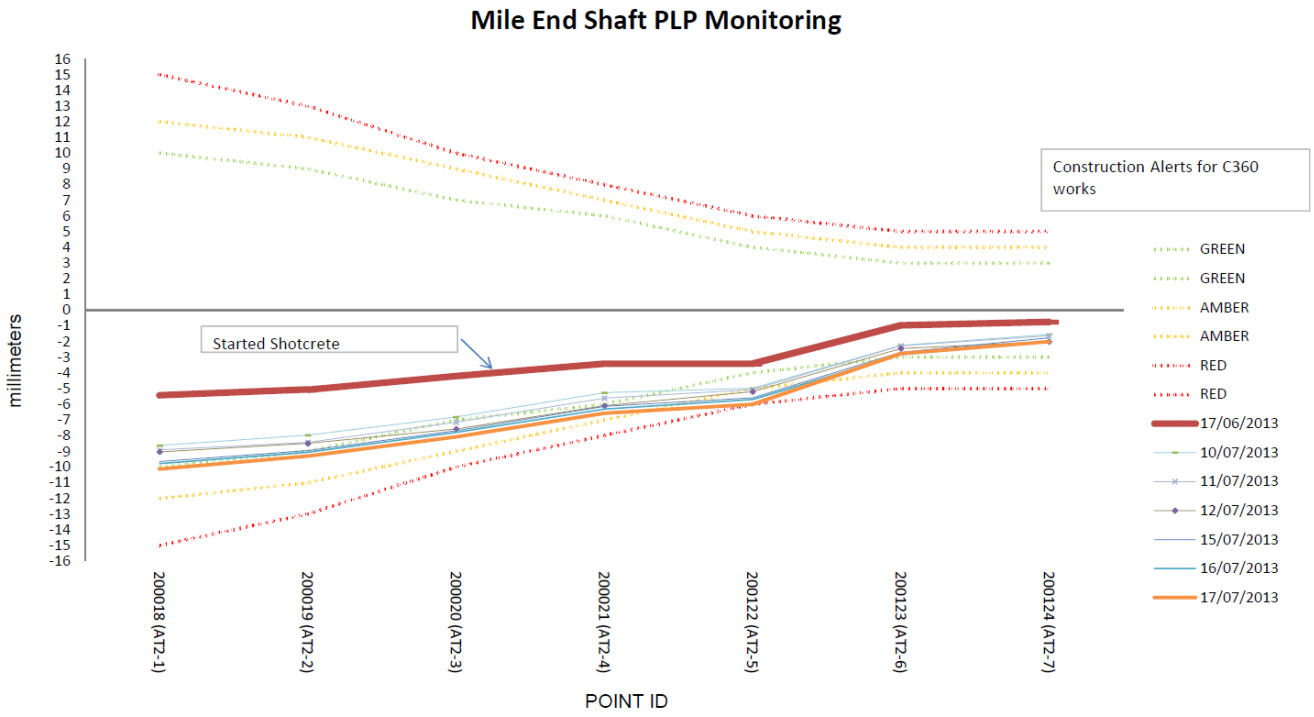

Figure AIII.6 - 17/07/2013

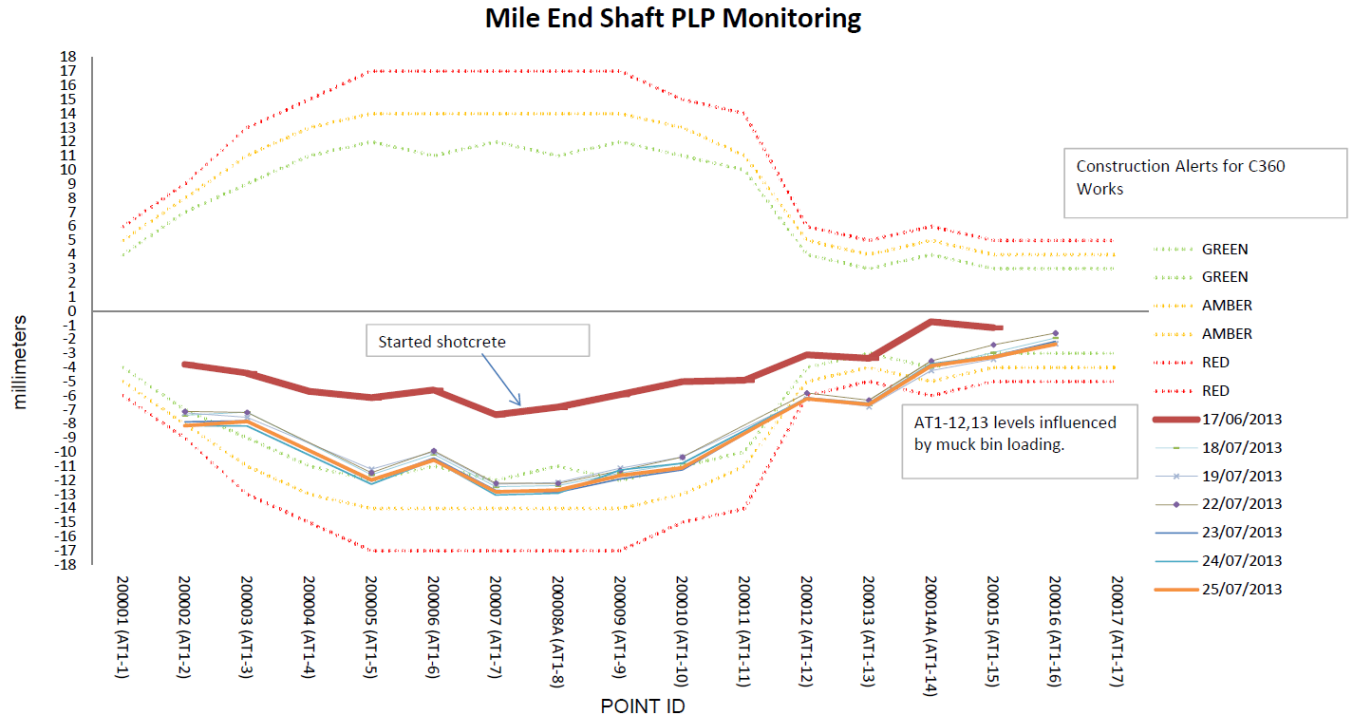

Figure AIII.7 - 25/07/2013

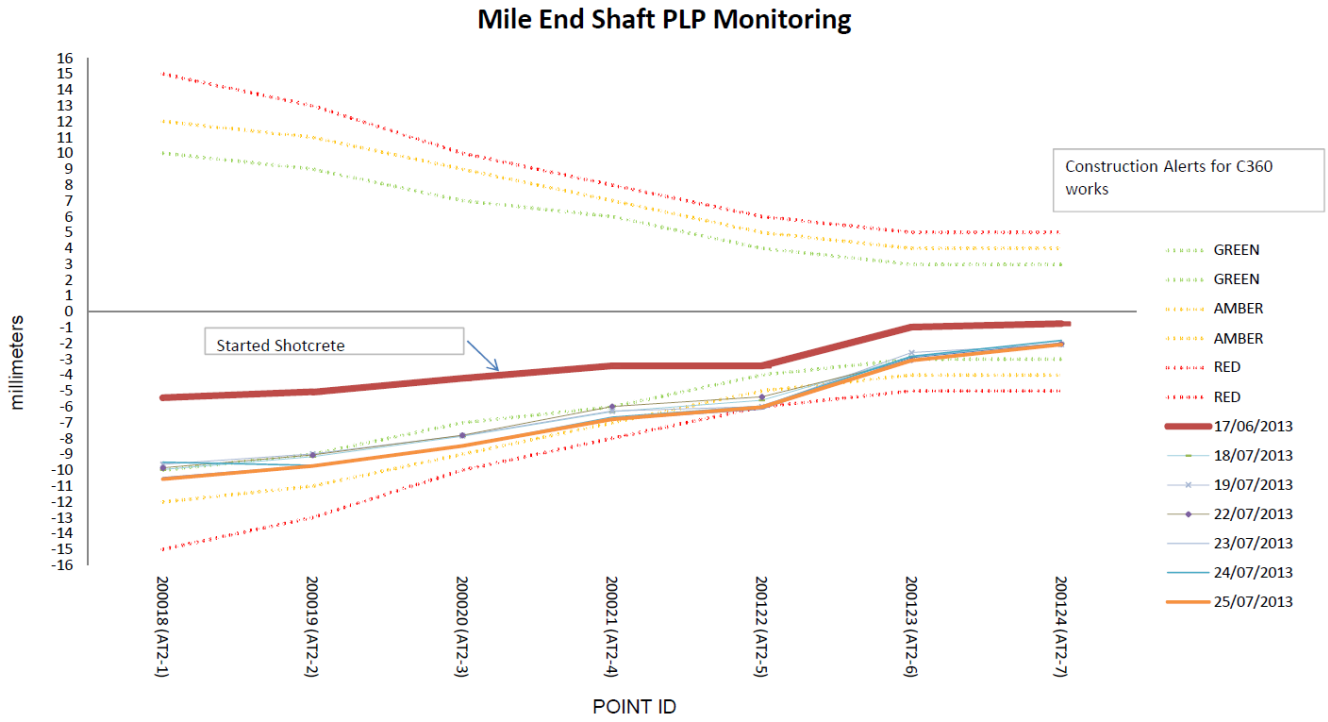

Figure AIII.8 - 25/07/2013